



ADVANCES IN CHEMICAL ENGINEERING

Volume 14

John L. Anderson

ADVANCES IN CHEMICAL ENGINEERING

Volume 14

This Page Intentionally Left Blank

ADVANCES IN CHEMICAL ENGINEERING

Editor-in-Chief

JAMES WEI

*Department of Chemical Engineering
Massachusetts Institute of Technology
Cambridge, Massachusetts*

Editors

JOHN L. ANDERSON

*Department of Chemical Engineering
Carnegie-Mellon University
Pittsburgh, Pennsylvania*

KENNETH B. BISCHOFF

*Department of Chemical Engineering
University of Delaware
Newark, Delaware*

JOHN H. SEINFELD

*Department of Chemical Engineering
California Institute of Technology
Pasadena, California*

Volume 14



ACADEMIC PRESS, INC.

Harcourt Brace Jovanovich, Publishers

San Diego New York Berkeley Boston
London Sydney Tokyo Toronto

COPYRIGHT © 1988 BY ACADEMIC PRESS, INC.

ALL RIGHTS RESERVED.

NO PART OF THIS PUBLICATION MAY BE REPRODUCED OR
TRANSMITTED IN ANY FORM OR BY ANY MEANS, ELECTRONIC
OR MECHANICAL, INCLUDING PHOTOCOPY, RECORDING, OR
ANY INFORMATION STORAGE AND RETRIEVAL SYSTEM, WITHOUT
PERMISSION IN WRITING FROM THE PUBLISHER.

ACADEMIC PRESS, INC.

San Diego, California 92101

United Kingdom Edition published by

ACADEMIC PRESS LIMITED

24-28 Oval Road, London NW1 7DX

LIBRARY OF CONGRESS CATALOG CARD NUMBER: 56-6600

ISBN 0-12-008514-3 (alk. paper)

PRINTED IN THE UNITED STATES OF AMERICA

88 89 90 91 9 8 7 6 5 4 3 2 1

CONTENTS

PREFACE	vii
-------------------	-----

Analysis and Synthesis of Resilient Heat Exchanger Networks

RICHARD D. COLBERG AND MANFRED MORARI

I. Introduction	1
II. Empirical versus Systematic Methods for HEN Resilience	3
III. Analysis of HEN Resilience	11
IV. Synthesis and Design of Resilient HENs	65
Nomenclature	89
References	91

Catalytic Hydrodemetallation of Petroleum

RICHARD J. QUANN, ROBERT A. WARE, CHI-WEN HUNG, AND JAMES WEI

I. Introduction	96
II. Metal Compounds in Petroleum	98
III. Residuum Hydrotreating Technology	134
IV. Reaction Kinetics and Diffusion in Catalytic Hydrodemetallation	158
V. Catalyst Deactivation	210
VI. Conclusions	248
References	251

The Safety Matrix: People Applying Technology to Yield Safe Chemical Plants and Products

KENT DAVIS

I. Introduction	262
II. Organization	271
III. Functional Roles	274
IV. Programs and Procedures	281
V. Society's Role	312
VI. Summary and Conclusions	316
References	318
INDEX	319

This Page Intentionally Left Blank

PREFACE

In a very short time since its announcement in November 1987, the National Research Council report, "Frontiers in Chemical Engineering: Research Needs and Opportunities," has become accepted as the point of departure in any discussion on the future of our profession. The report hails four principal frontiers: starting new technologies, maintaining leadership in established technologies, protecting and improving health, safety, and the environment, and developing systematic knowledge and generic tools. This report is required reading for all serious chemical engineers who are concerned about the future.

There are three chapters in this volume of *Advances in Chemical Engineering*. The chapter, "Analysis and Synthesis of Resilient Heat Exchanger Networks" by Colberg and Morari of Caltech, is concerned with the development of new generic tools. It provides an overview on the macroscale design of systems that are resilient and flexible to uncertainties and variations in system variables, such as flow rates and fouling of heat exchanger surfaces.

The chapter, "Catalytic Hydrodemetallation" by Quann and Ware of Mobil, Hung of Chevron, and Wei of MIT, is devoted to maintaining leadership in an established technology, namely oil refining. There are two topics with the greatest potential impact on our ability to increase the supply of clean premium transportation fuels of gasoline and kerosene: the liquefaction of ubiquitous and refractory methane and the upgrading of heavy and resid oils. This chapter provides a timely review of a principal problem in resid upgrading.

The chapter, "Safety Matrix: People Applying Technology to Yield Safe Chemical Plants and Products" by Davis of Dow Chemical, is concerned with protecting and improving safety in chemical plants. Dow Chemical has dramatically improved its safety record and seized a leadership position among chemical companies in the past decade. This improvement is not an accident, but the result of a dedicated attitude and systemic application that should be exported to the entire chemical industry. The lessons here would make us all winners and demonstrate that the chemical engineers are the solutions rather than the problems.

James Wei

This Page Intentionally Left Blank

ANALYSIS AND SYNTHESIS OF RESILIENT HEAT EXCHANGER NETWORKS

Richard D. Colberg and
Manfred Morari

Department of Chemical Engineering
California Institute of Technology
Pasadena, California 91125

I. Introduction	1
II. Empirical versus Systematic Methods for HEN Resilience	3
A. Why Empirical Methods Can Fail: Motivating Examples	3
B. Systematic Methods: Basic Problem Descriptions	8
III. Analysis of HEN Resilience	11
A. General Problem Formulations	11
B. Linear Resilience Analysis	28
C. Nonlinear Resilience Analysis	33
D. Class 2 Resilience Problems	59
E. Summary of HEN Resilience Analysis Techniques; Areas for Future Research	62
IV. Synthesis and Design of Resilient HENs	65
A. HEN Synthesis Based on a Flexibility Index Target	65
B. Multiperiod HEN Synthesis Using Structural Optimization	72
C. HEN Synthesis Using "Downstream (Disturbance) Paths"	82
D. Summary of Resilient HEN Synthesis Procedures; Areas for Future Research	85
Nomenclature	89
References	91

I. Introduction

Research on the synthesis of economically optimal heat exchanger networks (HENs) has been performed for over 15 years (Nishida *et al.*, 1981). As a result of this research, two general conclusions have emerged: (1) the optimum network generally features minimum or close to minimum utility consumption, and (2) the optimum network generally has a mini-

mum or close to minimum number of units (exchangers, heaters, and coolers).

As aids in synthesizing economically optimal HENs, targets have been developed to predict *before* synthesis the minimum utilities required (Hohmann, 1971; Raghavan, 1977; Linnhoff and Flower, 1978) and the minimum units required (Hohmann, 1971) for given values of the stream supply and target temperatures and heat capacity flow rates and an assumed value of minimum approach temperature ΔT_m . Thus most recent HEN synthesis algorithms decompose the synthesis problem into at least two stages: (1) targeting of minimum utilities and minimum units and (2) synthesis of a HEN structure with minimum utility consumption and with minimum or close to minimum number of units.

Most recent synthesis algorithms are also based upon the principles of the thermodynamic "pinch" (Linnhoff *et al.*, 1979; Umeda *et al.*, 1978). Recognition of the pinch provided great physical insight into the problem of HEN synthesis. The reader is assumed to be familiar with the principles of the pinch and with general methods for HEN synthesis [e.g., pinch design method (Linnhoff *et al.*, 1982; Linnhoff and Hindmarsh, 1983), structural optimization methods for selection of a minimum set of stream matches (Papoulias and Grossmann, 1983), and determination of the most economical network structure (Floudas *et al.*, 1986) from the predicted matches].

The difficulty with these synthesis methods is that they generate HENs for *fixed* nominal values of the stream supply temperatures and flow rates and for assumed nominal values of the heat transfer coefficients. In an industrial HEN, the supply temperatures and flow rates will vary (because of unpredictable environmental disturbances or because of predictable feedstock and throughput changes), and the heat transfer coefficients are highly uncertain (due to fouling, etc.). The HEN synthesized for nominal conditions must be *resilient* (flexible) to changes in supply temperatures and flow rates and to uncertainties in heat transfer coefficients.

In general, the entire process plant should be resilient. However, in a tightly energy-integrated plant, it is especially important that the HEN be resilient—if the HEN cannot operate, then neither can the plant.

In the past, HEN resilience was often assumed if the HEN could operate for perceived "worst" cases (i.e., combinations of highest and lowest temperatures and flow rates. However, as the next section of this chapter demonstrates, the worst cases for resilience may not agree with intuition (e.g., nonlinearities may cause the worst case for resilience to occur at intermediate values of temperature and flow rate).

A more sophisticated approach to analyzing HEN resilience is to use "shifting" arguments. By considering the effects of temperature and flow

rate disturbances as they are shifted and/or propagated toward the heaters and coolers (which can absorb the disturbances), one can gain physical insight into the problem of HEN resilience. However, the shifting arguments are difficult to apply quantitatively to HENs with several degrees of freedom (several exchangers more than the minimum required and/or stream splits), and it is difficult to study interactions between multiple disturbances.

In this chapter more systematic methods for HEN resilience analysis and three procedures for synthesis of resilient HENs are reviewed. Section II demonstrates how simple, empirical HEN resilience tests can fail and establishes the need for more systematic HEN resilience analysis methods. Section III presents several rigorous analysis methods, states the conditions when they are linear, and includes special nonlinear forms. Section IV reviews three procedures for synthesis of resilient HENs: (1) synthesis based on a resilience target (Colberg *et al.*, 1988); (2) "multiperiod" synthesis-analysis-resynthesis algorithm (Floudas and Grossmann, 1987b), which is an extension of the structural optimization synthesis algorithm for fixed stream conditions; and (3) synthesis using "downstream (disturbance) paths" (Linnhoff and Kotjabasakis 1986).

The scope of this chapter is limited to resilience of HENs in the steady state. Obviously, it is important that a HEN be controllable and that it be resilient to dynamic changes in temperature and flow rate (Morari *et al.*, 1985). However, dynamic resilience will not be addressed. Also, many of the resilience concepts reviewed here were developed for general chemical processes (Grossmann and Morari, 1983; Swaney and Grossmann, 1985a; Grossmann and Floudas, 1987; Linnhoff and Kotjabasakis, 1986). However, in this chapter they will be applied specifically to HENs.

II. Empirical versus Systematic Methods for HEN Resilience

A. WHY EMPIRICAL METHODS CAN FAIL: MOTIVATING EXAMPLES

The conventional procedure for introducing resilience in a HEN (or general process plant) is to use empirical overdesign. That is, a nominal or "conservative" basis is selected for designing and optimizing the HEN. Empirical safety factors based on past experience are applied to the equipment sizes and extra units are also often introduced. However, although this empirical procedure will in general add resilience and

flexibility of operation to a HEN, it has the following drawbacks:

1. Not much insight is gained on how much (if any) resilience is added for a given degree of overdesign.
2. The "most conservative" or "worst case" basis for design may not be the one the designer would intuitively expect.
3. Conditions that give rise to infeasible operation may not be detected since interactions among different exchangers are not explicitly taken into account.
4. The resulting oversized network may not operate efficiently and may not be optimal from an economic viewpoint.

The following two examples demonstrate these drawbacks of empirical overdesign.

Example 1 (from Grossmann and Morari, 1983). Traditional industrial practice generates resilient HENs by designing them for what are perceived to be "extreme" operating conditions. Naturally, if these extremes are selected properly, the HEN will perform satisfactorily for the whole range of expected conditions. This example demonstrates that the proper selection of "extremes" is far from trivial and that seemingly logical choices can lead to extremely poor systems.

The HEN shown in Fig. 1a was designed for the problem data shown. There are no other designs with fewer heat transfer units, and the approach temperatures fall nowhere below 10 K; therefore this structure is likely to be close to optimal economically. However, it is known that the heat capacity flow rate of stream S_{h1} can be as large as 1.85 kW/K at times. The natural approach of the design engineer would be to test his design for this extreme condition. The test reveals that the network structure also performs satisfactorily at this flow rate (Fig. 1b). It appears logical to expect that the structure can handle all flow rates in the range 1–1.85 kW/K.

Figure 1c reveals that this is not the case. *Even if exchanger 1 had infinite area* (ie., infinite overdesign factor), for a heat capacity flow rate of 1.359 kW/K the outlet temperature of stream S_{h1} cannot be decreased below 344 K. With a reasonable approach temperature difference of 10 K (Fig. 1d), the minimum attainable outlet temperature for stream S_{h1} is 375.4 K, corresponding to a target temperature violation of 52 K. If S_{h1} were the feed stream to a reactor, this design error could have serious consequences.

By switching the cooler from stream S_{h2} to S_{h1} the network can be made resilient (Fig. 1e). In all exchangers the approach temperatures exceed 10 K over the whole range of flow rate variations $1 \leq w_{h1} \leq 1.85$ kW/K and therefore capital costs remain reasonable. The example shows that

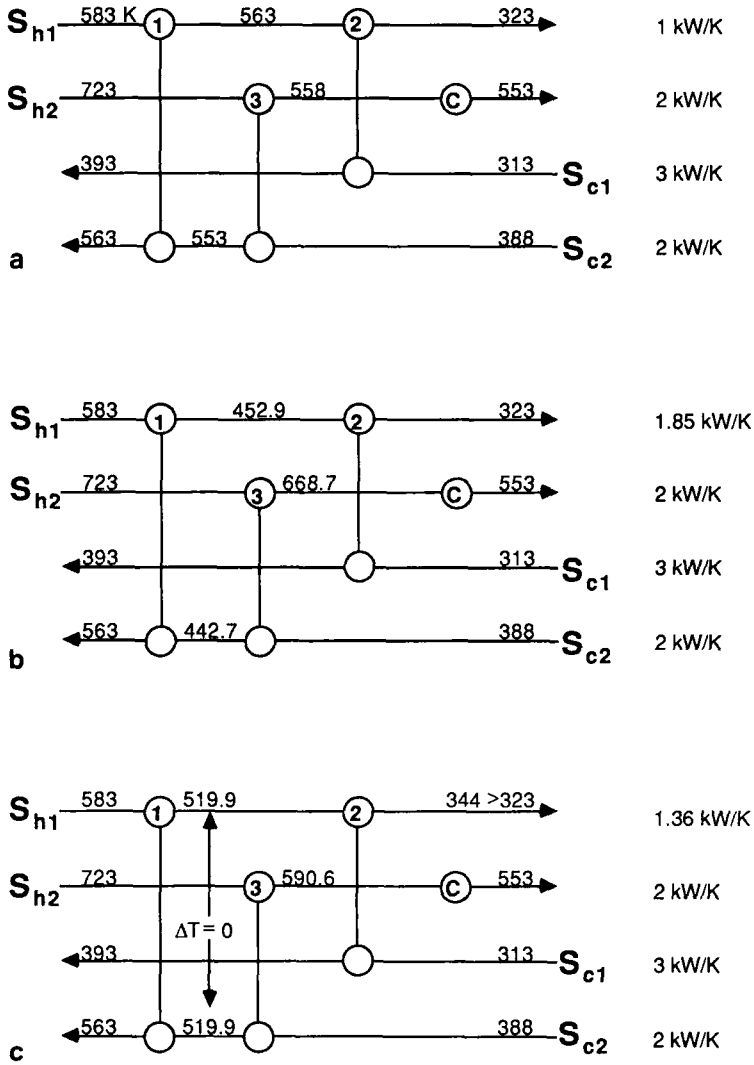


FIG. 1. HEN structures for Example 1: (a) Feasible for nominal flow rate $w_{h1} = 1.0$ kW/K. (b) Feasible for extreme flow rate $w_{h1} = 1.85$ kW/K. (c) Target temperature violation of 21 K with intermediate flow rate $w_{h1} = 1.359$ kW/K (with $\Delta T_m = 0$ K). (d) Target temperature violation of 52 K with intermediate flow rate $w_{h1} = 1.359$ kW/K (with $\Delta T_m = 10$ K). (e) Resilient for $1.0 \leq w_{h1} \leq 1.85$ kW/K. (f) Resilient for modified example ($T_{c2}^S = 393$ K).

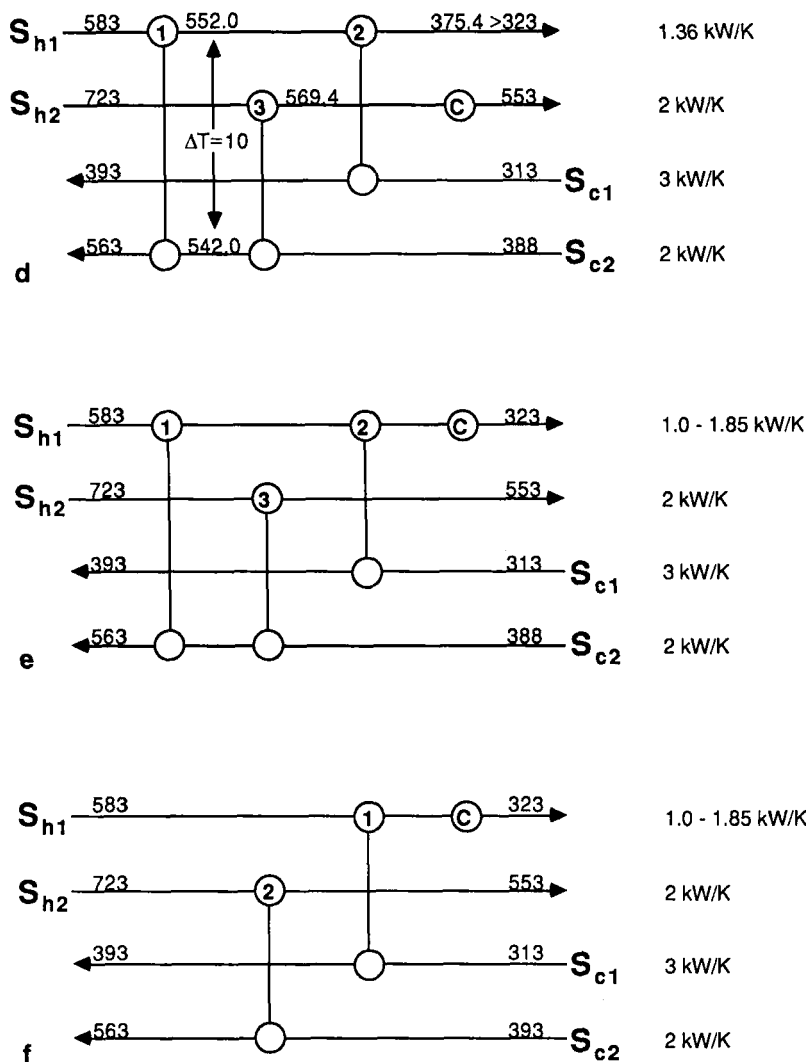


FIG. 1 (Continued)

resilience may not be obtained with additional exchangers or excessive oversizing, but simply by a proper redesign of the network structure.

Let us also look at the slightly modified problem in which the inlet temperature of stream S_{c2} is increased to $T_{c2}^s = 393$ K. The network structure in Fig. 1a suffers from the same deficiencies as before. A resilient structure

is shown in Fig. 1f. It involves only three heat exchangers, while the other structure had four. Selecting networks with a larger number of transfer units not only increases capital costs, but can *decrease* resilience. Resilience cannot be achieved by *ad hoc* addition of equipment, but by systematic design techniques based on a thorough understanding of the physicomathematical problem.

Example 2 (from Grossmann and Morari, 1983). In order to illustrate the problem of overlooking effects of interactions, consider the HEN shown in Fig. 2a. Note that in this case the outlet temperatures of streams S_{h1} and S_{c2} have been specified as inequalities: stream S_{h1} must be cooled down to at least 410 K, while stream S_{c2} must be heated up to at least 430 K.

Assume that the areas of exchangers 1 and 2 are sized for nominal values of heat transfer coefficients $U_1 = U_2 = 800 \text{ W/m}^2 \text{ K}$ and that the resulting areas are oversized by 20%. If such a design were implemented in practice, the following situation might occur.

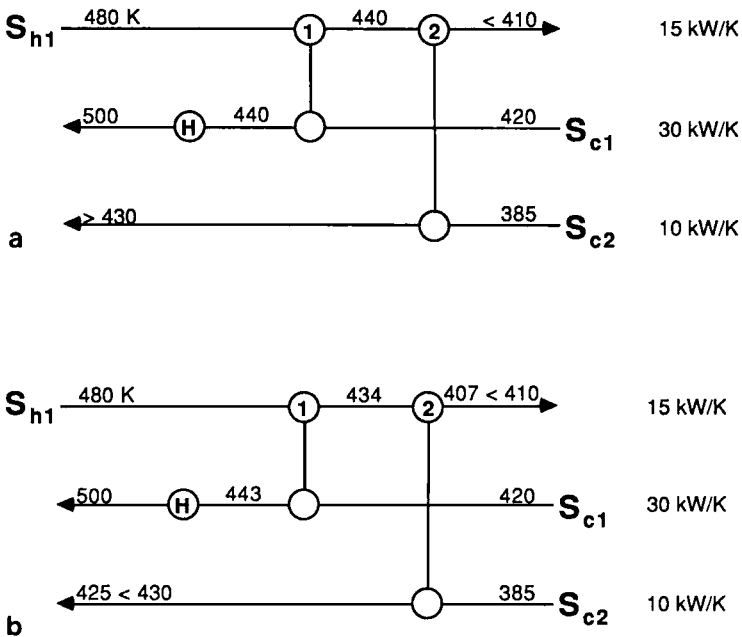


FIG. 2. HEN structure for Example 2: (a) Feasible with nominal heat transfer coefficients. (b) Infeasible with heat transfer coefficients +20% and -20% of their nominal values in exchangers 1 and 2, respectively.

Suppose that U_1 is 20% higher than its nominal value while U_2 is 20% lower. For such a case, as shown in Fig. 2b, the exit temperature of stream S_{h1} from exchanger 1 would drop from the expected 440 K down to 434 K owing to the larger heat transfer coefficient. However, with this change the temperature driving force in exchanger 2 is reduced, which when coupled with the lower heat transfer coefficient causes the outlet temperature of stream S_{c1} from this exchanger to be 425 K, or 5 K below the minimum temperature that was specified. Therefore, for this realization of heat transfer coefficients the network attains infeasible operation since it violates the temperature specification. This example illustrates the danger of overlooking interactions when using empirical overdesign.

It should be noted that this design satisfies the temperature specifications when both heat transfer coefficients are 20% lower than their nominal values, which intuitively would be regarded as the "worst" condition. Thus, this example also shows that identifying "worst" conditions for feasible operation may not always be obvious from intuition.

Another point of the example is related to the choice of areas such that temperature specifications are not violated for any deviation of U_1 and U_2 within $\pm 20\%$ of their nominal values. For instance, if one were to insist on oversizing the area of exchanger 1 by 20%, then the area of exchanger 2 would have to be oversized by 108%. On the other hand, if one were to oversize exchanger 2 by 23%, then exchanger 1 would not have to be oversized, but rather it could be *undersized* by 16%! This shows that the choice of a resilient design which is also economically optimal may not be obvious in general. Hence, the need for a systematic treatment of resilience and flexibility in process design should be evident.

B. SYSTEMATIC METHODS: BASIC PROBLEM DESCRIPTIONS

The previous examples clearly demonstrate the need for more systematic methods to treat HEN resilience. In particular, systematic methods are needed to determine how much, if any, resilience is gained for a given degree of overdesign, or whether resilience can be improved by simple structural changes; to rigorously handle process interactions and to correctly identify "worst case" operating conditions; and to synthesize the structure and determine the minimal amount of oversizing to yield an economically optimal, resilient HEN.

Before describing some basic problems in systematic analysis and synthesis of resilient HENs, we need to establish a common vocabulary of clearly defined terms. (Most of these definitions are adopted from Grossmann and Morari, 1983.)

Analysis means the study of the properties (economics, resilience, etc.) of a given design.

Design is the selection of variables (e.g., heat exchanger areas, maximum heater and cooler loads) which lead a given design structure (HEN topology or general process flow sheet) to have specified properties.

Synthesis is the generation of the process structure. The structural variables (existence or absence of a process unit—e.g., exchanger—or interconnection between process units) can be represented by binary integer variables.

Feasible refers to a process (HEN structure) which satisfies all physical constraints (nonnegative exchanger loads) and performance specifications (target temperatures, minimum approach temperature, specified energy recovery).

Control is the manipulation of a degree of freedom (e.g., heater, cooler or exchanger load, stream split fraction) in order to make a process feasible and/or economically optimal in the steady state. In this chapter, “control” is used in a static sense only; process dynamics are not considered.

Uncertainty range is the range of uncertain variables in a design problem. The uncertainty range can consist of “external” uncertainties (e.g., supply temperatures and flow rates) and/or “internal” uncertainties (e.g., heat transfer coefficients). The uncertainty range is typically specified in terms of finite upper and lower bounds on each of the uncertain variables.¹

Flexible refers to a process which remains feasible for every value of the uncertain variables in the uncertainty range despite *desired* changes to the process (e.g., supply temperature and flow rate variations due to feedstock changes).

Resilient processes are those which remain feasible for every value of the uncertain variables in the uncertainty range despite *undesired* changes to the process (e.g., environmental disturbances in supply temperatures, fouling of heat transfer surfaces). Mathematically, flexibility and resilience are the same problem; in this chapter, the two terms are used synonymously.

Several types of problems can be defined for the analysis and synthesis of resilient HENs. Some basic problems are verbally described here. In the next section, these problems are defined mathematically and interpreted graphically. In subsequent sections, algorithms are presented for solving these problems.

¹ In all of the resilience analysis techniques reviewed here, the uncertainty range can be extended to include variable target temperatures. In addition, if any of the uncertainties are correlated, then the uncertainty range should include only the independent uncertainties with all the dependent uncertainties expressed in terms of the independent ones.

1. *Feasibility Test*

For assumed, fixed values of the uncertain variables, can the “control variables” (degrees of freedom) be manipulated so as to make the HEN feasible (Saboo *et al.*, 1987a)? Note that feasibility of a HEN depends on several factors: assumed values of the uncertain variables, feasibility constraints (e.g., value of ΔT_m , specified level of energy recovery), values of the design and structural variables chosen by the designer *before* the feasibility test (or analogously before plant operation), and the fact that control variables are allowed to vary *during* the feasibility test (or analogously during plant operation).

Many earlier researchers neglected the fact that degrees of freedom are usually available in a process plant (HEN) which can be manipulated during plant operation so as to maintain feasibility (review by Grossmann *et al.*, 1983). By not allowing the control variables to vary, the feasibility test can be unnecessarily conservative.

2. *Resilience (Flexibility) Test*

Is the HEN feasible for *every* value of the uncertain variables in the expected uncertainty range? Note that whether a HEN is resilient depends upon the size of the expected uncertainty range (which the designer must estimate), in addition to the factors listed earlier which affect HEN feasibility. This test can be used to identify “worst case” values of the uncertain variables and to determine whether design changes make a formerly nonresilient HEN resilient in the specified uncertainty range. [Note that Halemane and Grossmann (1983) and Grossmann and Floudas (1987) call this test a “feasibility test” and that they have no specific name for the test with assumed, fixed values of the uncertain variables. In this chapter, we follow the terminology of Saboo *et al.* (1987)].

3. *Resilience (Flexibility) Index*

The resilience (flexibility) test is a yes–no test of HEN resilience in a specified uncertainty range. A more general problem is to measure the size of the largest uncertainty range for which the HEN is resilient (flexible). The resilience and flexibility indices are two different measures of the largest uncertainties (from assumed nominal values of the uncertain variables) for which a HEN remains feasible (Saboo *et al.*, 1985; Swaney and Grossmann, 1985a). Note that these indices depend upon the choice of nominal values for the uncertain variables. These indices can be used to determine how much resilience (flexibility) is gained for a given design change (overdesign or structural change) and to identify “worst case” values of the uncertain variables which limit HEN resilience.

4. *Synthesis of Resilient HENs*

The problem of synthesizing HENs which are both economically optimal and resilient can be posed in many forms. Should HEN cost be minimized only for “worst case” values of the uncertain variables (minimax strategy), or should the “expected” cost of the HEN—averaged over the expected frequency of occurrence of each value of the uncertain variables—be minimized? Should HEN feasibility be guaranteed only at the values of the uncertain variables which minimize cost or for the whole range of uncertain variables? Grossmann *et al.* (1983) review the approaches of several earlier researchers in uncertain process design. Later in this chapter, methods are presented to synthesize HENs in which the cost is minimized for several values of the uncertain variables (to approximate the minimax strategy) and which are resilient for the entire uncertainty range (Floudas and Grossmann, 1987b; Colberg *et al.*, 1988).

III. Analysis of HEN Resilience

A. GENERAL PROBLEM FORMULATIONS

In this section, general mathematical formulations and graphic interpretations are presented for several resilience analysis problems: (1) feasibility test, (2) resilience (flexibility) test, (3) flexibility index, and (4) resilience index.

1. *Feasibility Test*

The physical performance of a HEN can be described by the following set of constraints (Grossmann and Floudas, 1987):

$$h(d, z, x, \theta) = 0, \quad g(d, z, x, \theta) \leq 0 \quad (1)$$

where h is the vector of equations (mass and energy balances, energy recovery specification) which hold for steady-state operation and g is the vector of inequalities (target temperature and ΔT_m specifications; nonnegative load constraints) which must be satisfied if operation is to be feasible. The variables are classified as follows: d is the vector of design variables that define the HEN structure and exchanger sizes. These variables are fixed at the design stage and remain constant during plant operation. Here θ is the vector of uncertain variables (uncertain supply temperatures and flow rates, heat transfer coefficients, etc.). The vector z of control variables stands for the degrees of freedom that are available during operation and

which can be adjusted for different realizations of uncertain variables θ . Finally, x is the vector of state variables which is a subset of the remaining variables and which has the same dimension as h .

For a given HEN design d and for any realization of θ during operation, the state variables can in general be expressed as an implicit function of control variables z using equalities h ,

$$h(d, z, x, \theta) = 0 \Rightarrow x = x(d, z, \theta)$$

This allows elimination of the state variables, and the HEN performance specifications can be described with the following reduced set of inequality constraints:

$$g_m[d, z, x(d, z, \theta), \theta] = f_m(d, z, \theta) \leq 0 \quad (m \in M) \quad (2)$$

where M is the index set for the inequalities. It should be noted that elimination of the state variables is done at this point for the sake of simplicity in presentation; the actual numerical algorithms for analyzing HEN resilience do not require elimination of the equality constraints.

A HEN is feasible for assumed, fixed values of uncertain variables θ if control variables z can be found to satisfy the reduced set of constraints. The HEN feasibility test can be formulated as follows to minimize the maximum constraint violations (Halemane and Grossmann, 1983):

$$\psi(d, \theta) = \min_z \max_{m \in M} f_m(d, z, \theta) \quad (3)$$

This minimax problem can be converted to a simpler nonlinear program (NLP) by introducing a slack variable β to measure violations of the inequality constraints:

$$\psi(d, \theta) = \min_{z, \beta} \beta \quad (4)$$

subject to

$$f_m(d, z, \theta) \leq \beta \quad (m \in M)$$

The HEN is feasible for the assumed values of the uncertain variables θ if and only if $\psi \leq 0$.

In terms of the actual HEN feasibility constraints (including the equality constraints), NLP (4) can be expressed more explicitly as (Saboo *et al.*, 1987a)

$$\psi = \min_{u, v, \beta} \beta \quad (5)$$

subject to:

(A1) Energy balances on all exchangers, heaters, and stream splits:

$$A(u, w)t^S + B(u, v, w)v = b$$

(A2) Specified energy recovery:

$$\sum_k l_k^H = \alpha H(t^S, w)$$

(B1) ΔT_m constraints on all exchangers:

$$C(u, w)t^S + D(u, v, w)v + p \leq \beta e$$

(B2) Nonnegative exchanger and cooler loads:

$$E(u, w)t^S + Gv + r \leq \beta e$$

(B3) Nonnegative heater loads:

$$-l^H \leq \beta e$$

where t^S is the vector of supply temperatures; w the vector of inlet heat capacity flow rates;

$$\theta = \begin{bmatrix} t^S \\ w \end{bmatrix}$$

is the vector of uncertain variables (constant for feasibility test); u the vector of stream split fractions; t^I the vector of intermediate stream temperatures (between exchangers); l^H the vector of heater loads;

$$v = \begin{bmatrix} t^I \\ l^H \end{bmatrix}$$

is the vector of state and control variables (excluding stream split fractions); H the minimum heating requirement; α the factor by which heating target is relaxed from minimum heating requirement;

$$e = [1 \ 1 \ \cdots \ 1]^T$$

b , G , p , r are constant vectors and matrices; A , C , E are matrices whose elements are functions of u and w ; and B , D are matrices whose elements are functions of u , v , and w .

If the HEN has more than the minimum number of exchangers (say n_U more than the minimum) and n_T variable target temperatures, then $n_U + n_T$ of the intermediate stream temperatures and heater loads can be chosen as control variables. Stream split fractions are always available as control variables. These variables are adjusted to try to make the HEN feasible for the assumed, fixed values of the uncertain supply temperatures and flow rates. The HEN is feasible if and only if $\psi \leq 0$.

2. Resilience (Flexibility) Test

Resilience of a HEN represents its ability to accommodate uncertainty in a set of selected variables. The resilience properties of a HEN can be

completely described by the feasible region R (Fig. 3) in the space of uncertain variables:

$$R = \{\theta \mid \exists z] f_m(d, z, \theta) \leq 0 \forall m \in M\}$$

or equivalently

$$R = \{\theta \mid \psi(d, \theta) \leq 0\}$$

The boundary of R is determined by $\psi = 0$. Individual segments in the boundary of R are determined by $f_m = 0$, $m \in M$. Values of the uncertain variables θ lying inside feasible region R allow the control variables z to be adjusted so that all the feasibility constraints can be satisfied. For values of θ lying outside the feasible region, the control variables cannot be adjusted to satisfy all the feasibility constraints.

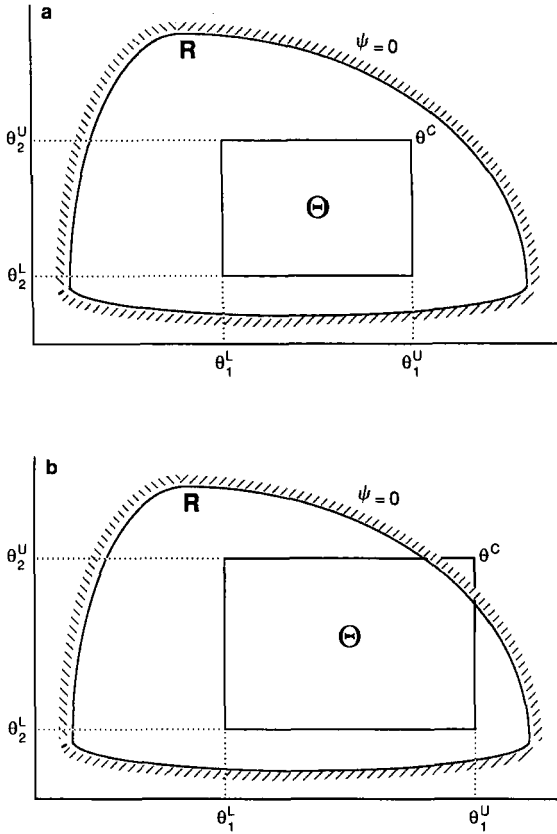


FIG. 3. Feasible region R and uncertainty ranges θ for resilient and nonresilient HENs: (a) Resilient HEN ($\theta \subset R$). (b) Nonresilient HEN ($\theta \not\subset R$).

The resilience (flexibility) test determines whether a HEN is resilient (flexible) throughout a specified uncertainty range Θ ,

$$\Theta = \{\theta \mid \theta^L \leq \theta \leq \theta^U\}$$

where θ^L and θ^U are vectors of lower and upper bounds, respectively, specified by the designer to describe the expected range of uncertainty. (Note that *resilience* and *flexibility* are used synonymously to describe the same test.) In other words, the resilience test determines whether the specified uncertainty range Θ lies entirely within feasible region R (see Fig. 3).

A HEN is resilient throughout uncertainty range Θ if and only if the HEN is feasible ($\psi \leq 0$) for all $\theta \in \Theta$. In mathematical terms, a HEN is resilient in Θ if and only if $\chi(d) \leq 0$, where

$$\chi(d) = \max_{\theta \in \Theta} \psi(d, \theta) \quad (6)$$

(Halemane and Grossmann, 1983). Substituting the definitions of ψ from Eqs. (3) and (4), two equivalent formulations for $\chi(d)$ in terms of the feasibility constraints are

$$\chi(d) = \max_{\theta \in \Theta} \min_z \max_{m \in M} f_m(d, z, \theta) \quad (7a)$$

and

$$\chi(d) = \max_{\theta \in \Theta} \min_{z, \beta} \beta \quad (7b)$$

subject to

$$f_m(d, z, \theta) \leq \beta \quad (m \in M)$$

If $\chi(d) > 0$, then at least one of the feasibility constraints is violated somewhere in the uncertainty range.

In terms of the actual HEN feasibility constraints (including the equality constraints), problem (7b) can be expressed more explicitly as (Saboo *et al.*, 1985a)

$$\chi(d) = \max_{\theta} \min_{u, v, \beta} \beta \quad (8)$$

subject to:

(A1) Energy balances on all exchangers, heaters, and stream splits:

$$A(u, w)t^S + B(u, v, w)v = b$$

(A2) Specified energy recovery:

$$\sum_k l_k^H = \alpha H(t^S, w)$$

(B1) ΔT_m constraints on all exchangers:

$$C(u, w)t^S + D(u, v, w)v + p \leq \beta e$$

(B2) Nonnegative exchanger and cooler loads:

$$E(u, w)t^S + Gv + r \leq \beta e$$

(B3) Nonnegative heater loads:

$$-t^H \leq \beta e$$

(B4) Uncertainty range:

$$\theta^L \leq \theta \leq \theta^U$$

where θ includes the uncertain supply temperature t^S and flow rates w and the control variables z are the degrees of freedom available in the intermediate stream temperatures and heater loads v and stream split fractions u .

The solution θ^C of max-min problem (8) defines a critical point for feasible operation—it is the point where uncertainty range Θ is closest to feasible region R if $\chi(d) \leq 0$ (Fig. 3a), or it is the point where maximum constraint violations occur if $\chi(d) > 0$ (Fig. 3b). In qualitative terms, the critical points in the resilience test are the worst case conditions for feasible operation.

In general, θ^C need not be a vertex of the uncertainty range (e.g., for some nonconvex feasible regions R). An algorithm for finding nonvertex critical points (active constraint strategy; Grossmann and Floudas, 1987) is described later. Swaney and Grossmann (1985a) establish sufficient conditions when the critical point must be a vertex of the uncertainty range. Of course, these conditions include the case when all the feasibility constraints (including the equality constraints) are linear. Section III,B discusses the conditions when the HEN feasibility constraints are linear.

When the critical point must be a vertex of the uncertainty range, the HEN is resilient ($\chi \leq 0$) if and only if it is feasible ($\psi \leq 0$) at every vertex. In mathematical terms, semiinfinite problem (6) reduces to a finite optimization problem

$$\chi(d) = \max_{l \in L_v} \psi(d, \theta^l) \quad (9)$$

where $\psi(d, \theta^l)$ is the value of the feasibility measure at corner point θ^l [obtained by solving problem (4) or (5)], L_v is the index set for the 2^{n_u} vertices, and n_u is the number of uncertain variables. The disadvantage of this approach is the large number of (N)LPs which must be solved (2^{n_u})

even if the number of uncertain variables is reasonably small. Swaney and Grossmann (1985b) and Grossmann and Floudas (1985, 1987) have developed algorithms (including the active constraint strategy for linear problems) which avoid the need to solve an (N)LP for every vertex.

Example 3 (adapted from Grossmann and Floudas, 1987). The HEN in Fig. 4 was designed for the heat capacity flow rates, target temperatures, and nominal stream supply temperatures shown. This HEN is to be tested for resilience in an uncertainty range of ± 10 K in all stream supply temperatures.

It can be shown that the resilience test for this HEN is linear (see Section III,B,1). Therefore the HEN is resilient if and only if it is feasible at every vertex of the specified uncertainty range.

The following linear program (LP) can be formulated to check HEN feasibility at specified values of the supply temperatures:

$$\psi = \min \beta$$

subject to the following energy balances,

$$HX\ 1: \quad 1.5(T_1^S - T_5) = 2(T_7 - T_3^S)$$

$$HX\ 2: \quad 1(T_2^S - T_6) = 2(563 - T_7)$$

$$HX\ 3: \quad 1(T_6 - T_2^T) = 3(393 - T_4^S)$$

load constraints,

$$HX\ 1: \quad T_2^S - T_7 \leq \beta$$

$$HX\ 2: \quad T_7 - 563 \leq \beta$$

$$HX\ 3: \quad T_4^S - 393 \leq \beta$$

$$C: \quad 350 - T_5 \leq \beta$$

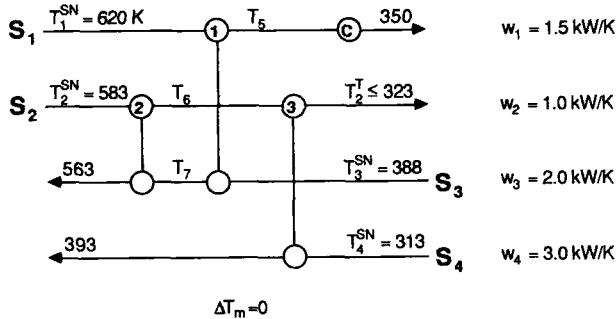


FIG. 4. HEN structure for Examples 3, 4, and 5.

ΔT_m constraints,

$$HX\ 1: \quad T_3^S - T_5 \leq \beta$$

$$HX\ 2: \quad T_7 - T_6 \leq \beta$$

$$HX\ 3: \quad T_4^S - T_2^T \leq \beta$$

and target temperature specification

$$T_2^T \leq 323$$

The energy recovery constraint reduces to $0 = 0$ since there are no heaters.

Application of this LP at each vertex of the uncertainty range yields the results shown in Table I. The HEN is not resilient since it is infeasible at several vertices. In particular, there are four critical vertices where $\psi_{\max} = 10.0$. At all four of these critical vertices, HEN feasibility is limited by ΔT_m violations in exchanger 2.

3. Flexibility Index

The resilience (flexibility) test is a yes–no test whether or not a HEN is resilient (flexible) in an expected uncertainty range. A more general

TABLE I
RESILIENCE TEST FOR EXAMPLE 3

Vertex				ψ	Active constraints		T_2^T (K)
δT_1^S (K)	δT_2^S (K)	δT_3^S (K)	δT_4^S (K)				
-10	-10	-10	-10	8.8	$HX\ 1\ \Delta T_m$	$HX\ 3\ \Delta T_m$	294.2
			+10 ^a	10.0	$HX\ 2\ \Delta T_m$	$T_2^T = 323$	323
		+10	-10	4.8	$HX\ 1\ \Delta T_m$	$HX\ 3\ \Delta T_m$	298.2
			+10 ^a	10.0	$HX\ 2\ \Delta T_m$	$T_2^T = 323$	323
	+10	-10	-10	0.8	$HX\ 1\ \Delta T_m$	$HX\ 3\ \Delta T_m$	302.2
			+10	0	$HX\ 2\ \Delta T_m$	$T_2^T = 323$	323
		+10	-10	-3.2	$HX\ 1\ \Delta T_m$	$HX\ 3\ \Delta T_m$	303
			+10	0	$HX\ 2\ \Delta T_m$	$T_2^T = 323$	323
		-10	-10	0	$HX\ 2\ \text{load}$	$HX\ 3\ \Delta T_m$	303
			+10 ^a	10.0	$HX\ 2\ \Delta T_m$	$T_2^T = 323$	323
+10	-10	-10	-10	0	$HX\ 2\ \text{load}$	$HX\ 3\ \Delta T_m$	303
			+10 ^a	10.0	$HX\ 2\ \Delta T_m$	$T_2^T = 323$	323
		+10	-10	0	$HX\ 2\ \text{load}$	$HX\ 3\ \Delta T_m$	303
			+10 ^a	10.0	$HX\ 2\ \Delta T_m$	$T_2^T = 323$	323
	+10	-10	-10	-6.7	$HX\ 2\ \text{load}$	$HX\ 3\ \Delta T_m$	303
			+10	0	$HX\ 3\ \Delta T_m$	$T_2^T = 323$	323
		+10	-10	-6.7	$HX\ 2\ \text{load}$	$HX\ 3\ \Delta T_m$	303
			+10	0	$HX\ 3\ \Delta T_m$	$T_2^T = 323$	323

^a Critical corner points.

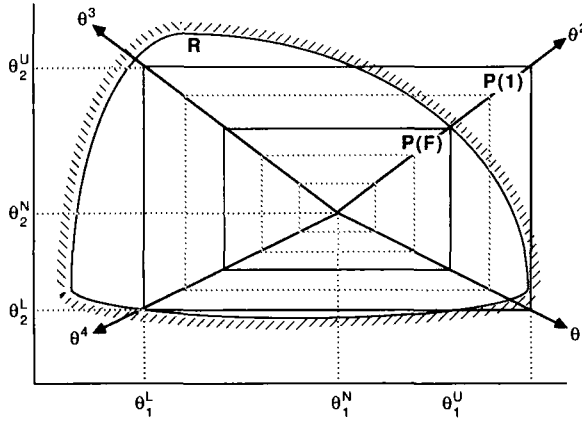


FIG. 5. Flexibility index F defines largest scaled hyperrectangle $\Theta(F)$ for which HEN is resilient.

approach is to measure the size of feasible region R with a numerical flexibility index.

The flexibility index can be defined by considering how much larger (or smaller) the expected uncertainty range Θ must be scaled so that it exactly fits inside feasible region R (Fig. 5). The family of scaled hyperrectangles $\Theta(s)$ can be parameterized by scale factor s as

$$\Theta(s) = \{\theta \mid (\theta^N - s \Delta\theta^-) \leq \theta \leq (\theta^N + s \Delta\theta^+)\}$$

where

$$\Delta\theta^+ = \theta^U - \theta^N \quad \text{and} \quad \Delta\theta^- = \theta^N - \theta^L$$

and $\Theta(1)$ represents the expected uncertainty range. Then flexibility index F is defined as the value of scale factor s for which the hyperrectangle $\Theta(s)$ exactly fits inside feasible region R [i.e., $\Theta(F)$ is the largest scaled hyperrectangle which can be inscribed in the feasible region (Swaney and Grossmann, 1985a)].

A HEN is resilient in an expected uncertainty range $\Theta(1)$ if and only if $F \geq 1$. This is the same information which the resilience (flexibility) test gives. But the flexibility index tells us even more. For instance if $F = 0.5$, we know that the HEN is not resilient in the specified uncertainty range; in addition, we know that the HEN can tolerate uncertainties only half as large as those expected.

Whether a HEN is resilient in a specified uncertainty range is independent of the choice of nominal values θ^N of the uncertain variables in that range. However, the actual value of the flexibility index F does depend on the choice of θ^N .

The problem of calculating the flexibility index can be mathematically formulated as

$$F(d) = \max_s s \quad \text{subject to} \quad \Theta(s) \subset R \quad (10)$$

In terms of resilience measure χ , this problem is equivalent to (Swaney and Grossmann, 1985a)

$$F(d) = \max_s s \quad \text{subject to} \quad \chi(d, s) \leq 0 \quad (11)$$

Using the definition of χ given by Eq. (7a), a formulation in terms of the feasibility constraints is

$$F(d) = \max_s s \quad \text{subject to} \quad \max_{\theta \in \Theta(s)} \min_z \max_{m \in M} f_m(d, z, \theta) \leq 0 \quad (12)$$

and

$$\Theta(s) = \{\theta \mid (\theta^N - s \Delta \theta^-) \leq \theta \leq (\theta^N + s \Delta \theta^+)\}$$

The solution θ^C of problem (12) defines the critical point where the scaled hyperrectangle $\Theta(F)$ meets the boundary of feasible region R (Fig. 5). Note that at the critical point, $\psi(d, \theta) = 0$. In general, θ^C need not correspond to a vertex of the hyperrectangle (e.g., for some nonconvex feasible regions R). An algorithm for finding nonvertex critical points (active constraint strategy; Grossmann and Floudas, 1985a) is described later in this chapter. Swaney and Grossmann (1987) establish sufficient conditions when the critical point must be a vertex of the hyperrectangle. Of course, these conditions include the case when all the feasibility constraints (including the equality constraints) are linear (Section III,B).

When the critical point must be a vertex of the hyperrectangle $\Theta(F)$, the simplest approach to calculating the flexibility index F is to maximize s in each vertex direction θ^l (Fig. 5) by the following (N)LP (Swaney and Grossmann, 1985a):

$$s^{l*}(\theta^l) = \max_{z, s^l} s^l \quad (13)$$

subject to

$$f_m(d, z, \theta) \leq 0 \quad (m \in M), \quad \theta = \theta^N + s^l \theta^l$$

Then the flexibility index is the smallest one of these:

$$F = \min_{l \in L_v} s^{l*} \quad (14)$$

The disadvantage of this approach is the large number of (N)LPs which must be solved (2^{n_u}) even if the number of uncertain variables is

reasonably small. Swaney and Grossmann (1985b) and Grossmann and Floudas (1985, 1987) have developed algorithms (including the active constraint strategy for linear problems) which avoid the need to solve an (N)LP for every vertex direction.

In terms of the actual HEN feasibility constraints (including the equality constraints), (N)LP (13) can be expressed more explicitly as

$$s^{I*}(\theta^I) = \max_{u,v,s} s^I \quad (15)$$

subject to:

(A1) Energy balances on all exchangers, heaters, and stream splits:

$$A(u, w)t^S + B(u, v, w)v = b$$

(A2) Specified energy recovery:

$$\sum_k l_k^H = \alpha H(t^S, w)$$

(B1) ΔT_m constraints on all exchangers:

$$C(u, w)t^S + D(u, v, w)v + p \leq 0$$

(B2) Nonnegative exchanger and cooler loads:

$$E(u, w)t^S + Gv + r \leq 0$$

(B3) Nonnegative heater loads:

$$-l^H \leq 0$$

(B4) Uncertainty directions:

$$\theta = \theta^N + s^I \theta^I$$

where

$$\theta^1 = \begin{bmatrix} \theta_1^L \\ \theta_2^L \\ \vdots \\ \theta_{n_u-1}^L \\ \theta_{n_u}^L \end{bmatrix} - \theta^N, \quad \theta^2 = \begin{bmatrix} \theta_1^L \\ \theta_2^L \\ \vdots \\ \theta_{n_u-1}^L \\ \theta_{n_u}^U \end{bmatrix} - \theta^N, \quad \dots, \quad \theta^{2^{n_u}} = \begin{bmatrix} \theta_1^U \\ \theta_2^U \\ \vdots \\ \theta_{n_u-1}^U \\ \theta_{n_u}^U \end{bmatrix} - \theta^N$$

and θ includes the uncertain supply temperatures t^S and flow rates w .

Example 4 (from Grossmann and Floudas, 1987). The flexibility index of the HEN structure in Fig. 4 is to be calculated with respect to an expected uncertainty range of + 10 K in all stream supply temperatures.

The supply temperatures shown in Fig. 4 are the assumed nominal values.

The following LP can be formulated to maximize the scale factor s^l in each vertex direction:

$$S^{l*} = \max s^l$$

subject to the following energy balances,

$$HX\ 1: \quad 1.5(T_1^S - T_5) = 2(T_7 - T_3^S)$$

$$HX\ 2: \quad 1(T_2^S - T_6) = 2(563 - T_7)$$

$$HX\ 3: \quad 1(T_6 - T_2^T) = 3(393 - T_4^S)$$

load constraints,

$$HX\ 1: \quad T_3^S - T_7 \leq 0$$

$$HX\ 2: \quad T_7 - 563 \leq 0$$

$$HX\ 3: \quad T_4^S - 393 \leq 0$$

$$C: \quad 350 - T_5 \leq 0$$

ΔT_m constraints,

$$HX\ 1: \quad T_3^S - T_5 \leq 0$$

$$HX\ 2: \quad T_7 - T_6 \leq 0$$

$$HX\ 3: \quad T_4^S - T_2^T \leq 0$$

target temperature specification,

$$T_2^T \leq 323$$

and vertex directions

$$\begin{bmatrix} T_1^S \\ T_2^S \\ T_3^S \\ T_4^S \end{bmatrix} = \begin{bmatrix} 620 \\ 583 \\ 388 \\ 313 \end{bmatrix} + s^l \theta^l, \quad s^l \geq 0$$

where

$$\theta^1 = \begin{bmatrix} -10 \\ -10 \\ -10 \\ -10 \end{bmatrix}, \quad \theta^2 = \begin{bmatrix} -10 \\ -10 \\ -10 \\ +10 \end{bmatrix}, \quad \dots, \quad \theta^{16} = \begin{bmatrix} +10 \\ +10 \\ +10 \\ +10 \end{bmatrix}$$

for the directions to the 16 vertices of the expected uncertainty range. Note

that the energy recovery constraint reduces to $0 = 0$ since there are no heaters.

Solution of the 16 LPs yields the results in Table II. The flexibility index is 0.5; thus the HEN can only tolerate uncertainties of ± 5 K in each stream supply temperature instead of the ± 10 K expected. In particular, there are four critical vertices ($s_{\min}^* = 0.5$). At all four of these critical vertices, HEN flexibility is limited by ΔT_m violations in exchanger 2.

4. Resilience Index

A primary disadvantage of the flexibility index is the need to solve 2^N (N)LPs corresponding to the vertex directions when the critical point must be a vertex of the hyperrectangle $\Theta(F)$. To decrease the required computational effort, Saboo *et al.* (1985) define a different index, the resilience index (RI), to measure the size of feasible region R .

The RI is defined as the largest *total* uncertainty which the HEN can tolerate while remaining feasible:

$$RI = \max_{\theta \in R} \min_z \sum_i |\theta_i - \theta_i^N| \quad (16)$$

TABLE II
FLEXIBILITY INDEX FOR EXAMPLE 4

Vertex direction				s^{I*}	Active constraints		T_2^T (K)
δT_1^S (K)	δT_2^S (K)	δT_3^S (K)	δT_4^S (K)				
-10	-10	-10	-10	0.56	HX 1 ΔT_m	HX 3 ΔT_m	307.4
			+10 ^a	0.5	HX 2 ΔT_m	$T_2^T = 323$	323
		+10	-10	0.7	HX 1 ΔT_m	HX 3 ΔT_m	306
			+10 ^a	0.5	HX 2 ΔT_m	$T_2^T = 323$	323
	+10	-10	-10	0.933	HX 1 ΔT_m	HX 3 ΔT_m	303.67
			+10	1.0	HX 2 ΔT_m	$T_2^T = 323$	323
		+10	-10	1.4	HX 1 ΔT_m	HX 3 ΔT_m	299
			+10	1.0	HX 2 ΔT_m	$T_2^T = 323$	323
		-10	-10	1.0	HX 2 load	HX 3 ΔT_m	303
			+10 ^a	0.5	HX 2 ΔT_m	$T_2^T = 323$	323
+10	-10	+10	-10	1.0	HX 2 load	HX 3 ΔT_m	303
			+10 ^a	0.5	HX 2 ΔT_m	$T_2^T = 323$	323
		-10	-10	3.0	HX 2 load	HX 3 ΔT_m	283
			+10	1.0	HX 2 ΔT_m	$T_2^T = 323$	323
	+10	-10	-10	3.0	HX 2 load	HX 3 ΔT_m	283
			+10	1.0	HX 2 ΔT_m	$T_2^T = 323$	323
		+10	-10	3.0	HX 2 load	HX 3 ΔT_m	283
			+10	1.0	HX 2 ΔT_m	$T_2^T = 323$	323

^a Critical corner points.

subject to

$$f_m(d, z, \theta) \leq 0 \quad (m \in M)$$

Geometrically, the RI defines the largest polytope P which can be inscribed in feasible region R . For example, in Fig. 6 any pair of lines drawn from the origin θ^N in the coordinate directions θ_1 and θ_2 to the edge of the polytope will have the same total length

$$RI = |\theta_1 - \theta_1^N| + |\theta_2 - \theta_2^N|$$

The solution θ^C of max-min problem (16) is the critical point which limits the RI; that is, it is the point where the largest inscribed polytope meets the feasible region R . In general, θ^C need not correspond to a vertex of the polytope (e.g., for some nonconvex feasible regions R). However, to date no general algorithm has been developed to find nonvertex critical points which limit the RI.

A sufficient condition that the RI be determined by a vertex critical point is that the feasible region R be convex. (Of course, a special case of this is when all the feasibility constraints are linear; see Section III,B.) Unfortunately, when flow rates or heat transfer coefficients are included in the uncertainty range, the feasible region can be nonconvex (see Examples 1 and 2 and Section III,C,3). Thus, current algorithms for calculating the RI are limited to temperature uncertainties only.

When the feasible region R is convex, the RI is also the largest *individual* uncertainty which the HEN can tolerate while remaining feasible (in addition to being the largest *total* uncertainty). Thus the simplest algorithm for calculating the RI is to maximize the individual uncertainties which the

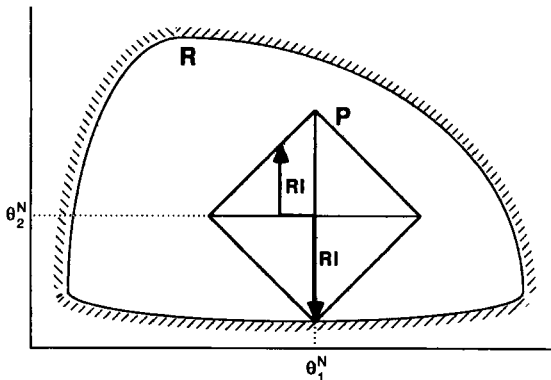


FIG. 6. Resilience index (RI) defines largest polytope P for which HEN is resilient.

HEN can tolerate in each of two directions (Saboo *et al.*, 1985):

$$\delta\theta_{l,\max}^+ = \max_z(\theta_l - \theta_l^N) \quad (17a)$$

subject to

$$f_m(d, z, \theta) \leq 0 \quad (m \in M), \quad \theta_l \geq \theta_l^N$$

and

$$\delta\theta_{l,\max}^- = \max_z(\theta_l^N - \theta_l) \quad (17b)$$

subject to

$$f_m(d, z, \theta) \leq 0 \quad (m \in M), \quad \theta_l \leq \theta_l^N$$

where θ consists of temperature uncertainties only. Then the RI is the smallest one of these maximum individual uncertainties:

$$RI = \min_l \{\delta\theta_{l,\max}^+, \delta\theta_{l,\max}^-\} \quad (18)$$

For convex feasible regions, the primary advantage of the resilience index should now be apparent: Only $2n_u$ (N)LPs need to be solved to determine the RI (since a polytope has only $2n_u$ vertices), while 2^{n_u} (N)LPs originally needed to be solved to determine the flexibility index (since a hyperrectangle has 2^{n_u} vertices). However, algorithms developed by Swaney and Grossmann (1985b) and Grossmann and Floudas (1985, 1987) dramatically decrease the number of (N)LPs which must be solved to determine the flexibility index and reduce the advantage of using the resilience index instead of the flexibility index. For nonconvex feasible regions, the active constraint strategy algorithm of Grossmann and Floudas (1987) can locate nonvertex critical points of the flexibility index, while no general algorithm is currently available to locate nonvertex critical points for the RI.

The RI can be scaled in terms of maximum expected uncertainties like the flexibility index. Then the RI would be an upper bound on the flexibility index, since the RI only considers uncertainties in each stream *individually*, while the flexibility index considers uncertainties in all streams *simultaneously*. However, for HENs it seems reasonable to assume that the uncertainty in each stream's supply temperature is roughly inversely proportional to that stream's heat capacity flow rate (i.e., that each stream is subject to roughly the same "load uncertainty"). Thus the RI is calculated in terms of load uncertainty δl_i^+ or δl_i^- , where

$$\delta l_i^+ = w_i(\delta\theta_i^+) = w_i(\delta T_i^{S+}), \quad \delta l_i^- = w_i(\delta\theta_i^-) = w_i(\delta T_i^{S-})$$

and w_i is the heat capacity flow rate of stream i and δT_i^{S+} (δT_i^{S-}) is the

positive (negative) uncertainty in the supply temperature of stream S_i relative to its nominal value.

Now in terms of the actual HEN feasibility constraints (including the equality constraints), (N)LPs (17) can be expressed more explicitly as (Saboo *et al.*, 1985)

$$\delta l_{i,\max}^+ = \max_{u, v, \delta l_i^+} \delta l_i^+ \quad (19)$$

subject to:

(A1) Energy balances on all exchangers, heaters, and stream splits:

$$A(u, w)t^S + B(u, v, w)v = b$$

(A2) Energy recovery specification:

$$\sum_k l_k^H = \alpha H(t^S, w)$$

(B1) ΔT_m constraints on all exchangers:

$$C(u, w)t^S + D(u, v, w)v + p \leq 0$$

(B2) Nonnegative exchanger and cooler loads:

$$E(u, w)t^S + Gv + r \leq 0$$

(B3) Nonnegative loads in all heaters:

$$-l^H \leq 0$$

(B4) Uncertainty directions:

$$t^S = t^{SN} + \begin{bmatrix} 1/w_1 & & \\ & \ddots & \\ & & 1/w_{n_s} \end{bmatrix} \delta l^{i+}$$

where

$$\delta l^{i+} = \begin{bmatrix} 0 \\ \vdots \\ 0 \\ \delta l_i^+ \\ 0 \\ \vdots \\ 0 \end{bmatrix}$$

and n_s is the number of streams. Similar (N)LPs are written for $\delta l_{i,\max}^-$.

Then

$$RI = \min_i \{\delta l_{i,\max}^+, \delta l_{i,\max}^-\} \quad (20)$$

Example 5 (adapted from Grossmann and Floudas, 1987). The resilience index is to be calculated for the HEN shown in Fig. 4. The following series of LPs is formulated to determine the maximum load uncertainty allowed in a positive direction on each stream:

$$\delta l_{i,\max}^+ = \max \delta l_i^+$$

subject to the same energy balance, ΔT_m , load, and target temperature constraints as in Example 4 and uncertainty directions for the four positive

$$\begin{bmatrix} T_1^S \\ T_2^S \\ T_3^S \\ T_4^S \end{bmatrix} = \begin{bmatrix} 620 \\ 583 \\ 388 \\ 313 \end{bmatrix} + \begin{bmatrix} 1/1.5 & 0 & 0 & 0 \\ 0 & 1/1.0 & 0 & 0 \\ 0 & 0 & 1/2.0 & 0 \\ 0 & 0 & 0 & 1/3.0 \end{bmatrix} \delta l^{i+}$$

where

$$\delta l^{1+} = \begin{bmatrix} \delta l_1^+ \\ 0 \\ 0 \\ 0 \end{bmatrix}, \quad \dots, \quad \delta l^{4+} = \begin{bmatrix} 0 \\ 0 \\ 0 \\ \delta l_4^+ \end{bmatrix}$$

uncertainty directions along the four streams. Similar LPs are also written for the four negative uncertainty directions. Note that the energy recovery constraint reduces to $0 = 0$ since there are no heaters.

Solution of the eight LPs gives the results in Table III. The RI is 19 kW and is limited by ΔT_m in exchangers 1 and 2 for a positive uncertainty in the supply temperature of stream 2.

In order to compare the resilience index with the flexibility index, suppose that the RI is scaled in terms of temperature rather than load. Then the temperature RI is 6.67 K (Table III), limited by positive uncertainty in the supply temperature of stream 4. (Note that the limiting uncertainty direction changes when the RI is rescaled from load to temperature.) This means that the HEN can tolerate uncertainty of 6.67 K in *any* individual stream supply temperature in either a positive or negative direction. Because of linearity and convexity, it also means that the HEN can tolerate a *total* temperature uncertainty $\sum_i |T_i^S - T_i^{SN}|$ of 6.67 K, no matter how the uncertainty is distributed among the streams. Note that this does not mean that the HEN can tolerate uncertainties of 6.67 K in all

TABLE III
RESILIENCE INDEX FOR EXAMPLE 5

Uncertainty direction	$\delta T^{+/-}$ (K)	$\delta I^{+/-}$ (kW)	Active constraints		T_2^T (K)
I_1^-	18.67	28	$HX\ 1\ \Delta T_m$	$HX\ 3\ \Delta T_m$	313
I_1^+	∞	∞			
I_2^-	19	19 ^a	$HX\ 1\ \Delta T_m$	$HX\ 2\ \Delta T_m$	322
I_2^+	330	330	$HX\ 1\ \text{load}$	$T_2^T = 323$	323
I_3^-	42.5	85	$C\ \text{load}$	$HX\ 3\ \Delta T_m$	313
I_3^+	165	330	$HX\ 1\ \text{load}$	$T_2^T = 323$	323
I_4^-	14	42	$HX\ 1\ \Delta T_m$	$HX\ 3\ \Delta T_m$	299
I_4^+	6.67 ^b	20	$HX\ 2\ \Delta T_m$	$T_2^T = 323$	323

^a Critical point for load RI.

^b Critical point for temperature RI

four streams *simultaneously*. In fact, the flexibility index (Example 4) tells us that the HEN can only handle uncertainties of ± 5 K in all four streams simultaneously.

B. LINEAR RESILIENCE ANALYSIS

Because of the ability of linear programs to guarantee a global optimum and because of the relative ease of solving LPs (as compared to NLPs), we wish to exploit the cases when HEN resilience analysis is linear. This section establishes sufficient conditions for linear HEN resilience analysis.

A type of problem called class 2 is not amenable to straightforward linear analysis. In this type of problem, the form of the energy recovery constraint changes when the stream population at the pinch changes somewhere in the uncertainty range. This section defines and describes the differences between class 1 and class 2 problems.

1. Sufficient Conditions for Linear Resilience Analysis

Saboo and Morari (1984) have determined the following sufficient conditions when analysis of HEN resilience is linear:

Theorem 1 (Corner Point Theorem). Assume the following: (1) constant heat capacities and no phase change, (2) supply and target temperature uncertainties only (no uncertainties in flow rates or heat transfer coefficients), (3) constant stream split fractions (Saboo *et al.*, 1987b), and

(4) “small” uncertainty range (“class 1” problem defined subsequently). If these assumptions are satisfied, then the HEN resilience analysis problem is linear. [In particular, matrices A , B , C , D , and E are constant in the feasibility test (5), resilience test (8), flexibility index problem (15), and resilience index problem (19).]

As a consequence of linearity (convexity), a HEN is resilient in a specified uncertainty range if and only if it is feasible at every corner point (vertex) of the uncertainty range.

Saboo *et al.* (1985) have shown that under the assumptions of the corner point theorem, HEN resilience analysis problems with specified exchanger areas (rather than specified ΔT_m) are also linear.

2. Definition of Class 1 and Class 2 Problems

The assumptions of the corner point theorem are rather restrictive. They are also straightforward except for the meaning of “small” uncertainty range (“class 1” problem).

In HEN synthesis, the pinch occurs at a stream supply, dew point, or bubble point (Saboo and Morari, 1984). A HEN resilience analysis problem is class 1 if the uncertainties are small enough that the stream population at the pinch is constant throughout the uncertainty range. If the uncertainties are too large, then the stream population at the pinch changes and the problem is class 2.

As an example, consider the stream data in Fig. 7, where the only uncertain variable is the supply temperature T_{h2}^S of stream S_{h2} . For an uncertainty range $470 \leq T_{h2}^S \leq 480$ K, the pinch is always caused by the supply of stream S_{h2} (Fig. 7a). Therefore this uncertainty range is class 1. However, if the uncertainty range is expanded to $460 \leq T_{h2}^S \leq 480$ K, then stream S_{h1} causes the pinch for $T_{h2}^S < 470$ (Fig. 7b), while stream S_{h2} still causes the pinch for $T_{h2}^S > 470$ (Fig. 7a). Thus for this larger uncertainty range, the stream population at the pinch changes, and the problem is class 2.

Special cases of class 2 resilience analysis problems include when the problem changes from pinched to unpinched (threshold) or when the problem changes from unpinched heating to unpinched cooling (or vice versa).

Saboo and Morari (1984) give the general test to determine whether a problem is class 1 or class 2. In their test the uncertainty range can include supply temperatures, target temperatures, and flow rates. (It would not matter whether the uncertainty range included heat transfer coefficients.) In this chapter, we restrict their test to problems with constant or piecewise constant heat capacities.

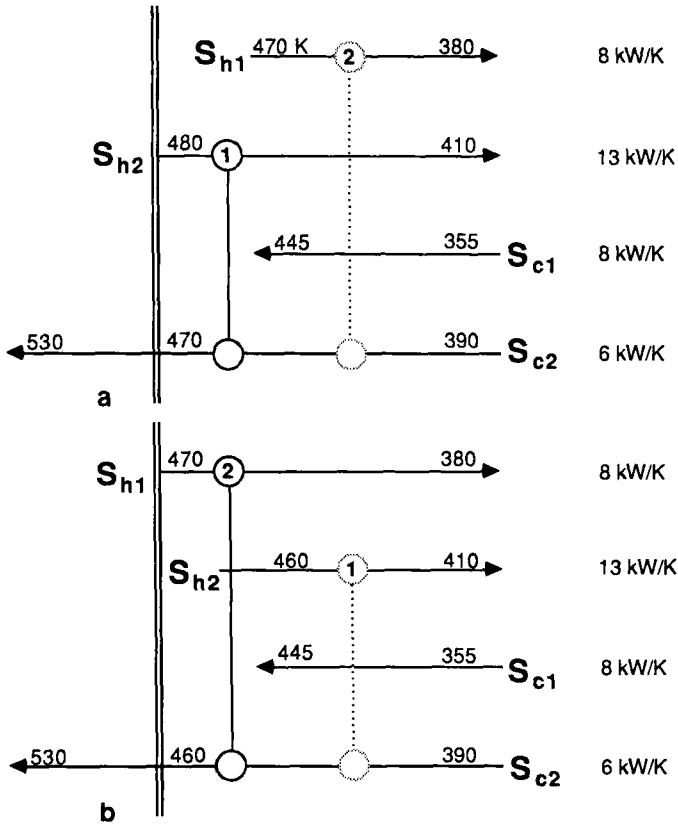


FIG. 7. Class 2 problem—stream population at pinch changes when T_{h2}^S changes: (a) $T_{h2}^S = 480$ K, (b) $T_{h2}^S = 460$ K.

Theorem 2. Let case B be the point in the uncertainty range which maximizes the HEN's cooling requirement and case C be the point which maximizes the HEN's heating requirement. (See Table IV for the supply temperatures, target temperatures, and flow rates corresponding to these two cases.) Then

a. For any point in the uncertainty range, the pinch temperature T_p is between the pinch temperatures for cases B and C:

$$T_p^C \leq T_p \leq T_p^B$$

where hot and cold stream temperatures T are shifted to account for partial contributions to ΔT_m (as in Linnhoff and Flower, 1978).

TABLE IV

SUPPLY TEMPERATURES, TARGET TEMPERATURES, AND FLOW RATES CORRESPONDING TO MAXIMUM HEATING AND MAXIMUM COOLING (WHEN ALL STREAMS HAVE CONSTANT HEAT CAPACITY AND NO PHASE CHANGE)

Case	Supply temperatures	Target temperatures	Hot stream flow rates	Cold stream flow rates
Case B (maximum cooling)	Highest	Lowest	Highest	Lowest
Case C (maximum heating)	lowest	highest	lowest	highest

b. The problem is class 1 if (i) the pinch is determined by the supply temperature, dew point, or bubble point of the same stream in both case B and case C (target temperatures cannot cause the pinch) and (ii) for any point in the uncertainty range, no stream supply temperature, target temperature², dew point, or bubble point is contained in the open temperature interval (T_p^C, T_p^B) , except for the stream supply, dew point, or bubble point temperature associated with the pinch. Otherwise the problem is class 2.

Class 2 problems cause difficulties in HEN resilience analysis because the form of the energy recovery constraint changes as the stream population at the pinch changes. The energy recovery constraint is an energy balance above the pinch limiting the heating used by the network to be less than or equal to the heating required above the pinch (multiplied by some relaxation factor). When the form of the energy recovery constraint changes, the reduced form of the ΔT_m and load constraints also changes. The following example illustrates how the form of the energy recovery, ΔT_m , and loan constraints changes and how this can create nonconvex feasible regions for class 2 problems.

Example 6 (adapted from Saboo et al., 1985). Consider the HEN in Fig. 8. Its resilience is to be tested in the uncertainty range

$$340 \leq T_{h2}^S \leq 380 \text{ K}, \quad 270 \leq T_{c2}^S \leq 300 \text{ K}$$

Performing a case B–case C analysis for these stream data, we find that for case B ($T_{h2}^S = 380 \text{ K}$, $T_{c2}^S = 300 \text{ K}$) 140 kW of cooling and no heating are required and that for case C ($T_{h2}^S = 340 \text{ K}$, $T_{c2}^S = 270 \text{ K}$) 260 kW of heating and no cooling are required. Therefore this problem changes from unpinched cooling to unpinched heating and is class 2.

² Saboo and Morari (1984) forgot to include target temperatures in their statement of this theorem. It can be shown by counterexample that target temperatures must be included.

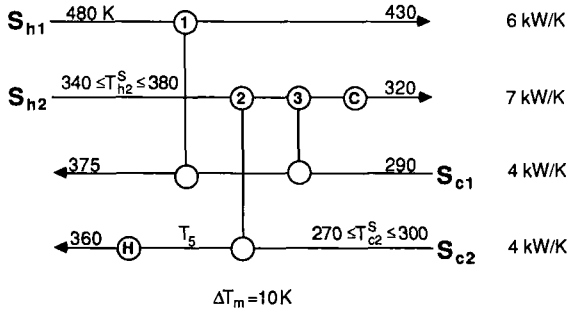


FIG. 8. HEN structure for Examples 6 and 12.

For the case when heating (and no cooling) is required, the energy recovery constraint is the net heating required by the network:

$$\ell^H = 4(375 - 290) + 4(360 - T_{h2}^S) - 6(480 - 430) - 7(T_{h2}^S - 320) \quad (a)$$

This constraint, along with the energy balances for the exchangers and heater, when substituted into the ΔT_m and load constraints for exchanger 2, yields

$$10 \leq T_{h2}^S - T_5 = 570 - 0.75T_{h2}^S - T_{c2}^S \quad (b)$$

$$0 \leq T_5 - T_{c2}^S = 1.75T_{h2}^S - 570 \quad (c)$$

The feasible region defined by constraints (a)–(c) is the convex region *below* the dashed line in Fig. 9. All other feasibility constraints for the HEN (for the heating only case) lie outside this region.

For the case when cooling (and no heating) is required, the energy recovery constraint reduces to $\ell^H = 0$. The ΔT_m and load constraints for exchanger 2 become

$$10 \leq T_{h2}^S - T_5 = T_{h2}^S - 360 \quad (d)$$

$$0 \leq T_5 - T_{c2}^S = 360 - T_{c2}^S \quad (e)$$

and the load constraint on the cooler becomes

$$0 \leq I^C = 6(480 - 430) + 7(T_{h2}^S - 360) - 4(375 - 290) - 4(360 - T_{c2}^S) \quad (f)$$

The feasible region defined by constraints (d)–(f) is the convex region *above* the dashed line in Fig. 9. Note that the form of the constraints, and thus the shape of the feasible region, changes between the heating only and cooling only cases.

Now consider the case when the network is allowed to use both heating

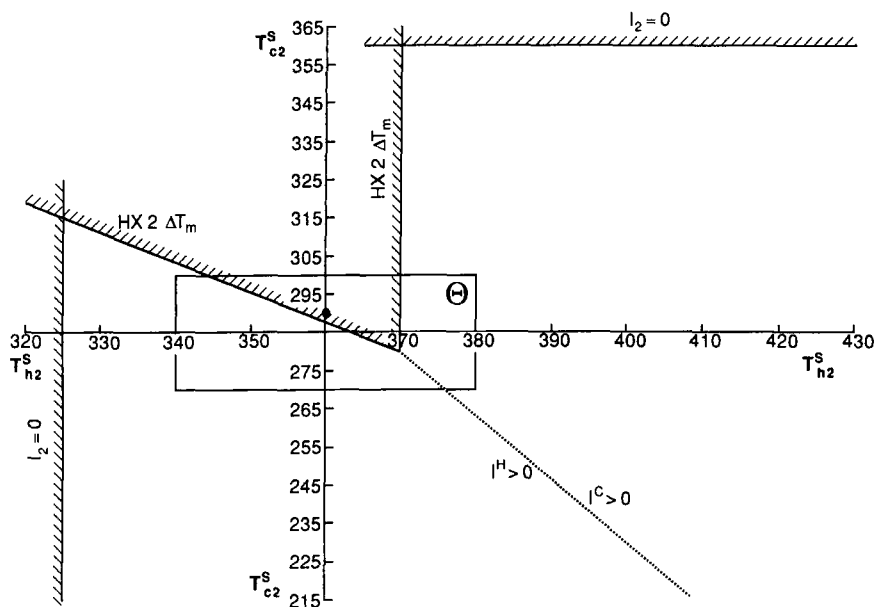


FIG. 9. Nonconvex feasible region for a class 2 problem (Examples 6 and 12).

and cooling. The feasible region for this case is the union of the feasible regions for the heating-only and cooling-only cases. (The dashed line in Fig. 9 is no longer a constraint; it is simply the boundary where the network switches from heating to cooling.) This new feasible region is nonconvex. In particular, the HEN is not feasible for the intermediate case ($T_{h2}^s = 360$ K, $T_{c2}^s = 295$ K), while it is feasible for all four corner points of the specified uncertainty range.

C. NONLINEAR RESILIENCE ANALYSIS

Heat exchanger network resilience analysis can become nonlinear and nonconvex in the cases of phase change and temperature-dependent heat capacities, varying stream split fractions, or uncertain flow rates or heat transfer coefficients. This section presents resilience tests developed by Saboo *et al.* (1987a,b) for (1) minimum unit HENs with piecewise constant heat capacities (but no stream splits or flow rate uncertainties), (2) minimum unit HENs with stream splits (but constant heat capacities and no flow rate uncertainties), and (3) minimum unit HENs with flow rate and temperature uncertainties (but constant heat capacities and no stream splits).

The nonlinear resilience tests developed by Saboo *et al.* (1987a,b) are each for a rather specific case. A more general resilience analysis technique based on the active constraint strategy of Grossmann and Floudas (1985, 1987) is also presented. The active constraint strategy can be used to test the resilience of a HEN with minimum or more units, with or without stream splits or bypasses, and with temperature and/or flow rate uncertainties (Floudas and Grossmann, 1987b).

1. Resilience Analysis with Piecewise Constant Heat Capacities

Most chemical processing plants include pure or multicomponent streams which change phase or which have strongly temperature-dependent heat capacities. Under these conditions the minimum approach temperature in a network can occur *anywhere* inside an exchanger. Therefore integral or differential equations are generally required to locate ΔT_m .

To allow algebraic equations to be used to locate ΔT_m , assume that the heat capacities can be approximated by piecewise constant functions of temperature, with discontinuities at temperature breakpoints T_{BR} . Then for each exchanger, ΔT_m can occur only at either end or at a breakpoint location inside the exchanger. However, a remaining difficulty is that since the intermediate stream temperatures are not known before the resilience test, the breakpoint locations are also not known *a priori*.

To deal with this difficulty, the energy balance and ΔT_m constraints are formulated by assuming that *all* breakpoints occur in *every* exchanger. (The energy recovery and load constraints are unaffected by the presence of breakpoints.) Then slack and integer variables are defined to correct the energy balance and ΔT_m constraints for each exchanger in which any temperature breakpoint does not occur (Saboo *et al.*, 1987a).

a. *Energy Balance Constraints.* To demonstrate the energy balance constraint with piecewise constant heat capacities, consider the heat exchanger in Fig. 10, where it is assumed that the hot stream has one tem-

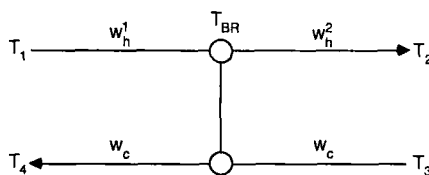


FIG. 10. Heat exchanger with temperature breakpoint in hot stream.

perature breakpoint,

$$w_h = \begin{cases} w_h^1, & T > T_{BR} \\ w_h^2, & T < T_{BR} \end{cases}$$

and that the cold stream has no breakpoint. The energy balance constraint is (Saboo *et al.*, 1987a)

$$w_c(T_4 - T_3) = w_h^1(T_1 - T_{BR}) + w_h^2(T_{BR} - T_2) + (w_h^1 - w_h^2) \eta_1 + (w_h^2 - w_h^1) \eta_3 \quad (21a)$$

Slack variables η are defined by

$$T_1 - T_{BR} + \eta_1 - \eta_2 = 0 \quad (21b)$$

$$T_{BR} - T_2 + \eta_3 - \eta_4 = 0 \quad (21c)$$

where integer variables m are used to allow only one of η_1 or η_2 (and only one of η_3 or η_4) to be nonzero:

$$\eta_1 \leq km_1 \quad (21d)$$

$$\eta_2 \leq k(1 - m_1) \quad (21e)$$

$$\eta_3 \leq km_2 \quad (21f)$$

$$\eta_4 \leq k(1 - m_2) \quad (21g)$$

$$\eta_1, \eta_2, \eta_3, \eta_4 \geq 0 \quad (21h)$$

$$m_1, m_2 = 0, 1 \quad (21i)$$

and k is an upper bound on the slack variables (e.g., the difference between the hottest and coldest temperatures in the network).

The energy balance without the slacks ($\eta_1 = \eta_3 = 0$) assumes that the temperature breakpoint occurs inside the exchanger. To demonstrate that the energy balance is correct when the breakpoint occurs outside, consider the case when the breakpoint is upstream of the exchanger ($T_{BR} > T_1 > T_2$). Then constraints (21b)–(21i) give

$$\eta_1 = T_{BR} - T_1, \quad \eta_2 = 0, \quad \eta_3 = 0,$$

$$\eta_4 = T_{BR} - T_2, \quad m_1 = 1, \quad m_2 = 0$$

and Eq. (21a) yields

$$w_c(T_4 - T_3) = w_h^2(T_1 - T_2)$$

which is the correct energy balance for the exchanger.

b. ΔT_m Constraints. If T_{BR} occurs inside the heat exchanger in Fig. 10, then ΔT_m can occur at either end or at the breakpoint inside the

exchanger. To set up the ΔT_m constraint at the breakpoint, an energy balance constraint [similar to Eq. (21a)] is first formulated to define temperature T_5 of the cold stream when the hot stream temperature is T_{BR} :

$$w_h^1(T_1 - T_{BR}) = w_c(T_4 - T_5) \quad (22)$$

Temperature T_5 has no physical meaning when the breakpoint occurs outside the exchanger. Then the ΔT_m constraint at the breakpoint is (Saboo *et al.*, 1987a)

$$T_{BR} - T_5 + K(m_1 + m_2) \geq \Delta T_m \quad (23)$$

where K is a sufficiently large positive constant. If the breakpoint occurs inside the exchanger, then both m_1 and m_2 are zero [from constraints (21b–21i)]. If the breakpoint occurs upstream ($m_1 = 1$) or downstream ($m_2 = 1$) of the exchanger, then the ΔT_m constraint at the breakpoint is not physically meaningful, and the term involving m_1 and m_2 forces the constraint to be satisfied.

The energy balance and ΔT_m constraints are easily extended to situations with multiple breakpoints (Saboo *et al.*, 1987a).

c. *Feasibility Test.* If all the restrictions of the corner point theorem are satisfied except that the heat capacities are allowed to be piecewise constant, then the following mixed-integer linear program (MILP) can be formulated to test HEN feasibility for assumed, fixed values of the uncertain temperatures (Saboo *et al.*, 1987a):

$$\psi = \min_{v, \beta, \eta, m} \beta \quad (24)$$

subject to:

(A1) Energy balances on all exchangers and heaters:

$$At^S + Bv + N\eta = b$$

(A2) Specified energy recovery:

$$\sum_k l_k^H = \alpha H$$

(B1) ΔT_m constraints on all exchangers:

$$Ct^S + Dv + O\eta + p \leq \beta e$$

(B2) Nonnegative exchanger and cooler loads:

$$Et^S + Gv + r \leq \beta e$$

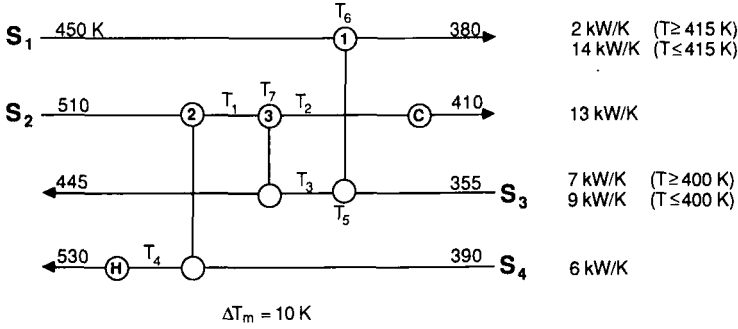


FIG. 11. HEN structure with temperature breakpoints for Example 7 (infeasible).

(B3) Nonnegative heater loads:

$$-l^H \leq \beta e$$

(B4) Definition of slack and integer variables:

$$I\eta - km \leq L, \quad \eta_k \geq 0, \quad m_k = 0, 1$$

The HEN is feasible if and only if $\psi \leq 0$.

Example 7 (from Saboo et al., 1987a). The HEN structure in Fig. 11 is to be tested if it is feasible for the supply temperatures shown. The heat capacities have two breakpoints: $T_{BR_1} = 415$ K in hot stream S_1 and $T_{BR_3} = 400$ K in cold stream S_3 .

In heat exchanger 1, T_5 is the temperature of cold stream S_3 corresponding to hot breakpoint T_{BR_1} . Hot stream temperatures T_6 and T_7 in exchangers 1 and 3, respectively, correspond to potential locations of cold breakpoint T_{BR_3} . The minimum heating requirement is 180 kW for a specified ΔT_m of 10 K.

The constraints for exchanger 1 are formulated as follows. For overall energy balance:

$$2(450 - 415) + 14(415 - 380) = 7(T_3 - 400) + 9(400 - 355) + (7 - 9)\eta_1$$

For energy balance to define temperature T_5 of stream S_3 corresponding to T_{BR_1} :

$$2(450 - 415) = 7(T_3 - 400) + 9(400 - T_5) + (7 - 9)\eta_1 + (9 - 7)\eta_3$$

For energy balance to define temperature T_6 of stream S_1 corresponding to T_{BR_3} :

$$2(450 - 415) + 14(415 - T_6) + (14 - 2)\eta_5 = 7(T_3 - 400) + 7\eta_1$$

For constraints defining slack variables η_i :

$$T_3 - 400 + \eta_1 - \eta_2 = 0, \quad 400 - T_5 + \eta_3 - \eta_4 = 0$$

$$415 - T_6 + \eta_5 - \eta_6 = 0$$

$$0 \leq \eta_1 \leq km_1, \quad 0 \leq \eta_2 \leq k(1 - m_1)$$

$$0 \leq \eta_3 \leq km_2, \quad 0 \leq \eta_4 \leq k(1 - m_2)$$

$$0 \leq \eta_5 \leq km_3, \quad 0 \leq \eta_6 \leq k(1 - m_3)$$

$$m_1, m_2, m_3 = 0, 1$$

where k is a sufficiently large positive number. For approach temperature constraints:

$$\text{At hot end:} \quad 450 - T_3 + \beta \geq 10$$

$$\text{At cold end:} \quad 380 - 355 + \beta \geq 10$$

$$\text{At } T_{BR_1}: \quad 415 - T_5 + \beta \geq 10$$

$$\text{At } T_{BR_3}: \quad T_6 - 400 + Km_1 + \beta \geq 10$$

where K is a sufficiently large positive number. For load constraint, the heat load of exchanger 1 will always be positive, since it is the only exchanger on stream 1. Note that the ΔT_m constraint at T_{BR_1} requires no integer variables [as opposed to Eq. (23)] since T_{BR_1} *must* occur inside exchanger 1. The ΔT_m constraint at T_{BR_3} requires only one integer variable since T_{BR_3} can occur only inside or downstream (but not upstream) of exchanger 1. Constraints for the other exchangers are formulated similarly.

Solution of the MILP gives $\psi = 7.2$ K. Therefore the network is infeasible. Both breakpoints T_{BR_1} and T_{BR_2} occur in heat exchanger 1. The corresponding temperatures are

$$T_5 = 412.2 \text{ K} \quad (\text{corresponding to } T_{BR_1} = 415 \text{ K})$$

$$T_6 = 408.7 \text{ K} \quad (\text{corresponding to } T_{BR_3} = 400 \text{ K})$$

The ΔT_m violations also occur inside heat exchanger 1:

$$\Delta T_m - (415.0 - 412.2) = 7.2 \text{ K}, \quad \Delta T_m - (408.7 - 400.0) = 1.3 \text{ K}$$

The structure can be made feasible by shifting the cooler from stream 2 to stream 1 to increase the temperature driving force in exchanger 1.

d. *Resilience Test.* Unfortunately, if the temperature breakpoints move to different exchangers when HEN feasibility is checked at different corner points of the uncertainty range, the corner point theorem may not

hold (Saboo *et al.*, 1987a). However, for HENs with a minimum number of units, an MILP can still be formulated which is a necessary and sufficient resilience test.

In a minimum unit HEN the intermediate stream temperatures and heater loads, and thus the breakpoint locations, are uniquely determined by the energy balance and energy recovery constraints. Thus for given supply temperatures and flow rates, the ΔT_m violations (and surpluses) and load violations (and surpluses) in each exchanger k are also uniquely determined.

The ΔT_m violations (γ_{T_k}) and surpluses (σ_{T_k}) can be defined by

$$T_1 - T_2 + \gamma_{T_k} - \sigma_{T_k} = \Delta T_m \quad (25a)$$

Integer variables m_{T_k} are used as follows to allow only one of γ_{T_k} or σ_{T_k} to be nonzero:

$$0 \leq \gamma_{T_k} \leq k_T m_{T_k} \quad (25b)$$

$$0 \leq \sigma_{T_k} \leq k_T (1 - m_{T_k}) \quad (25c)$$

$$m_{T_k} = 0, 1 \quad (25d)$$

where k_T is a sufficiently large number (larger than the maximum possible ΔT_m violation or surplus). Load violations γ_L and surpluses σ_L are defined similarly using integer variables m_L .

By using these definitions for ΔT_m and load violations and surpluses, the following MILP can be formulated to test the resilience of a minimum unit HEN with breakpoints (Saboo *et al.*, 1987a):

$$\chi = \max_{\theta} \sum_k (\gamma_{T_k} + \gamma_{L_k}) \quad (26)$$

subject to:

(A1) Energy balances on all exchangers and heaters:

$$At^S + Bv + N\eta = b$$

(A2) Specified energy recovery:

$$\sum_k l_k^H = \alpha H$$

(B1) ΔT_m constraints on all exchangers:

$$Cr^S + Dv + O\eta + p = \gamma_T - \sigma_T$$

(B2) Nonnegative exchanger and cooler loads:

$$Et^S + Gv + r = \gamma_L - \sigma_L$$

(B3) Nonnegative heater loads:

$$-l^H = \gamma_L^H - \sigma_L^H$$

(B4) Definition of slack and integer variables:

$$I\eta - km \leq L, \quad I\gamma_T - k_T m_T \leq 0,$$

$$I\sigma_T - k_T m_T \leq L_T, \quad I\gamma_L - k_L m_L \leq 0$$

$$I\sigma_L - k_L m_L \leq L_L, \quad I\gamma_L^H - k_L^H m_L^H \leq 0, \quad I\sigma_L^H - k_L^H m_L^H \leq L_L^H$$

$$m_k, m_{T_k}, m_{L_k}, m_{L_k}^H = 0, 1, \quad \eta_k, \gamma_{T_k}, \sigma_{T_k}, \gamma_{L_k}, \sigma_{L_k}, \gamma_{L_k}^H, \sigma_{L_k}^H \geq 0$$

(B5) Uncertainty range

$$\theta^L \leq \theta \leq \theta^U$$

where θ contains the uncertain supply temperatures. This MILP can be extended to include target temperatures in the uncertainty range. The HEN is resilient in the specified uncertainty range if and only if $\chi = 0$.

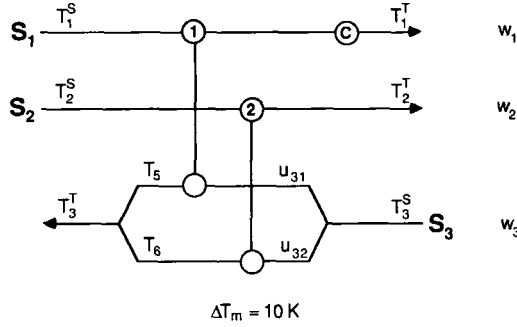
2. Resilience Analysis with Stream Splits

Resilience analysis for HENS can become nonlinear and nonconvex if varying stream split fractions are allowed. In this section nonlinear feasibility and resilience tests are presented for networks with stream splits, with the assumption that the network has a minimum number of units. This assumption often is not restrictive since many stream split networks do have a minimum number of units.

a. *Stream Split Constraints.* For HENs with a minimum number of units, the heater loads and intermediate stream temperatures are uniquely determined by the energy balance and energy recovery constraints. These equality constraints can be solved simultaneously to obtain explicit expressions for the heater loads and intermediate stream temperatures in terms of the stream supply temperatures and stream split fractions. These expressions can then be substituted into some of the ΔT_m constraints to form constraints on the stream split fractions (Saboo *et al.*, 1987b). The following example demonstrates this procedure.

Example 8 (from Saboo et al., 1987b). Resilience of the HEN in Fig. 12 is tested in Example 9. In this example, the constraints on the stream split fractions are formulated.

Note that the energy recovery constraint reduces to $0 = 0$ for this network since there are no heaters. The energy balance constraints for the two exchangers can be solved for intermediate stream temperatures T_5 and



Stream (i)	T_i^S (K)	T_i^T (K)	w_i (kW/K)
1	740	625	2
2	415-515	370	1
3	320	550	1

FIG. 12. Minimum unit HEN structure with stream split (Examples 8, 9, and 11).

T_6 to give

$$HX\ 1: \quad T_5 = T_3^S + \frac{w_3(T_3^T - T_3^S) - w_2(T_2^S - T_2^T)}{u_1 w_3} \quad (a)$$

$$HX\ 2: \quad T_6 = T_3^S + \frac{w_2(T_2^S - T_2^T)}{u_2 w_3} \quad (b)$$

The ΔT_m constraints for this network are

$$HX\ 1: \quad T_1^S - T_5 \geq \Delta T_m; \quad T_4 - T_3^S \geq \Delta T_m \quad (c)$$

$$HX\ 2: \quad T_2^S - T_6 \geq \Delta T_m; \quad T_2^T - T_3^S \geq \Delta T_m \quad (d)$$

Substituting for T_5 in $T_1^S - T_5 \geq \Delta T_m$ yields

$$-\frac{w_3(T_3^T - T_3^S) - w_2(T_2^S - T_2^T)}{u_1 w_3} \geq -\left[(T_1^S - \Delta T_m) - T_3^S\right] \quad (e)$$

Note that $T_1^S - \Delta T_m \geq T_5 \geq T_3^S$ for the network to be feasible. Therefore the right side of inequality (e) is negative, and (e) becomes

$$u_{31} \geq g_{31} \triangleq \frac{(w_2 T_2^T + w_3 T_3^T) - w_2 T_2^S - w_3 T_3^S}{(-w_3 \Delta T_m) + w_3 T_1^S - w_3 T_3^S} \quad (f)$$

Similarly, substituting for T_6 in $T_2^S - T_6 \geq \Delta T_m$ yields

$$u_{32} \geq g_{32} \triangleq \frac{(-w_2 T_2^T) + w_2 T_2^S}{(-w_3 \Delta T_m) + w_3 T_2^S - w_3 T_3^S} \quad (g)$$

These stream split constraints replace the two ΔT_m constraints used in their derivation.

In general, assuming that any exchanger may be connected to *either* a cold stream split or a hot stream split (but not to *both* a cold stream split and a hot stream split), the stream split constraints have the form

$$u_{ij} \geq g_{ij} \triangleq \frac{a_{ijo} + \sum_l a_{ijl} T_l^S}{c_{ijo} + \sum_l c_{ijl} T_l^S} \quad (27)$$

where u_{ij} is the stream split fraction of branch j in stream i and a_{ijo} , a_{ijl} , c_{ijo} , and c_{ijl} are constants depending on stream target temperatures, flow rates, and ΔT_m (Saboo *et al.*, 1987b). Under the same assumption, the load constraints can always be written in terms of unsplit streams. These results hold for any number of stream splits and for any number of exchangers connected to each branch of a stream split.

b. *Feasibility Test.* If all the restrictions of the corner point theorem are satisfied except that the stream split fractions are allowed to vary, then the following LP can be formulated to test the feasibility of a minimum unit HEN for assumed, fixed values of the uncertain temperatures (Saboo *et al.*, 1987b):

$$\psi = \min_u \beta \quad (28)$$

subject to:

(A1) Mass balance at each stream split:

$$\sum_j u_{ij} = 1 \quad \forall i$$

(B1) Constraints on stream split fractions:

$$u_{ij} + \beta \geq g_{ij} \triangleq \frac{a_{ijo} + \sum_l a_{ijl} T_l^S}{c_{ijo} + \sum_l c_{ijl} T_l^S}$$

(B2) Load and ΔT_m constraints not depending on u :

$$v_k \triangleq v_{ko} + \sum_l v_{kl} T_l^S \leq \beta$$

The minimum unit HEN with stream splits is feasible if and only if $\psi \leq 0$.

For the feasibility test, stream split constraints (B1) are *linear*! In particular, each g_{ij} is constant since the feasibility test is for specified supply temperatures. Also note that the energy balance and energy recovery constraints are not included in this feasibility test; they are used to determine constants a_{ijl} , c_{ijl} , and v_{kl} in the stream split, load, and ΔT_m constraints.

c. *Resilience Test.* For the resilience test, the stream split constraints are *no longer linear* since the supply temperatures are no longer constant but vary within an uncertainty range. In general, the stream split constraints are nonconvex and the corner point theorem cannot be applied. However, it is still possible to develop a sufficient test for HEN resilience.

The critical values of the uncertain supply temperatures limiting HEN resilience are those which maximize constraint functions g_{ij} and v_k . Constraints v_k are linear functions of supply temperatures T_l^S and constraints g_{ij} are monotonic functions of T_l^S (Saboo *et al.*, 1987b). Thus the critical points which maximize g_{ij} and v_k are corner points of the uncertainty range. To identify which of the corner points maximizes each of the constraint functions, one can simply examine the signs of the gradients of g_{ij} and v_k with respect to each of the T_l^S .

A necessary condition for the HEN to be resilient is that $v_{k,\max}$ be nonpositive for every k (Saboo *et al.*, 1987b). This condition is necessary since constraint functions v_k are linear in T_l^S and independent of stream split fractions u . If any of the $v_{k,\max}$ is positive, then one of the ΔT_m or load constraints in problem (28) is violated (at the critical corner point for $v_{k,\max}$) and no choice of stream split fractions u will make the network feasible (at that critical corner point). If all the $v_{k,\max}$ are nonpositive, then all of the ΔT_m and load constraints in problem (28) are satisfied at every corner point, and thus (by linearity in T^S) throughout the entire uncertainty range.

If all the $v_{k,\max}$ are nonpositive, then the ΔT_m and load constraints (which are independent of u) can be deleted from further consideration. The following LP can then be formulated to check whether the remaining constraints (which are functions of u) are satisfied (Saboo *et al.*, 1987b):

$$\chi = \min_{u, \beta} \beta \quad (29)$$

(A1) Mass balance at each stream split:

$$\sum_j u_{ij} = 1 \quad \forall i; \quad u_{ij} \geq 0 \quad \forall i, j$$

(B1) Constraints on stream split fractions:

$$u_{ij} + \beta \geq g_{ij,\max}$$

Note that the uncertain supply temperatures T^S are not included as optimization variables in LP (29), since the uncertainty range was already searched to calculate $g_{ij,\max}$.

The minimum unit HEN with stream splits is resilient if $\chi \leq 0$. This test is sufficient, but not necessary, for HEN resilience. It is necessary only if the same critical corner point maximizes all of the g_{ij} and v_k constraint functions simultaneously.

Example 9. Resilience of the minimum-unit stream-splitting HEN shown in Fig. 12 is to be tested in the uncertainty range $415 \text{ K} \leq T_2^S \leq 515 \text{ K}$. The stream split constraints were derived in Example 8 from the ΔT_m constraints on the hot ends of the exchangers.

The constraints for the resilience test are the following:

Stream split constraints:

$$HX \ 1: \quad u_{31} \geq g_{31} \triangleq \frac{(600 - T_2^S)}{410}$$

$$HX \ 2: \quad u_{32} \geq g_{32} \triangleq \frac{(T_2^S - 370)}{(T_2^S - 330)}$$

Load constraints:

$$HX \ 1: \quad v_1 \triangleq T_2^S - 600 \leq 0$$

$$HX \ 2: \quad v_2 \triangleq 370 - T_2^S \leq 0$$

$$C: \quad v_3 \triangleq 370 - T_2^S \leq 0$$

Mass balance at stream split:

$$u_{32} = 1 - u_{31}, \quad u_{31}, u_{32} \geq 0$$

The remaining ΔT_m constraints ($T_4 - T_3^S \geq 10$, $T_2^T - T_3^S \geq 10$) can be disregarded since for the values of the heat capacity flow rates chosen in this example, ΔT_m will always occur on the hot ends of the exchangers for any value of the stream split fractions.

The feasible region defined by these constraints is plotted in Fig. 13. The feasible region is nonconvex, and thus the corner point theorem does not hold. In particular, the HEN is not feasible for $422 \text{ K} \leq T_2^S \leq 508 \text{ K}$, even though it is feasible for the corner points of the uncertainty range: $T_2^S = 415 \text{ K}$ and $T_2^S = 515 \text{ K}$.

The resilience test correctly identifies that the HEN is not resilient in the specified uncertainty range. In order to apply the resilience test, the values of $v_{k,\max}$ and $g_{ij,\max}$ shown in Table V are calculated. The values of $v_{k,\max}$ are all nonpositive; thus the load constraints are satisfied throughout the

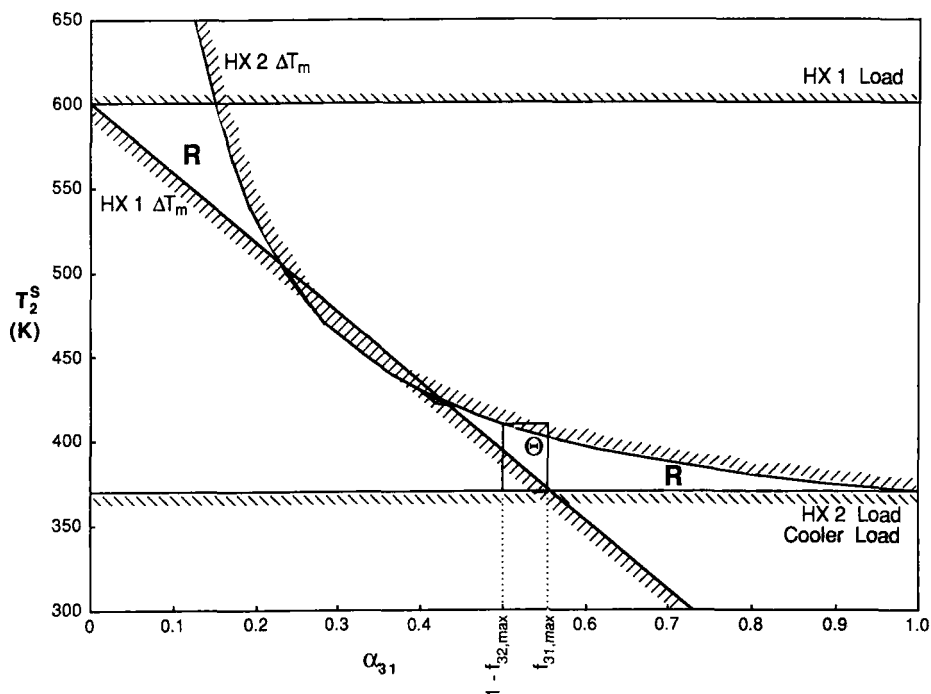


FIG. 13. Feasible region for stream splitting HEN structure (Examples 8, 9 and 11).

TABLE V

MAXIMUM VALUES OF RESILIENCE CONSTRAINT FUNCTIONS
 $v_{k,\max}$ AND $g_{ij,\max}$ IN AN UNCERTAINTY RANGE
 $415 \leq T_2^S \leq 515$ K (EXAMPLE 9)

Constraint function	Maximum value $V_{k,\max}$ or $g_{ij,\max}$	Critical corner point (K)
v_1	-85	$T_2^S = 515$
v_2	-45	$T_2^S = 415$
v_3	-45	$T_2^S = 415$
g_{31}	0.4512	$T_2^S = 415$
g_{32}	0.7838	$T_2^S = 515$

uncertainty range and can be deleted from further consideration. Now LP (29) is applied to test whether the stream split constraints are satisfied:

$$\chi = \min_{u_{31}, \beta} \beta$$

subject to

$$u_{31} + \beta \geq g_{31, \max} = 0.4512, \quad u_{31} - \beta \leq 1 - g_{32, \max} = 0.2162$$

Solution of this LP yields $\chi = 0.1175$. Since $\chi > 0$, the HEN is not resilient in the uncertainty range $415 \text{ K} \leq T_2^S \leq 515 \text{ K}$.

To show that this procedure is not a *necessary* test for resilience, consider the uncertainty range $370 \text{ K} \leq T_2^S \leq 410 \text{ K}$. This uncertainty range is shown in Fig. 13. Obviously, the HEN is resilient in this uncertainty range since for every value of T_2^S in the range, there is a value of u_{31} for which the network is feasible.

The resilience test incorrectly identifies the network as not being resilient. The values of $v_{k, \max}$ and $g_{ij, \max}$ for this uncertainty range are listed in Table VI. Since all the $v_{k, \max}$ are nonpositive, the load constraints are satisfied throughout the uncertainty range. To test the stream split constraints, LP (29) is applied:

$$\chi = \min_{u_{31}, \beta} \beta$$

subject to

$$u_{31} + \beta \geq g_{31, \max} = 0.5610, \quad u_{31} - \beta \leq 1 - g_{32, \max} = 0.5000$$

Solution of this LP yields $\chi = 0.0305$, thus implying that the network is not resilient in the new uncertainty range. The resilience test is conservative because LP (29) looks for values of stream split fractions u which, if held

TABLE VI
MAXIMUM VALUES OF RESILIENCE CONSTRAINT FUNCTIONS
 $v_{k, \max}$ AND $g_{ij, \max}$ IN AN UNCERTAINTY RANGE
 $370 \leq T_2^S \leq 410 \text{ K}$ (EXAMPLE 9)

Constraint function	Maximum value $v_{k, \max}$ or $g_{ij, \max}$	Critical corner point (K)
v_1	-190	$T_2^S = 410$
v_2	0	$T_2^S = 370$
v_3	0	$T_2^S = 370$
g_{31}	0.5610	$T_2^S = 370$
g_{32}	0.5000	$T_2^S = 410$

constant, would make the HEN resilient for the entire uncertainty range. From Fig. 13, for the uncertainty range $370 \text{ K} \leq T_2^S \leq 410 \text{ K}$, there is no single value of u_{31} which, if held constant, would make the HEN resilient for the entire uncertainty range.

3. Resilience Analysis with Flow Rate Uncertainties

When a HEN resilience problem includes uncertain flow rates, the energy balance, energy recovery, ΔT_m , and load constraints all can become nonlinear. Example 1 demonstrated that this can lead to non-convex problems and thus that the corner point theorem does not hold for flow rate uncertainties in general.

One reasonable simplifying assumption is a high correlation between the uncertain flow rates. Indeed, it is instructive to study the limiting case when a change in total process throughput changes all the flow rates proportionately. In this case, the changing flow rates simply rescale the resilience problem; that is, the flow rate changes can be factored out of the energy balance and energy recovery constraints and have no effect upon the ΔT_m and load constraints (Saboo *et al.*, 1987b). Therefore if all the flow rates vary proportionately, then the flow rate uncertainties can be ignored while testing the resilience of a HEN to temperature uncertainties. The rating for each heat exchanger is determined by the largest process throughput.

a. ΔT_m and Load Constraints. When the uncertain flow rates are not proportionate, the resilience test can still be simplified if the HEN has a minimum number of units. For a minimum unit HEN, the energy balance and energy recovery constraints can be solved simultaneously to give unique expressions for the heater loads and intermediate stream temperatures. Then these expressions can be substituted into the ΔT_m and load constraints to write the constraints explicitly in terms of the supply temperatures T^S and head capacity flow rates w .

Following this procedure, the ΔT_m constraint for an exchanger connected to hot stream S_i and cold stream S_j with uncertain flow rates has the general form (Saboo *et al.*, 1987b)

$$g_{ij}(w, T^S) \triangleq \frac{1}{w_i} \sum_l (a_{ijo} + a_{ijl} T_l^S) w_l - \frac{1}{w_j} \sum_l (c_{ijo} + c_{ijl} T_l^S) w_l - \Delta T_m \geq 0 \quad (30)$$

where a_{ijo} and c_{ijo} are equal to -1 , 0 , or $+1$ times a target temperature and

where a_{ijt} and c_{ijt} are equal to -1 , 0 , or $+1$. If heat capacity flow rates w_i and w_j are constant, then the ΔT_m constraint is required at only one end of the exchanger, depending upon the sign of $(w_i - w_j)$. However, if the flow rates vary enough that the sign of $(w_i - w_j)$ changes in the uncertainty range, then ΔT_m constraints are required at both ends of the exchanger.

The load constraint for an exchanger k with uncertain flow rates has the following general form (Saboo *et al.*, 1987b):

$$v_k(w, T^S) \triangleq \sum_l (v_{ko} + v_{kl} T_l^S) w_l \geq 0 \quad (31)$$

where v_{ko} equals -1 , 0 , or $+1$ times a target temperature and v_{kl} equals -1 , 0 , or $+1$.

b. *Resilience Test.* In general, ΔT_m and load constraints (30) and (31) are nonlinear and nonconvex, and the corner point theorem cannot be applied. However, it is still possible to develop a necessary and sufficient resilience test for HENs with a minimum number of units.

A minimum unit HEN with uncertain flow rates is resilient in a specified uncertainty range if and only if ΔT_m and load constraints (30) and (31) are satisfied throughout the uncertainty range; that is, the network is resilient if and only if

$$\min_{i,j,k} (g_{ij,\min}, v_{k,\min}) \geq 0 \quad (32)$$

where

$$g_{ij,\min} = \min_{\theta \in \Theta} g_{ij}, \quad v_{k,\min} = \min_{\theta \in \Theta} v_k \quad (33)$$

and θ contains the uncertain supply temperatures T^S and flow rates w in the uncertainty range Θ (Saboo *et al.*, 1987b).

Constraint functions v_k are monotonic in supply temperatures T^S and heat capacity flow rates w . Thus the critical point which minimizes v_k is a corner point of the uncertainty range. To identify which of the corner points minimizes each v_k , one can simply examine the signs of the gradients of each v_k with respect to each T_l^S and w_l .

Unfortunately, constraint functions g_{ij} are not necessarily monotonic. However, each g_{ij} has at most one stationary point with respect to flow rates w_i and w_j (Saboo *et al.*, 1987b). Standard nonlinear programming can be used to locate each stationary point. If the stationary point of g_{ij} lies outside the uncertainty range or if the stationary point is a maximum, then $g_{ij,\min}$ occurs at a corner point.

Saboo (1984) has generalized resilience test (32) to class 2 problems. However, his method is still limited to minimum unit HENs with no stream splits.

4. Active Constraint Strategy for Nonlinear Resilience Analysis

The nonlinear resilience analysis methods of the previous few sections, although rigorous, are limited to rather specific situations (Saboo *et al.*, 1987a,b): minimum unit HENs with piecewise constant heat capacities (but no stream splits or flow rate uncertainties), minimum unit HENs with stream splits (but constant heat capacities and no flow rate uncertainties), or minimum unit HENs with flow rate and temperature uncertainties (but constant heat capacities and no stream splits). Although it might be possible to combine these resilience analysis methods, the combined method would still be limited to HENs with a minimum number of units, and it would only be a sufficient test for resilience (at least for HENs with stream splits).

A more general algorithm, the active constraint strategy, has been developed by Grossmann and Floudas (1985, 1987) to analyze the resilience of many nonlinear processes in which the critical points limiting resilience need not be corner points of the uncertainty range. The active constraint strategy allows nonlinear resilience analysis of more general HENs than possible by earlier methods. In particular, it can be used to test the resilience of a HEN with minimum or more units, with or without stream splits or bypasses, and with temperature and/or flow rate uncertainties, but with constant heat capacities (Floudas and Grossmann, 1987b).

In addition, the active constraint strategy can save significant computational time in *linear* resilience analysis (86% in one example; Grossmann and Floudas, 1987) by eliminating the need to check HEN feasibility at every corner point. Thus, this strategy makes it practical to analyze the resilience of HENs with a large number of streams.

Grossmann and Floudas (1985, 1987) present both nonlinear and specialized linear forms of the active constraint strategy. Only the nonlinear form is discussed in this chapter.

The active constraint strategy has been developed for both the resilience (flexibility) test and the flexibility index (Grossmann and Floudas, 1985, 1987). However, only the active constraint strategy for the resilience test will be discussed here. Recall that the resilience test is based upon a resilience measure $\chi(d)$:

$$\chi(d) = \max_{\theta \in \Theta} \psi(d, \theta) \quad (6)$$

subject to

$$\Theta = \{\theta | \theta^L \leq \theta \leq \theta^U\}$$

where

$$\psi(d, \theta) = \min_{z, \beta} \beta \quad (4)$$

subject to

$$f_m(d, z, \theta) \leq \beta \quad (m \in M)$$

A HEN is resilient in a specified uncertainty range Θ if and only if $\chi(d) \leq 0$. If $\chi(d) > 0$, then at least one of the feasibility constraints f_m is violated somewhere in the uncertainty range. Geometrically, the resilience test determines whether uncertainty range Θ lies entirely within feasible region R .

The basic idea of the active constraint strategy is to use the Kuhn–Tucker conditions to identify the potential sets of active constraints at the solution of NLP (4) for feasibility measure ψ . Then resilience test problem (6) [or flexibility index problem (11)] is decomposed into a series of NLPs with a different set of constraints (a different potential set of active constraints) used in each NLP.

Floudas and Grossmann (1987b) have shown that for HENs with any number of units, with or without stream splits or bypasses, and with uncertain supply temperatures and flow rates but with constant heat capacities, the active constraint strategy decomposes the resilience test (or flexibility index) problem into NLPs which have a single local optimum. Thus the resilience test (or flexibility index) also has a single local optimum solution.

a. *Active Constraints in Resilience Analysis.* Resilience measure $\chi(d)$ is determined by the largest value of feasibility measure $\psi(d, \theta)$ in the specified uncertainty range Θ . Feasibility measure $\psi(d, \theta)$ is limited in turn by different sets of reduced inequality constraints f_m which become active at the solution of NLP (4). An understanding of the different sets of active constraints which determine ψ forms the basis of the active constraint strategy. The following example is designed to promote a deeper understanding of feasibility measure ψ and of the active constraints which limit it.

Example 10. Feasibility measure ψ is to be calculated for the HEN in Fig. 14 as a function of uncertain supply temperature T_3^S . Since the HEN

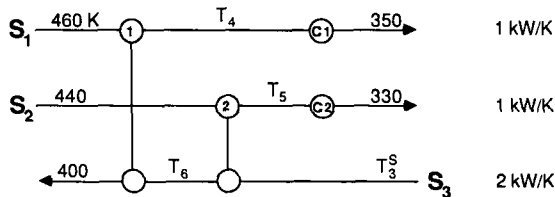


FIG. 14. HEN structure for Example 10.

has one more unit than the minimum required, one degree of freedom (control variable) can be manipulated to satisfy the feasibility constraints. Intermediate stream temperature T_5 is selected as the control variable.

Note that the energy recovery constraint reduces to $0 = 0$ since there is no heater in the network. The energy balances for the two exchangers can be solved simultaneously to yield the following expressions for intermediate stream temperatures T_4 and T_6 :

$$T_4 = 2T_3^S - T_5 + 100, \quad T_6 = T_3^S - 0.5T_5 + 220$$

These expressions can be substituted into the HEN ΔT_m and load constraints to yield the following LP for calculating ψ :

$$\psi(T_3^S) = \min_{T_5, \beta} \beta$$

subject to ΔT_m constraints

$$HX\ 1: \quad f_1 = T_5 - 2T_3^S + 260 \leq \beta$$

$$HX\ 2: \quad f_2 = T_3^S - T_5 + 10 \leq \beta$$

and load constraints

$$HX\ 1: \quad f_3 = 2T_3^S - T_5 - 360 \leq \beta$$

$$HX\ 2: \quad f_4 = T_5 - 440 \leq \beta$$

$$C\ 1: \quad f_5 = T_5 - 2T_3^S + 250 \leq \beta$$

$$C\ 2: \quad f_6 = 330 - T_5 \leq \beta$$

Figure 15 shows the feasible region for this HEN. With appropriate choice of control variable T_5 , the HEN is feasible for $295\text{ K} \leq T_3^S \leq 400\text{ K}$. Consider the three points labeled *A*, *B*, and *C* ($T_3^S = 340\text{ K}$; $T_5 = 380, 385, 390\text{ K}$). Table VII lists the values of f_i and β for each of these points. The value of β is minimized when two of the constraints become simultaneously active ($f_1 = f_2 = \beta_{\min} = -35$), which occurs at point *B*.

Table VII also lists values of $\psi = \beta_{\min}$ for other points labeled in Fig. 15. These values of ψ are plotted in Fig. 16. Note that $\psi \leq 0$ for $295\text{ K} \leq T_3^S \leq 400\text{ K}$, corresponding to the feasible range of T_3^S . The function $\psi(T_3^S)$ is piecewise linear. For each segment of $\psi(T_3^S)$, a different pair of active constraints (f_i, f_j) determines ψ . The pair of constraints active for each segment is noted on Fig. 16.

b. *Active Constraint Strategy.* In the previous example, different segments of the feasibility function ψ are all characterized by the same number of active constraints. In addition, HEN feasibility is always limited

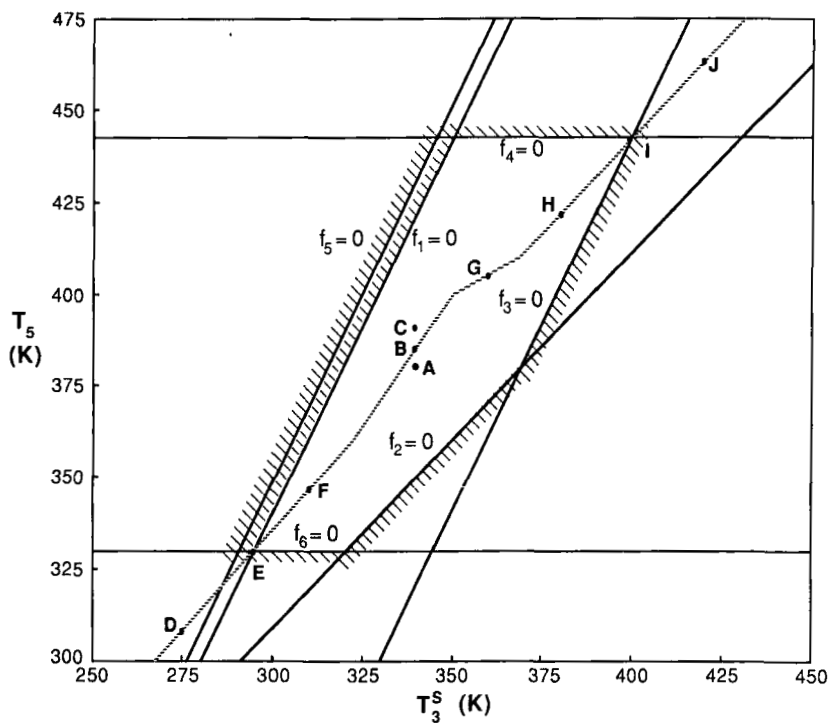
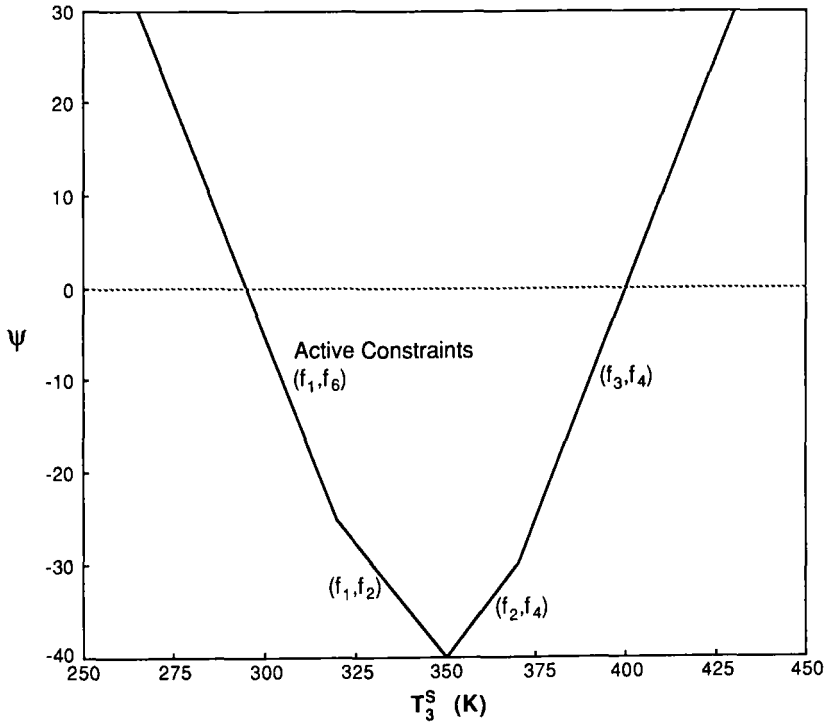


FIG. 15. Feasible region for Example 10.

TABLE VII

CALCULATION OF FEASIBILITY MEASURE ψ FOR EXAMPLE 10

Point	T_3^S	T_5	f_1	f_2	f_3	f_4	f_5	f_6	β
A	340	380	-40	-30	-60	-60	-50	-50	-30
B	340	385	-35	-35	-65	-55	-45	-55	-35
C	340	390	-30	-40	-70	-50	-40	-60	-30
Point	T_3^S	T_5	f_1	f_2	f_3	f_4	f_5	f_6	ψ
D	275	310	20	-25	-120	-130	10	20	20
E	295	330	0	-25	-100	-110	-10	0	0
F	310	345	-15	-25	-85	-95	-25	-15	-15
G	360	405	-55	-35	-45	-35	-65	-75	-35
H	380	420	-80	-30	-20	-20	-90	-90	-20
I	400	440	-100	-30	0	0	-110	-110	0
J	420	460	-120	-30	20	20	-130	-130	20

FIG. 16. Feasibility measure ψ for Example 10.

by the same number of active constraints in the resilience test of Example 3 (Table I), the flexibility index of Example 4 (Table II), and the resilience index of Example 5 (Table III). Swaney and Grossmann (1985a) have shown that this observation is general; that is, feasibility function ψ is characterized by a constant number of active constraints.

Theorem 3. Let n_z denote the number of control variables z and n_f the number of reduced inequality constraints f . If each $n_z \times n_z$ square submatrix of the Jacobian of f with respect to z ,

$$\begin{bmatrix} \frac{\partial f_1}{\partial z_1} & \frac{\partial f_1}{\partial z_2} & \dots & \frac{\partial f_1}{\partial z_{n_z}} \\ \frac{\partial f_2}{\partial z_1} & \frac{\partial f_2}{\partial z_2} & \dots & \frac{\partial f_2}{\partial z_{n_z}} \\ & & \ddots & \\ \frac{\partial f_{n_f}}{\partial z_1} & \frac{\partial f_{n_f}}{\partial z_2} & \dots & \frac{\partial f_{n_f}}{\partial z_{n_z}} \end{bmatrix}, \quad n_f \geq n_z + 1$$

is of full rank, then the number of active constraints ($f_m = \beta_{\min} = \psi$, $m \in M_A$) is equal to $n_z + 1$.

Note that this theorem is consistent with the number of active constraints in Examples 3, 4, 5, and 10. (If each square submatrix of the Jacobian is not of full rank, then the number of active constraints may be less than $n_z + 1$.)

Two important consequences leading to the active constraint strategy follow from Theorem 3 (Grossmann and Floudas, 1987). First, for given values of uncertain variables θ , the value of $\psi = \beta_{\min}$ can be uniquely determined from a square system of $n_z + 1$ active constraint equations in $n_z + 1$ unknowns ($z_1, \dots, z_{n_z}, \beta_{\min}$) rather than having to be determined by optimization. Second, resilience test problem (6) can be reduced to the following much simpler NLP:

$$\chi(d) = \max_{\theta \in \Theta} \beta_{\min} \quad (34)$$

subject to

$$f_m(d, z, \theta) \leq \beta_{\min} \quad (m \in M_A), \quad \Theta = \{\theta | \theta^L \leq \theta \leq \theta^U\}$$

where M_A is the set of $n_z + 1$ potentially active constraints at the corresponding value of θ . [The constraints in NLP (34) are written as inequality constraints rather than as equality constraints (as in Grossmann and Floudas, 1987), since all of the constraints may not be active if the submatrix of the Jacobian corresponding to constraint set M_A does not have full rank.]

The difficulty with problem (34) is that the set of active constraint equations M_A can change for different values of uncertain variables θ . The key feature of the active constraint strategy is its ability to identify potential sets of active constraints.

The potential sets of active constraints are identified by applying the Kuhn–Tucker conditions to NLP (4) for feasibility measure ψ (Grossmann and Floudas, 1985, 1987):

$$\sum_{m \in M} \lambda_m = 1 \quad (35a)$$

$$\sum_{m \in M} \lambda_m \frac{\partial f_m}{\partial z} = 0 \quad (35b)$$

$$\xi_m = \beta - f_m(d, z, \theta) \quad (m \in M) \quad (35c)$$

$$\lambda_m \xi_m = 0 \quad (m \in M) \quad (35d)$$

$$\lambda_m, \xi_m \geq 0 \quad (m \in M) \quad (35e)$$

where ξ_m and λ_m are the slack variable and Kuhn–Tucker multiplier, respectively, for constraint m . Equations (35a) and (35b) represent the

stationary points of the Lagrangian with respect to β and z , respectively; (35c) defines the slack variables; and (35d) and (35e) represent the complementary conditions.

Assuming that constraint functions f_m , $m \in M$, are all monotonic in z , the potential sets of active constraints can be determined from Kuhn-Tucker conditions (35b) and (35e) as follows (Grossmann and Floudas, 1987). If the constraint functions f_m are monotonic in z , then every component of $\partial f_m / \partial z$ is one signed for all z for each possible value of θ . Since $\lambda_m \geq 0$ must hold for each constraint $m \in M$ [Eq. (35e)], Eq. (35b) identifies the different sets of $n_z + 1$ constraints which can satisfy the Kuhn-Tucker conditions (different potential sets M_A of $n_z + 1$ active constraints).

To illustrate, reconsider Example 10, which has one control variable $z = T_5$. The reduced constraint functions have the following gradients with respect to z :

$$\begin{aligned} \frac{\partial f_1}{\partial z} &= 1, & \frac{\partial f_2}{\partial z} &= -1, & \frac{\partial f_3}{\partial z} &= -1 \\ \frac{\partial f_4}{\partial z} &= 1, & \frac{\partial f_5}{\partial z} &= 1, & \frac{\partial f_6}{\partial z} &= -1 \end{aligned}$$

Since there is one control variable, by Theorem 3 feasibility measure ψ is determined by two active constraints. Since for each pair of active constraints the corresponding Kuhn-Tucker multipliers λ_m must be non-negative [Eq. (35e)], each pair of active constraint functions must have gradients of opposite sign [Eq. (35b)]. Thus the potential sets of active constraints are

$$\begin{aligned} (f_1, f_2), (f_1, f_3), (f_1, f_6), (f_2, f_4), (f_2, f_5) \\ (f_3, f_4), (f_3, f_5), (f_4, f_6), (f_5, f_6) \end{aligned}$$

From Example 10 (Fig. 16), the actual sets of active constraints are

$$(f_1, f_2), (f_1, f_6), (f_2, f_4), (f_3, f_4)$$

Now the active constraint strategy for performing the resilience test can be summarized (Grossmann and Floudas, 1987) as follows.

1. Identification of potential sets of active constraints:
 - a. For every $m \in M$, compute $\partial f_m / \partial z$ and determine the sign of each component of the gradients.
 - b. Using Kuhn-Tucker conditions (35b) and (35e), identify the $k = 1, \dots, n_A$ potential sets of $n_z + 1$ active constraints, $M_A(k) = \{m \mid m \in M \text{ and } m \text{ is one of the } n_z + 1 \text{ active constraints}\}$.

2. Determine the trial resilience measure χ^k for each potential set of active constraints $M_A(k)$.
 - a. If $M_A(k)$ involves only upper and lower bound constraints $\theta_{l(k)}^L \leq \theta_{l(k)} \leq \theta_{l(k)}^U$, then

$$\chi^k(d) = \frac{1}{n_k} \left[\sum_{l(k) \in M_A(k)} \theta_{l(k)}^L - \sum_{l(k) \in M_A(k)} \theta_{l(k)}^U \right] \quad (36)$$

where index $l(k)$ represents the components of θ involved in the upper and lower bound constraints in $M_A(k)$ and n_k is total number of upper and lower bound constraints (Grossmann and Floudas, 1987).

- b. Otherwise, solve the following version of NLP (34):

$$\chi^k(d) = \max_{\theta \in \Theta, z, \beta_{\min}} \beta_{\min} \quad (34^k)$$

subject to

$$f_m(d, z, \theta) \leq \beta_{\min} \quad (m \in M_A(k)), \quad \Theta = \{\theta | \theta^L \leq \theta \leq \theta^U\}$$

3. Determine the overall resilience measure $\chi(d)$:

$$\chi(d) = \max_{k=1, \dots, n_A} \chi^k(d)$$

4. The HEN is resilient in the specified uncertainty range Θ if and only if $\chi(d) \leq 0$.

It should be noted that the active constraint strategy is equivalent to an explicit enumeration of all potential sets of active constraints. This explicit enumeration could also be performed by a mixed-integer nonlinear program (MINLP), with integer variables denoting whether particular constraints are active. Grossmann and Floudas (1987) present the form of this MINLP, but it is not solvable with current algorithms. The active constraint strategy decomposes the MINLP into a series of solvable NLPs. In the case of linear constraints, the MINLP reduces to a MILP, which is solvable by standard branch and bound techniques. Grossmann and Floudas (1987) also present forms of the active constraint strategy where the equality constraints are handled explicitly (rather than being substituted into the inequality constraints) and when no control variables are present (e.g., minimum unit HENs with fixed target temperatures and no stream splits).

Example 11. The active constraint strategy is to be used to test the resilience of the same stream splitting HEN as in Example 9 (Fig. 12) in the uncertainty range $\Theta = \{T_2^S | 415 \leq T_2^S \leq 515 \text{ K}\}$.

Note that the energy recovery constraint reduces to $0 = 0$ since there is no heater in this network. The energy balances for both exchangers and the stream split can be solved simultaneously for intermediate stream tempera-

tures T_4 , T_5 , and T_6 to yield

$$T_4 = 0.5T_2^S + 440, \quad T_5 = \frac{1}{u_{31}}(600 - T_2^S) + 320,$$

$$T_6 = \frac{T_2^S - 370}{1 - u_{31}} + 320$$

When these expressions for T_4 , T_5 , and T_6 are substituted into the ΔT_m , load, and stream split constraints, the following NLP can be written for feasibility measure ψ :

$$\psi = \max_{u_{31}, \beta} \beta$$

subject to ΔT_m constraints

$$HX\ 1: \quad f_1 \triangleq \frac{600 - T_2^S}{u_{31}} - 410 \leq \beta$$

$$HX\ 2: \quad f_2 \triangleq \frac{T_2^S - 370}{1 - u_{31}} - T_2^S + 330 \leq \beta$$

load constraints

$$HX\ 1: \quad f_3 \triangleq 0.5T_2^S - 300 \leq \beta$$

$$HX\ 2: \quad f_4 \triangleq 370 - T_2^S \leq \beta$$

$$C: \quad f_5 \triangleq 185 - 0.5T_2^S \leq \beta$$

and stream split constraints

$$f_6 \triangleq -u_{31} \leq \beta, \quad f_7 \triangleq u_{31} - 1 \leq \beta$$

The feasible region determined by these constraints (with $\beta = 0$) is shown in Fig. 13.

The gradients of the constraint functions f_i with respect to control variable u_{31} are

$$\frac{\partial f_1}{\partial u_{31}} = -\frac{600 - T_2^S}{u_{31}^2} < 0 \quad \forall T_2^S \in \Theta$$

$$\frac{\partial f_2}{\partial u_{31}} = \frac{T_2^S - 370}{(1 - u_{31})^2} > 0 \quad \forall T_2^S \in \Theta$$

$$\frac{\partial f_3}{\partial u_{31}} = \frac{\partial f_4}{\partial u_{31}} = \frac{\partial f_5}{\partial u_{31}} = 0$$

$$\frac{\partial f_6}{\partial u_{31}} = -1, \quad \frac{\partial f_7}{\partial u_{31}} = 1$$

Thus, from Kuhn–Tucker condition (35b), the potential sets of active constraints are identified as shown in Table VIII. For each potential set of active constraints $M_A(k)$, NLP (34^k) is formulated to determine trial resilience measure $\chi^{(k)}$. For example, for potential set $M_A(1) = \{(f_1, f_2)\}$, the following NLP is solved:

$$\chi^{(1)} = \max_{T_2^S, u_{31}, \beta} \beta$$

subject to

$$f_1 \triangleq \frac{600 - T_2^S}{u_{31}} - 410 \leq \beta, \quad f_2 \triangleq \frac{T_2^S - 370}{1 - u_{31}} - T_2^S + 330 \leq \beta$$

$$415 \leq T_2^S \leq 515 \text{ K}$$

The solution of NLP (34^k) for each potential set of active constraints is summarized in Table VIII.

The resilience measure for this stream-splitting HEN is

$$\chi = \max_k \chi^k = \chi^1 = 5.7159$$

Thus the HEN is not resilient in the specified uncertainty range. The worst case condition for resilience is given by the solution of NLP (34^k) corresponding to $M_A(1) = \{(f_1, f_2)\}$. At this solution, constraints $f_1 \leq 0$ ($HX 1 \Delta T_m$) and $f_2 \leq 0$ ($HX 2 \Delta T_m$) are most violated when $T_2^S = 462.2 \text{ K}$ and $u_{31} = 0.3315$ (compare with Fig. 13).

Note that in Table VIII, u_{31} violates the stream split constraints ($0 \leq u_{31} \leq 1$) at some of the solutions of NLP (34^k); for example, $u_{31} < 0$ at the solution of NLP (34¹⁸). This means that *potential* set of active constraints $M_A(18) = \{(f_5, f_7)\}$ is *not* active at the solution of the resilience test problem, since u_{31} violates the nonnegativity constraint [which was not included in NLP (34¹⁸)]. However, u_{31} does satisfy the constraint $u_{31} \leq 1$ ($f_7 \leq 0$), since this constraint was included in NLP (34¹⁸).

Note also that some of the gradients $\partial f_i / \partial u_{31}$ are zero and thus that this problem does not strictly satisfy the conditions of Theorem 3. The result of this is either of the following.

1. For given T_2^S , the solution of NLP (34^k) may not be uniquely determined by a system of $n_z + 1$ equality constraints in $n_z + 1$ unknowns (u_{31} and β). For example, in Table VIII, for $M_A(10) = \{(f_3, f_4)\}$ and $M_A(11) = \{(f_3, f_5)\}$, u_{31} is arbitrary at the solution of NLP (34^k). In this case, only a subset of $M_A(k)$ may actually be active.

2. Nonlinear program (34^k) may have no feasible solution [e.g., for $M_A(14) = \{(f_4, f_5)\}$]. If this is the case, then *potential* set $M_A(k)$ *cannot* be active at the solution of the resilience test problem.

TABLE VIII

RESILIENCE TEST WITH ACTIVE CONSTRAINT STRATEGY FOR EXAMPLE 11

k	Potential set of active constraints	Solution of NLP (34 ^k)		
		T_2^S (K)	u_{31}	χ^k
1	(f_1, f_2)	462.2	0.3315	5.716
2	(f_1, f_3)	515	0.2313	-42.5
3	(f_1, f_4)	415	0.5068	-45.0
4	(f_1, f_5)	415	0.4774	-22.5
5	(f_1, f_7)	415	0.4519	-0.5482
6	(f_2, f_3)	515	-0.0175 ^a	-42.5
7	(f_2, f_4)	415	-0.1250 ^a	-45
8	(f_2, f_5)	415	0.2800	-22.5
9	(f_2, f_6)	515	0.2153	-0.2153
10	(f_3, f_4)	446.67	Arbitrary	-76.67
11	(f_3, f_5)	485	Arbitrary	-57.5
12	(f_3, f_6)	415	42.5 ^a	-42.5
13	(f_3, f_7)	515	-41.5 ^a	-42.5
14	(f_4, f_5)	No feasible solution	No feasible solution	No feasible solution
15	(f_4, f_6)	415	45 ^a	-45
16	(f_4, f_7)	415	-44 ^a	-45
17	(f_5, f_6)	415	22.5 ^a	-22.5
18	(f_5, f_7)	415	-21.5 ^a	-22.5
19	(f_6, f_7)	Arbitrary	0.5	-0.5

^a These *potential* sets of active constraints turn out *not* to be active in resilience problem (6) since the constraints on u_{31} ($0 \leq u_{31} \leq 1$) are violated.

D. CLASS 2 RESILIENCE PROBLEMS

All the resilience analysis methods presented so far require that the form of the energy recovery constraint remain the same throughout the uncertainty range (class 1 problem). If the uncertainty range is sufficiently large, then the stream population at the pinch changes, thus changing the form of the energy recovery constraint (class 2 problem). When the form of the energy recovery constraint changes, then the reduced form of the ΔT_m and load constraints also changes (after the energy recovery and energy balance equality constraints are solved for the state variables and expressions for the state variables are substituted into the ΔT_m and load

constraints). Example 6 earlier in this chapter demonstrated that class 2 problems can be nonconvex even if all the constraints are linear.

A practical disadvantage of class 2 problems is that extra exchangers are often required because of changes in the pinch stream population. For example, reconsider the class 2 problem in Fig. 7. In Fig. 7a, the ΔT_m constraint imposed by the pinch at T_{h2}^S requires the presence of exchanger 1 (matching streams S_{c2} and S_{h2}), while exchanger 2 (matching streams S_{c2} and S_{h1}) can be completely bypassed. However, in Fig. 7b, the new pinch location at T_{h1}^S requires the presence of exchanger 2, while exchanger 1 can be completely bypassed. Thus for the class 2 uncertainty range, both exchangers are required, while for a class 1 uncertainty range ($460 \leq T_{h2}^S \leq 470$ K or $470 \leq T_{h2}^S \leq 480$ K), only one of the two exchangers is required. As a result, requiring strict resilience for class 2 problems (including that the energy recovery specification be satisfied throughout the uncertainty range) can make a HEN's capital cost quite high.

For quality control or safety considerations, it is essential that a HEN meet specified target temperatures, whether or not it achieves specified energy recovery. Thus for industrial problems with large uncertainty ranges, it may be desirable to design networks which are merely *operable*, rather than resilient, that is, to require that the network meet all target temperatures while satisfying the ΔT_m and load constraints, but allowing the energy recovery constraint to be violated at some points in the uncertainty range. Requiring that a HEN be operable rather than strictly resilient allows some extra heating to be used occasionally in order to lower capital costs.

Assuming that all the restrictions of the corner point theorem are satisfied except that class 2 problems are allowed, HEN resilience analysis without the energy recovery constraint is convex even for class 2 problems, since all the other constraints are still linear. This leads to the following modification of the corner point theorem (Saboo *et al.*, 1987b).

Theorem 4. Assume that all the restrictions of the corner point theorem are satisfied except that class 2 problems are allowed.

a. Then a HEN is operable in a specified uncertainty range if and only if it is operable at every corner point of the uncertainty range.

b. An upper bound on the minimum heating necessary for the HEN to be operable at a specified point θ in the uncertainty range is given by a linear combination of the minimum heating targets at all the corner points:

$$H_{\min} \leq \sum_{l \in L_v} y^l H^l \quad (37)$$

where y^l are determined such that

$$\theta = \sum_{l \in L_v} y^l \theta^l \quad (38)$$

Here θ^l are the values of the uncertain variables and H^l the minimum heating target at corner point l and L_v is the index set for the corner points.

Example 12 (from Saboo et al., 1987b). For the HEN structure in Fig. 8, the problem of analyzing resilience in an expected uncertainty range of

$$340 \leq T_{h1}^S \leq 380 \text{ K}, \quad 270 \leq T_{c2}^S \leq 300 \text{ K}$$

is class 2 (Example 6). However, the HEN is operable at all four corner points (Fig. 9) and thus is operable throughout the uncertainty range.

The minimum heating requirement at each corner point is

$$H^1 = 260 \text{ kW} \quad \text{at} \quad \theta^1 = (340, 270)$$

$$H^2 = 0 \text{ kW} \quad \text{at} \quad \theta^2 = (380, 270)$$

$$H^3 = 140 \text{ kW} \quad \text{at} \quad \theta^3 = (340, 300)$$

$$H^4 = 0 \text{ kW} \quad \text{at} \quad \theta^4 = (380, 300)$$

Thus at the intermediate uncertainty point

$$\theta = \begin{bmatrix} 360 \\ 295 \end{bmatrix} = y^1 \begin{bmatrix} 340 \\ 270 \end{bmatrix} + y^2 \begin{bmatrix} 380 \\ 270 \end{bmatrix} + y^3 \begin{bmatrix} 340 \\ 300 \end{bmatrix} + y^4 \begin{bmatrix} 380 \\ 300 \end{bmatrix} \quad (a)$$

an upper bound on the minimum heating requirement is

$$H_{\min} \leq y^1(260) + y^2(0) + y^3(140) + y^4(0) \quad (b)$$

However, since there are four unknowns (y^1, y^2, y^3, y^4) and only two equations in system (a), the choice of the unknowns is not unique. The following LP is formulated to find the choice of y^1, y^2, y^3, y^4 which minimizes the upper bound on H_{\min} :

$$H_{\min} \leq \min_{y^1, y^2, y^3, y^4, H} H$$

subject to

$$H = 260y^1 + 0y^2 + 140y^3 + 0y^4$$

$$360 = 340y^1 + 380y^2 + 340y^3 + 380y^4$$

$$295 = 270y^1 + 270y^2 + 300y^3 + 300y^4$$

$$y^1, y^2, y^3, y^4 \geq 0$$

Solution of this LP yields $H_{\min} \leq 47.8$ kW, with $y^1 = y^2 = 0$, $y^3 = 0.3417$, and $y^4 = 0.6417$. The actual heating requirement at this intermediate uncertainty point is $H_{\min} = 20$ kW.

The preceding theorem describes an *operability test* for class 2 HENs. Similarly, by omitting the energy recovery constraint from flexibility index problem (15) or resilience index problem (19), an *operability index* could be defined for class 2 HENs.

To rigorously analyze the resilience of class 2 HENs, and not just the operability, requires more complicated algorithms that are beyond the scope of this chapter. Saboo (1984) presents a mixed-integer linear program (MILP) for testing the resilience of minimum unit HENs to temperature uncertainties and a quadratic program (QP) for testing the resilience of HENs with more than minimum units. In addition, he presents an algorithm (based on solving a series of NLPs) for testing the resilience of minimum unit HENs with both temperature and flow rate uncertainties. Saboo (1984) also presents an algorithm for calculating the resilience index of class 2 HENs. However, all of these algorithms are limited to HENs with constant heat capacities and no phase change and constant stream split fractions.

E. SUMMARY OF HEN RESILIENCE ANALYSIS TECHNIQUES; AREAS FOR FUTURE RESEARCH

Several HEN resilience analysis techniques have been reviewed in this chapter. These techniques are all variations of three basic problems.

1. The resilience (flexibility) test determines whether a HEN structure is resilient (flexible) in a given uncertainty range.
2. The flexibility index determines the largest uncertainty range (scaled hyperrectangle) for which the HEN is resilient. The flexibility index is scaled in terms of an expected uncertainty range ($\theta^N - F \Delta\theta^- \leq \theta \leq \theta^N + F \Delta\theta^+$).
3. The resilience index, another measure of the largest uncertainties for which the HEN remains feasible, is the size of the largest *total* uncertainty load (polytope region) which the HEN can tolerate.

Different algorithms are required to solve these three basic resilience analysis problems depending on whether the problem is linear, nonlinear, or class 2. A HEN resilience problem is linear under the following conditions (corner point theorem, Saboo and Morari, 1984): (1) constant heat capacities and no phase change, (2) temperature uncertainties only

(no uncertain flow rates or heat transfer coefficients), (3) constant stream split fractions, and (4) class 1 uncertainty range.

If the HEN resilience problem is linear, then the three basic analysis techniques can be implemented as follows.

1. For the resilience (flexibility) test, a HEN is resilient (flexible) in a specified uncertainty range if and only if it is feasible at every corner point of the uncertainty range.

2. The flexibility index can be calculated by determining the largest scaled uncertainty s^k which the network can tolerate in the direction of each of the k corner points of the uncertainty range. Then the flexibility index is

$$F = \min_k s^k$$

3. The resilience index can be determined by maximizing the load uncertainty l_i which the network can tolerate in either a positive or negative direction in each stream supply temperature. Then the resilience index is

$$RI = \min_i (l_i^-, l_i^+, \max)$$

Different algorithms are required if the HEN resilience problem is nonlinear. Special algorithms were presented for testing the resilience of minimum unit HENs with piecewise constant heat capacities, stream splits, or simultaneous flow rate and temperature uncertainties. A more general algorithm, the active constraint strategy, was also presented which can test the resilience or calculate the flexibility index of a HEN with minimum or more units, stream splits and/or bypasses, and temperature and/or flow rate uncertainties, but with constant heat capacities.

In the case of class 2 resilience problems, the temperature or flow rate uncertainties are large enough that the stream population at the pinch changes somewhere in the uncertainty range, thus changing the form of the energy recovery constraint. More complicated algorithms (Saboo, 1984) are required to rigorously analyze resilience for these problems. However, for class 2 problems it may be more practical to require that the HEN merely be operable rather than strictly resilient. A HEN is operable throughout a specified uncertainty range if and only if it is operable at every corner point of the uncertainty range.

Several powerful HEN resilience analysis algorithms have been reviewed in this chapter, including the active constraint strategy (Grossmann and Floudas, 1985, 1987) which can test the resilience of the most general HEN. However, many common industrial HENs still cannot be analyzed with present techniques. For example, no technique has been

reported which can analyze the resilience of a HEN with uncertain flow rates and temperatures *and* phase change. Also, no *rigorous* technique (with a single local optimum) has been reported which can analyze HEN resilience with respect to *area* constraints (rather than ΔT_m constraints), except when the HEN satisfies all the restrictions of the corner point theorem (Saboo *et al.*, 1985).

In order to extend present resilience analysis techniques to more general HENs, the following areas of research seem useful.

1. Develop more general techniques to analyze the resilience of HENs with minimum or more units, stream splits and/or bypasses, temperature and/or flow rate uncertainties, *and* temperature-dependent heat capacities and phase change. It may be possible to extend the active constraint strategy to heat capacities with a specific temperature dependence (e.g., $C_p = a + bT + cT^2$). It might also be possible to handle phase change with the active constraint strategy (e.g., by using breakpoints as in Section III,C,1) if this approach will lead to mixed-integer nonlinear programs which are solvable (e.g., by the outer approximation algorithm of Duran and Grossmann, 1986).

2. Develop more general techniques to test the resilience of HENs with area constraints instead of (or in addition to) ΔT_m constraints. It is possible to include area constraints in the active constraint strategy. However, the active constraint strategy for the resilience test may not satisfy the (sufficient) conditions for a single local optimum when logarithmic mean ΔT (ΔT_{LM}) is used. It may have a single optimum when arithmetic mean ΔT is used or when a Taylor series approximation of ΔT_{LM} is used. These approximations could be used to find a starting point to initialize the NLPs of the active constraint strategy with ΔT_{LM} .

3. Develop techniques to test the resilience of HENs with uncertain heat transfer coefficients (e.g., heat transfer coefficients as a function of flow rate, but with uncertain function parameters). It is possible to extend the active constraint strategy to heat transfer coefficients with bounded uncertainties (not as a function of flow rate), but then the active constraint strategy may not have a single local optimum solution.

4. Develop techniques to test the resilience of class 2 HENs with stream splits and/or bypasses, temperature and/or flow rate uncertainties, and temperature-dependent heat capacities and phase change. It may be possible to extend the active constraint strategy to class 2 problems. This would allow resilience testing of class 2 problems with stream splits and/or bypasses and temperature and/or flow rate uncertainties. However, the uncertainty range would still have to be divided into "pinch regions" (as in Saboo, 1984).

IV. Synthesis and Design of Resilient HENs

Research on the synthesis of economically optimal HENs has been performed by various investigators for over 15 years (Nishida *et al.*, 1981). Several powerful synthesis methods have evolved, including the pinch design method (Linnhoff *et al.*, 1982; Linnhoff and Hindmarsh, 1983) and methods based on structural optimization [to predict a minimum set of stream matches (Papoulias and Grossmann, 1983) and to determine the most economical network structure (Floudas *et al.*, 1986) from the predicted matches]. However, these methods synthesize networks only for fixed, assumed nominal values of any uncertain supply temperatures and flow rates and uncertain heat transfer coefficients.

The analysis techniques presented earlier in this chapter can be used to test the resilience of a synthesized network, and evolutionary changes can be made to the network, if necessary, to improve its resilience. However, this type of procedure may require many evolutionary synthesis–analysis iterations, and it may not be obvious which evolutionary changes are required to improve a network’s resilience. Obviously, better methods are needed which incorporate resilience into the synthesis procedure itself.

Two such methods to synthesize HENs, which are both economically optimal and resilient, have evolved from the resilience analysis techniques reviewed. These methods are (1) synthesis of HEN structure based on a flexibility index (FI) target (Colberg *et al.*, 1988) and (2) synthesis of HEN structure and design (sizing) of individual exchangers based on structural optimization algorithms for multiperiod operation (e.g., for multiple critical points which limit resilience) (Floudas and Grossmann, 1987b). In addition, Linnhoff and Kotjabasakis (1986) have introduced the simple but intuitively appealing concept of “downstream (disturbance) paths” for synthesis of resilient HENs. All these methods are discussed here. However, emphasis is on how resilience aspects are incorporated into the synthesis algorithms rather than on the mechanics of the synthesis algorithms themselves.

A. HEN SYNTHESIS BASED ON A FLEXIBILITY INDEX TARGET

Just as targets for minimum required utilities, units, and heat transfer area can guide a designer in synthesizing an economically optimal HEN, a target for maximum possible resilience (flexibility) can guide the designer in synthesizing a resilient HEN. And just as the economic targets simplify the search for an economically optimal HEN (by restricting the search to networks with minimum utility consumption), the flexibility index target

simplifies the search for a resilient HEN [by identifying the “critical” operating condition (supply temperatures and flow rates) and constraint (e.g., appearance of a new pinch) most likely to limit resilience].

1. *Flexibility Index Target*

Colberg *et al.* (1988) define the “general” resilience (flexibility) target as the maximum amount of resilience that could be incorporated into a HEN structure synthesized for given nominal stream data if the designer were to consider *all* possible HENs synthesized for that stream data. They show that such a target is arbitrarily large (i.e., for *any* given nominal values of uncertain stream data, it is *always* possible to synthesize a HEN structure which is resilient for *all* physically meaningful combinations of the uncertain supply temperatures, target temperatures, and heat capacity flow rates). In particular, infinitely cyclic HEN structures (or finite ones with a sufficient number of stream splits) can achieve this general resilience target. These particular structures can mimic the composite curves for any set of supply and target temperatures and flow rates [i.e., the temperature–enthalpy profile of each hot (cold) stream in the structure can always mimic the temperature–enthalpy profile of the hot (cold) composite curve]. And since the composite curves can be constructed for all physically possible temperatures and flow rates, the structures are resilient for all such temperatures and flow rates.

This general resilience target is not very practical. (1) Complex, costly HEN structures are generally required to achieve it; and (2) designing for *all* physically possible uncertainties is unrealistic (overly ambitious). A practical resilience target should be achievable with reasonable HEN structures (i.e., structures with few more units or stream splits than the number required for nominal stream data). A practical resilience target can be defined by restricting the target to class 1 uncertainty ranges (Colberg *et al.*, 1988). Larger, class 2 uncertainty ranges generally require HEN structures with a greater number of exchangers in order to satisfy ΔT_m at a number of different pinches (see Section III,D).

In order to quantify this resilience (flexibility) target, it can be defined in terms of the flexibility index. Then the resilience target—the class 1 flexibility index target—is the flexibility index of the largest possible class 1 uncertainty range (scaled with respect to the designer-specified expected uncertainty range) for the given nominal stream data (Colberg *et al.*, 1988).

For simple problems with a small number of streams and a small number of uncertain parameters, the class 1 FI target can be determined simply by trial-and-error plotting of the composite curves (Colberg *et al.*, 1988). The size of a class 1 uncertainty range is generally limited by its case B

(maximum cooling) and case C (maximum heating) corner points (see Theorem 3 in Section III,B,2). Starting from the nominal stream data, one can vary the uncertain supply temperatures and flow rates in the direction of the case B and case C corner points of the expected uncertainty range (see Table IV) and plot several sets of composite curves as the uncertain parameters vary. If a problem is pinched for the nominal stream data, the scaled uncertainty range is class 1 as long as (1) the pinch-causing stream is the same for the case B and case C corner points of the scaled uncertainty range, as well as for the nominal operating point; (2) the stream populations above and below the pinch are the same for the case B, case C, and nominal operating points; and (3) none of the stream supply, target, dew point, or bubble point temperatures (or breakpoint temperatures in the case of piecewise constant heat capacities) overlaps the range of pinch temperatures. If a problem is threshold heating (cooling) for the nominal stream data, the scaled uncertainty range is class 1 as long as the problem is also threshold heating (cooling) for both the case B and case C corner points of the scaled uncertainty range.

Trial-and-error plotting of composite curves is impractical for problems with a large number of streams, a large number of uncertain parameters, or correlated uncertainties. Colberg *et al.*, (1988) present a nonlinear program (NLP) to calculate the class 1 FI target for these (and simpler) problems.

Example 13 (from Colberg et al., 1988). Consider the nominal stream data given in Table IX. Stream S_{c2} causes the pinch for these data.

Assume that the supply temperature T_{h2}^S and heat capacity flow rate w_{h2} of hot stream S_{h2} are uncertain. Figure 17 shows a "pinch behavior diagram" as T_{h2}^S and w_{h2} vary. The nominal stream data are indicated with an asterisk. For every combination of uncertain parameters T_{h2}^S and w_{h2} in

TABLE IX
NOMINAL STREAM DATA FOR
EXAMPLES 13 AND 14.^a

Stream	T^S (K)	T^T (K)	w (kW/K)
S_{h1}	390	338	4.0
S_{h2}	400	283	6.0
S_{c1}	298	498	5.0
S_{c2}	358	388	10.0

^a After shifting to account for $\Delta T_m = 10$ K.

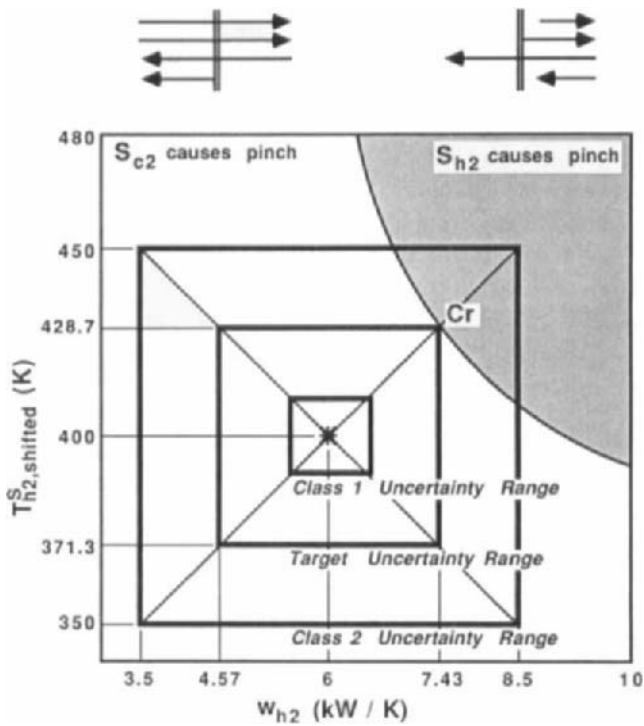


FIG. 17. “Pinch behavior diagram” illustrating class 1, class 2, and target uncertainty ranges for Example 13.

the unshaded portion of this diagram, stream S_{c2} causes the pinch. For all values of T_{h2}^S and w_{h2} in the shaded portion of this diagram, stream S_{h2} causes the pinch. If an uncertainty range includes both shaded and unshaded regions of this diagram, then it is class 2; otherwise it is class 1.

Figure 17 shows an uncertainty range as it increases in size. The smallest uncertainty range is class 1—for every combination of T_{h2}^S and w_{h2} in the range, stream S_{c2} causes the pinch, and the stream populations above the pinch (S_{h1} , S_{h2} , S_{c1} , S_{c2}) and below the pinch (S_{h1} , S_{h2} , S_{c1}) are constant. The largest uncertainty range is class 2—in one corner of the uncertainty range stream S_{h2} causes the pinch, while in the remainder of the uncertainty range stream S_{c2} causes the pinch. The middle-size uncertainty range (the “target uncertainty range”) corresponds to the resilience target—it is at the transition between class 1 and class 2. If the uncertainties were any larger (in the direction of increasing T_{h2}^S or increasing w_{h2}), then this uncertainty range would become class 2. The point labeled “Cr” in Fig. 17 limits the size of the target operating range; this point is called the

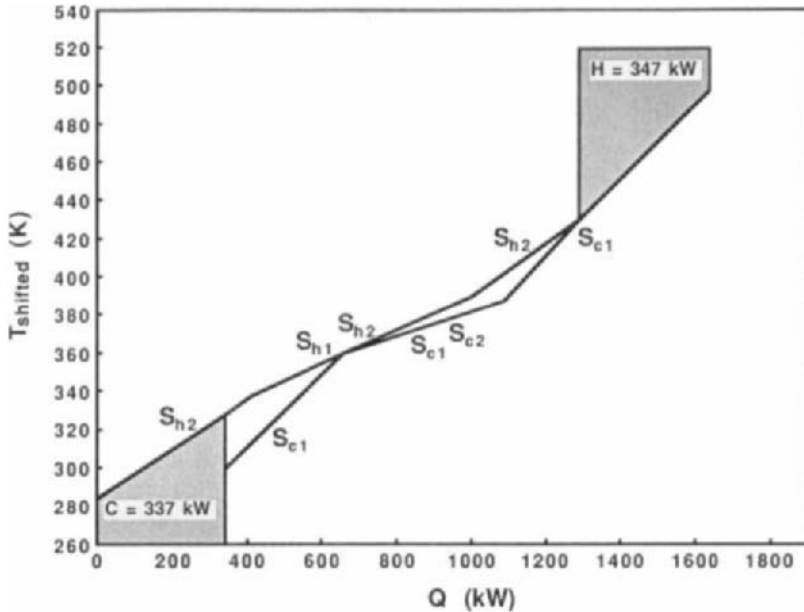


FIG. 18. Composite temperature-enthalpy curves for the critical uncertainty point of Example 13.

“critical uncertainty point.” At this point, *both* stream S_{h2} and stream S_{c2} cause pinches, as shown in the composite curves in Fig. 18. Thus the “critical constraint” which limits resilience in this example is the appearance of a new pinch at the supply of stream S_{h2} .

Suppose that the designer specifies as the expected uncertainty range the smallest uncertainty range shown in Fig. 17 ($\Delta T_{h2}^S = \pm 10$ K; $\Delta w_{h2} = \pm 0.5$ kW/K). Then the class 1 FI target (F^*) has the value 2.87 ($F^* \Delta T_{h2}^S = \pm 28.7$ K; $F^* \Delta w_{h2} = \pm 1.44$ kW/K); the size of the target uncertainty range is scaled relative to the size of the expected uncertainty range. Note that the class 1 FI target can also have a value less than 1.0 if the expected uncertainty range specified by the designer is class 2.

2. Use of the Class 1 Flexibility Index Target in HEN Synthesis

In the synthesis of resilient HENs, use of the class 1 flexibility index target offers two important features (Colberg *et al.*, 1988):

1. The size of the target (compared to 1) tells the process engineer if the expected uncertainty range is class 1 or class 2, and thus predicts (in a qualitative sense) how difficult it is to synthesize a resilient HEN for the expected uncertainty range.

2. Calculation of the FI target identifies the critical uncertainty point and constraint most likely to limit resilience, and thus identifies the supply temperatures and flow rates (in addition to the nominal ones) to which the process engineer should pay special attention.

To use the size of the class 1 FI target F^* to judge the difficulty of synthesizing a HEN resilient in a specified expected uncertainty range, consider three cases.

(1) $F^* \gg 1$. In this case, the expected uncertainty range is class 1 and is *much* smaller in size than the target uncertainty range. Since the uncertainties in the expected uncertainty range are relatively small (compared to the largest uncertainties in the target uncertainty range), traditional synthesis methods for fixed (nominal) stream conditions should be sufficient. Of course after designing the HEN, the designer should verify whether or not it is resilient in the desired expected uncertainty range.

(2) $F^* \approx 1$. Now the expected uncertainty range is class 1 but is close in size to the target uncertainty range. Since the expected uncertainty range is class 1, one can still “have it all;” that is, one can still synthesize a HEN structure with a “practical” number of units (qualitatively, few more units than the number required for nominal conditions) which is resilient—while using minimum utilities—throughout the expected uncertainty range. However, since the expected uncertainty range is close in size to the target uncertainty range, synthesis may be more difficult (Colberg *et al.*, 1988). Example 14 below illustrates one crude procedure for synthesizing a resilient HEN in this case. This procedure uses the critical uncertainty point as well as the nominal stream data to synthesize the HEN structure.

(3) $F^* < 1$. Now the expected uncertainty range is class 2 and one can no longer “have it all”—some trade-off must be made (Colberg *et al.*, 1988). The most common trade-off is to require minimum utility consumption only at the nominal operating point and at the corner points of the uncertainty range, and to allow extra utility consumption for other points in the uncertainty range. Alternatively, the designer could require minimum utility consumption throughout the uncertainty range, with a consequent increase in the number of units. Or the designer could decrease the size of the expected uncertainty range (e.g., by imposing tighter control on the surrounding process).

Unlike the economic HEN synthesis targets (for nominal stream conditions), the class 1 FI target is a “soft” target—the process engineer can actually exceed the target (i.e., design for class 2 uncertainty ranges by making one of the trade-offs discussed above). Whether the process engineer chooses to meet, not meet, or even exceed the resilience target

depends upon economic factors, including the cost of *not* being resilient (e.g., lost production). Likewise, whether or not the engineer chooses to meet the (nominal) economic targets depends upon resilience (as well as safety, controllability, and so on).

By calculating the class 1 FI target, the process engineer can identify the critical uncertainty point and critical constraint (appearance of new pinches, nonnegative heating or cooling, and so on). This uncertainty point and constraint limit the resilience of a completely countercurrent (e.g., infinitely cyclic) HEN structure able to mimic the composite curves; thus they seem the *most likely* uncertainty point and constraint to limit the resilience of a practical but well-designed (almost completely countercurrent) HEN structure.

The following example demonstrates, by means of a crude synthesis procedure, how the class 1 FI target can be used as a synthesis tool. By using the target to identify the critical uncertainty point and constraint, the process engineer can consider resilience *during* the early stages of synthesizing a resilient, economic HEN, rather than adding resilience *after* synthesis of an economic (for nominal conditions) HEN. Knowledge of the critical constraint (e.g., appearance of a second pinch) tells the process engineer exactly where to place exchangers and stream splits in order to best achieve resilience.

Example 14 (from Colberg et al., 1988). For the nominal stream data of Example 13 (Table IX), synthesize a “practical” HEN structure which is as resilient as possible for uncertainties in the supply temperature and heat capacity flow rate of stream S_{h2} , based on “expected” uncertainties of $\Delta T_{h2}^S = \pm 10$ K and $\Delta w_{h2} = \pm 0.5$ kW/K. In other words, synthesize a HEN structure to achieve the class 1 FI target based on this expected uncertainty range. [Note that here we have specified the “expected” uncertainties to establish the relative sizes of the two uncertainties (i.e., to establish the aspect ratio of the rectangular expected uncertainty range), rather than to specify absolute sizes of the uncertainties for which to design].

Step 1. Calculate the class 1 FI target. The target was determined graphically in Example 13. The target, $F^* = 2.87$, is limited by a critical uncertainty point of $F^* \Delta T_{h2}^S = +28.7$ K, $F^* \Delta w_{h2} = +1.43$ kW/K (i.e., $T_{h2}^S = 428.7$ K after shifting to account for ΔT_m , and $w_{h2} = 7.43$ kW/K), and a critical constraint involving the appearance of a second pinch at the supply of stream S_{h2} (Fig. 17).

Step 2. Synthesize a HEN structure for the critical uncertainty point. Since the critical uncertainty point limits resilience, it is the uncertainty

point with the tightest design constraints (in this case due to the appearance of simultaneous pinches at S_{c2} and S_{h2}). Thus we synthesize for this point before considering the nominal stream data. A structure [obtained by the pinch design method (Linnhoff and Hindmarsh, 1983)] is shown in Fig. 19a. The four shaded exchangers are required to satisfy ΔT_m at the pinch caused by S_{c2} ; the blackened exchanger and heater are required to satisfy ΔT_m at the pinch caused by S_{h2} .

Step 3. Synthesize a HEN structure for the nominal stream data as similar as possible to the structure synthesized for the critical uncertainty point. Such a structure is shown in Fig. 19b. The shaded exchangers are required to satisfy ΔT_m at the pinch.

Step 4. Merge the two separate structures into a single structure. In this case, merging is trivial because of the strong similarity between the two designs; we merely add the heater on S_{c2} for the nominal structure to the structure synthesized for the critical uncertainty point. The resulting structure is shown in Fig. 19c.

Step 5. Test the resilience of the merged structure. (Before this test we only know that the merged structure is feasible for both the nominal stream data and the critical uncertainty point. We do not know yet if the structure is resilient throughout the desired uncertainty range.) The flexibility index of the merged HEN structure is 2.87. Thus the structure achieves the class 1 FI target and is resilient throughout the target uncertainty range.

Step 6. Try to reduce the number of units in the merged HEN structure (e.g., by loop-breaking; Su and Motard, 1984). The only loop in this structure is shown by the dashed lines in Fig. 19c. (Since the pinch caused by stream S_{c2} occurs for every point in the uncertainty range, we are not considering loops which straddle this pinch so that we can maintain minimum utility consumption throughout the uncertainty range.) Eliminating any unit in this loop except the match between streams S_{h2} and S_{c1} reduces the flexibility index to zero (i.e., the structure becomes infeasible even for nominal conditions); eliminating the S_{h2} - S_{c1} match reduces the flexibility index to 0.57. Thus no unit can be deleted from the merged HEN structure without a loss of resilience.

B. MULTIPERIOD HEN SYNTHESIS USING STRUCTURAL OPTIMIZATION

To automatically synthesize HENs operable ("resilient" without any constraint on energy recovery; see Section III,D) in a specified range of uncertain temperatures and flow rates, Floudas and Grossmann (1987b) have developed computer algorithms which iteratively synthesize a HEN, analyze its operability, and resynthesize a more operable HEN if neces-

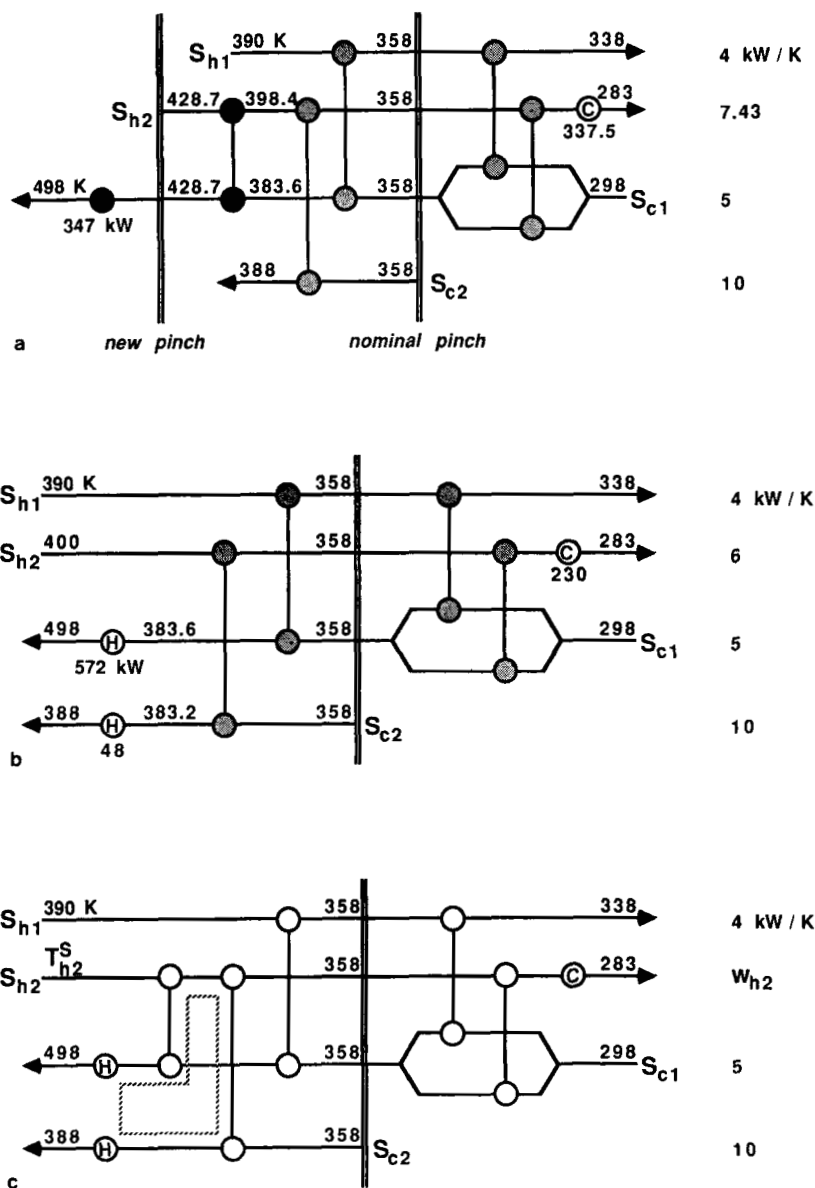


FIG. 19. HEN structures for Example 14: (a) Synthesized for critical uncertainty point, (b) synthesized for nominal stream data, and (c) merged structure which achieves the class 1 FI target.

sary. In particular, they have combined the multiperiod synthesis algorithm of Floudas and Grossmann (1986, 1987a) with special forms of the operability test and flexibility index (without the energy recovery constraint) reviewed earlier in this chapter. By requiring operability in the specified uncertainty range rather than strict resilience, Floudas and Grossmann (1987b) avoid the issue of class 1–class 2 problems. They also restrict their synthesis procedure to constant heat capacities.

The multiperiod synthesis algorithm of Floudas and Grossmann (1986, 1987a) generates HENs which are feasible for each of several periods of operation (i.e., for each of several critical points which may limit operability) and which have a minimum number of units, a minimum investment cost (given the predicted minimum number of units), and a minimum utility cost for each period. The multiperiod synthesis algorithm guarantees HEN feasibility (operability) only at the discrete periods of operation. The operability test (or the flexibility index without the energy recovery constraint) ensures that the HEN is operable throughout the entire uncertainty range. (Note that maximum energy recovery—minimum utility consumption—is also guaranteed only for the discrete periods of operation, and not for the entire uncertainty range.) If the HEN is not operable throughout the uncertainty range, then the critical point for operability (i.e., the combination of uncertain supply temperatures and flow rates where the HEN feasibility constraints are most violated) is added as a new period of operation, and the multiperiod synthesis algorithm is applied again to generate a more operable HEN.

The multiperiod synthesis–analysis–resynthesis algorithm is actually decomposed into two stages (Floudas and Grossmann, 1987b):

1. The stage of matches includes the following.
 - a. Synthesis: Predict a minimum set of stream matches, and the heat transferred in each match, which will lead to a minimum unit HEN feasible for each period of operation and which has minimum utility cost during each period (Floudas and Grossmann, 1986).
 - b. Analysis: Apply the active constraint strategy to the “operability³ test at the stage of matches” to determine whether the predicted set of matches can lead to an operable HEN.
 - c. Iteration: If the predicted set of matches can lead to an operable HEN, then proceed to stage 2. Otherwise, add the critical point for operability as a new period of operation and repeat stage 1.

³ Floudas and Grossmann (1987b) actually call this the *feasibility test at the stage of matches*. However, since Floudas and Grossmann do not include an energy recovery constraint, we are calling this the *operability test at the stage of matches* in order to remain consistent with the terminology of Saboo *et al.* (1987b).

2. The stage of structure includes the following.
 - a. Synthesis: Derive the HEN superstructure from the predicted set of stream matches. (The HEN superstructure consists of the predicted stream matches and mathematical "piping" connecting the matches in all possible series, parallel, and bypass combinations.) Optimize the superstructure to determine the actual structure and exchanger areas which minimize total investment cost⁴ (Floudas and Grossmann, 1987a).
 - b. Analysis: Apply the active constraint strategy to the "flexibility index at the stage of structure" to determine whether the actual HEN is operable.
 - c. Iteration: If the HEN is operable in the specified uncertainty range, then stop. Otherwise, add the critical point for operability as a new period of operation and repeat stage 2.

Decomposition of the multiperiod synthesis–analysis–resynthesis algorithm into these two stages is possible because any feasible (operable) set of matches predicted by the first stage can always be translated into a feasible (operable) HEN in the second stage (Floudas and Grossmann, 1987b). The operability test in stage 1 ensures that the set of matches can lead to an operable HEN. However, even if a set of matches does pass the operability test in stage 1, an operability test (or corresponding flexibility index) is still necessary in stage 2. This is because even though the operable set of matches can always be translated into an operable HEN, not all HENs translated from the set of matches will necessarily be operable; that is, operability of a HEN depends upon the details of its structure (the order in which the matches are connected) as well as upon the set of matches themselves.

The steps of the multiperiod synthesis–analysis–resynthesis algorithm can now be summarized as follows (Floudas and Grossmann, 1987b).

Step 1. Select a finite number of periods of operation (i.e., sets of values of the uncertain supply temperatures and flow rates). Typically, the nominal operating point is selected, as well as some combinations of upper and lower bounds on the uncertain variables [e.g., bounds corresponding to maximum heating, maximum cooling, maximum heat exchange, and maximum required heat transfer area, as suggested by Marselle *et al.* (1982)].

⁴ Note that the investment cost is minimized for a HEN superstructure with a fixed number of units (matches). If the number of units could vary, then the investment cost might be minimized even further.

Step 2. Formulate and solve the LP transshipment model of Papoulias and Grossmann (1983) for each period of operation to determine the minimum utility cost and pinch location for each period.

Step 3. Formulate and solve the multiperiod MILP transshipment model of Floudas and Grossmann (1986) to determine a minimum set of stream matches for feasible operation in all the periods and the heat transferred in each match in each period.

Step 4. Apply the operability test at the stage of matches (with the active constraint strategy). The form of this operability test is described in the next section. (a) If the set of matches cannot lead to an operable HEN, then add the critical point for operability as another period of operation and return to step 2. (b) If the set of matches can lead to a HEN operable in the specified uncertainty range, then go to step 5.

Step 5. Derive the multiperiod superstructure based upon the matches and heat transferred in each match predicted by the multiperiod MILP transshipment model. Formulate an NLP to optimize the superstructure (Floudas and Grossmann, 1987a) to give the HEN structure and exchanger sizes which minimize investment cost.

Step 6. Apply the active constraint strategy to the flexibility index (F) at the stage of structure (without the energy recovery constraint). The form of this flexibility index problem is described in a later section. (a) If $F \geq 1$, then the HEN is operable in the specified uncertainty range. Stop. (b) If $F < 1$, then add the critical point for operability as another period of operation and return to step 5.

1. *Operability Test at the Stage of Matches*

The operability test (resilience test in Section III,A,2, but without the energy recovery constraint) is applied at the stage of matches to determine whether the predicted stream matches can lead to an operable HEN. The general form of this operability test is

$$\chi(d) = \max_{\theta \in \Theta} \psi(d, \theta) \quad (39)$$

where $\psi(d, \theta)$ is determined by the LP

$$\psi(d, \theta) = \min_{z, \beta} \quad (40)$$

subject to:

Equality constraints

(A1) Energy balances on each hot process and utility stream in each "temperature interval" (TI) of the multiperiod MILP transshipment model. Each energy balance involves the "residuals" (heat cascaded) to and from the TI and the heat transferred in each stream match in the TI.

- (A2) Energy balances on each cold process and utility stream in each TI.
- (A3) Zero residual to the hottest TI and from the coldest TI.

Inequality constraints

- (B1) Residuals of $-\beta$ or more
- (B2) Heat loads in each stream match of $-\beta$ or more

where θ contains the uncertain supply temperatures and flow rates and z the control variables. Note that ΔT_m will automatically be satisfied if all the residuals are nonnegative (because of the way the TIs are defined). The matches lead to an operable HEN if and only if $\chi \leq 0$. Floudas and Grossmann (1987b) give the specific form of the constraints in this operability test. The constraints are nonlinear in general; however, they are linear for fixed values of the uncertain supply temperatures and flow rates.

Floudas and Grossmann (1987b) show that the solution (critical point) of problem (39) must be a corner point of the uncertainty range. Thus operability test (39) can be simplified to

$$\chi(d) = \max_{l \in L_v} \psi(d, \theta^l) \quad (41)$$

where $\psi(d, \theta^l)$ is calculated at corner point θ^l of the uncertainty range and L_v is the index set of all the corner points. Problem (41) can be solved by a series of LPs (40) for $\psi(d, \theta^l)$, one at each corner point of the uncertainty range. Alternatively, to avoid exhaustive evaluation of all the corner points, the active constraint strategy can be applied directly to operability test (39).

2. Flexibility Index at the Stage of Structure

The flexibility index at the stage of structure ensures that the HEN translated from the operable matches is itself operable in the specified uncertainty range. A yes-no operability test at the stage of structure could be used to ensure operability of the HEN. Instead, Floudas and Grossmann (1987b) choose to use the more general flexibility index (as reviewed in Section III,A,3, but without the energy recovery constraint) since it also provides information on the largest scaled uncertainty range in which the HEN remains operable.

The general form of the flexibility index at the stage of structure (without the energy recovery constraint) is

$$F(d) = \max_s \quad (42)$$

subject to

$$h(d, z, \theta) = 0$$

$$\max_{\theta \in \Theta(s)} \min_z \max_{m \in M} g_m(d, z, \theta) \leq 0$$

$$\Theta(s) = \{\theta \mid \theta^N - s \Delta\theta^- \leq \theta \leq \theta^N + s \Delta\theta^+\}, \quad s \geq 0$$

where equality constraints $h(d, z, \theta)$ consist of

- (A1) Mass balances for each splitter
- (A2) Mass balances for each mixer
- (A3) Energy balances for each mixer
- (A4) Energy balances for each exchanger
- (A5) Area constraints for each exchanger without bypass

and inequality constraints $g(d, z, \theta)$ consist of

- (B1) Area constraints for each exchanger with bypass
- (B2) ΔT_m constraints for each exchanger
- (B3) Nonnegative loads for each exchanger, heater, and cooler
- (B4) Nonnegative flow rates

Floudas and Grossmann (1987b) give the specific form of these constraints. The energy balance and area constraints are, in general, nonlinear.

The critical point for the flexibility index is, in general, not a corner point of the uncertainty range (e.g., see Section III,C,2 on stream splits or Section III,C,3 on flow rate uncertainties). Thus, Floudas and Grossmann (1987b) use the active constraint strategy to solve problem (42). Floudas and Grossmann (1987b) show that the active constraint strategy applied to the flexibility index at the stage of structure has a single local optimum if area constraints (A5) and (B1) are excluded. When the area constraints are included, the active constraint strategy may have multiple local optima.

Example 15 (from Floudas and Grossmann, 1987b). A HEN is to be designed for the nominal stream data shown in Table X. Due to changes in the process feedstocks, an uncertainty range is defined for the flow rates (i.e., ± 0.4 kW/K of the nominal point) and supply temperatures of hot

TABLE X
NOMINAL STREAM CONDITIONS FOR EXAMPLE 15

Stream	w (kW/K)	T^S (K)	T^T (K)
S_{h1}	1.4	583	323
S_{h2}	2	723	553
S_{c1}	3	313	393
S_{c2}	2	388	553

stream S_{h1} (± 10 K) and cold stream S_{c2} (± 5 K). The objective is to design a HEN which is operable for the specified uncertainty range and which features the minimum investment cost, fewest number of units, and minimum utility cost.

Suppose that only two periods of operation are considered in the first iteration of the synthesis procedure. The selected periods correspond to (1) maximum total heat exchange (i.e., w_{h1}^U , w_{c2}^U , T_{h1}^U , T_{c2}^L , and (2) maximum cooling (i.e., w_{h1}^U , w_{c2}^L , T_{h1}^U , T_{c2}^U). Solving the LP transshipment model for each period with a specified ΔT_m of 10 K yields

Period 1	Period 2
$H_{\min} = 0$	$H_{\min} = 0$
$C_{\min} = 178$ kW	$C_{\min} = 330$ kW
No pinch	No pinch

By formulating and solving the multiperiod MILP transshipment model for these two periods of operation, the following set of matches is identified:

$$S_{h1}-S_{c2}, \quad S_{h2}-S_{c1}, \quad S_{h2}-S_{c2}, \quad S_{h1}-CW$$

where CW denotes cooling water. The solution of this model was obtained by using the computer code LINDO (Schrage, 1981) and required 2.4 sec (DEC-20). By applying the operability test at the stage of matches and solving LP (40) at each of the 16 corner points, the operability measure was found to be $\chi(d) = 128$. This solution was obtained by using the computer code LINDO in 20.5 sec. Positive $\chi(d)$ implies that the preceding selection of matches cannot result in an actual operable network.

The critical uncertainty point for $\chi(d) = 128$ is introduced (i.e., w_{h1}^L , w_{c2}^L , T_{h1}^L , T_{c2}^U) as a third period of operation, which in fact corresponds to the condition of maximum heating. This third period features utility loads of $H_{\min} = 58$ kW and $C_{\min} = 0$, with no pinch point. Then by formulating and solving the multiperiod MILP transshipment model for the three periods of operation, the following set of matches is predicted:

$$H-S_{c2}, \quad S_{h1}-S_{c1}, \quad S_{h1}-S_{c2}, \quad S_{h2}-S_{c2}, \quad S_{h2}-CW$$

where H denotes steam. This solution was obtained by using the computer code LINDO in 2.76 sec. The corresponding heat exchanged at each match is shown in Table XI. By applying the operability test in the stage of matches, it was found that $\chi(d) = 0$. This required the solution of LP (40) at each of 16 corner points (21 sec). Since the operability measure $\chi(d)$ is zero, this implies that the preceding selection of matches predicted by the multiperiod MILP transshipment model can result in an operable HEN.

TABLE XI
MATCHES AND HEAT EXCHANGED IN EACH OPERATING PERIOD IN EXAMPLE 15

Unit	Match	Heat exchanged (kW)		
		Period 1	Period 2	Period 3
1	H-S _{c2}	0	0	58
2	S _{h1} -S _{c1}	240	240	240
3	S _{h1} -S _{c2}	246	246	10
4	S _{h2} -S _{c2}	162	10	340
5	S _{h2} -CW	178	330	0

To automatically determine the network structure that is feasible for these three periods of operation and that features minimum investment cost, as well as minimum utility cost for each period, the automatic synthesis approach for multiperiod networks by Floudas and Grossmann (1987a) is utilized. The value of ΔT_m was relaxed to 1 K for this design stage. In the first step of this approach, the multiperiod superstructure is derived by using the five predicted matches. Then by formulating the superstructure as an NLP and using the values of the overall heat transfer coefficients and cost data shown in Table XII, the resulting NLP is solved by using the computer code MINOS/AUGMENTED (Murtagh and Saunders, 1981). This NLP features 108 variables, 57 nonlinear constraints, and 60 linear constraints. The CPU time for solving this NLP was 24.8 sec.

TABLE XII
OVERALL HEAT TRANSFER COEFFICIENTS AND
COST DATA FOR EXAMPLE 15^a

Match	U_{ij} (kW/m ² K)	A_{ij} (m ²)
H-S _{c2}	0.08	23.77
S _{h1} -S _{c1}	0.08	103.83
S _{h1} -S _{c2}	0.08	56.583
S _{h2} -S _{c2}	0.08	23.315
S _{h2} -CW	0.08	13.013

^a $C_{ij} = 4333A_{ij}^{0.6}$ (\$), A in m². Steam cost (573 K): 171.428×10^{-4} (\$/kW hour). Cooling water cost (303–323 K): 60.576×10^{-4} (\$/kW hour)

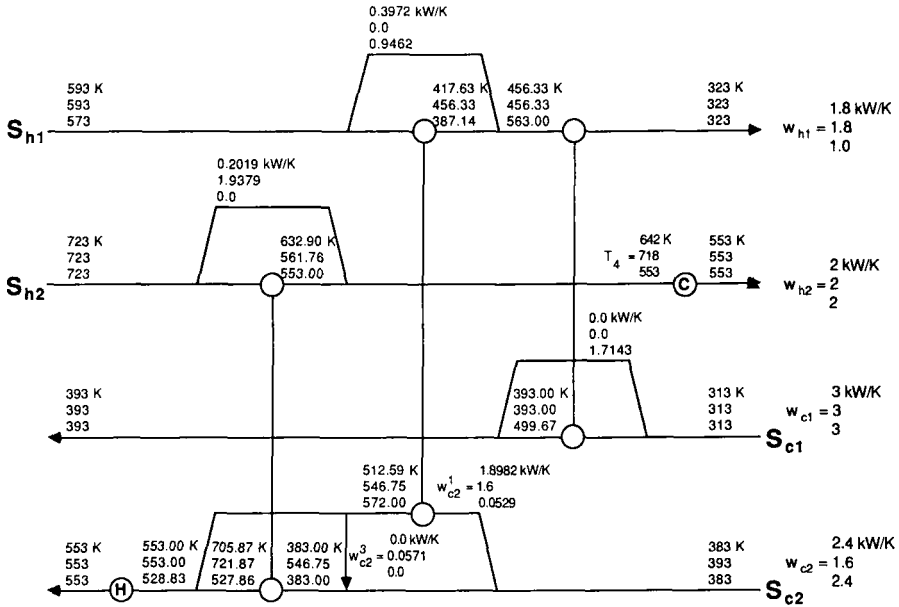


FIG. 20. Operable HEN synthesized for Example 15.

The solution of this optimization problem provides the HEN shown in Fig. 20, where flow rates and temperatures are listed for the three operating periods. The areas of the heat exchangers are given in Table XII. Notice that there is splitting of cold stream S_{c2} into two branches. Bypasses are also involved in stream S_{c1} (match S_{h1} – S_{c1}), stream S_{h1} (match S_{h1} – S_{c2}), and stream S_{h2} (match S_{h2} – S_{c2}). This network, which is feasible for the three operating periods that are considered, features a minimum investment cost of \$196,900 and a minimum utility cost of \$1.078/hour for operating period 1, \$1.999/hour for period 2, and \$0.9943/hour for period 3.

To test for operability of the HEN in the specified uncertainty range, the active constraint strategy is applied to the flexibility index at the stage of structure (without the energy recovery constraint). First, constraints (A1)–(A5) and (B1)–(B4) are developed for this network. Since there are nine equations and 12 unknowns, there exist three control variables which have been selected to be $z_1 = w_{c2}^1$, $z_2 = w_{c2}^3$, $z_3 = T_4$ (see Fig. 20). Using the information from the gradients of the feasibility constraints with respect to the control variables, four active sets of constraints are identified. Then, solving an NLP for each active set of constraints, it was found

that the flexibility index is $F = 1$, which implies that the network configuration derived in the preceding step is not only economical and energy efficient, but also operable for the full uncertainty range. The solution of the four NLPs required 22.4 sec. Hence, the total computer time that was required to solve this problem was 94 sec.

C. HEN SYNTHESIS USING "DOWNSTREAM (DISTURBANCE) PATHS"

Kotjabasakis and Linnhoff (1986) introduced the concept of "downstream (disturbance) paths" for synthesis of resilient HENs (or more general processes). This simple concept provides an excellent physical understanding of structural HEN resilience. It also can be used to study the qualitative effects of varying an uncertain parameter (e.g., a supply temperature and/or flow rate) upon specified fixed parameters (e.g., target temperatures) and to suggest design changes to eliminate or counteract these effects early in the structural design stage. The concept of downstream paths is best illustrated by example.

Example 16 (from Linnhoff and Kotjabasakis, 1986). Consider the HEN structure in Fig. 21. Based on a physical understanding of the HEN structure and without the need to solve any linear programs, we wish to investigate two questions. (1) Will varying a specified uncertain supply temperature and/or flow rate affect a given fixed target temperature? (2) What design changes might be used to eliminate these effects?

In the HEN structure in Fig. 21, all the streams except S_{c1} have heaters or coolers which can be used to control their target temperatures (though extra utility may be required to do so). Thus in this example we will concentrate on maintaining the target temperature of stream S_{c1} .

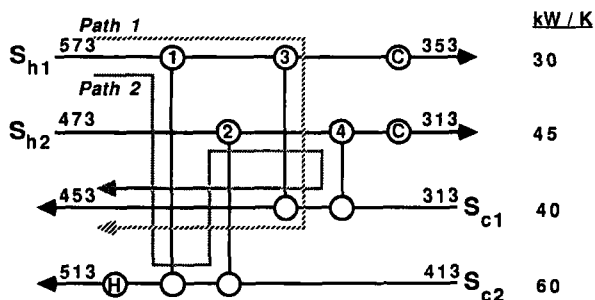


FIG. 21. Two paths from T_{h1}^S to T_{c1}^T , (1) Completely downstream and (2) partially upstream.

Consider the effect of varying T_{h1}^S upon T_{c1}^T . Figure 21 shows two "paths" from the supply of S_{h1} to the target of S_{c1} . A "path" is an unbroken connection between any two points in the HEN grid diagram. It seems obvious that a varying supply temperature or flow rate can affect a (fixed) target temperature only if they are physically connected by a "path" through streams and heat exchangers. Path 1 in Fig. 21 carries a change in T_{h1}^S downstream along S_{h1} , through exchanger 3, and downstream along S_{c1} . Path 2 carries the change downstream along S_{h1} , through exchanger 1, and *upstream* S_{c2} . However, the effect of a changing supply temperature or flow rate *cannot* travel upstream. Thus a changing supply temperature or flow rate can affect a (fixed) target temperature only if there is a path connecting the two which is completely downstream.

Now consider the effect of varying T_{c2}^S upon (fixed) T_{c1}^T . Figure 22a shows two completely downstream paths between T_{c2}^S and T_{c1}^T . We wish to consider possible design changes which can eliminate the effect of varying T_{c2}^S upon T_{c1}^T .

(1) *Break downstream path.* If the ΔT_m (or area) and load constraints of the remaining exchangers allow it, removing exchanger 3 will break path 1 between T_{c2}^S and T_{c1}^T , as shown in Fig. 22b.

(2) *Insert upstream element.* If the ΔT_m (or area) and load constraints allow it, exchangers 2 and 4 can be interchanged to block path 2, as shown in Fig. 22c. Here we have inserted exchanger 4 *upstream* of exchanger 2. If the changes in Figs. 22b and 22c are possible, then we can eliminate the effect of varying T_{c2}^S upon (fixed) T_{c1}^T *without* the need for any overdesign.

(3) *Apply manipulation.* If ΔT_m (or area) and load constraints do not allow the changes in Figs. 22b and 22c, then manipulation (of an exchanger bypass) might be used to counteract the effect of changing T_{c2}^S upon (fixed) T_{c1}^T . Figure 23 shows that there are downstream paths from all four exchangers to the target of stream S_{c1} . Thus a bypass around any one of the four exchangers can be used to counteract the effect of changing T_{c2}^S upon T_{c1}^T . Of course the effect of manipulating the chosen bypass upon the other target temperatures must also be considered.

In the previous example, several design changes were considered in order to eliminate or counteract the effect of a changing supply temperature upon a fixed target temperature. The best choice of design change depends on trade-offs between capital and energy costs; that is, removing exchanger 3 to give Fig. 22b might require adding area to the other exchangers and/or increasing heating and cooling, while the changes in Fig. 23 (adding an exchanger bypass) require adding area.

Kotjabasakis and Linnhoff (1986) demonstrate the use of sensitivity tables for a quick (but qualitative) means of evaluating these trade-offs and

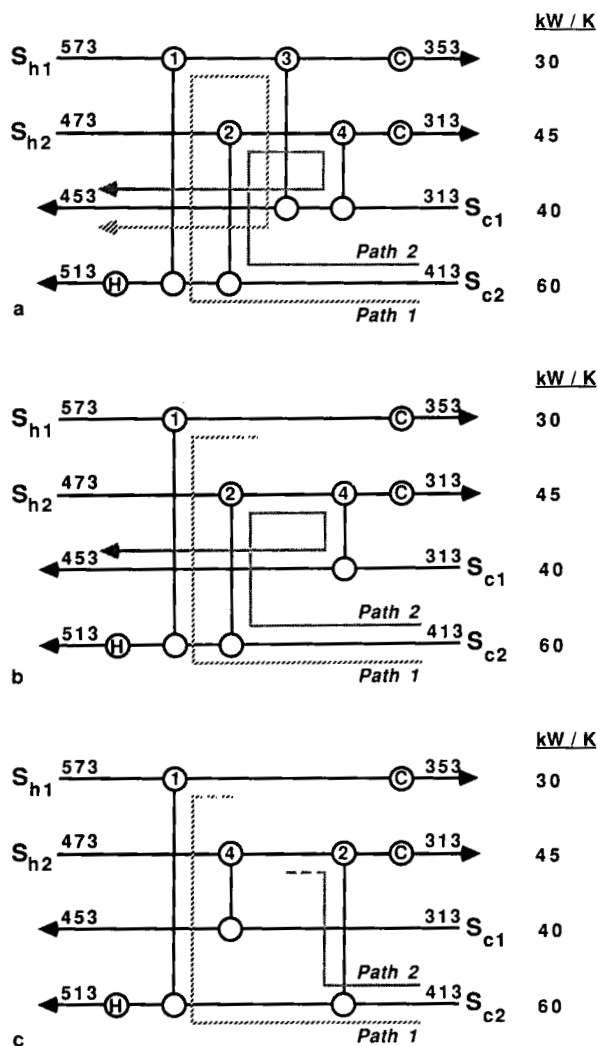


FIG. 22. Two design changes to block downstream paths. (a) Original design, (b) remove exchanger 3 to break path 1, and (c) insert exchanger 4 upstream of exchanger 2 to block path 2.

eliminating obviously expensive design choices. However, these sensitivity tables do not consider the nonlinearity of area (capital cost) as a function of the uncertain supply temperatures and flow rates, and they do not consider interactions between two simultaneously varying supply temperatures or between two paths connecting the same supply and target temperatures.

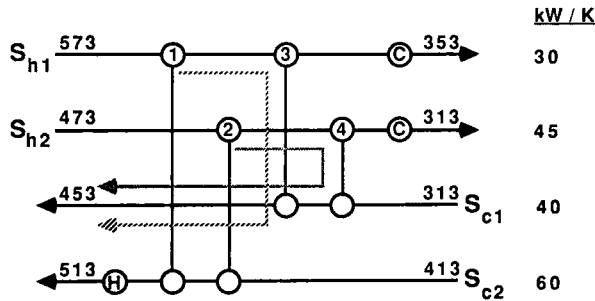


FIG. 23. Downstream paths from all four exchangers allow manipulation of T_{cl}^T .

Thus simulation (e.g., the feasibility test in Section III,A,1 with area constraints replacing the ΔT_m constraints) and costing should be used to evaluate the final design choices.

In addition, the sensitivity tables do not consider the inherent nonlinearity of the HEN resilience problem. Thus while the use of downstream paths and sensitivity tables may guarantee feasible HEN operation for specified discrete values of supply temperatures and flow rates, they do not guarantee feasible HEN operation for intermediate supply temperatures and flow rates [unless *all* paths between varying and fixed parameters have been blocked, as in Fig. 22b, or unless the assumptions of the corner point theorem (Section III,B,1) are satisfied]. More rigorous testing (e.g., using one of the techniques discussed in Section III) may be necessary to guarantee resilience for intermediate supply temperatures and flow rates.

D. SUMMARY OF RESILIENT HEN SYNTHESIS PROCEDURES; AREAS FOR FUTURE RESEARCH

Three methods for synthesis of HENs which are economically optimal and resilient have been reviewed in this chapter: (1) synthesis of HEN structure based on a class 1 flexibility index (FI) target (Colberg *et al.*, 1988); (2) synthesis of HEN structure and design (sizing) of individual exchangers using mixed-integer optimization algorithms for multiperiod operation (Floudas and Grossmann, 1987b); and (3) synthesis of HEN structure based on "downstream (disturbance) paths" (Linnhoff and Kotjabasakis, 1986).

The class 1 FI target is the flexibility index of the largest possible class 1 uncertainty range for given nominal stream data. For simple problems it can be calculated by trial-and-error plotting of the composite curves. For larger problems, or problems with correlated uncertainties, the target can be calculated with a NLP (Colberg *et al.*, 1988).

The class 1 FI target serves two important uses during synthesis of resilient HENs.

1. The size of the target (relative to 1) tells the designer if the expected uncertainty range is class 1 or class 2, and thus whether trade-offs must be made to achieve resilience in the expected uncertainty range.

2. Calculation of the target identifies the critical uncertainty point and constraint most likely to limit resilience.

Use of the class 1 FI target as a HEN synthesis tool offers a number of attractive features.

1. Knowledge of the critical uncertainty point and constraint allows the designer to strategically place exchangers and stream splits where they will most improve resilience. This feature tends to minimize the number of synthesis-analysis iterations required to achieve a resilient HEN.

2. The class 1 FI target can be used to predict the trade-off between a *constant* value of ΔT_m and resilience, and energy and resilience (Colberg *et al.*, 1988).

3. The target attempts to consider economics, albeit indirectly (Colberg *et al.*, 1988). It indirectly limits the number of exchangers (by limiting the target to class 1 uncertainty ranges), and places bounds on utility consumption and network area (implicitly through use of the composite curves, or by constraints in the NLP).

The class 1 FI target also suffers a few disadvantages.

1. It is limited to class 1 problems.

2. It cannot handle uncertain heat transfer coefficients.

3. Although the FI target can consider ΔT_m varying as a function of uncertain supply temperatures and flow rates (e.g., by using the *nominal* energy, area, and units targets to predict an economic optimum ΔT_m), this dependence must be specified *before* plotting any composite curves or solving the NLP. Thus the trade-off between cost and resilience is not accurately considered (i.e., ΔT_m should reflect the cost of overdesign to achieve resilience as well as the cost of energy, units, and area for nominal operating conditions).

The second synthesis procedure reviewed in this chapter, based on mixed-integer optimization, iteratively synthesizes a HEN, analyzes its operability, and resynthesizes a more operable HEN if necessary (Floudas and Grossmann, 1987b). In particular, this procedure combines the multi-period, mixed-integer synthesis algorithm of Floudas and Grossmann (1986, 1987a) with specific forms of the operability test at the stage of matches

and flexibility index at the stage of structure (with active constraint strategy) developed by Floudas and Grossmann (1987b).

The synthesis procedure of Floudas and Grossmann (1987b) is one of the most powerful in the open literature for solving practical HEN synthesis problems and has a number of attractive features.

1. It synthesizes a HEN which is resilient *and* which has the minimum number of units required for resilience, minimum investment cost, and minimum utility cost for each period of operation.

2. It not only synthesizes the HEN structure, but also designs (sizes) the individual exchangers.

3. It synthesizes and designs the HEN automatically from given stream and cost data.

4. By decomposing the synthesis problem into the "stage of matches" and the "stage of structure," the synthesis procedure can handle large problems with reasonable computational effort.

However, these same features also have the following drawbacks.

1. Although HENs with reasonable cost should be obtained by separately minimizing energy cost, number of units, and investment cost, this procedure does not necessarily minimize total cost. In particular, the choice of ΔT_m for energy targeting and for predicting the stream matches is not optimized to consider the trade-off between energy and capital costs (as in Ahmad and Linnhoff, 1984). Even more important, different values of ΔT_m will generally be optimal for different periods of operation in the synthesis procedure. Also, investment cost is minimized only for a fixed set of matches.

2. By decomposing the HEN synthesis problem into the stages of matches and structure, this procedure might make it difficult for the designer to directly influence the shape of the synthesized network (i.e., how should the stage of matches be influenced in order to achieve a desired change at the stage of structure?). For example, this procedure does not seem to allow the designer to easily constrain stream splitting (like Saboo *et al.*, 1986) and might be difficult to apply in revamp synthesis.

3. The synthesis procedure guarantees minimum energy cost only for the discrete periods of operation considered, and not for the whole uncertainty range (especially for class 2 problems).

4. The analysis portion of the procedure is limited to constant heat capacities.

The concept of "downstream (disturbance) paths" (Linnhoff and Kotjabasakis, 1986) is a simple and intuitively appealing tool for evolutionary synthesis of resilient HENs. It can be used to identify the qualitative effects of varying uncertain supply temperatures and flow rates upon (fixed) target

temperatures, and to identify potential design changes to eliminate or counteract these effects. The qualitative use of downstream paths has several attractive features.

1. It is simple (no calculations required).
2. It provides great physical insight into the structural resilience of a HEN.

However, the quantitative use of downstream paths suffers several disadvantages.

1. It is difficult to consider interactions among two or more supply temperatures or flow rates changing simultaneously.
2. It is difficult to consider interactions among two or more paths between the same supply temperature (or flow rate) and target temperature.
3. It is difficult to consider nonlinear effects on HEN resilience.

These disadvantages are apparent in the use of sensitivity tables (Kotjabasakis and Linnhoff, 1986) combined with downstream paths.

In addition, both the FI target-based synthesis procedure and the multiperiod synthesis procedure suffer from the fact that they synthesize a HEN for a *specified* uncertainty range and cannot directly consider the trade-off between resilience and total HEN cost. At present, the best way of evaluating this trade-off with these methods is to synthesize HENs for several different sizes of the uncertainty range and then to compare the HENs. The downstream path method (combined with sensitivity tables) evaluates this trade-off much more easily and directly (subject to the quantitative limitations discussed above).

The class 1 FI target (Colberg *et al.*, 1988) combined with the pinch design method (Linnhoff *et al.*, 1982; Linnhoff and Hindmarsh, 1983) for synthesis of an initial HEN, and the use of downstream paths (Linnhoff and Kotjabasakis, 1986) to improve resilience (or reduce cost), yields a very flexible synthesis method with great physical insight into structural HEN resilience (both through the use of downstream paths and knowledge of the critical uncertainty point and constraint). This combined method allows the designer to evaluate trade-offs between capital and energy, but can be difficult to apply to problems with many streams or where several or dissimilar designs must be merged (Example 14). The multiperiod synthesis-analysis-resynthesis algorithm of Floudas and Grossmann (1987b) is easy to apply even to large problems with many critical uncertainty points (periods of operation), but cannot directly evaluate trade-offs between capital and energy (unless one iterates ΔT_m), and is not flexible enough to allow the designer to influence the synthesized HEN (e.g., to constrain

stream splitting or to perform revamp synthesis). The "ideal" algorithm for resilient HEN synthesis should combine the desirable features of both of these algorithms. Possible areas of research to develop a more ideal synthesis algorithm include the following.

1. Develop methods for predicting energy–capital–resilience trade-offs by use of the energy, units, area, and FI targets. In particular, develop an area target which considers the total *installed* HEN area required for resilience, including the area which might be bypassed for nominal stream conditions.

2. In the multiperiod synthesis–analysis–resynthesis algorithm of Floudas and Grossmann (1987b), minimize the total HEN cost rather than separately minimizing energy and capital costs. This can be accomplished at least at the stage of structure by treating utility loads and loads of the stream matches as variables in the superstructure, rather than as constants predicted by the LP transshipment model (Papoulias and Grossmann, 1983) and the multiperiod MILP transshipment model (Floudas and Grossmann, 1986).

3. In order to properly consider the trade-offs between capital, energy, and resilience at the stage of matches, investigate the "optimum" choice of ΔT_m . Actually, in an ideal synthesis algorithm, these trade-offs should be evaluated directly and not by means of a possibly artificially chosen value of ΔT_m .

4. In order to make the multiperiod synthesis–analysis–resynthesis algorithm more flexible (and to extend it later to revamp synthesis), investigate how to constrain stream splitting.

5. Extend the multiperiod synthesis–analysis–resynthesis algorithm to handle temperature-dependent heat capacities and phase change and uncertain heat transfer coefficients.

Nomenclature

- | | |
|---|--|
| a Constant used in stream split constraint (27) ⁵ or constant used in ΔT_m constraint with uncertain flow rates (30) | B Matrix used in general form of energy balance constraint (5) |
| A Matrix used in general form of energy balance constraint (5) | c Constant used in stream split constraint (27) or constant used in ΔT_m constraint with uncertain flow rates (30) |
| b Vector used in general form of energy balance constraint (5) | c_p Heat capacity, kJ/kg K |

⁵ Numbers in parentheses refer to the first equation in which a symbol is used.

- C Matrix used in general form of ΔT_m constraint (5)
 C_{\min} Minimum cooling requirement, kW
 d Vector of design variables (1)
 D Matrix used in general form of ΔT_m constraint (5)
 e Vector of ones, $[1 \ 1 \ \cdots \ 1 \ 1]^T$ (5)
 E Matrix used in general form of load constraint (5)
 f Vector of reduced inequality constraints (2)
 F Flexibility index, dimensionless (10)
 g_{ij} Constraint on split fraction of branch j on stream i (27) or ΔT_m constraint on exchanger connected to streams S_i and S_j with uncertain flow rates (30)
 G Matrix used in general form of load constraint (5)
 h Vector of equality constraints (1)
 H Minimum heating requirement, kW (5)
 I Identity matrix
 k Upper bound on slack variables η (21)
 k_L Upper bound on slack variables γ_L and σ_L (25)
 k_T Upper bound on slack variables γ_T and σ_T (25)
 I^H Vector of heater loads, kW (5)
 L Matrix used to define integer variables m (24)
 L_L Matrix used to define integer variables m_L (26)
 L_T Matrix used to define integer variables m_T (26)
 m Integer variables determining in which exchanger each temperature breakpoint occurs (21)
 m_L Integer variables used in equality form of load constraint with temperature breakpoints (26)
 m_T Integer variables used in equality form of ΔT_m constraint with temperature breakpoints (25)
 M Index set for reduced inequality constraints (2)
 M_A Index set for active reduced inequality constraints (34)
 n_A Number of potential sets of active constraints M_A
 n_f Number of reduced inequality constraints f
 n_z Number of control variables (degrees of freedom) z
 n_θ Number of uncertain variables θ
 N Matrix used in general form of energy balance constraint with temperature breakpoints (24)
 O Matrix used in general form of ΔT_m constraint with temperature breakpoints (24)
 p Vector used in general form of ΔT_m constraint (5)
 P Polytope region defined by resilience index
 r Vector used in general form of load constraint (5)
 R Region for feasible operation of a HEN
 RI Resilience index, kW (16)
 s Scale factor for family of hyperrectangles used to define the flexibility index, dimensionless (10)
 t Vector of temperatures
 T Temperature, K
 u_{ij} Split fraction of branch j on stream i , dimensionless
 U Heat transfer coefficient, kW/m² K
 v Vector of state and control variables $[r^I, I^H]$ (5)
 v_k k th load or ΔT_m constraint function not depending on any stream split fractions (28) or load constraint function for exchanger k with uncertain flow rates (31)
 w_i Heat capacity flow rate of stream S_i , kW/K
 x Vector of state variables
 z Vector of control variables (degrees of freedom) (1)

Greek Letters

- α Factor by which to relax minimum heating target, dimensionless (5)
 β Slack variable for measuring worst violation of feasibility constraints (4)

γ_L	Load violation, kW (26)		
γ_T	ΔT_m violation, K (25)		
δl	Supply temperature uncertainty expressed in terms of load, kW (19)		
δT	Uncertainty in (supply) temperature, K (19)		
$\delta \theta$	Uncertainty (in any uncertain variable) (17)		
ΔT	Approach temperature, K		
ΔT_m	Minimum approach temperature allowed in a HEN, K		
ΔT_s	Smallest approach temperature actually occurring in a HEN, K		
$\Delta \theta$	Expected uncertainty (in any uncertain variable) (12)		
η	Slack variables for determining in which exchangers each temperature breakpoint occurs, K ((21)		
θ	Vector of uncertain variables (supply temperatures, flow rates, and/or heat transfer coefficients)		
Θ	Hyperrectangular uncertainty range		
λ	Kuhn-Tucker multiplier (35)		
ξ	Kuhn-Tucker slack variables (35)		
σ_L	Load surplus, kW (26)		
σ_T	ΔT_m surplus, K (25)		
χ	Resilience measure (6)		
ψ	Feasibility measure (3)		
		<i>Subscripts</i>	
		BR	Breakpoint (discontinuity in piecewise constant heat capacity)
		i	Stream index
		j	Stream index
		k	Exchanger (or heater) index
		l	Uncertainty direction (along a single stream)
		L	Load constraint
		m	Index for reduced inequality constraints
		<i>Superscripts</i>	
		C	Critical (uncertainty point)
		H	Heater (load)
		I	Intermediate (stream temperature)
		l	Uncertainty direction (toward a vertex of the uncertainty range)
		L	Lower bound (on uncertain variable)
		N	Nominal (value of uncertain variable)
		S	Supply (temperature)
		T	Target (temperature)
		U	Upper bound (on uncertain variable)
		+	Positive uncertainty direction
		-	Negative uncertainty direction

References

- Ahmad, S., and Linnhoff, B., Overall cost targets for heat exchanger networks. *ICHEME Annu. Rese. Meet.*, Bath, Apr. (1984).
- Colberg, R. D., Morari, M., and Townsend, D. W., A resilience target for heat exchanger network synthesis. *Comp. Chem. Eng.*, in press (1988).
- Duran, M. A., and Grossmann, I. E., A mixed-integer nonlinear programming algorithm for process systems synthesis. *AIChE J.* **32**, 592 (1986).
- Floudas, C. A., and Grossmann, I. E., Automatic generation of multiperiod heat exchanger network configurations. *Comp. Chem. Eng.* **11**, 123 (1987a).
- Floudas, C. A., and Grossmann, I. E., Synthesis of flexible heat exchanger networks for multiperiod operation. *Comp. Chem. Eng.* **10**, 153 (1986).
- Floudas, C. A., and Grossmann, I. E., Synthesis of flexible heat exchanger networks with uncertain flowrates and temperatures. *Comp. Chem. Eng.* **11**, 319 (1987b).
- Floudas, C. A., Ciric, A. R., and Grossmann, I. E., Automatic synthesis of optimum heat exchanger network configurations. *AIChE J.* **32**, 276 (1986).

- Grossmann, I. E., and Floudas, C. A., Active constraint strategy for flexibility analysis in chemical processes. *Comp. Chem. Eng.* **11**, 675 (1987).
- Grossmann, I. E., and Floudas, C. A., A new approach for evaluating flexibility in chemical process design. *Proc. Process Syst. Eng. PSE '85, Cambridge, IChemE Symp. Ser.* **92**, 619 (1985). *Process Syst. Eng.* (1985b).
- Grossmann, I. E., and Morari, M., Operability, resiliency and flexibility—process design objectives for a changing world. *Int. Conf. Found. Computer-Aided Process Design, 2nd, Snowmass, CO* (1983).
- Grossmann, I. E., Halemane, K. P., and Swaney, R. E., Optimization strategies for flexible chemical processes. *Comp. Chem. Eng.* **7**, 439 (1983).
- Halemane, K. P., and Grossmann, I. E., Optimal process design under uncertainty. *AIChE J.* **29**, 425 (1983).
- Hohmann, E. C., Optimum networks for heat exchange. Ph.D. thesis, Univ. of So. Calif. (1971).
- Kotjabasakis, E., and Linnhoff, B., Sensitivity tables for the design of flexible processes (1)—How much contingency in heat exchanger networks is cost effective? *Chem. Eng. Res. Des.* **64** (1986).
- Linnhoff, B., and Flower, J. R., Synthesis of heat exchanger networks: I. Systematic generation of energy optimal networks. *AIChE J.* **24**, 633 (1978).
- Linnhoff, B., and Hindmarsh, E., The pinch design method for heat exchanger networks. *Chem. Eng. Sci.* **38**, 745 (1983).
- Linnhoff, B., and Kotjabasakis, E., Downstream paths for operable process design. *Chem. Eng. Prog.* **82** (5), 23 (1986).
- Linnhoff, B., Mason, D. R., and Wardle I., Understanding heat exchanger networks. *Comp. Chem. Eng.* **3**, 295 (1979).
- Linnhoff, B., Townsend D. W., Boland, D., Hewitt, G. F., Thomas, B. E. A., Guy, A. R., and Marsland R. H., "A User Guide on Process Integration for the Efficient Use of Energy," IChemE, available from Pergamon, Oxford, 1982.
- Marselle, D. F., Morari, M., and Rudd, D. F., Design of resilient processing plants—II. Design and control of energy management systems. *Chem. Eng. Sci.* **37**, 259 (1982).
- Morari, M., Grimm, W., Oglesby, M. J., and Prosser, I. D., Prosser, Design of resilient processing plants—VII. Design of energy management system for unstable reactors—new insights. *Chem. Eng. Sci.* **40**, 187 (1985).
- Murtagh, B. A., and Saunders, M. A., A projected Lagrangian algorithm and its implementation for sparse nonlinear constraints, and MINOS/AUGMENTED user's manual, Technical Reports SOL 80-1R and SOL 80-14, Systems Optimization Laboratory, Dept. of Operations Research, Stanford Univ., CA (1981).
- Nishida, N., Stephanopoulos, G., and Westerberg, A. W., A review of process synthesis. *AIChE J.* **27**, 321 (1981).
- Papoulias, S. A., and Grossmann, I. E., A structural optimization approach in process synthesis. II: Heat recovery networks. *Comp. Chem. Eng.* **7**, 707 (1983).
- Raghavan, S., Heat exchanger network synthesis: a thermodynamic approach. Ph.D. thesis, Purdue Univ. (1977).
- Saboo, A. K., Synthesis and analysis of resilient heat exchanger networks. Ph.D. thesis, Univ. of Wisc., Madison (1984).
- Saboo, A. K., and Morari, M., Design of resilient processing plants—IV. Some new results on heat exchanger network synthesis. *Chem. Eng. Sci.* **39**, 579 (1984).
- Saboo, A. K., Morari, M., and Colberg, R. D., Resilience analysis of heat exchanger networks—Part I: Temperature dependent heat capacities. *Comp. Chem. Eng.*, **11**, 399 (1987a).

- Saboo, A. K., Morari, M., and Colberg, R. D., Resilience analysis of heat exchanger networks—Part II: Stream splits and flowrate variations. *Comp. Chem. Eng.*, **11**, 457 (1987b).
- Saboo, A. K., Morari, M., and Colberg, R. D., RESHEX—an interactive software package for the synthesis and analysis of resilient heat exchanger networks. Part II: Discussion of area targeting and network synthesis algorithms. *Comp. Chem. Eng.* **10**, 591 (1986).
- Saboo, A. K., Morari, M. and Woodcock, D. C., Design of resilient processing plants—VIII. A resilience index for heat exchanger networks. *Chem. Eng. Sci.* **40**, 1553 (1985).
- Schrage, L., "User's Manual—Linear, Integer and Quadratic Programming with LINDO." Scientific Press, Palo Alto, California, 1981.
- Swaney, R. E., and Grossmann, I. E., An index for operational flexibility in chemical process design. Part II: Computational algorithms. *AIChE J.* **31**, 631 (1985b).
- Umeda, T., Itoh, J., and Shiroko, K., Heat exchange system synthesis. *Chem. Eng. Prog.* **74**, (7), 70 (1978).

This Page Intentionally Left Blank

CATALYTIC HYDRODEMETALLATION OF PETROLEUM

Richard J. Quann and Robert A. Ware

**Paulsboro Research Laboratory
Mobil Research and Development Corporation
Paulsboro, New Jersey 08066**

Chi-Wen Hung

**Chevron Research Company
Richmond, California 94802**

James Wei

**Department of Chemical Engineering
Massachusetts Institute of Technology
Cambridge, Massachusetts 02139**

I. Introduction	96
II. Metal Compounds in Petroleum	98
A. Composition of Petroleum	98
B. Metal-Bearing Compounds in Petroleum	101
C. Distribution of Nickel and Vanadium Compounds	109
III. Residuum Hydrotreating Technology	134
A. Introduction	134
B. The Role of Hydroprocessing in Residuum Conversion	135
C. Developments in RDS-HDM Hydroprocessing Technology	145
D. Commercial Residuum Hydroprocessing Catalysts	153
IV. Reaction Kinetics and Diffusion in Catalytic Hydrodemetallation	158
A. Model Compound Hydrodemetallation Studies	158
B. Hydrodemetallation of Petroleum Oils and Residuum	184
V. Catalyst Deactivation	210
A. Mechanisms of Catalyst Deactivation	212
B. Dynamics of Reactor-Bed Deactivation	228
C. Modeling of Catalyst Deactivation	234
VI. Conclusions	248
References	251

I. Introduction

The depletion of the world's reserves of low-sulfur crude oils is leading to an increase in refinery utilization of low-quality, heavy crudes to meet the demand for lighter, more valuable products such as motor gasoline, diesel fuel, jet fuel, and petrochemical feedstocks. These heavy crudes are characterized by sulfur contents of 1 to 6 wt. %, nitrogen of 0.1 to 0.6 wt. %, and high concentrations of polyaromatic asphaltenic structures which are concentrated primarily in the 345°C+ (650°F+) atmospheric residuum or 565°C+ (1050°F+) vacuum residuum, termed "the bottom-of-the-barrel" fraction. The presence of numerous sulfur and nitrogen species in the crude reduces the quality of the refined product and poses serious environmental hazards in the form of SO_x and NO_x emissions in combustion. These heteroatoms (S, N) also act as catalyst poisons, making for difficult and expensive processing in catalytic conversion steps such as catalytic cracking and reforming (Gates *et al.*, 1979). In response to the heavier crude slate, the residuum hydrotreating capability of refineries is on the increase. Total free world capacity has increased from approximately 200,000 barrels per stream day (BPSD) in 1970 to 1,200,000 BPSD in 1986 (Lasher and Lasher, 1986). Hydrodesulfurization is a primary objective of residuum hydrotreating, but the removal of other contaminants (including nitrogen, oxygen, and Ramsbottom carbon) has become more important in recent years.

In crude oils, nearly half of the metallic elements in the periodic table have been identified as trace elements (Yen, 1975). Of these, vanadium and nickel are the most abundant and troublesome. Iron is sometimes present, typically in a form and concentration which are easily processed, and therefore is not as troublesome as vanadium and nickel found in most petroleums. In the process of residuum hydrotreating, metal compounds undergo hydrodemetallation (HDM) reactions simultaneously with the removal of sulfur, nitrogen, and oxygen species. When a hydroprocessed residuum is to be charged to a fluid catalytic cracking unit or to be used as turbine fuel, it is desirable to remove metal compounds via HDM to prevent poisoning of the cracking catalysts and erosion of the furnace linings and turbine blades. Even then the reactions of metal compounds create problems. During hydrotreating, for instance, these metals deposit on the catalyst and cause fouling of active sites, which leads to rapid catalyst deactivation. After longer exposure times, the accumulation of metals causes pore mouth plugging and occludes the less severely poisoned interior pore structure of the hydrotreating catalyst. It is estimated for feeds with metal content in excess of 200 ppmw that hydrotreating catalyst consumption exceeds 1 lb per 10 barrels of feed; this can have a significant impact on process economics (Nelson, 1976).

A better understanding of the chemical nature of the metal compounds, the mechanisms of HDM reactions, and metal deposition phenomena would establish a basis for developing improved hydroprocessing catalysts and reactors. A goal of research in this area is to develop catalysts with greater metals tolerance and operational life in reactors.

The scope of this review is to present in one publication a discussion of the elements of physical chemistry, heterogeneous catalysis, and reaction engineering that are necessary for a basic understanding of catalytic hydrodemetallation. Emphasis is centered on vanadium and nickel removal since these are the most abundant metals in petroleum. This chapter covers four major subject areas in separate sections. Each section is written with the aim of consolidating the most recent advances and summarizing the state of the art by relying on the authors' own experiences and extensive reference to the literature. Subject areas are identified where the evidence does not lend itself to a single interpretation in the hope that this will encourage further investigation of these challenging subjects.

In Section II, the nature of the metal compounds in petroleum oils is discussed to establish a basic understanding of the targeted reactants. The chemical composition of the host petroleum and residuum is described, including a discussion of the two classes of metal compounds: (1) metalloporphyrins and (2) nonporphyrin metals. The troublesome asphaltenes will also be described. Comparison is made between the characteristics of vanadium and nickel complexes and their distribution in residua.

In Section III, commercial residuum hydroprocessing technology is discussed to establish the role and requirements of hydroprocessing in the overall refinery residuum conversion scheme. Commercial residuum hydroprocessing catalysts and residuum hydrodesulfurization (RDS)-hydrodemetallation (HDM) technology are reviewed briefly.

In Section IV, the kinetics and mechanisms of catalytic HDM reactions are presented. Reaction pathways and the interplay of kinetic rate processes and molecular diffusion processes are discussed and compared for demetallation of nickel and vanadium species. Model compound HDM studies are reviewed first to provide fundamental insight into the complex processes occurring with petroleum residua. The effects of feed composition, competitive reactions, and reaction conditions are discussed. Since development of an understanding of the kinetics of metal removal is important from the standpoint of catalyst lifetime, the effect of catalyst properties on reaction kinetics and on the resulting metal deposition profiles in hydroprocessing catalysts are discussed.

In Section V, deactivation of catalyst pellets and reactor beds during residuum hydroprocessing is considered. The chemical nature of the metal deposits is described, including a discussion of the physical distribution of these poisons in aged catalysts and reactor beds. Models to predict

catalyst and reactor performance during deactivation are developed from the theory of diffusion and reaction to interpret these experimental observations. The importance of catalyst properties, feedstock properties, and operating conditions on deactivation rates and catalyst lifetime is demonstrated.

In the last section, future perspectives for the study of residuum hydroprocessing and the rational design of hydrodemetallation catalysts and processes are offered.

II. Metal Compounds in Petroleum

A. COMPOSITION OF PETROLEUM

Petroleum is a complex, wide-boiling-range mixture of hydrocarbon and nonhydrocarbon organic compounds that extends from the simplest alkanes to highly complex structures with molecular weights in the thousands. The systematic variation in the composition of petroleum as a function of boiling point is illustrated in Fig. 1. With increasing boiling point or carbon number, the concentration of cyclic and aromatic compounds increases, as does the complexity of the mixture. The material boiling below about 345° (650°F), having a minimum of nonhydrocarbon or heteroatom- (O, N, S) bearing molecules, is readily converted in a refinery

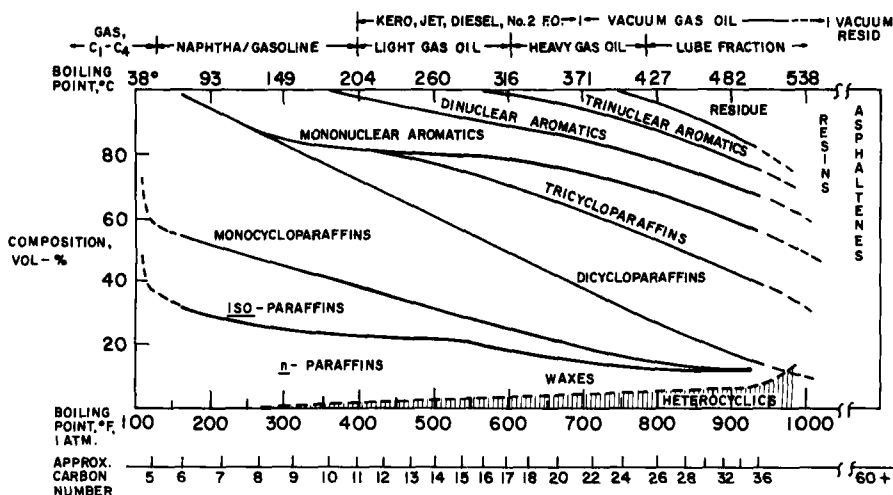


Fig. 1. Relative quantities and boiling range of major hydrocarbon classes in the crude oil from Ponca City Field (Venuto and Habib, 1978).

to valuable transportation fuels. The heavy oil, comprised of material boiling above 345°C, contains a significant amount of impurities and must undergo extensive treatment and upgrading in the refinery to yield quality transportation fuels. Alternatively, heavy oil can be blended to lower-valued fuel oil and asphalt products. Although the most common impurities in petroleum are the heteroatoms, many trace metals in the form of organometallic compounds are also present at measurable levels (Erickson *et al.*, 1954), with some in sufficient quantities to cause environmental concerns about oil-fired power plants or processing problems in refineries. Nickel and vanadium are usually the most abundant metals occurring in petroleum and are therefore of greatest interest and concern.

The portion of the petroleum that has a boiling point of more than 345°C (650°F) is most frequently referred to as the atmospheric residuum. Typically, the crude oil contains 20–50 vol% of atmospheric residuum. Selected properties of various atmospheric residua are compared in Table I. While impurities such as sulfur can be distributed over a wide boiling range, metals are generally concentrated in the 540°C+ (1000°F+) fraction. This high boiling fraction has been termed the vacuum residuum because vacuum distillation of the atmospheric residuum is required to isolate the 540°C+ fraction from the lower-boiling material. The vacuum residuum contains the hydrocarbons of highest molecular weight in petroleum. In addition, asphaltenes tend to concentrate in the vacuum residuum. Asphaltenes are, by definition, a solubility class of material that precipitates from the oil to form a solid when the oil is treated with a selected solvent. Asphaltenes are thought to be a complex mixture of high-boiling, polar, aromatic, high-molecular-weight compounds that, when precipitated from the oil, contain a disproportionate amount of impurities, including the heteroatoms and nickel and vanadium compounds. Because of these characteristics, asphaltenes are the most difficult component in petroleum to process.

Nickel and vanadium in petroleum exist as soluble organometallic complexes that fall into two categories: metal porphyrins and nonporphyrin metal complexes. Both the porphyrins and the nonporphyrins may be distributed over a wide boiling range (350–650°C+), reflecting significant variations in molecular weight, structure, and polarity. Metal porphyrins and nonporphyrin metal complexes also tend to precipitate as part of the asphaltene material to an extent that varies with the source of the crude oil.

This section will review the nature of nickel and vanadium compounds present in petroleum oil, beginning with a detailed discussion of the metal compound categories and their molecular structure. The final section of this discussion will consider the manner in which these two classes of metal-bearing compounds are distributed or associated in the oil.

TABLE I
PROPERTIES OF VARIOUS ATMOSPHERIC RESIDUA^a

Crude oil origin	Residuum type ^b	1000°F (LV %) ^c	Gravity (°API)	Sulfur (wt. %)	Nitrogen (wt. %)	Ramsbottom carbon (wt. %)	Asphaltenes (wt. %) ^d	Metals (ppm)		
								Nickel	Vanadium	Iron
Iranian										
Heavy	Ar	46	14.7	2.52	0.47	9.5	6.7	57	166	4
Light	Ar	41	18.1	2.36	0.29	6.8	—	26	71	2
Kuwait	Ar	46	14.6	4.10	0.22	11.1	3.5	22	77	1
Arabian										
Heavy	Ar	53	12.7	4.24	0.28	12.3	10.2	28	78	4
Light	Ar	42	16.2	3.10	0.17	8.4	2.3	6	33	7
Maya (Mexico)	Ar	60	8.8	4.50	0.54	18.3	15.0	70	433	16
Isthmus (Mexico)	Ar	39	15.7	2.84	0.24	8.6	2.1	14	86	25
Alaskan North Slope	Ar	45	15.4	1.58	0.34	8.3	1.7	16	43	3
Beta (California)	Ar	57	8.3	4.31	1.06	13.2	10.5	156	180	84
France-Wilmington (California)	Ar	54	10.0	2.18	0.79	13.0	5.9	73	84	50
Hondo (California)	Ar	62	8.5	6.49	0.87	13.5	14.2	130	249	2
Santa Maria (California)	Ar	66	5.3	6.43	0.86	17.0	17.6	156	318	36
Kern River (California)	Ar	49	10.2	1.16	0.94	9.3	3.3	88	47	47
Jobo (Venezuela)	Ar	65	6.8	4.24	0.54	16.2	14.4	93	450	15
Monogas/Morichal (Venezuela)	Ar	58	8.6	3.54	0.51	13.8	11.1	114	387	11
Bachaquero (Venezuela)	Ar	59	10.1	2.79	0.57	14.3	8.4	61	507	33
Boscan (Venezuela)	Ar	72	6.3	5.9	0.69	18.2	13.5	130	1553	6
Sumatran Light (Indonesia)	Ar	40	26.5	0.16	0.18	5.1	1.9	15	1	10
Tia Juana (Venezuela)	Ar	37	17.3	1.78	0.33	8.3	—	25	185	—
Athabasca (Canada)	Crude	—	5.9	4.9	0.41	14.9	11.4	86	167	—
Lloydminster (Canada)	Crude	—	14.5	4.3	—	8.1	—	40	100	—
Cold Lake (Canada)	Crude	—	10.0	4.4	0.39	12.8	10.8	62	164	—

^a Sources: Speight (1981), Yen (1973), and Chevron (unpublished data).

^b Ar: atmospheric resid.

^c 1000°F + vol % of atmospheric resid.

^d Heptane insoluble.

B. METAL-BEARING COMPOUNDS IN PETROLEUM

1. *Porphyrin Metal Compounds*

The porphyrins in petroleum, often referred to as petroporphyrins, have been extensively studied due to their utilization as geological biomarkers for characterizing the age and origin of the petroleum source (Sundararaman, 1985). The oldest and by far the most widely accepted explanation for the origin of petroporphyrins was proposed by Treibs (1936). Treibs assumed that petroporphyrins were derived from the chlorophylls of aquatic life. He also suggested a sequence of chemical reactions that could account for the transformation of chlorophylls to petroporphyrins. After some modifications, Yen (1975) also presented a scheme for the transformation of chlorophyll to several vanadyl petroporphyrins. A similar scheme was also proposed by Baker and Palmer (1978). The origin of nickel and vanadium in the porphyrin-type compounds is not clear. Many have concluded that the biological material is the source of the metals in petroleum. However, nonbiological origin of nickel and vanadium such as from reservoir rock minerals is also possible. Detailed discussions of the origin of metallopetroporphyrins and nonporphyrin metals in petroleum have been presented by Filby (1975), Yen (1975), and Baker and Palmer (1978).

The basic skeleton of porphyrin is porphine ($C_{20}H_{14}N_4$), a closed ring of four pyrrole groups bridged by methine-carbon atoms at the α -carbon positions, as shown in Fig. 2. Compounds referred to as porphyrins may have various substituents replacing the hydrogen at the eight β -pyrrolic carbon positions and at the four methine bridge carbon positions. Although porphine itself does not occur in nature, porphyrins are found in nature both in the free form and complexed with metals. The petroporphyrins referred to in this chapter are the porphyrins found in petroleum. The petroporphyrins only exist as metalloporphyrins, with free-base petroporphyrins virtually absent from petroleum. A characteristic physical property of porphyrins and metalloporphyrins is their intense color from the absorption bands in the visible and ultraviolet range. Each type of porphyrin and metalloporphyrin has a distinct spectrum that is used for identification and quantitative measurement.

Metalloporphyrins are formed by the chelation of a metal ion into the porphyrin structure. This involves the incorporation of the metal ion into the center of the tetrapyrrole ring with the simultaneous displacement of two protons from the pyrrolic nitrogen atoms. Nickel is present in petroleum as Ni (II), and it sits in the plane of the four pyrrole rings comprising the porphyrin. The vanadium is present as V (IV), but exists in

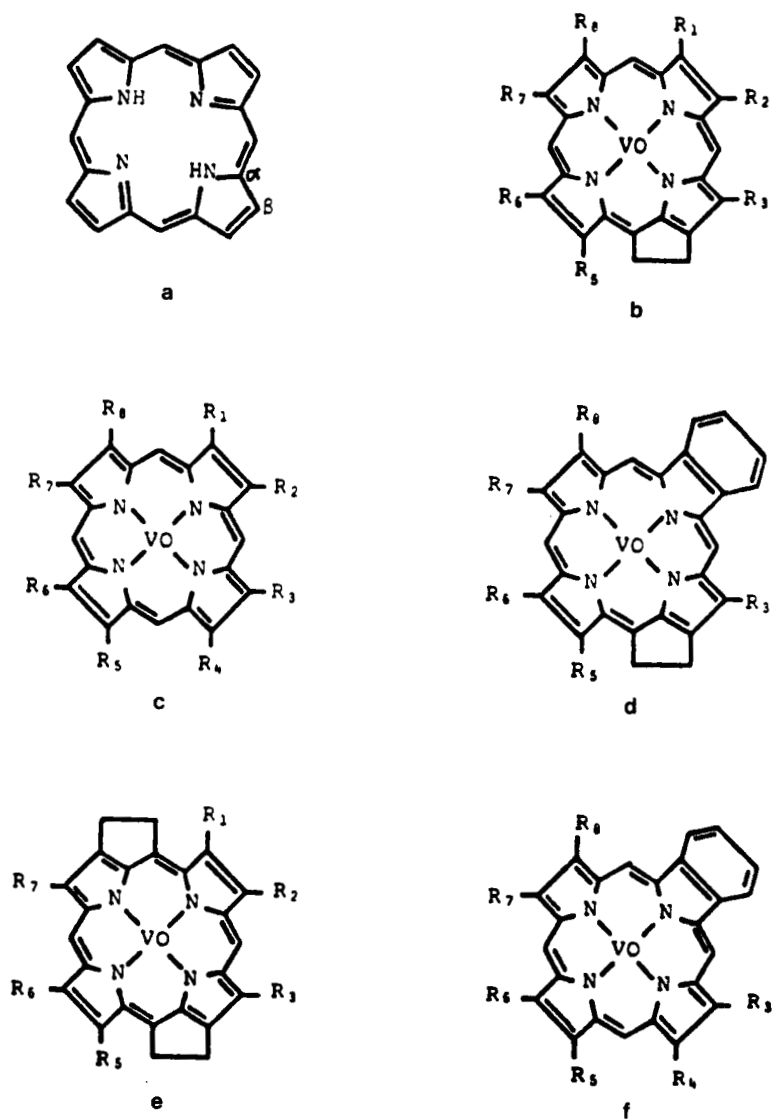


FIG. 2. Porphyrin skeletal structure and metalloporphyrins found in petroleum: (a) porphyrine, (b) DPEP, (c) etioporphyrin, (d) Rhodo-DPEP, (e) Di-DPEP, (f) Rhodo-Etio.

petroleum as the vanadyl VO (2+). The oxygen in the vanadyl group is perpendicular to the porphyrin plane and the vanadium atom lies 0.48 Å above the porphyrin plane in vanadyl deoxophylloerythroetioporphyrin (DPEP) petroporphyrins (Petersen and Alexander, 1968).

The prevalence of nickel and vanadium in petroporphyrins in comparison with other metals is a consequence of both the stronger chelating strength of Ni and V in the porphyrin nucleus and the higher solubility constant of Ni and V sulfide during the formation of petroporphyrins. The chelating strength of Fe, for example, is not as strong as Ni and V (Buchler, 1975). The iron petroporphyrin has not been detected in crude oils (Filby, 1975).

The amount of metal porphyrin in a petroleum varies considerably in terms of both absolute concentration and as a percentage of metal compounds among different petroleums. A comparison of the total metals content and of the percentage of the metals occurring as porphyrins is shown in Table II for various petroleums.

The majority of metallopetroporphyrins in crude oil can be classified into two groups, a DPEP series and an etioporphyrin (Etio) series (Sugihara *et al.*, 1970; Yen, 1975; Baker and Palmer 1978). Each group consists of a series of alkyl homologues in the range C₂₅–C₃₉. However, petroporphyrins in the range of C₂₅–C₅₀ for DPEP series and as high as C₅₀–C₆₀ for other types of petroporphyrins have been reported by Barwise

TABLE II
METALLOPORPHYRIN CONTENT IN PETROLEUMS^a

Crude source	Total Ni + V in 650°F + (ppm)	Wt. % (Ni + V) as Ni + V metallopetroporphyrins
Agha Jari	97	34
Gach Saran (Iran)	223	16–22
Kuwait	99	14
Arabian Heavy (Saudi Arabia)	106	6
Bachaquero (Venezuela)	568	9–14
Morichal (Venezuela)	501	21
Boscan (Venezuela)	1683	19–25
Tia Juana (Mexico)	210	3–10
Wilmington (California)	157	22–34
Santa Maria (California)	474	8
Beta (California)	336	28
Maya (Mexico)	503	13

^a Sources: Biggs *et al.* (1985), Speight (1981), Costantinides and Arich (1963), and Dean and Whitehead (1963).

TABLE III
EQUATIONS TO CALCULATE THE MOLECULAR WEIGHT OF HOMOLOGOUS
SERIES OF PETROPORPHYRINS

Type of porphyrins	Carbon number of basic structure	Molecular weight (free base) ^{a,b}
Etio	20	$310 + 14n$
DPEP	22	$336 + 14n$
Rhodo-Etio	24	$360 + 14n$
Rhodo-DEPE	26	$386 + 14n$
Di-DPEP	24	$362 + 14n$

^a n is the number of methylene groups attached to the porphyrin nucleus.

^b For molecular weight of vanadyl porphyrins, add 65 to molecular weight of corresponding free-base porphyrins. For nickel porphyrins, add 56.

and Whitehead (1980). The equations for calculating the molecular weight of homologous series of petroporphyrins are shown in Table III. The molecular weight of a vanadyl DPEP porphyrin is only 443, but a C₅₀ vanadyl DPEP porphyrin has a molecular weight of 793. A more detailed discussion of the molecular weight distributions and the petroporphyrin isomers has been presented by Baker and Palmer (1978).

Both Etio and DPEP series complexed with Ni and V exist in petroleum (Baker *et al.*, 1967). The DPEP series differs from the Etio series by having a cycloalkano ring (Fig. 2). Baker *et al.* (1967) and Yen and Silverman (1969) measured the porphyrin types in several petroleum. The ratio of the DPEP to the Etio series as well as the width of the distribution in molecular weight due to alkyl substituents are used as indicators for estimating the geological age and source of a given petroleum. For example, samples with a wide molecular weight distribution are more mature as are those with more Etio than DPEP. Etio is believed to be formed from DPEP over time to release the isocyclic strain in DPEP. Samples with high DPEP/Etio series ratio, coupled with a narrow distribution of molecular weight may also reflect the nonmarine origin of the petroporphyrins. Therefore, high Etio/DPEP ratios are characteristic of relatively old formations (Baker *et al.*, 1967; Yen and Silverman, 1969; Baker and Palmer, 1978). In addition to the DPEP and the Etio series, other types of metallopetroporphyrins have been found (Fisher and Dunning, 1961; Baker, 1966; Baker *et al.*, 1967; Barwise and Whitehead, 1980) including the Di-DPEP, Rhodo-Etio, and Rhodo-DPEP. Figure 2 shows the structures of these types of vanadyl petroporphyrins.

The Rhodo-type petroporphyrins are usually found in formations of old age and may contain one or more benzo rings fused to the pyrrole rings.

The equations calculating the molecular of homologous series of Rhodo porphyrins are also given in Table III. The Rhodo porphyrins have a higher molecular weight for the same number of methylene groups attached to the porphyrin nucleus. The cycloalkano and benzo groups are not considered as part of the methylene groups. Barwise and Whitehead (1980) studied the vanadyl petroporphyrins of Boscan and Iranian residua and observed all five aforementioned types of vanadyl petroporphyrins.

The molecular dimension of metallopetroporphyrins will vary, of course, with the chain length of their alkyl homologues. Baker *et al.* (1967) and Baker and Palmer (1978) studied the molecular weight distributions of the petroporphyrins obtained from several crude oils and found that weighted average molecular weights of porphyrin mixtures, based on metal-free porphyrins, are in the range of 450–480 with average carbon numbers of only C_{30} to C_{32} . The diameter for the basic porphine struture is only 8–10 Å. A C_{32} metallopetroporphyrin with four ethyl and four methyl groups as substituents on the eight β -pyrrolic carbons will have a diameter of 11 to 13 Å. Even a hypothetical C_{60} metallopetroporphyrin with eight pentyl groups as substituents has a diameter of no more than 25 Å. Petersen and Alexander (1968) presented both the intramolecular atomic distances and the interatomic angles for vanadyl DPEP, which can be used to calculate the diameter of a metallopetroporphyrin with known alkyl substituents.

Comprehensive references on the structure, physical properties, and chemistry of porphyrins and metalloporphyrins include (1) "Porphyrins and Metalloporphyrins," edited by K. M. Smith (1975). (2) "The Role of Trace Metals in Petroleum" edited by T. F. Yen (1975), and (3) "The Porphyrins," Vols. I–VIII, edited by D. Dolphin (1978). Methods for isolation and identification of petroporphyrins have been discussed by Sugihara *et al.* (1970), Barwise and Whitehead (1980), Baker and Palmer (1978), and Sundararaman (1985).

2. Nonporphyrin Metal Compounds

Unlike metalloporphyrins, the nonporphyrinic metal compounds are poorly characterized with respect to molecular structure and properties. Examining the nature of the nickel and vanadium in these compounds is important from the standpoint that often most of the Ni and V in a petroleum is nonporphyrinic, as shown in Table II. Sugihara *et al.* (1970) suggested that the nonporphyrin metal compounds comprise a wide variety of coordinated complexes resulting from the reaction of inorganic forms of the metals with polar organic molecules. Larson and Beuther (1966) speculated that the nonporphyrinic metal complexes are simply

heteroatom aromatic ring structures resembling porphyrins, except that they contain sulfur and nitrogen in various proportions. Yen (1975) postulated several types of nonporphyrinic metal. He proposed two major categories of Ni and V nonporphyrinic compounds: (1) hydroporphyrins, arylporphyrins, and porphyrin-degraded products and (2) Ni and V complexes of tetradentate-mixed ligands.

Hydroporphyrins are similar to porphyrins in structure except that at least one of the double bonds on the methine bridge and/or the pyrrole groups is hydrogenated. Arylporphyrins are highly aromatic porphyrins. Examples of vanadyl hydroporphyrins, vanadyl arylporphyrins, and porphyrin-degraded products are shown in Fig. 3. The metals are still coordinated to four nitrogen atoms from the pyrrole group. In many cases the physical properties such as size, UV-VIS spectra, and solubility in solvent are different than those of a typical porphyrin due to either interrupted conjugation or increased aromaticity. Yen (1975) and Barwise

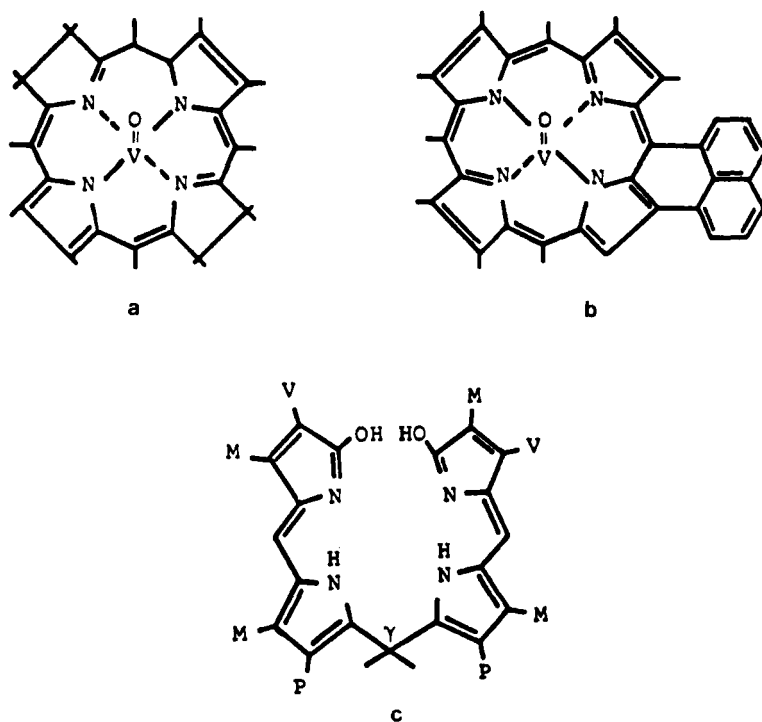


FIG. 3. Nonporphyrinic metals: (a) vanadyl hydroporphyrin, (b) vanadyl arylporphyrin (highly aromatic porphyrin), (c) porphyrin-degraded product (bilirubin). (Yen, 1975).

and Whitehead (1980) reported that the Rhodo porphyrin also has different visible spectrum than other porphyrins.

The Ni and V complexes of tetradentate-mixed ligands are associated with the heteroatom or polar complexes in the crude. The ligands can be comprised of four atoms from N, S, and O. Electron spin resonance (ESR), also called electron paramagnetic resonance (EPR), is an important tool in the research on the nature of ligand types and other properties related to the nonporphyrinic metal compounds (Tynan and Yen, 1969). Based on ESR studies, Dickson *et al.* (1972) reported that fractions of Kuwait residuum have vanadyl VO ligand coordination of N_2O_2 (two N plus two O) or S_4 (four S), depending on the polarity of the fraction. Dickson and Petrakis (1974) found from EPR measurements that vanadium was bound as the vanadyl, but that three different environments existed for the vanadyl in a West Mara crude (Venezuela), including N_2OS , S_2O_2 , or N_3O . Asaoka *et al.* (1983) found N_4 to dominate the ligand types in the Boscan crude. Yen (1975) proposed that nonporphyrin chelates were similar to the porphyrins in structure except that sulfur or oxygen replaced the nitrogen of the pyrrole ring.

Some researchers have doubted whether nonporphyrin metal compounds exist at all in petroleum (Goulon *et al.*, 1984; Berthe *et al.*, 1984). This speculation is based on the similarities in spectral features of petroleum-bound metals and model-metal porphyrin compounds from selected petroleums under the examination of x-ray absorption, photoelectron, and laser desorption spectroscopies. Interpretation of spectra from these methods, however, is uncertain and difficult given the lack of sufficient data on model compounds, particularly nonporphyrin metals and in a petroleum environment or matrix.

Reynolds *et al.* (1985, 1987) examined petroleum porphyrin and nonporphyrin metals independently with EPR after methanol extraction of porphyrins from the petroleum. Table IV shows the EPR-derived coordination spheres of vanadyl nonporphyrin fractions of various crudes. The Ni and V coordinated to four nitrogens (N_4 type) could be petroporphyrin precursors and derivatives as previously discussed or tetradentate-mixed ligands in which N does not necessarily come from a pyrrole group. Considerable variability in the vanadyl coordination among different crude oils is evident. Figure 4 illustrates some proposed metal complexes that may exist in petroleum (Yen, 1975).

Fish and Komlenic (1984) and Fish *et al.* (1984) employed size exclusion chromatography-high-pressure liquid chromatography (SEC-HPLC) with element detection to determine the molecular weight distribution of metal-bearing compounds in four heavy petroleums. The observed

TABLE IV
EPR-DERIVED COORDINATION SPHERES OF VANADYL
NONPORPHYRIN FRACTIONS^a

Crudes	Coordination ^{b,c}
Beta (California)	NOS ₂
Morichal (Venezuela)	N ₄ (NOS ₂)
Maya (Mexico)	N ₂ OS, S ₂ O ₂ , N ₃ O, NOS ₂
Arabian Heavy (Saudi Arabia)	N ₄ , NOS ₂
Boscan (Venezuela)	N ₄

^a Source: Reynolds *et al.* (1985).

^b The multiple choices given indicate that more than one coordination sphere can be assigned by the EPR study.

^c A remote choice is indicated in parentheses.

molecular weight distribution of vanadyl compounds was very broad, ranging from less than 400 to over 9000. Although the existence of very high molecular weight compounds must be questioned on the basis of possible intermolecular associations, the significance of these results is that 30 to 50% of the vanadyl compounds have a molecular weight of less than 900,

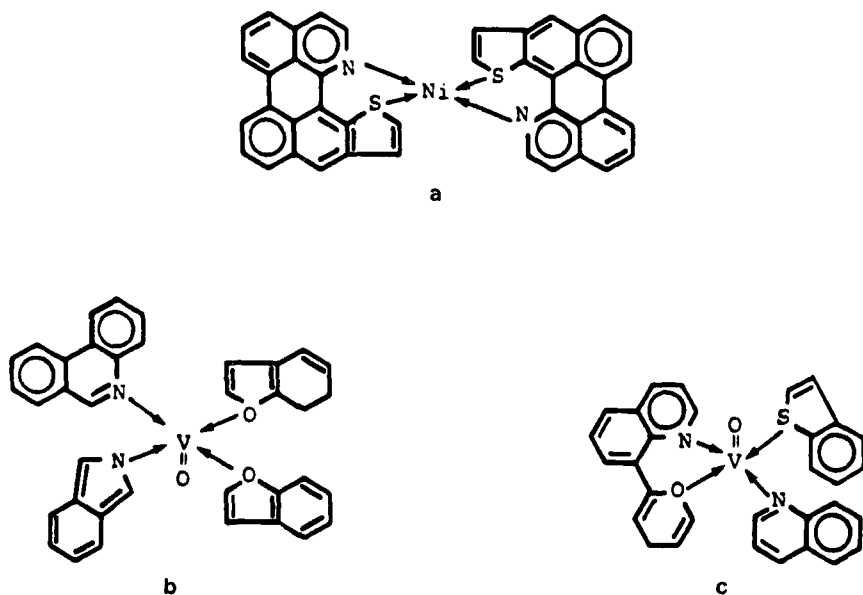


FIG. 4. Possible metal complexes in petroleum: (a) $\text{Ni}(\text{N}_2\text{S}_2)$, (b) $\text{VO}(\text{N}_2\text{O}_2)$, (c) $\text{VO}(\text{N}_2\text{SO})$ (Yen, 1975).

with 13 to 31% less than 400. The presence of vanadyl compounds with molecular weight less than that possible for vanadyl porphyrins is definitive evidence for the occurrence of nonporphyrin metals. Similar observations were reported for nickel-bearing compounds. The nature of the high-molecular-weight metal-bearing compounds will be discussed in Section II,C,3,c.

C. DISTRIBUTION OF NICKEL AND VANADIUM COMPOUNDS IN PETROLEUM

Fractionation of petroleum in the refinery, to obtain streams with specific boiling ranges for various downstream processes, is performed by distillation in a crude unit. To determine how Ni and V compounds are distributed as a function of boiling point is, therefore, useful for evaluating their impact in the refinery. Petroleum may also be fractionated by solvent separation and chromatography to obtain more detailed information on the distribution of Ni and V compounds. This section will review the available literature on how metals are distributed in petroleum by boiling point and solubility class. It will also include some discussion of the structure of heavy oil in general and asphaltenes in particular. Vercier *et al.* (1981) have provided an excellent review of methods and procedures involved in petroleum fractionations.

1. *Distribution of Nickel and Vanadium in Petroleum by Boiling Point*

An effective laboratory distillation method, molecular distillation or short-path distillation, is used to obtain cut points as high as 705°C (1300°F) without severe cracking of the feedstock. Using this method, Dean and Whitehead (1963) obtained data on the distribution of total Ni and V and metallopetroporphyrins in various distillation fractions. This data, shown in Table V, reveals that the absolute percent of the distribution varies among the crudes but that some general trends exist. Practically less than 1% of Ni and V is in the 500°C– fraction with only a small percentage of Ni and V present in the 500–650°C fraction. However, more than 70% of Ni and V in this fraction occur as porphyrins. Apparently, the metal porphyrins are more volatile and, therefore, have lower molecular weight or lower polarity resulting in fewer intermolecular associations than the nonporphyrin metals. The majority of Ni and V, appears in the 650°C+ fraction and as nonporphyrins. The difference between the Ni and V distributions is not significant given the accuracy of the data. Other similar studies

TABLE V
DISTRIBUTION OF NI AND V IN FRACTIONS SEPARATED BY DISTILLATION^a

Crude	Wt. % of crude	Approximate boiling point (°C)	Vanadium (% total)	Nickel (% total)	% Metal as metalloporphyrin
Boscan (Venezuela)	40	<500	<1	<1	—
	14	500–630	7	5	87
	46	>630	93	95	20
Overall	100%		1200 ppm	103 ppm	25%
Gach Saran (Iran)	69	<490	<1	<1	—
	16	490–660	14	8	80
	15	>660	86	92	6
Overall	100%		107 ppm	33 ppm	16%
Kuwait (Kuwait)	71	<510	<1	<1	—
	10	510–650	6	1	77
	4	650–690	8	4	70
	15	>690	86	95	8
Overall	100%		31 ppm	8 ppm	14%

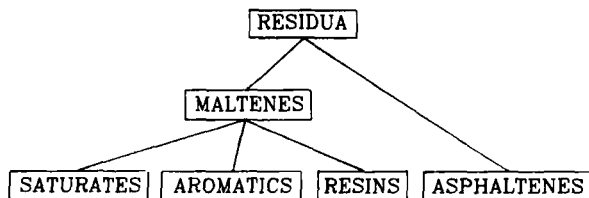
^a Raw data obtained from Dean and Whitehead (1963) by molecular distillation. The data have been rearranged and reinterpreted to normalize the percent closure.

(Barwise and Whitehead, 1980) led to the following additional information: (1) Sulfur-containing compounds are more volatile than metal-bearing compounds. More than 20% of the sulfur appears in 500°C–fraction, with less than 50% of the sulfur occurring in the 650°C+ fraction. (2) The volatility of metallopetroporphyrins varies with their type and degree of substitution. The Rhodo petroporphyrins tend to concentrate more in the heavier fractions than the other types of petroporphyrins.

2. Metal Porphyrin and Nonporphyrin Distribution in Petroleum Solubility Classes

Petroleum can be fractionated into four generic types of materials representing general chemical properties. These include saturated hydrocarbons, aromatic hydrocarbons, resins, and asphaltenes. The standard ASTM separation procedure (D2007) for isolating the asphaltenes and the other components in petroleum is based on solubility behavior and chromatography, as shown in Fig. 5. Commercially, many refineries utilize solvent separations to produce a solvent deasphalted oil which has lower impurity levels.

Asphaltenes are thought to be the most complex, high-molecular-weight, high-boiling components in petroleum. Asphaltenes constitute a solubility class of materials consisting primarily of highly polar and



- ASPHALTENES
 - PENTANE 40/1 BY VOLUME INSOLUBLE
- MALTENES
 - PENTANE 40/1 BY VOLUME SOLUBLE
- SATURATES
 - ELUTION THROUGH ATTAPULGUS CLAY AND SILICA
- AROMATICS
 - ELUTION THROUGH ATTAPULGUS CLAY BUT RETAINED ON SILICA
- RESINS
 - RETAINED ON ATTAPULGUS CLAY

FIG. 5. Standard ASTM (D2007) procedure for separation of asphaltene and other generic components in petroleum (after Reynolds, 1985).

aromatic species which may be quite varied on a molecular basis. By definition, asphaltene is the precipitate obtained when a petroleum or a bitumen is mixed with 40 volumes of a relatively light paraffin, usually pentane. Precipitated asphaltene appears as a dark brown or black solid, generally soluble in benzene, pyridine, and other polar solvents. Asphaltene cannot be separated by distillation from the crude oil on a commercial scale because of their high boiling point range. Resins are less polar, less aromatic, and of lower molecular weight than asphaltene. The asphaltene content of the atmospheric residuum from various petroleum generally falls in the range 2–20 wt. %, as shown in Table I.

The amount of asphaltene precipitate from one crude oil is dependent on the carbon number of the alkane solvent. A decrease in the solvent carbon number results in an increase in the asphaltene precipitate. This observation would suggest that asphaltene and resin are not greatly different materials. Rather, a continuum exists in the solubility behavior. An increase in boiling point in heavy oil is generally accompanied by an increase in both aromaticity and in the concentration of heteroelements or polar aromatic molecules (Corbett, 1969). Similarly, there is a gradual

transition in chemical properties from soluble to insoluble or oil to asphaltene, depending on the properties of the solvent. Boiling point and solubility tend to correlate inasmuch as the more insoluble portions of heavy oil are also more likely to contain the highest-boiling molecules. Resins are believed to solubilize asphaltenes in petroleum through peptization, having chemical properties intermediate to asphaltenes and oils. An asphaltene is generally not stable or soluble in its parent petroleum if the resins have been extracted (Koots and Speight, 1975).

Dean and Whitehead (1963) found that a portion of metalloporphyrins precipitates with the asphaltenes but that the majority is recovered with the resin. Erdman and Harju (1963) examined the different solvent fractions of several crude oils to determine the distribution of nonporphyrins. Asphaltenes, as shown in Table VI, do not necessarily contain all nonporphyrins.

The distributions of Ni, V, N, and S in several atmospheric residuum fractions (Reynolds, 1985) are shown in Table VII. As is evident from the table, the distributions of heteroatoms and metals in the fractions vary greatly with the petroleum source. The Kern River resid is considerably different than that from the other petroleum in having a low asphaltene

TABLE VI

CONCENTRATIONS OF VANADIUM COMPLEXES, PORPHYRIN AND NONPORPHYRIN, IN FRACTIONS OF FOUR CRUDE OILS^a

		Vanadium concentration (ppm)			
	Fraction	Boscan	La Luna	Baxterville	Belridge
Present as porphyrin complexes	Crude oil	350	56	46.7	17
	Asphaltene	868	200	230	180
	Resin	622	460	73	31
	Oil	21.6	9.05	0.56	2.7
Present as nonporphyrin complexes	Crude oil	784	152	~0	15
	Asphaltene	3612	2740	~0	95
	Resin	439	370	~0	58.7
	Oil	9.8	3.3	(0.2)	~0
		Total vanadium present as nonporphyrin complexes (%)			
	Fraction	Boscan	La Luna	Baxterville	Belridge
	Crude oil	69	73	~0	47
	Asphaltene	81	93	~0	35
	Resin		45	~0	65
	Oil		27	+	~0

^a Source: Erdman and Harju (1963).

TABLE VII

DISTRIBUTION OF Ni, V, N, AND S SOLUBILITY AND CHROMATOGRAPHIC FRACTIONS OF ATMOSPHERIC RESIDS^a

Crude	Wt. %	Wt. % of total				TGA residue	
		Sulfur	Nitrogen	Vanadium	Nickel	(% of fraction)	H/C
Maya (Mexico)							
Saturate	20.7	0.9	3.3	0	0	1.0	1.94
Aromatic	26.5	24.6	8.2	0.4	3.3	0.3	1.52
Resin	29.9	39.0	39.6	17.9	17.7	13.9	1.30
Asphaltene	20.6	36.3	48.9	81.7	79.0	44.8	1.14
Arabian Heavy (Saudi Arabia)							
Saturate	20.1	<1	6.7	0	0	0.4	1.95
Aromatic	31.0	29.6	8.4	3.4	10.4	0.7	1.57
Resin	31.2	46.3	43.8	25.2	28.2	13.2	1.32
Asphaltene	12.2	23.9	41.1	71.4	61.8	46.0	1.16
Beta (California)							
Saturate	9.4	<1	1.9	0	0	1.1	1.89
Aromatic	23.1	23.9	2.0	1.6	2.1	0.6	1.60
Resin	41.1	51.8	53.3	18.4	38.9	21.3	1.40
Asphaltene	18.8	24.2	42.9	80.1	59.1	39.1	1.25
Kern River (California)							
Saturate	21.8	<1	2.7	0	0	0.5	1.87
Aromatic	28.7	30.7	4.2	7.5	4.5	0.5	1.44
Resin	37.6	60.3	77.2	52.8	63.0	9.9	1.39
Asphaltene	5.5	8.8	15.8	39.8	32.5	42.6	1.17

^a Source: Reynolds (1985).

content as well as a low percentage of heteroatoms and metals in the asphaltene fraction. For all petroleum, sulfur is found primarily in the aromatic, resin, and asphaltene fractions, with only less than 1% of sulfur appearing in the saturate fraction. Nitrogen occurs almost exclusively in the resin and asphaltene fractions, with less than 15% of the nitrogen appearing in the saturate plus aromatic fractions. More than 85% of Ni and V appear in the resin and asphaltene fractions. Except for the Kern River residuum, more than 60% of Ni and V occur in the asphaltene fraction. Forty to 50% of the materials in the asphaltene fraction remain as residue in thermogravimetric analysis (TGA). The H/C ratios decreases from about 1.9 for saturate fraction to 1.2 for asphaltene fraction. Drushel (1979) examined an unnamed atmospheric residuum and observed similar trends, with the following additional observations: (1) The sulfur distributes evenly through vacuum gas oil (VGO) and vacuum residuum fractions, and (2) as much as 30% of metals appear in the C_5 -insoluble and C_7 -soluble fraction, which is part of C_5 asphaltene, but not part of C_7 asphaltene. This suggests that the alkane used to precipitate asphaltenes can change the apparent distribution of metals.

Additional insight can be obtained with the successive use of various light paraffin and polar solvents as a separation strategy. Dean and Whitehead (1963) obtained C_7 asphaltenes, a C_5 -insoluble- C_7 -soluble fraction (part of the resin), an acetone-immiscible fraction from the C_5 -soluble fraction and an acetone-miscible fraction for both Boscan and Gach Saran (Iranian Heavy) crude oils. They found that the vanadium was more concentrated in the C_7 asphaltene and C_5 -insoluble- C_7 -soluble fractions, especially in the C_7 asphaltene fraction. However, the metallopetroporphyrins were mostly concentrated in the C_5 -insoluble- C_7 -soluble and the acetone-miscible fractions. According to their data, only 5% of the metals in the asphaltenes are identified as metallopetroporphyrins. This is consistent with the expectation that metal porphyrins are less polar than the metal nonporphyrins.

Filby (1975) separated a tertiary California oil into a low-molecular-weight methanol-soluble fraction, a methanol-insoluble-pentane-soluble fraction (resin), and a C_5 asphaltene fraction. He observed that less than 5% of the Ni is present in the methanol-soluble fraction, exclusively as Ni porphyrins. More than 50% of the total Ni was found in the resin fraction, of which 64% occurred as Ni porphyrins. About 40% of the total Ni was found in the asphaltene fraction, of which 49% of the Ni present was in the porphyrin form.

After solubility fractions are obtained through precipitation and chromatography, gel permeation chromatography (GPC) may be used to obtain molecular weight information. Using GPC, Filby (1975) observed that

while most of the asphaltene nickel is detected in the MW 4000–8000 GPC fraction, a substantial amount of resin nickel appears in both MW 300–1000 and MW4000–8000 fractions. Also, compared with the nonporphyrin nickel, more nickel porphyrins are detected in the lower-molecular-weight fractions. It is important to realize that a metal-bearing molecule's presence in MW4000–8000 fractions does not necessarily imply that a metal-bearing molecule has a molecular weight of 4000–8000. Sugihara *et al.* (1970) used GPC and other techniques to study the metal porphyrins in Boscan asphaltenes. They observed that the metal porphyrins in the GPC high-molecular-weight fraction of the asphaltenes are associated with much larger molecules via intermolecular bonding and, therefore, appear to have a much higher molecular weight distribution. This will be discussed in more detail in the next section. Sugihara *et al.* (1970) also suggested that more of the nonporphyrin metals, because of higher polarity, are expected to associate with the asphaltenes and, therefore, not appear in the GPC low-molecular-weight fraction. The preceding two studies, plus the aforementioned study by Dean and Whitehead (1963), indicate that nonporphyrin metals tend to associate with the highly polar asphaltene fraction.

3. *Asphaltene Structure*

Since a significant if not a major portion of the metal porphyrins and nonporphyrins in petroleum are associated, albeit by precipitation, with the asphaltenes, some discussion must be devoted to the physical and chemical nature of asphaltenes. Furthermore, a disproportionate quantity of heteroatoms and catalyst coke precursors also reside in the asphaltene-type material. Despite numerous studies, however, the chemical structure of the asphaltene fraction remains speculative. This is due to the difficulty of isolating and identifying individual compounds in the high boiling range because of increased molecular size, complexity, and variety. Many investigators have approached the problem by proposing average molecular structures. The most accepted model, and one of the earliest, is that asphaltene molecules consist primarily of large, pericondensed, polynuclear aromatic centers with attached alkyl and alicyclic systems and with appreciable heteroelement (O, N, S) content including heterocycles. These early concepts, as well as the more recent information on the structure of asphaltenes and the association of metals with asphaltenes, are reviewed in this section.

a. *Asphaltene Chemical Structure.* Most of the early information available on the chemical nature of petroleum asphaltenes was obtained by

spectroscopic methods, including x-ray diffraction (XRD), proton nuclear magnetic resonance (HNMR), electron spin resonance (ESR), and infrared (IR). Using the structural information determined by these methods with additional molecular weight and elemental composition measurements, many investigators developed molecular models for asphaltenes. Yen (1972) and Speight and Moschopedis (1979) have provided excellent reviews of this early work.

The early spectroscopic studies using IR (Chelton and Traxler, 1957) and nuclear magnetic resonance (NMR) (Williams, 1959) observed both aromatic and alkyl structures in asphaltenes. Visible-UV spectroscopic studies by Erdman *et al.* (1958) indicated that asphaltenes and resins from the same petroleum source have a similar chemical structure but that significant variations existed among different petroleum. This is consistent with the observation that the resin-asphaltene interaction is specific in that the resins from one petroleum do not readily solubilize the asphaltene from another petroleum (Koots and Speight, 1975).

Yen *et al.* (1961) examined the structure of isolated petroleum asphaltenes by using XRD. From the diffraction pattern they were able to calculate the aromaticity, defined as the number of aromatic carbon atoms over the total carbon atoms. The aromaticity ranged from 0.26 to 0.53 for petroleum asphaltenes. In addition, the characteristic dimensions of an asphaltene were obtained by the XRD method. The asphaltene model developed by Yen *et al.* (1961) from these observations is presented in Fig. 6 with characteristic molecular dimensions. The model consists of

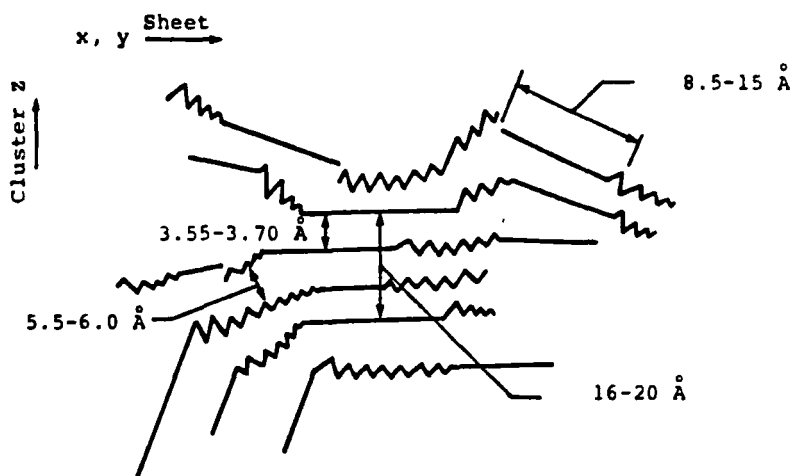


FIG. 6. Model of asphaltene structure (wavy lines represent the zigzag configuration of a saturated carbon chain or a loose net of naphthenic rings and straight lines represent the edge of flat sheets of condensed aromatic rings) (Yen *et al.*, 1961).

stacked aromatic sheets with alkyl or alicyclic substituents. Although the model has been generally accepted as a conceptual representation of an asphaltene, it does not necessarily depict the nature of asphaltenes in petroleum or in solution. Rather, the XRD spectra represent the short-range ordering of the precipitated or solid asphaltene sample. The reliability of using XRD to determine aromaticity has also been questioned by Ebert *et al.* (1982, 1985) on the basis that the diffraction band arising from stacked aromatic carbons does not reveal the aromatic portions not associated with stacks. Tynan and Yen (1969) proposed that the aromatic sheets are bound by π - π interaction or coordination through heteroatoms in the sheets with a dissociation energy of about 14 kcal/mole.

Yen and Erdman (1962) further investigated the same asphaltenes with HNMR to reveal additional chemical features including the shape or compactness of the polynuclear aromatic sheets and the extent and type of substitution on the aromatic perimeter. The HNMR technique provides for a determination of hydrogen types from which carbon types can be calculated (Brown and Ladner, 1960). The degree of substitution is defined as the number of carbon atoms directly attached to the peripheral carbons or to edge aromatic carbons over the total number of aromatic carbon atoms on the peripheral of the aromatic sheet. The extent of substitution varied between 0.48 and 0.70 for the asphaltenes, with slightly higher substitution observed for corresponding resins. The ratio of the number of peripheral aromatic carbons to the total number of aromatic carbons (C_p/C_a) provides a measure of the compactness and size of individual polynuclear aromatic nuclei. For asphaltenes of a different origin, the calculated C_p/C_a ratio varied from 0.34 to 0.53, corresponding to 7 to 19 condensed rings. The structures of the substituents were not as confidently determined because of uncertainties in determining naphthenic hydrogen. Nevertheless, an average structure of a hypothetical Lagunillas oil asphaltene molecule, shown in Fig. 7, was constructed on the basis of the NMR spectra and elemental analysis. This NMR-derived structure, with a molecular weight of about 1000, would correspond to a single sheet of the asphaltene model shown in Fig. 6.

Speight (1970) also applied the NMR method to an Athabasca bitumen. The asphaltene, resin, and oil fraction had 50%, 40%, and 28% aromatic carbon atoms, respectively. The peripheral to total aromatic ratio (C_p/C_a) was about 0.40 for the asphaltene, corresponding to a 12-ring center. The oil fraction has a C_p/C_a of 0.92, corresponding to 1 or 2 aromatic rings, and a slightly higher degree of substitution (58% versus 52%) on the peripheral carbons. The high molecular weight (~ 5500) for the asphaltenes led Speight to propose that an asphaltene molecule was probably composed of several 12-ring-type aromatic structures joined by alkyl side chains and, thus, having 40 or more aromatic rings per molecule.

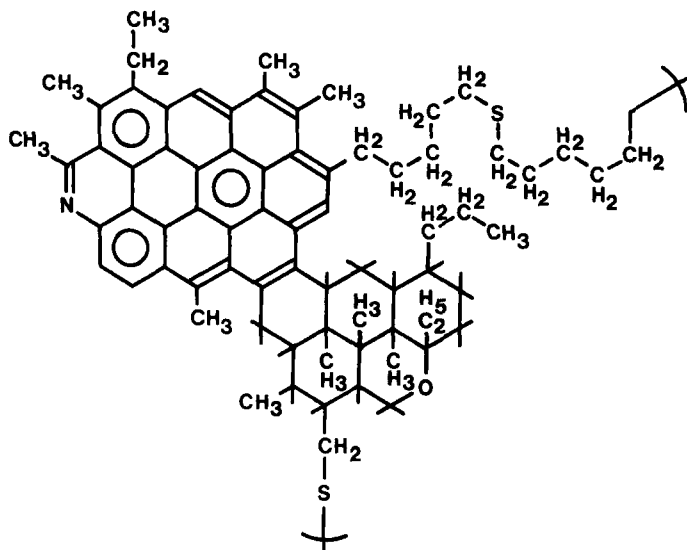


FIG. 7. Hypothetical molecular formula of an asphaltene molecule constructed from HNMR analysis of the Lagunillas oil asphaltene (Yen, 1972).

Of the saturated carbon atoms, 50% or more were paraffinic rather than naphthenic or alpha to the aromatic structure.

Koots and Speight (1975) reported the NMR-determined structures of pentane-insoluble asphaltenes and the corresponding resins from petroleum. The resins have rather small aromatic systems with a C_p/C_a ratio in the 0.85 to 1.0 range, characteristic of 1 or 2 rings. Several of the resin samples had C_p/C_a ratios as low as that calculated for 3-to 4-ring systems. Asphaltenes, on the average, again appeared to have a minimum of 7 rings but as many as 19 rings. Although the resins had a greater H/C ratio, their heteroelement content was not lower than that of the asphaltenes.

Dereppe *et al.* (1978) determined more detailed information on the naphthenic portion of asphaltenes by utilizing both proton and ^{13}C NMR spectroscopy. Shale oil asphaltenes contained 2 to 10 naphthenic rings and 2 to 6 aromatic rings with no relationship between the relative amounts of ring types. Further, fractionation of petroleum by precipitation in a series of paraffin solvents (Speight, 1971) and in heptane-benzene mixtures (Ferris *et al.*, 1967) has yielded asphaltene samples of varying molecular weight. Speight (1971) has shown that the NMR C_p/C_a condensation index decreases systematically from 0.55 to 0.35 with increasing molecular weight of the asphaltene fraction from 2694 to 8160. The pentane-soluble resin had the same apparent ring structure as the lowest-molecular-weight asphaltene. Ferris *et al.* (1967) observed that the heteroelement content, aromaticity, and size of the aromatic nuclei (by NMR) increase as a

function of molecular weight from oil to resin to asphaltene. However, their study indicated that these properties are constant as a function of molecular weight of the fractionated asphaltene. Ferris *et al.* (1967) did observe a definite increase in free radical concentration with increasing asphaltene molecular weight by using ESR. They also proposed that the asphaltene aromatic centers are interconnected by alicycle or alkyl linkages.

Heteroatoms in petroleum tend to concentrate in the higher-boiling compounds and in the asphaltenes (Speight, 1981; Corbett, 1969). Until recently, very little effort had been put into determining the nature and distribution of heteroatoms in the high-boiling fractions of petroleum. McKay and Latham (1981) and Grizzle *et al.* (1981) reported the distribution of heteroatoms in distillates and residues. The concentration of O, N, and S increases with boiling point, as shown in Table VIII for four petroleum heavy ends. The concentration of heteroelements, particularly nitrogen, is greater for asphaltenes than for resins (Koots and Speight, 1975; Speight, 1981; Boduszynski, 1985).

Early mass spectroscopic studies (Clerc and O'Neal, 1961) of asphaltenes identified that heteroatoms can exist in ring systems, including polyfunctional systems. This is consistent with thermal decomposition studies (Yen, 1971) in which virtually none of the nitrogen and only a fraction (~20%) of the sulfur are lost during treatment. In contrast, most of the oxygen is released. Oxidation rate studies have also indicated that O, N, and S are located in relatively stable chemical configurations, again inferring heterocycle structure (Erdman and Ramsay, 1961).

Tynan and Yen (1969) have suggested that the association of aromatic sheets in the asphaltene macrostructure may occur through coordination of heterocycles. The aromatic sheets may have defect centers with heteroelements providing coordination centers for metals (Yen, 1974).

McKay *et al.* (1981a-c), using IR spectroscopy, identified the presence of phenol-, carboxylic acid-, amide-, pyrrole-, and pyridine-type polar compounds in the high-boiling distillates (370–675°C) and residues (675°C+) of several petroleum (see Table VIII). In all cases the concentration of these polar compound types increased with boiling point in comparison to saturate and aromatic nonhydrocarbons. Grizzle *et al.* (1981) observed a similar trend, with nitrogen tending to be more concentrated in the heavier fractions than sulfur.

The presence of relatively high concentrations of heteroelements may lead to significant molecular associations via hydrogen bonding. Petersen (1967) studied H bonding in petroleum asphaltenes by using the IR stretching bands of OH and NH. Phenolic and alcoholic OH and pyrrole-type NH acids existed primarily as H-bonded intermolecular association complexes. Petersen (1967) also suggested that π bases were important in

TABLE VIII
DISTRIBUTION OF O, N, S, AND POLAR COMPOUNDS BY BOILING POINT^a

Crude oil	Boiling range (°C)	Wt. % of distillate or residue					Wt. %			Wt. % of acid fraction			
		Acids	Bases	Neutral nitrogen compounds	Saturate hydro- carbons	Aromatic hydro- carbons	Wt. %			Carboxylic acids	Phenols	Amides	Pyrroles
							Nitrogen	Sulfur	Oxygen				
Wilmington (California)	370–535	5.6	6.8	4.2	36.9	46.5	0.46	1.58	—	62	15	3	13
	535–675	9.3	12.7	21.3	20.8	36.0	0.86	2.15	—	48	12	13	22
	>675	18.0	19.0	41.0	4.0	15.0	1.62	2.57	1.46	33	12	25	30
Gach Saran (Iran)	370–535	1.7	2.1	2.3	48.5	46.5	0.22	1.85	—	4	31	26	36
	535–675	5.4	8.7	8.9	31.6	45.4	0.44	2.61	—	4	21	24	41
	>675	17.0	25.0	14.0	8.0	30.0	1.18	3.69	0.76	14	7	47	16
South Swan Hills (Alberta)	370–535	1.8	2.2	1.9	65.9	29.7	0.15	0.28	—	4	34	15	47
	535–675	3.5	4.5	5.6	57.5	28.9	0.27	0.46	—	7	25	24	37
	>675	12.0	13.0	10.0	34.0	27.0	0.55	0.53	1.20	24	13	30	16
Recluse (Wyoming)	370–535	1.4	1.1	0.9	74.1	22.5	0.07	0.12	—	11	24	3	56
	535–675	2.9	3.3	3.0	68.8	21.9	0.16	0.34	—	4	24	8	58
	>675	9.0	10.0	8.0	44.0	26.0	0.56	0.37	0.78	14	24	23	25

^a Source: McKay and Latham (1981).

H bonding. In a later study, Petersen *et al.* (1971) identified associated complexes of 2-quinolones with carboxylic acids. The 2-quinolones had been previously detected in petroleum heavy oils (Copelin, 1964; Snyder *et al.*, 1968). Model compound studies (Petersen *et al.*, 1971) of dimer and mixed dimer formation with 2-quinolone and carboxylic acids suggest strong association with enthalpies in the 8- to 10-kcal/mole range.

Barbour and Petersen (1974) observed strong H-bonding basicity of asphaltenes with phenol, having enthalpy of interactions between 6 and 8 kcal/mole. Phenol-base interactions for π aromatic bases are typically as low as 0.5 kcal/mole but can reach 9 kcal/mole for nitrogen- or sulfur-containing molecules (Barton *et al.*, 1972; Osawa *et al.*, 1967; Whetsel, 1968).

b. *Asphaltene Molecular Weight and Size.* Perhaps the most questionable area in the investigation of asphaltene structure is the determination of molecular weight. Indeed, data on molecular weight reported in the literature have varied considerably, depending on the measurement technique, asphaltene concentration, and solvent used for the determination. For example, ultracentrifugation studies (Winniford, 1963; Ray *et al.*, 1957; Wales and van der Waarden, 1964) have obtained molecular weight measurements as high as 300,000. Viscosity (Fischer and Schram, 1959), ebullioscopic (Griffin *et al.*, 1958), and vapor pressure osmometry (Altgelt, 1968) methods yield significantly lower values, typically in the 1000–5000 range. By comparison, the average condensed aromatic nuclei with alkyl and alicycle substituents, derived from NMR spectroscopic measurements, has a molecular weight of 600 to 1000. Some investigators have accounted for the difference in NMR structure and other measurements by proposing that C–C bonds (Ferris *et al.*, 1967; Speight and Moschopedis, 1979) or sulfur bridges (Ignasiak *et al.*, 1977) link several condensed polycyclic aromatic centers to yield macromolecules of repeating structure. Resins were also thought to have the same basic structure as the asphaltenes but to be monomeric with respect to number of aromatic nuclei per molecule and, therefore, of much lower molecular weight. The more current view, however, is that the association of molecules into clusters is primarily responsible for molecular weight measurements that exceed ~2000. The colloidal properties of asphaltenes in petroleum, or of separated asphaltenes in a solvent, are indicative of these strong intermolecular associations. The precipitation phenomena observed in the separation methods are an obvious indication of the importance of intermolecular associations.

Nollensteyn (1924) originally proposed that asphaltenes present in a hydrocarbon medium associated into micelles, with adsorbed resins acting

as a transition layer from oil to asphaltene. High-resolution electron microscopic studies of asphaltenes from an evaporated benzene solution revealed 20- to 30-Å particles (Dickie *et al.*, 1969).

Dickie and Yen (1967) advanced the concept that a definable average macrostructure, similar to the micelle concept, exists for asphaltenes, with the different molecular weight measurement techniques revealing the different microstructural features. The molecular weight of 500 to 800 measured by mass spectroscopy or XRD in their study correspond to the individual polynuclear aromatic sheet weights with their saturated substituents. The 2000–8000 range measured by vapor pressure osmometry (VPO), gel permeation chromatograph (GPC), and electron microscopy correspond to the stacking of four to six sheets (Fig. 6) into particles by intermolecular forces. From ESR studies, Tynan and Yen (1969) have suggested that π - π interaction or coordination through heteroatoms results in the stacking of the sheets. Micelles are formed by the association of two or more particles. Ultracentrifugation and GPC measurements in the 40,000 range (Altgelt, 1965) would reflect the association of particles into micelles. To what extent lower molecular-weight components aggregate in unaltered petroleum or the high-boiling resid fraction is uncertain.

Asphaltenes display low solubility in solvents used for molecular weight determinations. They tend to associate even in dilute solutions of relatively good solvents (Winniford, 1963). It was also suggested that resins absorbed on precipitated asphaltenes can affect molecular weight measurements (Speight, 1981). Girdler (1965) and Altgelt (1968), observed that the molecular weight of asphaltenes, as measured by VPO, are dependent on the solvent used. This was attributed to the effect solvent polarity has on the extent of association of asphaltene molecules. Moschopedis *et al.* (1976) have also shown that the VPO-measured molecular weight of a sample decreased by about a factor of two to three with increasing dielectric constant of the solvent. The association-dissociation phenomenon as measured by apparent molecular weight is also dependent on temperature (100–300°C), with the lowest observed molecular weight in the range 1000–2000. The apparent VPO molecular weight in benzene varied by more than a factor of three for different petroleum asphaltenes. Interestingly, the differences between asphaltenes of different origin were greatly minimized by use of highly polar solvents (Moschopedis *et al.*, 1976; Dickson *et al.*, 1969). Viscometry and rheological studies (Mack, 1960; Lorenz *et al.*, 1961) of asphaltene-like materials have also revealed aggregation phenomena. Viscosity behavior resembles that of relatively low molecular weight material associated through relatively weak bonds stable only at low shear rates.

At present, it is uncertain whether the measurement of molecular weight or size of asphaltenes removed from the petroleum has any significance with respect to the state of the parent polar material in petroleum or in the resid at hydroprocessing conditions. Most of the information available from analytical studies has been obtained on precipitated asphaltenes. Separation of asphaltenes from the petroleum by treatment with an alkane solvent disrupts the complex solubility equilibrium that exists between the oil, resin, and asphaltene fraction. Furthermore, the precipitation of asphaltenes does not generate chemically defined components (Boduszynski *et al.*, 1977; McKay *et al.*, 1978; Boduszynski, 1979). A petroleum or petroleum residuum is a mixture containing a wide range of molecular weights and chemically functional components. The use of analytical techniques, such as NMR, that obtain only average properties on whole precipitated samples has led to the concepts about average structure and high molecular weight which greatly oversimplify the complexity of the high-boiling residue. Solubility and boiling point are dependent not only on molecular weight, but also on molecular interactions brought about by functional groups containing heteroatoms involved in hydrogen bonding (Long, 1979). Highly polar aromatics of lower molecular weight may precipitate under the same solvent treatment or boil near the same temperature as higher-molecular-weight nonpolar or less polar aromatics.

Although the residuum is a mixture too complex for isolating chemically pure components, asphaltene investigators in recent years have developed techniques that separate residuum molecules on the basis of compound class rather than solubility class. These studies, discussed next, have greatly modified the concepts of asphaltene structure.

Boduszynski *et al.* (1980) described an elaborate new separation procedure for isolating and concentrating chemically defined compound types rather than solubility types. A residuum (675°C+) is first fractionated by chromatography with an ion and cation resin to isolate acids and bases, followed by coordination chromatography on ferric chloride Attapulgas clay to separate the remaining neutral Lewis base and hydrocarbon fraction. This latter component is further separated into saturate and aromatic hydrocarbons over silica gel.

The acid, base, and neutral Lewis base fractions consist of polar molecules capable of hydrogen bonding and, therefore, of intermolecular association. These polar fractions, which constitute nearly two-thirds of the 675°C+ residuum, have high concentrations of heteroelements in comparison to the nonpolar aromatic and saturate hydrocarbons, as shown in Table IX for the residuum from a Russian crude oil. Infrared spectroscopy of the acid fraction revealed mostly pyrroles with phenols but only traces of

TABLE IX
PROPERTIES OF GENERIC FRACTIONS OF THE ASPHALT FROM A RUSSIAN OIL^a

Fraction	% of Asphalt	Wt. %					Average molecular weight		
		Carbon	Hydrogen	Sulfur	Nitrogen	Oxygen ^b	VPO ^c	VPO ^d	FIMS
Asphaltenes	16	84.05	7.84	4.42	1.48	2.21	4015	4068	873
Polar aromatics—2	3	81.90	8.49	3.62	1.00	4.99	3075	—	1104
Polar aromatics—1	45	83.99	9.61	3.69	0.78	2.53	1405	1448	1020
Naphthene—aromatics	32	85.10	10.84	2.91	0.14	1.01	1062	1148	1234
Saturates	4	85.88	13.51	0.19	0.07	0.35	1036	—	1127

^a Source: Boduszynski *et al.* (1980).

^b By difference.

^c In benzene.

^d In methylene chloride.

carboxylic acids and quinolones. The base fraction contained mostly pyridine nitrogen with small amounts of amides and pyrroles. The neutral Lewis base fraction is expected to contain appreciable polynuclear aromatics, which are efficient π electron donors. Amides and pyrroles were identified as the predominant functional forms of the neutral Lewis base.

Field ionization mass spectrometry (FIMS) was applied to the different compound classes by Boduszynski *et al.* (1980). The FIMS molecular weight envelopes shown in Fig. 8 illustrate the similar but wide molecular weight distribution for each compound class. Furthermore, the FIMS molecular weight of about 1000 are considerably lower than those obtained by other methods in which intermolecular association may influence measured values. This is evident in Table IX by the comparison of VPO

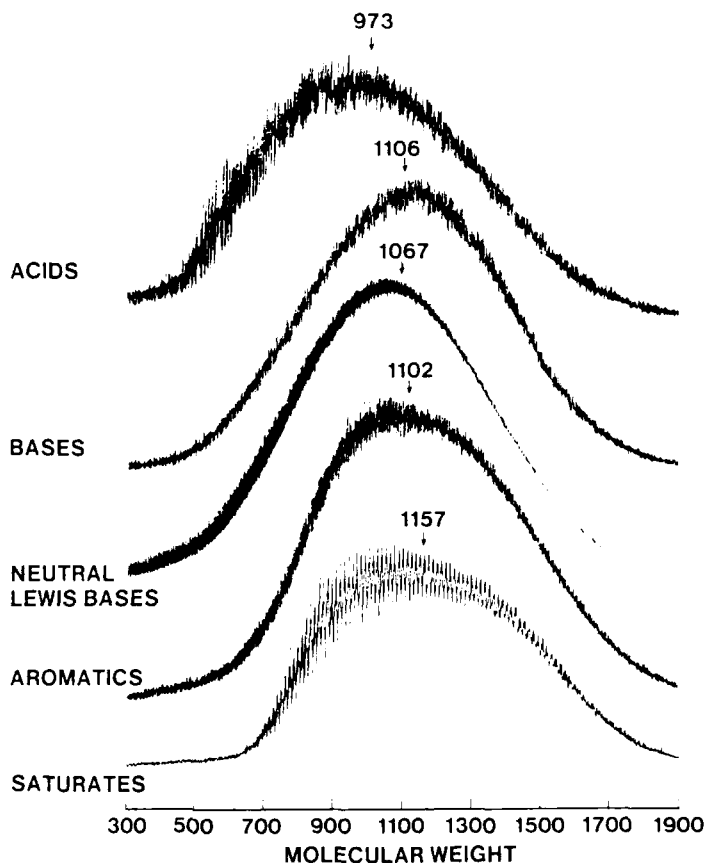


FIG. 8. Field ionization mass spectroscopy envelopes of compound classes in petroleum (Boduszynski *et al.*, 1980).

and FIMS measurements for molecular weight. Intermolecular association via hydrogen bonding appears to result in the higher molecular weight obtained by the VPO method.

Boduszynski *et al.* (1980) also employed the more conventional separation procedure based on solubility properties (Corbett, 1969) to provide asphaltene and maltene samples from the 675°C+ residuum. Asphaltenes are isolated by precipitation in an alkane solvent, with further separation of maltenes by chromatography in solvents of increasing elution strength. The FIMS results in Fig. 9 illustrate, significantly, that asphaltenes are not necessarily the highest-molecular-weight components in residuum. Asphaltenes have, rather, a relatively low but broad distribution of molecular weights.

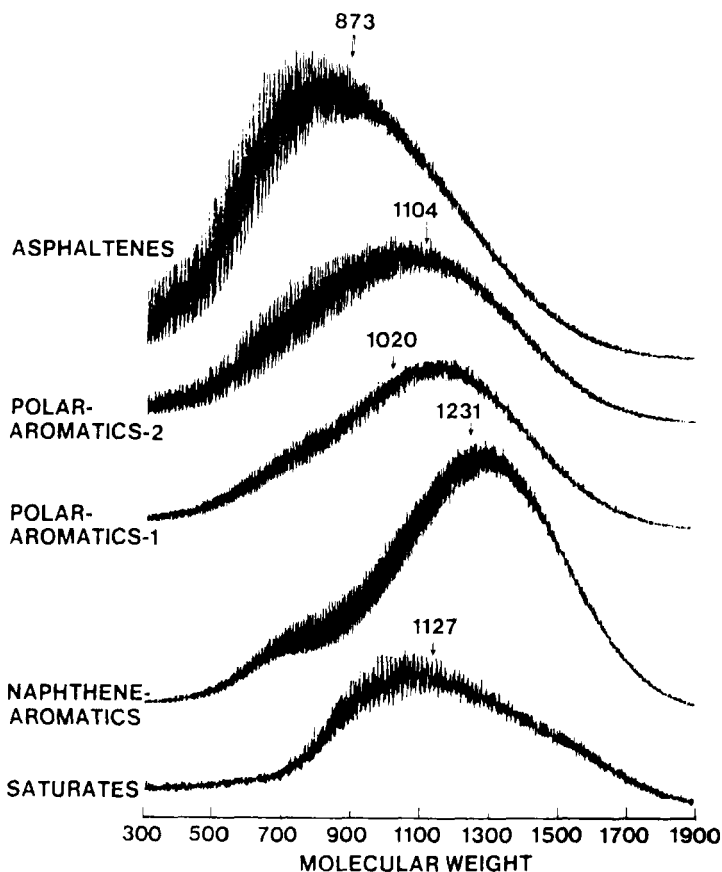


FIG. 9. Field ionization mass spectroscopy envelopes of petroleum generic fractions (Boduszynski *et al.*, 1980).

Infrared analysis of the asphaltenes revealed the presence of mostly pyrroles and phenols with minor amounts of carboxylic acid and 2-quinolones, similar to that found in the acid compound class. On the basis of these findings, molecular weight apparently does not play as significant a role in determining the solubility properties of the residuum as chemical functionality. The authors also reported that treatment of the acid-and base-free residuum with an alkane solvent does not generate a precipitate. Evidently, the OH and NH functional groups capable of strong H-bonding associations determine association behavior. As shown in Table X, the VPO molecular weight of asphaltenes far exceeds that of the FIMS of asphaltenes or acids. The discrepancy between VPO and FIMS values decreases with decreasing heteroatom content.

McKay and Latham (1981) have also determined compound class distributions in the high-boiling distillates and the residua for four crude oils. As shown in Table VIII, the content of heteroatom compounds increases with increasing boiling point. The 675°C+ residuum may have nearly 10 times the acids, bases, or neutral Lewis (pyrrolic and amides unreactive to column resins) bases compared to the VGO portion (370–535°C). Grizzle *et al.* (1981) have also employed compound class separations and have observed similar trends. McKay and Latham (1981) calculated that each acid, base, or neutral nitrogen molecule in the <675°C residuum contains three to five heteroatoms.

The concept of average molecular structure that others have adopted for asphaltenes is questionable (Boduszynski, 1983) in view of the wide molecular weight distributions and varying chemical functionality. Even narrow boiling point cuts, particularly at the higher boiling ranges, can yield molecules having a wide range of molecular weights and structure. Boiling point generally correlates with molecular weight but only within a compound class. Thus, a narrow boiling point cut would consist of relatively light heteroatom-containing polar molecules and relatively high molecular weight saturated hydrocarbons.

c. *Metal Porphyrin and Nonporphyrin Association with Asphaltenes.* Asphaltene metals correspond to the porphyrin and nonporphyrin metals which precipitate with the asphaltenes during the standard solvent separation procedure (ASTM Test D2007). Nickel and vanadium enrichment in the asphaltenes was discussed earlier. The significance of differentiating between asphaltene and nonasphaltene metals from a processing standpoint was based on the early concept that asphaltenes were micelles having enormous molecular weight and dimensions comparable to that of the catalyst pores. Catalyst design for the conversion of these large micelles, if they existed at hydroprocessing conditions, would be different

TABLE X
PROPERTIES OF THE COMPOUND CLASSES IN A RUSSIAN CRUDE OIL ASPHALT^a

Fraction	Wt. %						Average molecular weight		
	Asphalt	Carbon	Hydrogen	Sulfur	Nitrogen	Oxygen ^b	VPO ^c	VPO ^d	FIMS
Total asphalt	100	84.91	10.03	3.35	0.90	0.81	1448	1550	1048
Acids	21	83.76	8.53	3.81	1.46	2.44	2310	2277	973
Bases	19	81.78	9.81	3.69	1.73	2.99	1702	1459	1106
Neutral Lewis bases	29	83.76	9.98	2.66	0.48	3.12	1490	1459	1067
Aromatic hydrocarbons	24	85.19	9.78	2.61	0.14	2.28	1084	1207	1102
Saturate hydrocarbons	7	85.47	13.06	0.48	0.04	0.95	1030	950	1157

^a Source: Boduszynski *et al.* (1980).

^b By difference.

^c In benzene.

^d In methylene chloride.

than that for simple isolated porphyrin molecules. The current view on asphaltenes, as described in the preceding section, is that asphaltenes are primarily polar molecules of MW 300–1000 which precipitate in the alkane solvent and may display aggregation behavior in their native petroleum. Certain metal-bearing porphyrins and nonporphyrins may also coprecipitate from the petroleum under the same solvent treatment and associate in the petroleum with asphaltene components. At present, it is uncertain whether the large macrostructure model of Yen (Fig. 6), with metals located in the defects of aromatic sheets bound by π – π interactions or hydrogen bonding in the native crude oil or resid, exist or whether the large agglomerates observed in isolated samples are just artifacts of the separation methods. The most important question, however, is to what extent intermolecular associations involving metal porphyrins and nonporphyrins, such as π – π stacking and H bonding, take place at hydroprocessing conditions. This section will examine the nature of the interaction between metal-bearing porphyrins and nonporphyrins with the so-called asphaltenes in petroleum.

Asphaltenes may contain both porphyrin and nonporphyrin metals, depending upon the origin of the crude oil. Yen *et al.* (1969) characterized the vanadium complexes in a petroleum asphaltene by mass spectroscopy, optical spectroscopy, and ESR. Porphyrins (Etio and DPEP), acid-resistant porphyrin macrocycles of increased aromaticity (Rhodo), and nonporphyrins with mixed donor complexes were identified. Baker (1966) and Baker *et al.* (1967) extracted porphyrins from Boscan crude oil asphaltenes and also found Etio and DPEP as the two major porphyrin series. These homologous series range in molecular weight by 7 to 18 methylene groups. Gallegos (1967) observed by mass spectroscopy that asphaltenes and maltenes from a Boscan crude oil had nearly identical porphyrins in terms of mass distribution.

Porphyrin and nonporphyrin metals associated with asphaltenes have not been easy to identify in terms of molecular structure. This is partly due to the fact that the characteristics (i.e., spectra) of all possible model nonporphyrin compounds have not been studied. Nonporphyrin metals are probably small polar molecules that precipitate as asphaltenes (Filby, 1975) or complex at defect sites in large aromatic sheet structures of the type shown in Fig. 10. Porphyrins with increased aromaticity and systems with low aromaticity due to discontinued ring conjugation are both characterized as nonporphyrin species. These compounds do not have the characteristic visible absorption spectra and hence are not readily identified. It is also possible that some of the porphyrin in the residuum may not be extracted and identified due to intermolecular association with the asphaltene-generating molecules.

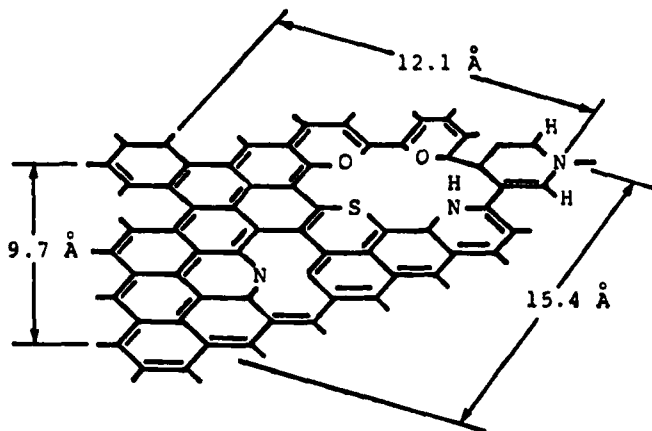


FIG. 10. Possible defect site in an aromatic sheet of the asphaltene (Tynan and Yen, 1969).

Nonporphyrin metal compounds generally have higher polarity and therefore exhibit a greater tendency for intermolecular association. This is evident in the greater proportion of nonporphyrins associated with asphaltene and in SEC-HPLC studies on metal-bearing compounds. The continuous SEC-HPLC elution time profiles of vanadium compounds in Fig. 11 for a crude oil (a), its porphyrins from methanol extraction (c), and the residuum oil (b) (nonporphyrins) remaining after methanol extraction illustrate significant apparent size differences or degrees of association (Biggs *et al.*, 1985). The nonporphyrin vanadium composites exhibit a much broader and apparently higher molecular weight profile than the vanadium porphyrins. Spencer *et al.* (1982) have also observed significant differences in the size of porphyrin and nonporphyrin metals by using SEC. They observed that the nonporphyrin fraction had a much higher molecular weight of 2000 to 3000, while porphyrins were only in the range 600–800. Since these studies use solvents as a mobile medium for SEC-HPLC, the measured sizes of nonporphyrin metal compounds may not represent their state in the environment of the original oil. In some cases, Biggs *et al.* (1985) reported slight increases in the nonporphyrin molecular weights after porphyrin extraction. Presumably, the extraction treatment also removed some of the polar compounds which help disperse the highly polar nonporphyrin metals and asphaltene.

Fish and Komlenic (1984) and Fish *et al.* (1984) have demonstrated that the vanadyl compounds associated with apparently high molecular weight fractions (2000+) observed by SEC-HPLC can, to a certain extent, be extracted as low-molecular-weight compounds with an aqueous pyridine solution. Nearly all of these extracted vanadyl compounds from either the

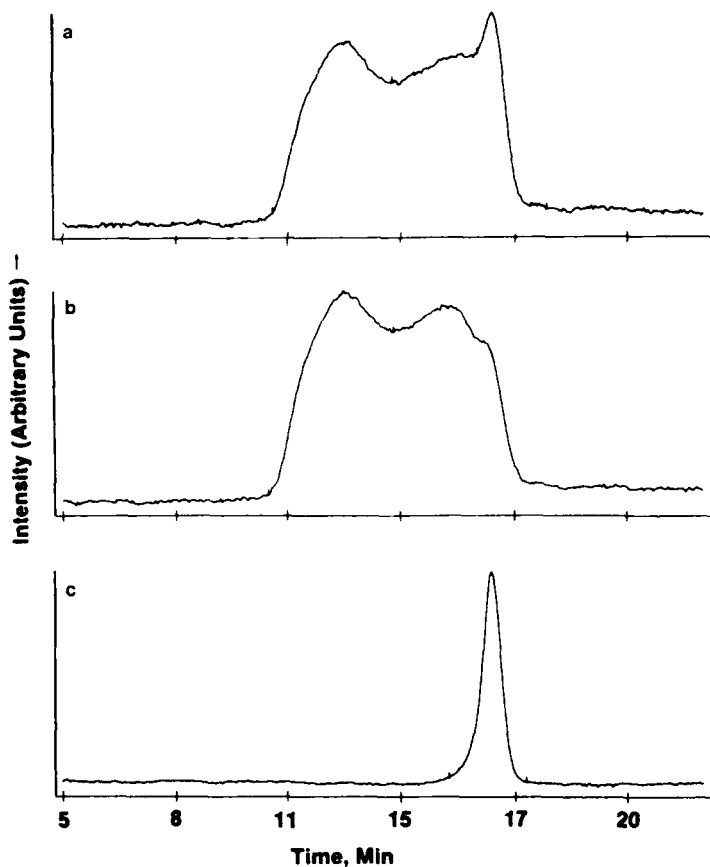


FIG. 11. Vanadium elution profiles from SEC-HCLP with element selective detection: (a) Morichal crude, (b) residual oil, (c) porphyrin fraction (Biggs *et al.*, 1985).

whole crude oil or its precipitated asphaltenes have actual molecular weights of less than 900, with the greatest proportion having molecular weights of less than 400, as shown in Table XI. The low molecular weights (less than 400) imply nonporphyrinic compounds. Since only 5 to 18% and 50 to 87% of the vanadyl compounds in the precipitated asphaltenes and whole petroleum, respectively, were extractable, it is possible that high-molecular-weight (2000+) metal compounds exist. More likely, however, this reveals the complex solubility equilibrium for these materials, with stronger associations resulting from or remaining after the extraction. The difference in the amounts extracted between the whole petroleum and the precipitated asphaltenes also reflects the effect that disrupting existing equilibrium has on the strength of intermolecular association. Without the resin solvent power in the whole petroleum,

TABLE XI

PERCENT VANADIUM IN EACH MOLECULAR WEIGHT CATEGORY OF VANADYL COMPOUNDS IN THE FOUR HEAVY CRUDE PETROLEUMS AND THEIR ASPHALTENES, MALTENES, ASPHALTENE POLAR EXTRACTS, AND EXTRACTED ASPHALTENES BY 50/100/1000 Å SEC-HPLC-GFAA ANALYSIS^{a,b}

	Boscan				Cerro Negro				Wilmington				Prudhoe Bay			
	>2000	900– 2000	400– 900	<400	>2000	900– 2000	400– 900	<400	>2000	900– 2000	400– 900	<400	>2000	900– 2000	400– 900	<400
Heavy crude																
Petroleum	28	20	23	29	31	22	20	26	31	29	23	17	28	23	19	30
Petroleum after																
extraction	32.6	23.7	23.6	20.1	37.9	33.2	19.9	9	40.2	28.3	16.8	14.7	34.6	30.5	22.9	11.9
Asphaltene	33	19	19	29	34	16	16	34	37	16	17	30	56	15	12	17
Maltenes	29	24	27	21	33	26	25	16	18	32	32	17	23	34	30	13
Asphaltene																
extract	0	4	31	65	0	5	26	69	9	14	25	52	0	0	13	87
Extracted																
asphaltene	58	16	15	11	59	15	12	14	80	10	8	2	85	8	4	4

^a Sources: Fish *et al.* (1984) and Fish and Kolmenic (1984).

^b Percentage of total vanadium determined by method of summing peak heights digitized with an integrator for the molecular weight region designated.

precipitated asphaltenes apparently exhibit stronger asphaltene–asphaltene interactions (Fish *et al.*, 1984) resulting in “hardened” micelles. Even after dissolution in highly polar solvent mediums such as pyridine, asphaltenes isolated by precipitation from the crude oil have apparent average diameters of 70 to 90 Å (Hall and Herron, 1979).

Although nickel compounds have not been examined to the same extent as vanadium compounds, reverse-phase HPLC studies by Fish *et al.* (1984) have demonstrated that nickel nonporphyrins are significantly more polar than the vanadyl nonporphyrins and are therefore expected to be more strongly associated.

The effect of temperature on the association of vanadium compounds in asphaltenes was investigated by Tynan and Yen (1969). Using electron spin resonance (ESR), they observed both anisotropic and isotropic hyperfine structures of vanadium, interpreted as bound or associated and free vanadium, from asphaltenes precipitated for a Venezuelan petroleum and reintroduced to various solvents. Higher temperatures and more polar solvents resulted in a transition from bound to free vanadium, as shown in Fig. 12. At 282°C, only 1% of the anisotropic spectrum was observed. An activation energy of 14.3 kcal/mole was observed for the transition.

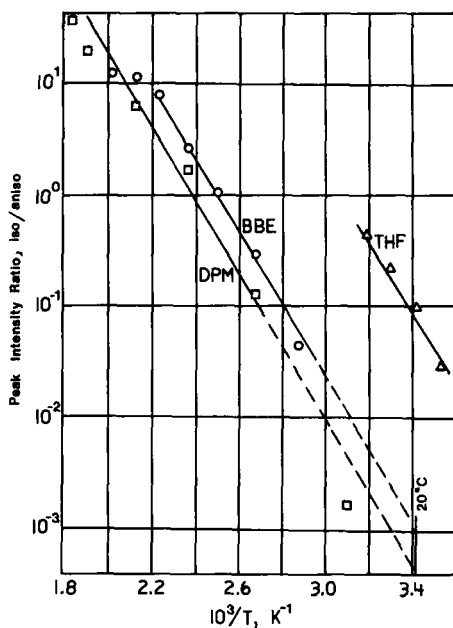


FIG. 12. Temperature dependence of the ratio of isotropic vanadium to anisotropic vanadium in asphaltenes in solutions of diphenylmethane (DPM), benzyl *n*-butyl ether (BBE), and tetrahydrofuran (THF) (Tynan and Yen, 1969).

Asaoka *et al.* (1983) also observed by ESR the temperature dependence of association with values ranging from 15 to 17 kcal/mole for asphaltenes. Dickson and Petrakis (1970) employed infrared spectroscopy and observed a 17.4-kcal/mole heat of dissociation for the dimer of vanadyl mesoporphyrin IX dimethyl ester. Although these values are significantly greater than the 2- to 8-kcal/mole range type of H bonding, it appears unlikely that ultralarge metal-bearing micellar entities or intermolecular associations exist in oil or the residuum at hydroprocessing conditions.

III. Residuum Hydrotreating Technology

A. INTRODUCTION

Residuum processing has become a major consideration in refinery process planning in recent years. Increasingly heavier crude supplies and a declining residual fuel oil market necessitate technology beyond the traditional routes such as visbreaking, coking, and low-severity hydrosulfurization (HDS) for producing transportation and fuel oils from residua (Gibson *et al.*, 1983; Siewert *et al.*, 1985). Heavy petroleum oils are troublesome due to their high levels of sulfur, nitrogen, coke precursors, and trace metals such as Ni and V. Furthermore, the residuum contains a lower ratio of hydrogen to carbon than desired lighter products, and so conversion requires that the hydrogen-to-carbon ratio be altered either by hydrogen addition or carbon rejection or by both.

Many upgrading technologies for converting 345°C+ (650°F+) atmospheric residuum or 565°C+ (1050°F+) vacuum residuum into lighter, more valuable products are described in the literature (*Hydrocarbon Processing*, 1986). No single process is likely to be a universal choice for all applications and potential bottom-of-the-barrel feedstocks. Several significant factors must be considered when choosing the appropriate residuum-processing scheme. These include product yield and quality, capital investment, operating costs (including the cost of the catalyst), process reliability, environmental constraints, and by-product disposal.

The technologies listed in Table XII are those that have been demonstrated on a commercial scale. Other technologies at various levels of development are described in the technical and patent literature.

This section will focus on the various hydroprocessing technologies that have been commercialized or are in a pilot stage near commercialization. Reactor design characteristics that differentiate the technologies will be highlighted. Included in this section is an overview of the properties and applications of commercial residuum hydroprocessing catalysts.

TABLE XII

RESIDUUM CONVERSION ALTERNATIVES^a

Thermal processing	Catalytic cracking
Visbreaking	Residuum FCC
Delayed coking	Hydroprocessing
Fluid coking	Residuum hydrotreating
Eureka	Residuum hydrocracking
Solvent processing	H-Oil
Deasphalting	LC-Fining
Gasification	Combinations (residuum hydrotreating plus)
Partial oxidation	Coking
Flexicoking	Deasphalting
	FCC

^a From Howell *et al.* (1985).

B. THE ROLE OF HYDROPROCESSING IN RESIDUUM CONVERSION

The first major processing units in a typical refinery are the crude oil distillation towers. These stills are used to separate the oil by boiling point such that each subsequent processing unit will have the appropriate boiling range feedstock. Crude oil distillation is most efficiently achieved by separation at atmospheric pressure followed by a separation under vacuum. The atmospheric distillation typically removes the 345°C– (650°F–) components. The 345°C+ bottom fraction from the atmospheric still is then fed to a vacuum distillation tower (25–40 mm Hg) which removes the remaining 565°C– (1050°F–) material from the 565°C+ vacuum residuum. The vacuum still is necessary for the heavier portion of the crude oil since the high temperatures necessary to vaporize the 345°C+ atmospheric residuum at atmospheric pressure would cause thermal degradation.

Distilled petroleum fractions are frequently subjected to further refining to satisfy the market demand for products that would be impossible to achieve by direct distillation of these materials from crude oil. The reader is referred to texts by Gary and Handwerk (1975) and Speight (1980) for additional details on petroleum refining technology.

Hydrotreating processes are typically used in petroleum refining to remove organic sulfur, nitrogen, and oxygen compounds from distilled oil fractions. These organic heteroatom compounds form SO_x and NO_x emissions if present during combustion of petroleum fuels. These emissions pose serious environmental hazards. Similarly, these heteroatoms act as poisons in catalytic cracking and reforming processes in refining (Gates *et al.*, 1979). These poisons increase operating costs and reduce the quality of the finished petroleum product. Hydroprocessing is also used to add

hydrogen to the residua. Hydrogenation reduces coking in subsequent catalytic or thermal cracking of the residua.

Hydrotreating is conducted under conditions of elevated temperature and pressure at which the oil is contacted with hydrogen over a catalyst, typically CoO–MoO₃ or NiO–MoO₃ on γ -Al₂O₃. The catalysts are produced in the oxide form and are sulfided before or during use in the reactor. Depending on the feedstock's boiling range, the hydrotreating severity varies widely, as indicated in Table XIII (Speight, 1981). Residuum feedstocks which contain the majority of the heteroatom contaminants are processed under conditions suitable for the catalysts to promote simultaneously hydrodesulfurization (HDS), hydrodenitrogenation (HDN), hydrodeoxygenation (HDO), and conversion of metal species through hydrodemetallation (HDM) reactions. Unlike S, N, and O, which are removed as gaseous products (H₂S, NH₃, and H₂O), elimination of Ni and V from petroleum results in metal deposition on, and thus irreversible fouling of, the hydrotreating catalysts (Nelson, 1976). This serious catalyst deactivation is a major problem in residuum hydrotreating and can often result in prohibitively expensive catalyst replacement costs.

Residuum hydroprocessing was first developed to produce low-sulfur fuel oil (LSFO). The early commercial applications took place in Japan during the late 1960s. Distillate HDS catalysts were applied to residua with relatively minor modifications to the catalyst properties. Metals poisoning was significant but tolerable since most early applications processed feeds with relatively low metals content at modest HDS severities. During the 1970s the demand for low-sulfur (1 wt. % or less) fuel oil increased dramatically in Japan and other world markets in response to stricter environmental regulations to achieve air pollution abatement. The inadequate supply of sweet crude oil necessitated improvements in residuum desulfurization (RDS) technology. Typical of these pioneering RDS commercial operations was Gulf's Residual Hydrodesulfurization Process, Type II, first commercialized in 1970 in Japan by Nippon Mining Company, Ltd. (Kaparakos *et al.*, 1984; Paraskos *et al.*, 1974). A simplified process flow diagram in Fig. 13 shows the single-reactor system. Filtered resid feed was combined with hydrogen gas and charged to the reactor, where desulfurization and demetallation occurred. Catalysts were developed for 75% desulfurization of Middle Eastern residua and tailored to accommodate deposits of nickel and vanadium as high as 60 wt. % of fresh catalyst. Catalyst life was 6 months. Product yields and properties for desulfurization of Kuwait and Khafji atmospheric tower bottoms to 1 wt. % sulfur 345°C+ LSFO are listed in Table XIV. Typical of desulfurization processes for fuel oil production, the distillate and naphtha yields are low (~11 vol %). Some conversion of residuum to gas oils and even to

TABLE XIII

EFFECT OF FEEDSTOCK TYPE ON DESULFURIZATION CONDITIONS^a

Feedstock	Process condition									
	Boiling range		Temperature		Hydrogen pressure		Hydrogen rate (scf/bbl)	LHSV	Catalyst life	
	°C	°F	°C	°F	psi	MPa			Months	bbl/lb
Naphtha	70–170	160–340	300–370	570–700	100–450	0.7–3.1	250–1500	5–8	36–48	500–1200
Kerosene	160–240	320–465	330–370	625–700	150–500	1.0–3.4	500–1500	4–6	36–48	300–600
Gas oil	240–350	465–660	340–400	645–750	150–700	1.0–4.8	1000–2000	2–6	36–48	200–400
Vacuum gas oil	350–650	660–1200	360–400	680–750	450–800	3.1–5.5	1000–4000	1–3	36–48	50–350
Residua	>650	>1200	370–450	700–840	750–2250	5.2–15.5	1500–10,000	0.1–2	3–24	2–50

^a From Speight (1981) and edited by authors.

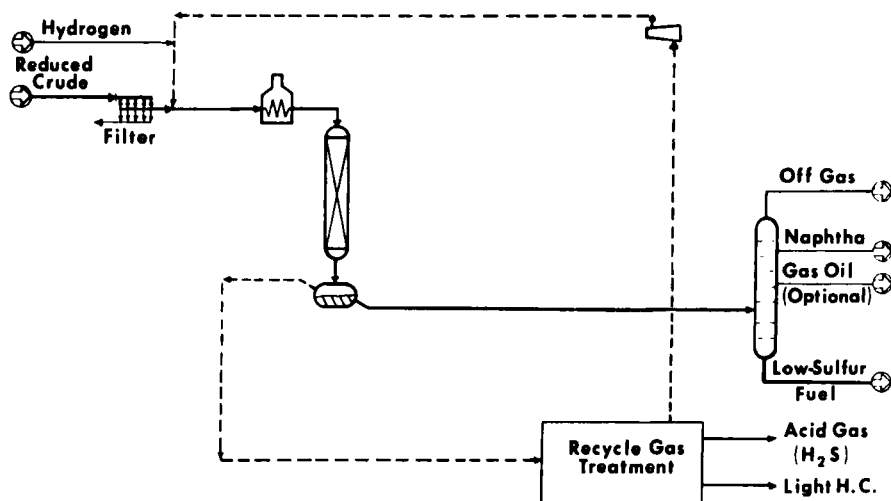


FIG. 13. Schematic flow diagram showing single fixed-bed reactor residuum hydro-processing coupled with distillation equipment to produce LSFO (Paraskos *et al.*, 1974).

TABLE XIV

YIELDS AND PROPERTIES FOR DESULFURIZATION OF KUWAIT AND KHAFJI 345°C+ ATMOSPHERIC RESIDUA^a

Chargestock	Kuwait		Khafji	
	Feed	Product	Feed	Product
Yields, run average				
H ₂ S, wt %		3.1		3.6
NH ₃ , wt %		<0.1		0.1
C ₁ -C ₄ , wt %		0.9		0.7
C ₅ -190°C naphtha, vol %		2.4		1.8
190-345°C distillate, vol %		4.6		13.2
345°C+ LSFO, vol %	100	92.9	100	86.2
Hydrogen consumption, scf/bbl		515		685
345°C+ LSFO properties				
Gravity, API	15.7	20.3	13.7	18.9
Sulfur, wt %	3.8	1.0	4.36	1.0
Nitrogen, wt %	0.22	0.18	0.26	0.23
Ramsbottom carbon, wt %	8.2	4.8	11.6	7.6
Nickel, ppm	16	5.5	28	—
Vanadium, ppm	50	9	90	14
Pour point, °C	18	15	13	10
Viscosity, cS at 100°C	37.1	17.4	59.3	31.9
% HDS		76		81
% HDN		26		26
% HDM		80		—

^a Source: Paraskos *et al.* (1974).

light products is evident by the distillate yields in these RDS operations; but until recently, the primary role of the RDS has been to produce LSFO.

In newer RDS applications the hydroprocessing unit is an integral part of the overall crude oil upgrading scheme to produce transportation fuels such as gasoline and kerosene. The RDS unit may operate independently of, or in combination with, other refinery conversion units, depending on the particular feedstock and product demand (Howell *et al.*, 1985; Siewert *et al.*, 1985). Hydroprocessing requirements and catalyst requirements are dictated by the processing route chosen.

Significant conversion of residuum directly to final products can be accomplished by operating a residuum hydrotreater at higher severity. Sulfur conversions in the range 80–95% are now routinely accomplished in the industry (Bridge *et al.*, 1975; Yamamoto, 1977; Young and Richardson, 1977). Typical of these designs for more severe operation is the use of multiple reactors and, possibly, multiple catalyst beds within reactors, as indicated by the simplified process flow diagram in Fig. 14. Recycle gas quench points are provided between reactors, and between beds if necessary, to control reactor temperature for maximum retention of catalyst activity during the cycle. The hydroprocessing unit operates in conjunction with distillation equipment to produce final product quality 345°C– fuels. Hydrodemetallation is necessary in this application to protect the primary hydrodesulfurization and boiling range conversion catalyst from being

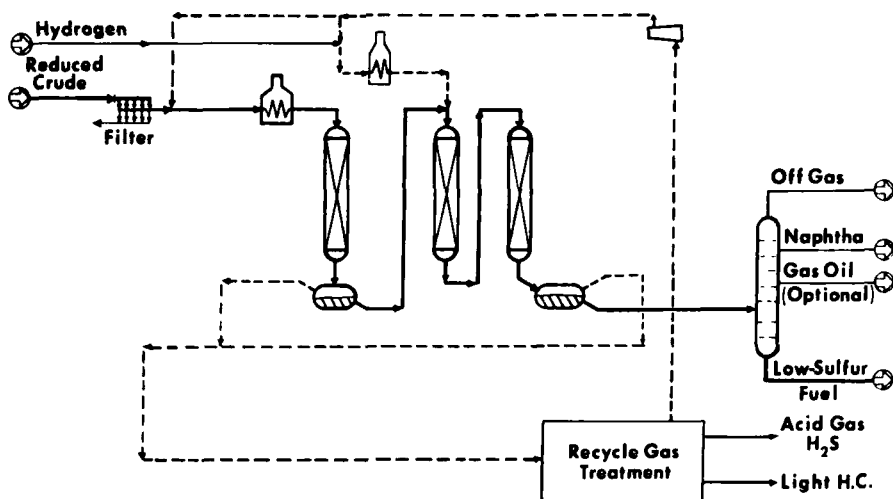


FIG. 14. Schematic flow diagram showing multiple fixed-bed reactor residuum hydroprocessing coupled with distillation equipment for high-severity RDS (Paraskos *et al.*, 1974).

TABLE XV

YIELDS AND PROPERTIES FOR HIGH-SEVERITY RDS OF KUWAIT 345°C+
ATMOSPHERIC RESIDUUM^a

	Feed	0.3% Sulfur fuel	0.1% Sulfur fuel
Yields, run average			
H ₂ S, wt %		3.73	3.93
NH ₃ , wt %		0.12	0.17
C ₁ -C ₄ , wt %		0.89	1.14
C ₅ -190°C naphtha, vol %		3.8	4.6
190-345°C distillate, vol %		12.5	14.0
345°C+ fuel oil, vol %	100	85.6	83.5
Hydrogen consumption, scf/bbl		650	725
190°C+ fuel properties			
Gravity, API	16.6	22.8	23.3
Sulfur, wt %	3.8	0.33	0.11
Nitrogen, wt %	0.22	0.14	0.10
Ramsbottom carbon, wt %	9.0	3.8	3.2
Nickel, ppmw	15	1.5	0.5
Vanadium, ppmw	45	2.6	1.2
Pour point, °C	15	2	-9
Viscosity, cS at 100°C	54.5	18.2	15.9
% HDS		91	97
% HDN		40	57
% HDM		93	97

^a Source: Campagna *et al.* (1982).

poisoned quickly by metal deposition. Demetallation catalysts with extended life and high metals capacity are desired.

Yields and properties for high-severity desulfurization of Kuwait atmospheric tower bottoms are contained in Table XV. Residuum conversion to lighter products is apparent by the higher distillate yields relative to low-severity yields indicated in Table XIV. The LSFO product properties affected to the greatest extent with increasing severity are sulfur, viscosity, and pour point.

The cut point of low-sulfur fuel oils will depend upon several factors including the RDS severity and the availability of additional upgrading equipment to produce higher-value transportation fuels. Blending the entire 345°C+ stream as LSFO is one option. Alternatively, the 345-540°C (650-1000°F) gas oil fraction, low in heteroatom content, is an attractive hydrocracking or catalytic cracking feedstock for producing diesel, jet, and gasoline fuels (Kanazawa *et al.*, 1984). This also reduces the yield of LSFO. The remaining 540°C+ vacuum residuum may be suitable as LSFO blending material directly, without the need for light cutter stocks,

provided that the sulfur content and viscosity are sufficiently reduced in the RDS.

An alternative processing strategy for disposing of the 540°C+ RDS bottoms shown in Fig. 14, other than as LSFO, is to send the entire 345°C+ stream to a catalytic cracker. The combination of residuum hydrotreating–fluidized catalytic cracking (FCC) has the potential to significantly upgrade residuum to lighter, more valuable products (Hohnholt and Fausto, 1985, 1986). For this scheme to operate economically, the hydrotreated residuum must have low metals (10–20 ppm) and nitrogen (<2000 ppm) content to avoid excessive catalyst consumption in the FCC and to maintain gasoline yield. The Ramsbottom carbon content of the FCC feed must also be low enough (<5 wt. %) to stay within the FCC regenerator constraints. The reduction of Ramsbottom carbon by hydrogenation effectively reduces the FCC coke yield and the regenerator air blower demand. In addition, the conversion of polynuclear aromatics to monoaromatics, naphthenes, and paraffins improves gasoline yield in the FCC. Sulfur must be low enough to meet environmental limits for the FCC regenerator flue gas. In this processing scheme, high-activity HDM catalysts are desirable. Properties of several Middle Eastern feedstocks hydrotreated for FCC processing are listed in Table XVI. High levels of metals removal are apparent.

The combination of residuum hydrotreating and delayed coking can offer considerable flexibility and capacity in handling heavy crudes (Teichman *et al.*, 1982; Beaton *et al.*, 1986. Such a configuration is shown schematically in Fig. 15. Vacuum gas oil and residuum from distillation units are processed in the RDS unit to lower the heteroatom content and effect a partial boiling range conversion of the oil. The 540°C– product is suited for additional upgrading in cracking units due to its low sulfur, nitrogen, and polycyclic aromatic content. The 540°C+ hydrotreated residuum is processed in the delayed coker by itself or in combination with raw vacuum residuum to further yield light products and gas oils, in addition to coke.

The residuum hydroprocessing–coking combination offers several advantages over coking alone. The RDS–coking scheme produces a greater volume of higher-value liquid products and less coke. These liquid products are lower in sulfur and nitrogen and have a higher hydrogen-to-carbon ratio which makes them superior feedstocks for further downstream processing. The remaining coke, reduced in quantity, is also of higher quality. The reduced sulfur and metals in the uncovered residuum enables production of higher-value anode-grade coke. The degree of hydrotreating prior to coking will be dictated by balancing product demands with operating expenses. Complete demetallation is rarely

TABLE XVI
PROPERTIES OF RDS FEEDSTOCKS AND PRODUCTS PRIOR TO CATALYTIC CRACKING^a

Feedstock	Paraffinic Middle East atmospheric residuum		Typical Middle East atmospheric residuum		Middle East atmospheric residuum and 15% Venezuelan atmospheric residuum	
	Feed	Product	Feed	Product	Feed	Product
345°C+ properties						
Gravity, API	21.0	25.0	17.5	23.6	17.0	22.1
Sulfur, wt %	1.8	0.22	2.7	0.25	3.0	0.37
Nitrogen, ppm	1600	818	1700	947	2400	1465
Concarbon, wt %	3.9	1.1	6.0	1.8	7.3	3.5
V and Ni, ppmw	13	0.4	22	1.0	85	12.4
Viscosity, cS at 50°C	82.6	61.1	130.8	71.9	152.5	84.9
% HDS		88		91		88
% HDN		49		44		39
% HDM		97		95		85

^a Source: Hohnholt and Fausto (1986).

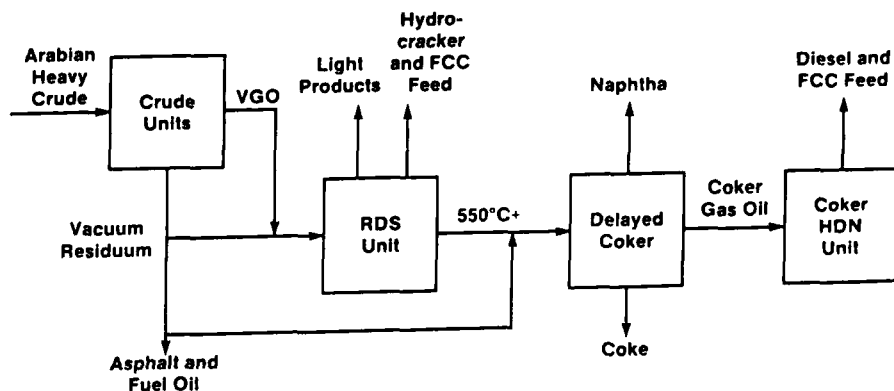


FIG. 15. Schematic flow diagram showing residuum hydroprocessing in combination with delayed coking to produce cracking feeds and light products (Howell *et al.*, 1985).

necessary prior to coking; 80–90% desulfurization and 70–80% demetallation are common, as illustrated in Table XVII for Arab Heavy RDS prior to coking. A long catalyst lifetime and high metals tolerance are likely to be more important than high activity in this application.

Another processing option involves the use of solvent deasphalting (SDA) to treat the vacuum residuum prior to hydroprocessing (Hung *et al.*,

TABLE XVII
PROPERTIES OF RDS FEEDSTOCK AND PRODUCTS
PRIOR TO COKING^a

Feedstock	Arab Heavy 405°C+	
	Feed	Product
Yields, vol %		
C ₅ –345°C	—	12
345–550°C	45	34
550°C+	55	37
Hydrogen consumption, scf/bbl		900
C ₅ + properties		
Gravity, API	12.1	21.6
Sulfur, wt %	4.2	0.6
Ramsbottom carbon, wt %	13.7	6.0
Nickel, ppmw	29	10
Vanadium, ppmw	102	26
Iron, ppmw	4	0
% HDS		88
% HDM		79

^a Source: Howell *et al.* (1985).

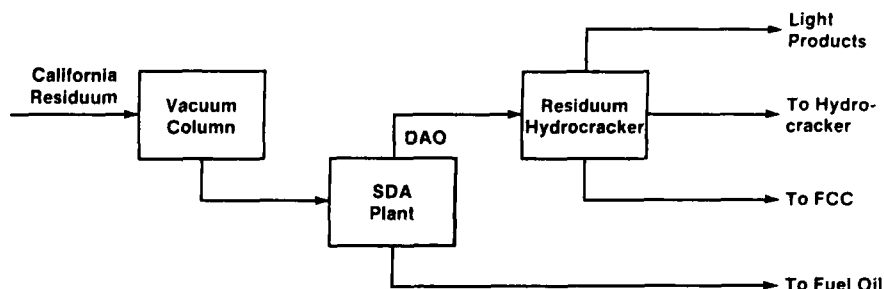


FIG. 16. Schematic flow diagram showing solvent deasphalting (SDA) combined with residuum hydrocracking (Howell *et al.*, 1985).

(1986b). The deasphalted oil (DAO) is sent to a DAO hydrocracker for conversion and upgrading to yield low sulfur and nitrogen content light products and cracker feeds, as depicted in Fig. 16. The asphalt fraction (up to 50% of the residuum) can be sent directly to a coker or blended with cutter stock as high-sulfur fuel oil (HSFO). This process route is particularly well suited for feedstocks in which the sulfur, metal, and Ramsbottom carbon contaminants are concentrated in the asphaltene portion of the residuum. In this application it is desirable to use high-activity catalysts

TABLE XVIII

FEED AND PRODUCT PROPERTIES FOR DAO HYDROCRACKER^a

Feedstock	California DAO	
	Feed	Product
Yields, vol %		
C ₅ -345°C	0	35
345-540°C	30	45
540°C+	70	25
345°C+ properties		
Gravity, API	15	26.3
Sulfur, wt %	1.5	0.005
Nitrogen, wt %	0.6	0.05
Ramsbottom carbon, wt %	5	1
Nickel, ppmw	20	<0.1
Vanadium, ppmw	8	<0.1
Iron, ppmw	15	<0.1
% HDS		>99
% HDN		92
% HDM		>99

^a Source: Hung *et al.* (1986a).

capable of promoting boiling range conversion simultaneously with heteroatom removal. Generally, the 540°C+ (1000°F+) conversion is 45–75% with a 345°C– (650°F–) yield of 25 to 50% of the DAO feed. Metals content of the DAO is generally low, as the example in Table XVIII illustrates. Graded catalyst beds have been developed which are capable of removing essentially all of the DAO metals and sulfur and high levels of nitrogen, while effecting the boiling range conversion.

C. DEVELOPMENTS IN RDS–HDM HYDROPROCESSING TECHNOLOGY

This section provides an overview of current residuum hydroprocessing technology with the intent of highlighting differences between the operation of the processes and their ability to upgrade the heavier feedstocks. Currently, the commercial operating capacity for residuum hydroprocessing in the Free World is close to 1.2 million BPSD, as indicated in Table XIX. This capacity reflects technology licensed by several companies. Process conditions, reactor type, and catalysts used for each of these commercially licensed technologies are compared in Table XX. Also included in this table are several technologies in near-commercial stages of development. These emerging technologies reflect the continued interest in residuum hydroprocessing. For additional information, the reader is referred to reviews by Speight (1981) and Schuetze and Hofmann (1984) and to references cited in this section for individual processes.

The distinction in Table XX between hydrotreating and hydrocracking processes is frequently misleading when residuum hydroprocessing is being considered. Hydrotreating conventionally has been referred to processes

TABLE XIX
COMMERCIAL RESIDUUM HYDROPROCESSING OPERATING CAPACITY,
FREE WORLD, JANUARY 1986^a

Process	Licensor	Units	Total capacity (BPSD) ^{b,c}
RDS/VRDS/RHDS	Chevron/Gulf	12	488,100
RCD/BOC UNIBON	UOP, Signal	5	132,900
Unicracking/HDS	UNOCAL Corp.	3	201,000
Residfining	Exxon	2	138,000
H-Oil	HRI/Cities	4	115,500
LC-Fining	Lummus/Cities	1	60,000
HDS	Shell	1	45,000

^a Source: Lasher and Lasher (1986).

^b Includes DMO/DAO units. Chevron has a 32,000 BPSD DAO hydrocracker; UOP has three DMO units with a total capacity of 84,200 BPSD.

^c Excludes units under construction.

TABLE XX
HYDROPROCESSING TECHNOLOGY^a

Process	Operating conditions			H ₂ consumption (scf/bbl)	Reactor type	Catalyst	Commercial operation
	Temperature (°C)	Pressure (psig)	LHSV (hr ⁻¹)				
Hydrotreating	350–440	750–3000	0.1–2	550–1600	Fixed bed	Group VIB and VIII on Al ₂ O ₃	Yes
Chevron RDS or VRDS					Fixed bed		Yes
Exxon RESIDfining					Fixed bed		Yes
Gulf RDS					Fixed bed		Yes
Shell RDS					Fixed bed without bunker flow		
UNOCAL Unicracking/RDS					Fixed bed		Yes
UOP RCD/BOC Unibon					Fixed bed		Yes
Hydrocracking							
CANMET	470	1500	3	1300	Slurry	Fe/Coal	No
Chiyoda ABC	390–420	1100–2300	0.5–1.5	500–650	Fixed bed	CoMo/Mg–Si	No
Combi-VEBA	430–470	1800–4350	0.4–1.0	1000–1800	Slurry/ fixed bed	Lignitic coke/ HDS catalyst	No
Dynacracking, HR	480	400–600	—	—	Fluid bed	Inert particles	No
H-Oil	430–470	1400–3000	0.5–1.5	800–1100	Ebullated bed	Group VIB, VIII	Yes
LC-Fining	430–470	1400–3000	0.5–1.5	750–1400	Expanded bed	Group VIB, VIII	Yes
M-Coke, Exxon	440	2000–3000	1	500–800	Slurry	Mo/coke	No
UOP Aurabon	450	2000–3000	0.5–2.0	700	Slurry	Oil metals (V, Ni)	No

^a From Schuetze and Hofmann (1984) and edited by authors.

for improving petroleum product quality, such as HDS and HDN. Boiling range conversion generally does not exceed 25%. With hydrocracking, boiling range conversion to lighter distillate products in excess of 50% is commonly attained simultaneously with the removal of sulfur and nitrogen, if present. Upgrading metal-containing feeds, by their very nature, requires processing of high-boiling-range, high-molecular-weight material. In this case, both heteroatom (sulfur, nitrogen, and metals) removal and boiling range conversion are required to provide the desired product yield and quality.

Reactor design is a key element in each process listed in Table XX. The method of feed introduction, the arrangement of the catalyst bed, and the mode of operation have an impact on the ability to process residua. For this reason, classification by reactor type provides a convenient and appropriate distinction for discussing hydroprocessing technology. The most common reactor designs include fixed beds, ebullated or expanded beds and slurry beds, and moving-bed reactors. These classifications are discussed in more detail next.

1. *Fixed-Bed Reactors*

The most common reactor design for residuum hydroprocessing is the down-flow, fixed-bed reactor shown in Fig. 14. This technology is utilized in the Chevron RDS and VRDS (Gibson *et al.*, 1983); Chiyoda Asphaltenic Bottom Cracking (ABC) (Takeuchi *et al.*, 1983; Komatsu *et al.*, 1986); Exxon RESIDfining (Sosnowski *et al.*, 1981); Gulf RDS (Vanik *et al.*, 1977; Kaparakos *et al.*, 1984), now licensed by Chevron; UNOCAL Unicracking/RDS (Miller *et al.*, 1983); and UOP RCD/BOC Unibon Process (Sikonia, 1980). Feedstock and hydrogen are introduced at the top of the reactor and flow or trickle down over the catalyst bed. The name "trickle-bed reactor," commonly used when referring to these fixed-bed reactors, originates from this flow pattern. The efficiency of the reactor requires proper liquid distribution at the reactor inlet to ensure wetting of the stationary catalyst and uniform flow throughout the bed. With fixed-bed reactors it is common to use multiple reactors and/or catalyst zones, as previously illustrated in Fig. 14. This design feature enables injection of cold hydrogen or recycle gas between stages to quench reaction exotherms and control temperature. The Gulf RDS, Type IV design allows for interstage gas removal after the first reactor (Paraskos *et al.*, 1974). This minimizes the deleterious effects of high concentrations of H_2S and NH_3 cascading on subsequent catalytic reaction zones. Staging also allows for liquid redistribution. The high efficiency of the UNOCAL process is attributed in part to a proprietary liquid distribution system (Richardson *et al.*, 1979).

Special graded reactors and catalyst beds are frequently employed in fixed-bed designs to deal with high-metals chargestocks. Gulf (Kaparakos *et al.*, 1984) and UNOCAL (Richardson *et al.*, 1979) technologies utilize a separate guard-bed reactor to protect the principal hydrotreating catalyst from potential plugging material in the residuum feed. This guard bed typically contains a large-pore, low-activity catalyst with a high capacity for particulates and metals deposits. Chevron RDS technology utilizes graded catalyst beds to maintain catalyst performance and combat excessive reactor pressure drop in the presence of high quantities of deposited metals (Howell *et al.*, 1985). The first catalyst zone contains a large-pore, low-HDS-activity catalyst tailored for high metals capacity. Subsequent catalyst zones contain higher-activity catalysts for the desired degree of sulfur removal and boiling range conversion. The use of multiple beds versus single beds generally depends on the operating philosophy of the company designing the technology and the feedstock characteristics.

In fixed-bed reactors the catalyst bed is poisoned progressively. (See the discussion in Section V). Deactivation from metals deposits occurs at the inlet and moves through the bed, gradually depleting the active catalyst zone. To combat the declining activity, the operating temperature is continually increased during the length of the run to maintain a target product property or yield. However, this results in a gradual shift in the properties and yields of the entire product slate owing to differences in the activation energies of the numerous reactions occurring. This policy of increasing operating temperature ceases when a process or metallurgical constraint is reached, at which time the run is terminated. The fixed-bed reactor must be taken off stream to regenerate the catalyst or to replace the catalyst if it has been severely contaminated by metals. In either case, the time-consuming procedure contributes to costly downtime. Reduction of cycle time can be especially acute with feedstocks containing suspended particulate matter such as dirt, rust, and scale. Bed plugging by such material may lead to excessive pressure drop, which forces reactor shutdown before the catalyst is deactivated. Flow channeling and nonuniform liquid and gas distribution within the reactor may also develop and reduce performance efficiency.

2. *Ebullated, Expanded, and Slurry-Bed Reactors*

The ebullated, expanded, and slurry-bed reactors utilize a fluent catalyst zone unlike the stationary catalyst design of fixed-bed reactors. This design overcomes several of the problems encountered when processing residua in fixed-bed catalytic reactors. The commercial H-Oil[®] process (Eccles *et al.*, 1982; Nongbri and Tasker, 1985) employs the ebullated-bed, whereas the

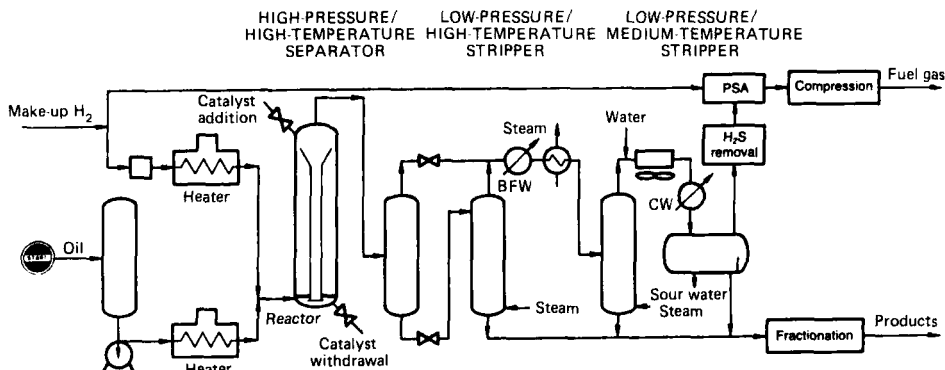


FIG. 17. Schematic flow diagram of residuum hydroprocessing unit utilizing LC-Fining expanded-bed reactor (van Driesen and Fornoff, 1985).

C-E Lummus/Cities Service LC-Fining process licensed by AMOCO (van Driesen and Fornoff, 1985; Beaton *et al.*, 1986) utilizes an expanded-bed reactor. A flow diagram of the LC-Fining process is shown in Fig. 17. The Canadian DOE CANMET process (Menziez *et al.*, 1981), the Exxon M-Coke (Bearden and Aldridge, 1981), and the UOP Aurabon (Anderson *et al.*, 1982) processes now in pilot plant stages of development employ slurry reactors.

In the ebullated-bed and expanded-bed reactors, liquid chargestock and hydrogen are introduced at the bottom and product is taken from the top. The upward flow of reactor liquid, achieved by internal liquid recycle pumps and recycle gas and hydrogen, is used to expand the catalyst bed and maintain the entire reactor contents, including catalyst, backmixed. Catalyst in the form of extrudates or as particles may be used; $\frac{1}{32}$ - and $\frac{1}{25}$ -in. catalyst extrudates are common. Isothermal operation is typical with these reactors due to the mixing, which provides an efficient means for contacting the oil, hydrogen, and catalyst; both temperature and concentration gradients are minimized. The exothermic heat of reaction can be easily dissipated. However, stagnant zones are known to develop and careful monitoring is required to prevent growth of such zones, which can lead to unstable and runaway conditions.

Slurry reactors achieve a similar intimate contacting of oil and catalyst and yet may operate with a lower degree of backmixing than the ebullated or expanded bed. In the slurry design, heavy oil is mixed with finely divided catalyst particles and fed upward, with hydrogen, through an "empty" reactor vessel. Oil and catalyst flow concurrently and may approach plug-flow behavior.

Reactor designs utilizing fluent catalyst beds facilitate the continuous addition and withdrawal of catalyst during operation. The averaged activity of the catalyst inventory reaches a steady state that results in constant product quality. This is a major difference compared to fixed-bed units in which reaction selectivities are changing during the run in response to increases in operating temperature necessary to combat declining activity. Similarly, aged catalyst can be withdrawn and fresh catalyst introduced without shutting down the hydroprocessing reactor. This increased operating factor decreases refinery maintenance costs associated with catalyst dumping and reloading.

Feedstocks containing high levels of mineral and particulate matter are ideally suited for these types of reactors. The solid suspended material in the feed will circulate throughout the expanded catalyst bed without causing frequent plugging problems and with no increase in pressure drop. Residuum conversion in excess of 65 vol % is possible even with high-metals feeds, as shown in Table XXI. This high-severity operation is possible without a severe penalty in operating factor due to the ability to continually add fresh catalyst to maintain high-activity inventory. Also, the use of small catalyst extrudates without a pressure drop penalty results in a considerable advantage in reaction rate relative to $\frac{1}{16}$ -in. extrudates in

TABLE XXI
YIELD AND PRODUCT QUALITY FOR HIGH-CONVERSION LC-FINING OF
LLOYDMINSTER/COLD LAKE RESIDUA^a

	Feed ^b	LC-Fining case I	LC-Fining case II
Yields			
C ₄ -, wt %	—	8.3	10.6
C ₅ -205°C, vol %	—	15.2	25.7
205-345°C, vol %	—	23.7	39.9
345-524°C, vol %	31	40.9	29.5
524°C+, vol %	69	24.1	10.3
Hydrogen consumption, scf/bbl		1160	1655
524°C+ conversion, vol %		65	85
% HDS		84	84
345-524°C properties			
Gravity, API	16.0	19.8	17.5
Sulfur, wt %	3.3	0.60	1.1
524°C+ properties			
Gravity, API	2.6	3.4	-4.5
Sulfur, wt %	5.7	2.2	3.3

^a Source: Van Driesen and Fornoff (1985).

^b Feed contains approximately 190 ppmw V and 90 ppmw Ni.

fixed-bed reactors. Reactions in these smaller catalysts occur with higher effectiveness factors owing to reductions in diffusional limitations, and the catalysts are less susceptible to pore-mouth plugging by metal deposits.

3. Moving-Bed Reactor

The Shell RDS process is unique in its utilization of a moving-bed or bunker reactor (van Zijl Langhout *et al.*, 1980). This reactor operates upstream of a conventional fixed-bed, trickle-flow reactor. In the moving-bed configuration, catalyst, oil, and process gases are introduced at the top of the bed, as depicted in Fig. 18. Oil trickles down over the catalyst, and the catalyst particles themselves slowly pass down through the bed under the force of gravity as the catalyst is withdrawn at the base. Catalyst velocity is generally significantly lower than the superficial velocity of the oil. This movement of catalyst allows continuous addition and withdrawal of catalyst as necessary to maintain the appropriate level of activity. Steady-state catalyst activity results in constant bunker reactor product quality. This is highly desirable when further hydrotreating of the product is practiced. High stream factors also result from the moving catalyst since replacement is possible without interrupting operation. The moving-bed reactor is especially attractive upstream of the primary desulfurization reactor if high-metals feedstocks are to be processed. An inexpensive, sacrificial catalyst with a high metals capacity and low HDS activity is

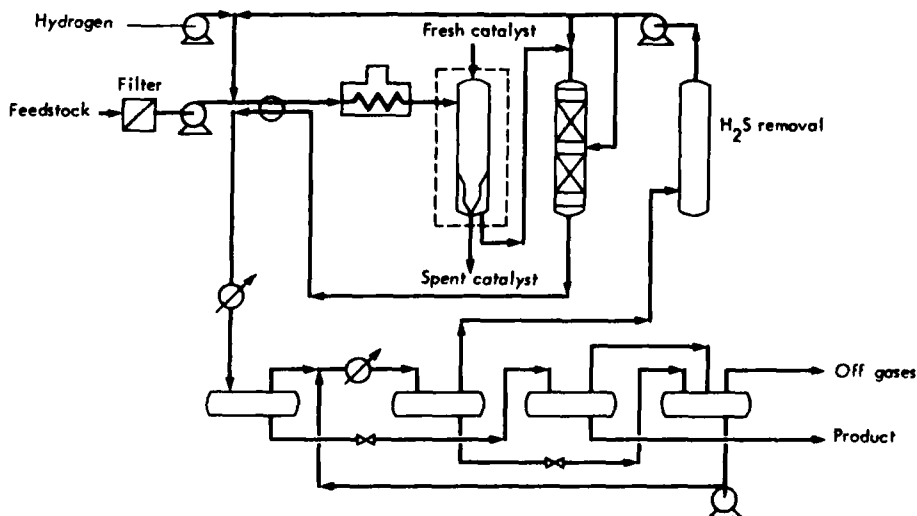


FIG. 18. Schematic flow diagram of residuum hydroprocessing unit utilizing Shell bunker reactor upstream of fixed-bed reactor (Speight, 1981).

TABLE XXII
SHELL BUNKER-FLOW CONVERSION OF VENEZUELAN RESIDUA^a

	Venezuelan 1 vacuum residuum		Venezuelan 2 atmospheric residuum	
	Feed	Product	Feed	Product
C ₅ + properties				
Gravity, API	6.8	11.4	5.7	11.1
Sulfur, wt %	3.2	2.3	5.9	3.6
Metals, ppmw	750	180	1500	320
C ₇ asphaltenes, wt %	13	8	17	6
Viscosity, cS at 100°C	4800	130	4310	480
Pour point, °C	>50	10	50	8
% HDS		28		40
% HDM		76		79

^a Source: van Zijl Langhout *et al.* (1980).

typically employed in the moving-bed reactor to protect downstream HDS catalysts from metal poisoning. This demetallation catalyst is generally used on a once-through basis and then discarded. The severe grinding and abrasion encountered in the moving-bed reactor requires strong, attrition-resistant catalysts. Pilot plant data in Table XXII illustrate the ability of the bunker reactor to handle high-metals Venezuelan residua. The example illustrates the low HDS relative to HDM activity of the catalysts typically used in the bunker reactor. Further hydroprocessing is required to achieve high levels of desulfurization.

4. Miscellaneous Reactor Configurations

Two additional hydroprocessing technologies have advanced to near-commercial, pilot plant stages of development and reflect additional reactor configurations. The Dynacracking process of Hydrocarbon Research, Inc. (Rakow and Calderon, 1981), combines thermal hydrocracking and coke gasification in separate zones of a single-reactor vessel. Residuum oil is fed into a well-mixed, isothermal fluidized bed of inert particles in the upper section of the reactor, where hydrocracking occurs to gaseous products and coke. Metals in the oil deposit on the fluidized particles and contribute a catalytic component to the hydrocracking reactions. The fluidized, metal- and coke-laden particles eventually move down to the lower section of the reactor, passing through a stripper to remove unconverted heavy-liquid hydrocarbons. There the particles are gasified by using oxygen and steam to produce a H₂-CO mixture which

both fluidizes and provides hydrogen and heat to the upper hydrocracking zone. Solid particles may be withdrawn from the gasifier to maintain the proper metal inventory in the reactor. Once in operation the combined reactors run in thermal balance. Feeds with high particulate content pose no plugging problem to this process. Hydrogen consumption is low, but liquid products generally require additional downstream hydroprocessing prior to use.

The VEBA Combi-Cracking (VCC) process originated from development work in coal liquefaction technology (Graeser and Niemann, 1982; Graeser *et al.*, 1986). The VCC process combines two steps, liquid-phase hydrogenation or hydrocracking of the heavy residuum and gas-phase hydrotreating of the products. The initial liquid-phase hydroprocessing is conducted in tubular reactors using a once-through catalyst of "Bayer" mass or lignitic carbonization coke which is slurried with the oil. The once-through catalyst avoids complications of catalyst deactivation and regeneration. The second stage of gas-phase hydrotreating is carried out in fixed-bed reactors with conventional HDS catalysts. The VCC process provides flexibility for processing a variety of heavy feeds, including those with high solids contents, to high conversions.

D. COMMERCIAL RESIDUUM HYDROPROCESSING CATALYSTS

Residuum hydroprocessing catalysts constitute the most demanding component of residuum upgrading technology. This fact is reflected in the outpouring of literature from catalyst development laboratories. Catalysts designed for fixed-bed reactors dominate the technical literature, reflecting the relative maturity and current commercial prominence of fixed-bed technology. Many of these catalysts are, however, appropriate for other reactor configurations, particularly the ebullated and expanded-bed reactors.

Residuum-hydrotreating catalysts typically contain 1 to 8 wt.% group VIII metal oxide and 3 to 20 wt.% group VIB metal oxide dispersed on a high-surface-area support, typically alumina. An important consideration in the formulation of the catalyst is the level of acidity of the support material. Introduction of acidic components into the support such as amorphous silica-alumina, phosphorus (Fitz and Rase, 1983), or zeolites (Sue and Fujita, 1986) may be desirable in applications where higher hydrocracking activity is desired. Conversely, low-acidity or neutral supports are used when deactivation due to excessive coking is to be avoided (Maier *et al.*, 1986). Physical properties of the catalysts reflect the properties of the support. Bulk density ranges from 0.4 to 0.7 g/ml, whereas pore volume varies from 0.4 to 1.5 ml/g and surface area typically ranges

from 50 to 300 m²/g. The average pore diameter of hydrotreating catalysts ranges from 40 to 400 Å, but catalysts with bimodal pore structures may contain some pores as large as 1000 to more than 10,000 Å.

Newer catalyst formulations have achieved improved control of hydroprocessing reactions by adjustments in the catalytic activity level. Catalysts intended for disposal after processing high-metals residua have avoided using high-metals loadings and combinations of expensive group VIII and VIB metals. Instead, low loadings or catalysts comprised of Ni and V supported on Al₂O₃ have been used with the intention of seeding the demetallation reactions and then relying on metals deposited from the oil to maintain activity (Toulhoat *et al.*, 1985).

Recent developments have also focused on catalysts having a low tendency toward coke formation and catalysts with tailor-made physical properties to accomodate higher metal deposition loadings. As discussed in Sections IV and V, pore size, pore size distribution, and particle size and shape are critical factors in determining activity and stability in residuum processing. However, high catalyst activity and high catalyst stability are a difficult combination to achieve. Maximum metals tolerance is achieved when the metal-bearing species fully penetrate the catalyst pore structure, but this leads to poisoning of the inner sites for further reaction. Conversely, if metal penetration is shallow due to fast reaction or controlled pore size, the inner portions of the catalyst remain active, but are soon inaccessible to reactants due to pore-mouth plugging by metal deposition (Douwes *et al.*, 1980). The selection of the optimum HDM catalyst will generally be case specific and determined by residuum feed properties, process operating conditions, and product quality requirements (Hung *et al.*, 1986a). Hydrodemetallation catalysts which permit deep metals penetration and uniformly accumulate metals deposits are desired when the HDM catalyst metals capacity is controlling run length. Conversely, when run length is not limited by the metals capacity of the HDM catalyst, catalysts with high activity for HDM and perhaps moderate activity for HDS and Ramsbottom carbon conversion are desirable. Finally, high-activity HDM catalysts which also have high HDS and Ramsbottom carbon removal activities find application with low-metals-content feeds, with which there is little chance of exhausting the metals capacity of the catalysts during the run length.

The variety of applications and the market growth potential have attracted numerous entries into the residuum hydroprocessing catalyst market, as indicated by the compilation of commercial vendors and catalysts in Table XXIII. Catalysts are available in an assortment of shapes, sizes, and formulations, but detailed information on catalytic metals, support composition, pore size, and pore size distribution is sketchy.

TABLE XXIII

COMMERCIAL RESIDUUM HYDROPROCESSING CATALYSTS^a

Company	Catalyst designation	Feed and/or application	Form ^b	Bulk density (lb/ft ³)	Support	Catalytic metals	Notes
AKZO Chemie/Ketjen	KF H-Oil	Resid HDT	Cylinder	—	Alumina	Co-Mo and Ni-Mo	Different particle sizes available
	KF 643/644	HDM	AO	45	Alumina	Ni-Mo	
American Cyanamid Co.	HDS-1442A/B	Resid or VGO	Cylinder	34	Alumina	Co-Mo	
	HDS-1443A/B	Resid or VGO	Cylinder	36	Alumina	Ni-Mo	
Catalyst and Chemicals Industries Co., Ltd.	CDS-R2	Resid HDS	Cylinder	42	—	—	
	CDS-R9	Resid HDS	Cylinder	42	—	—	
	CDS-DM-1	Resid HDM	Cylinder	36	—	—	
Chevron Research Co.	ICR 105	Resid HDT	P	49	—	—	Tailored pore size supports
	ICR 106	DAO	P	—	—	—	
	ICR 114	DAO	P	—	—	—	
	ICR 121	DAO, resid HDT	P	43	—	—	
	ICR 122	DAO, resid HDT	P	30	—	—	
	ICR 124	DAO, resid HDT	P	30	—	—	
	ICR 125	Resid HDT	P	—	—	—	
	ICR 129	Resid HDT	P	—	—	—	
Exxon Research & Engineering Co.	RT-2	Resid	—	—	—	Co-Mo + Ni-Mo	
	RT-228	Resid	—	—	—	Co-Mo + Ni-Mo	
	RT-621	Resid	—	—	—	Co-Mo + Ni-Mo	
Gulf Research & Development	A/VR-A	Resid HDS, <75%	Cylinder	32-40	Alumina	P	$\Delta P < A/VR-A$ Coke resistant
	A/VR-B	Resid HDS, <75%	Multi-lobe	30-38	Alumina	P	
	A/VR-C	Resid, 75-93% HDS	Cylinder	33-41	Alumina	P	

(Continued)

TABLE XXIII (Continued)

Company	Catalyst designation	Feed and/or application	Form ^b	Bulk density (lb/ft ³)	Support	Catalytic metals	Notes
156 Haldor Topsoe	A/VR-D	Resid, 75–93% HDS	Multi-lobe	33–41	Alumina	P	$\Delta P < A/VR-C$
	A/VR-E	Resid, >93% HDS	Cylinder	33–42	Alumina	P	Deep HDS, regenerable
	A/VR-F	Resid, >93% HDS	Multi-lobe	31–40	Alumina	P	$\Delta P < A/VR-E$
	A/VR-G	Resid HDS, <75%	Cylinder	34–40	Alumina	P	Alternative metals
	A/VR-H	Resid HDS, <75%	Multi-lobe	32–38	Alumina	P	A/VR-A $\Delta P < A/VR-G$
	A/VR-I	Resid HDS, HDM	Multi-lobe	30–37	Alumina	P	Metals tolerant
	TK-709	DAO, resid	Ring, cylinder	25(R), 33(C)	—	Mo	Low HDS, high HDM
	TK-710	DAO, resid	Ring, cylinder	31(R), 40(C)	—	Co–Mo	>HDS than TK-709
	TK-711	DAO, resid	Ring, cylinder	31(R), 40(C)	—	Ni–Mo	>HDS than TK-709
	TK-750	DAO, resid	Ring, cylinder	31(R), 40(C)	—	Co–Mo	>HDS than TK-710
	TK-751	DAO, resid	Ring, cylinder	31(R), 40(C)	—	Ni–Mo	>HDS than TK-711
	TK-770	DAO, resid	Cylinder	45	—	Co–Mo	High HDS, low HDM
	TK-771	DAO, resid	Cylinder	45	—	Ni–Mo	High HDS, low HDM
Harshaw/Filtrol	Filtrol 107	Resid	Klover™ leaf	38–39	Alumina	P	

Katalco Corp.	Filtrol 102	Resid	Extru-	—	Alumina	P	size < Filtrol 107 HDM, high HDS
	Filtrol 106	Resid	date	37-38	Alumina	P	
	KAT-4000	Resid HDT	Cylinder	34	Alumina	Co-Mo	Bimodal psd
	KAT-5000	Resid HDT	Cylinder	34	Alumina	Ni-Mo	
	DM-500	Resid HDM	Sphere	23	Alumina	Ni-Mo	
	LC-Fining	Resid, tar	Cylinder	Low	Alumina	Co-Mo or Ni-Mo	
	HMC 841	Resid HDT	Sphere	—	Alumina	Ni-Mo	
	HMC 849	Resid HDM	Sphere	—	Alumina	Ni-Mo	
	HMC 845	Resid HDT, HDM	Sphere	—	Alumina	Ni-Mo	
Shell Chemical	S327	Resid, FCC feed	Cylinder	50	Alumina	Ni-Mo	Metals resistant
	S127	Resid HDS	Cylinder	44	Alumina	Ni-Mo	Initial HDS
	S227	Resid HDS	Cylinder	44	Alumina	Ni-Mo	Deep HDS
	S147	Resid HDS	Cylinder	44	Alumina	Co-Mo	Initial HDS
	S247	Resid HDS	Cylinder	44	Alumina	Co-Mo	Deep HDS
UNOCAL Corp.	RF-11	Resid HDS	Shaped ext.	P	P	P	Bifunctional catalyst
	RF-25	Resid HDM	Shaped ext.	P	P	P	
	RF-100	Resid HDS	Shaped ext.	P	P	P	
	RF-200	Resid HDM	Shaped ext.	P	P	P	Bifunctional catalyst
	RF-220	Resid HDM	Shaped ext.	P	P	P	Bifunctional catalyst
UOP Process Division	RCD-5	Resid HDS	Sphere	41	Alumina	Co-Mo	Metals tolerant
	RCD-5A	Resid HDS	Sphere	46	Alumina	Co-Mo	High HDS activity
	RCD-7	DAO, HDM oil	Cylinder	53	Alumina	Co-Mo	High HDS + CCR
	RCD-8	Resid, DAO	Cylinder	36	P	P	High HDM, metals tolerant
United Catalysts, Inc.	C20-6-01	Full-range HDS	Cylinder	38	Alumina	Co-Mo	

^a From Corbett (1985) and edited by authors.

^b AQ = asymmetric quadrilobe; P = proprietary; ext. = extrudate.

Vendors consider this information proprietary and are hesitant to reveal catalyst preparation methods and properties that may jeopardize their marketing position. No attempt has been made in Table XXIII to identify advantages or redundancies in different manufacturers' catalyst products.

IV. Reaction Kinetics and Diffusion In Catalytic Hydrodemetallation

This section presents an overview of the chemistry and mechanisms of HDM reactions. Like HDS, HDN, and HDO, the basic chemical concept of the HDM process is to selectively remove the heteroatom species, in this case the metal, from the organic moiety with minimal conversion of the remaining petroleum. Demetallation results from chemical transformations of the metal-bearing compound on the catalyst surface coupled with diffusional transport to and from the active sites. Unlike sulfur, nitrogen, and oxygen, which are removed as gaseous products (H_2S , NH_3 , and H_2O), elimination of nickel and vanadium results in their deposition on the hydrotreating catalyst and deactivation of the catalyst through fouling and pore blockage. The resulting metal deposition ultimately determines the catalysts' total metals capacity and useful operating lifetime.

Reaction studies with model compounds representative of the metal species in petroleum are discussed to provide insight into the fundamental rate processes which occur. It will be demonstrated that this information can be used to successfully interpret the behavior of real feedstocks in commercial hydrotreating reactors.

A. MODEL COMPOUND HYDRODEMETALLATION STUDIES

Despite the importance of hydrodemetallation reactions and their intimate relationship to HDS, HDN, and HDO, relatively little is understood of the underlying fundamentals. Only recently have model compounds been used to explore the intrinsic reactivity of metal-bearing compounds and the nature of the catalytic sites responsible for these reactions. This is in sharp contrast to the wealth of model compound information existing in the literature on HDS (Gates *et al.*, 1979; Mitchell, 1980; Vrinat, 1983), HDN (Katzer and Sivasubramanian, 1979; Satterfield and Yang, 1984; Ho, 1988) and HDO (Furimsky, 1983; Satterfield and Yang, 1983).

The use of model compounds eliminates many of the complicated and competing catalytic reactions encountered with petroleum residuum, enabling a clearer picture of the inherent reactions to be ascertained.

1. Metalloporphyrin Demetallation Studies

a. *Reaction Pathways.* Investigation of the reactivity of metal species representative of those in heavy oils have been reported with metalloporphyrins, as shown in Fig. 19. Etio- and octaethyl-type porphyrins have been identified in crude oil and comprise up to 50% of the metal in the

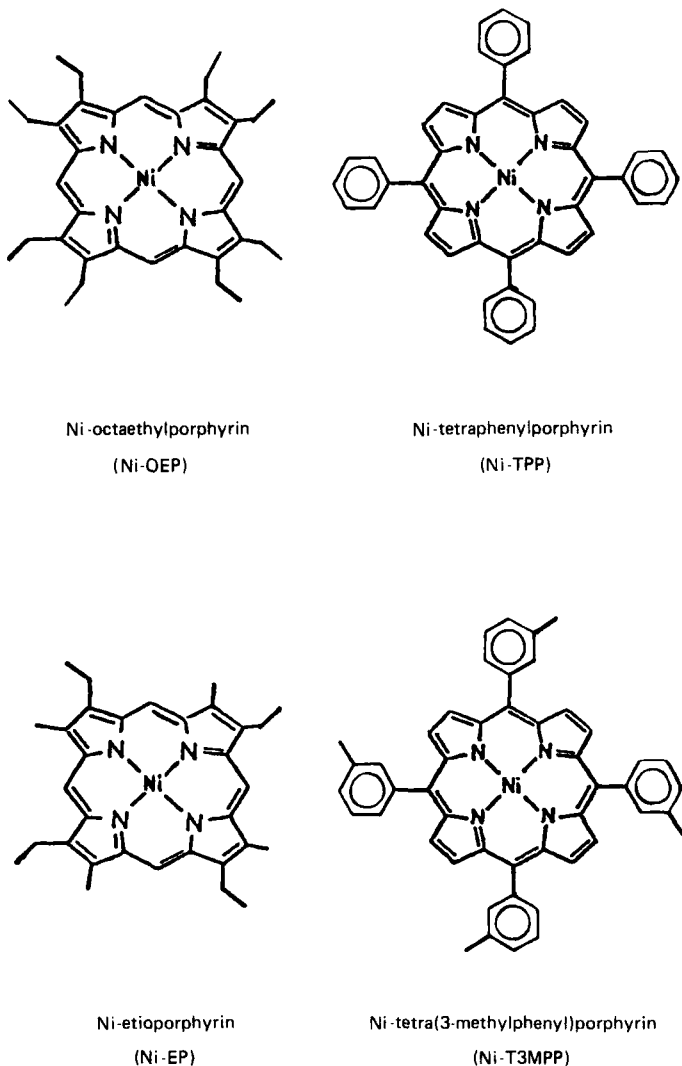
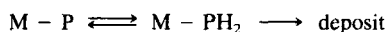


FIG. 19. Nickel analogs of model metalloporphyrins used in demetallation studies.

free porphyrin fraction (Baker and Palmer, 1978). Tetraphenyl-type porphyrins have not been identified in oil but may be representative of bound porphyrins of higher aromaticity existing in the petroleum asphaltenes (Vaughan *et al.*, 1970).

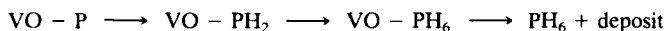
Pioneering model compound HDM work was first conducted by Hung and Wei (1980). Fractional order kinetics for total metal removal centered around 0.5 were observed for the demetallation of Ni- and VO-etioporphyrin and Ni-tetraphenylporphyrin on oxide CoMo/Al₂O₃ at industrial hydroprocessing conditions. The presence of hydrogen and active metals, Co and or Mo, on the Al₂O₃ support was demonstrated to be required for demetallation activity. Total metal removal rates less than the disappearance of feed porphyrin indicated the presence of intermediate metal species during demetallation. The intermediate was speculated to be a hydrogenated metalloporphyrin termed metallochlorin.

Agrawal and Wei (1984) isolated the metallochlorin and confirmed that the apparent fractional order kinetics resulted from a sequential mechanism much like HDS and HDN reactions. The hydrodemetallation of both nickel- and vanadyl-etioporphyrins on oxide CoMo/Al₂O₃ proceeded through two mechanistically different steps, an initial reversible hydrogenation followed by a terminal hydrogenolysis step



where P represents the starting porphyrin. Metal deposition occurs from the dihydrogenated metalloporphyrin intermediate (M-PH₂) not originally in the oil.

Complementary model compound HDM work confirmed the sequential mechanisms. Rankel (1981) and Rankel and Rollman (1983) observed hydrogenated metalloporphyrins including metallochlorin in the demetallation of Ni-octaethylporphyrin and Ni- and VO-tetraphenylporphyrins on sulfided CoMo/Al₂O₃. Kameyama *et al.* (1981, 1982, 1985) reported vanadyl-tetraphenylporphyrin demetallated through multiple hydrogenated intermediates on sulfided CoMo/Al₂O₃:



Suprisingly, no tetrahydrogenated metal species were detected.

Hydrodemetallation pathways for Ni-etioporphyrin and Ni-tetra(3-methylphenyl)porphyrin are shown in Fig. 20. Both are characterized by a sequential hydrogenation-hydrogenolysis global mechanism, but important differences are apparent. Ware and Wei (1985a) rationalized the differences in porphyrin reactivity on the basis of porphyrin molecular structure. Structural differences on the periphery of the metalloporphyrin, in particular the substituent groups at the β -pyrrolic and methine bridge

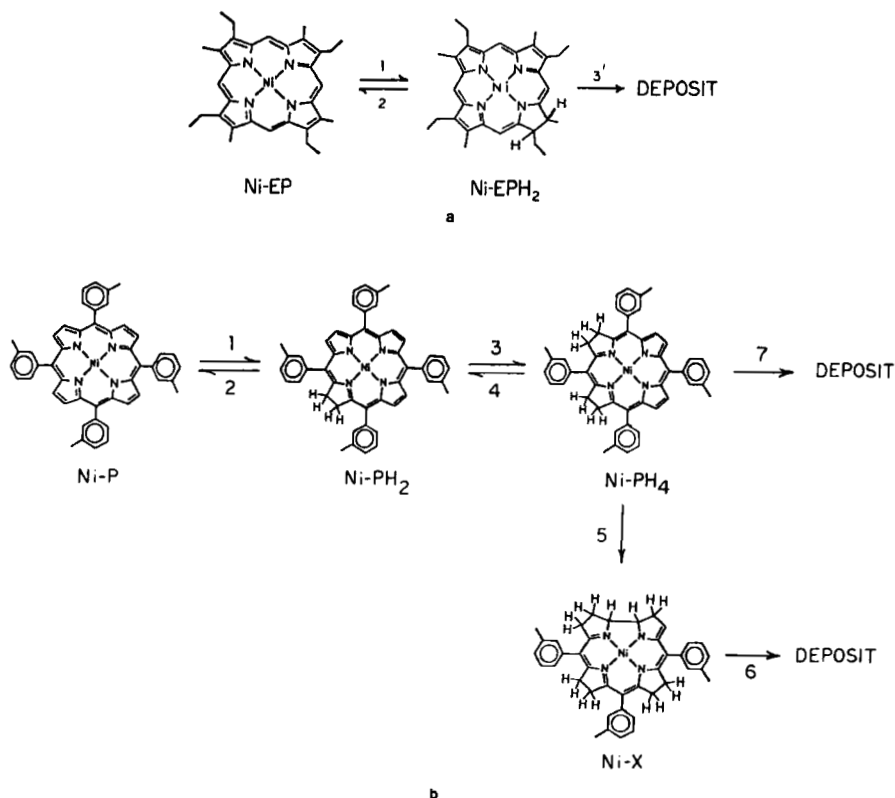


FIG. 20. Demetallation reaction pathway for (a) Ni-etio- and (b) Ni-tetra(3-methylphenyl) porphyrin (Ware and Wei, 1985a).

carbon positions influence, through steric and chemical means, the complexity of the reaction pathways.

The initial porphyrin hydrogenation on a pyrrole ring results in the least disruption of the porphyrin macrocycle under the HDM conditions. Minor strain is introduced into the macrocycle to accommodate the pyrroline ring (Scheer, 1978) although the porphyrin aromaticity is not significantly interrupted (Smith, 1975). However, pyrrole ring hydrogenation does disrupt the local electron density of the neighboring methine bridge carbons, enhancing their reactivity toward electrophilic attack (Fuhrhop, 1978). Etio-type porphyrins with open methine bridges are susceptible to further hydrogenation and reaction at these sites, which leads to cleavage of the macrocyclic ring. This explains why metal-free porphyrinic rings indicative of direct metal abstraction are not observed.

Once the porphyrin ring is open, the metal is deposited on the catalyst. Open chain tetrapyrrolic structures (M-biliverdenates) are unstable under catalytic hydrogenation conditions (Subramanian and Fuhrhop, 1978). The ease of this sequence with Ni-etiochlorophyll (Ni-etio) is apparent by the lack of stable metal intermediates other than the chlorin (M-PH₂).

Multiple hydrogenated porphyrinic intermediates are detected by UV-visible spectroscopy during the demetallation of Ni-tetra(3-methylphenyl) porphyrin (Ware and Wei, 1985a). Evidence from Ni-tetra(3-methylphenyl) porphyrin (Ni-T3MPP) catalytic demetallation studies by Weitkamp *et al.* (1983, 1984) on CoMo/Al₂O₃ also support this observation. The more extensive hydrogenation of Ni-T3MPP (TPP types in general) is a consequence of porphyrin basicity and less steric hindrance relative to Ni-etiochlorophyll. The electron-donating influence of the methyl, ethyl substituents in Ni-etio renders the β -pyrrolic positions more basic and less susceptible to reduction than Ni-T3MPP, in which only hydrogen atoms exist at these positions. Reduction potentials for the two porphyrins measured by P. Hambright (personal communication) confirm this difference. Reduction potential values for Ni-T3MPP are lower compared to Ni-etio, implying a greater ease of reducibility, as is observed. Greater accessibility to hydrogenation sites is also provided by the smaller β -pyrrolic groups in TPP-type porphyrins. Formation of the tetrahydro species is selectively at adjacent pyrrole rings, termed metalloisobacteriochlorins (Ni-PH₄) (Scheer, 1978).

Two metal deposition routes are observed with Ni-T3MPP (TPP types in general) on CoMo/Al₂O₃ (Ware and Wei, 1985a). The direct deposition step from Ni-PH₄ depicted in Fig. 20b is similar to macrocyclic ring cleavage with Ni-etiochlorophyll. A second product from Ni-PH₄ has been determined on the basis of spectroscopic and mass spectroscopic data to be a nonporphyrinic, contracted ring, Ni-corrin-type intermediate, termed Ni-X. The tolyl group stabilizes the methine carbon as a leaving group during formation of the contracted ring. The central nickel exerts a strong templating effect during this concerted reaction. The contracted macrocyclic ring (15 member) is preferred for Ni²⁺ because the Ni-N bond length in the corrin structure is more ideal than in the hydrogenated porphyrin ligand (16-member ring) (Angst *et al.*, 1981; Busch *et al.*, 1977). A second macrocyclic ring cleavage step is required for metal deposition from Ni-X.

An analogous ring contraction-carbon elimination reaction with Ni-etiochlorophyll would require loss of a methyl group which is energetically prohibitive. Formation of a methyl carbonium ion, for example, is energetically 50 kcal/mole higher than the corresponding xylyl carbonium ion.

Demetallation of VO-tetraphenylporphyrins is less likely than the nickel analogs to generate contracted rings. Unlike Ni²⁺, the VO²⁺ group has a radius slightly larger than can be accommodated in the plane of the

porphyrin ligand (Yen, 1975). Contraction of a 16- to 15-member macrocyclic ring is unlikely to provide an energetically favorable coordination cavity for VO^{2+} . West (1984), Hung and Wei (1980), and Kameyama *et al.* (1981, 1982, 1985) detect only hydrogenated porphyrinic intermediates in the demetallation of VO-TPP. No evidence for contracted ring intermediates has been reported.

Studies by Ware and Wei (1985a) and Webster (1984) reveal that the individual demetallation networks are unique to the porphyrin and not dependent upon the catalyst. On oxide and sulfided CoMo/ Al_2O_3 , and on group VIII metal/ Al_2O_3 catalysts under reducing conditions, metalloporphyrins undergo structural changes involving loss of aromaticity by hydrogenation to "activate" the molecule prior to ring cleavage and metal deposition.

In the presence of H_2S an alternative demetallation pathway has been suggested to compete with the catalytic hydrogenative route. Strong coordination by sulfur to the vanadium or nickel may weaken the metal-nitrogen bonds in the porphyrin molecule leading to direct metal abstraction (Dautzenberg and De Deken, 1985; Takeuchi *et al.*, 1985). Rankel (1981) reports that the hydrogenative route predominates with metalloporphyrins in the presence of a CoMo catalyst. Only at elevated temperatures ($>400^\circ\text{C}$) is the direct abstraction route by H_2S expected to dominate.

b. *Intrinsic Reaction Kinetic Studies.* Several investigators have measured the intrinsic kinetics of metal removal from model oils comprised of metalloporphyrins. Experiments have been conducted in both batch autoclave reactors and plug flow tubular reactors. Quantitative interpretation of the results has ranged from measurement of total metal removal rates to detailed reaction network analysis based on the identification and quantification of stable reaction intermediates.

Summarized in Table XXIV are results of HDM studies in which total metal removal rates were measured. Discrepancies in reaction order with respect to the total metal concentration are apparent. This reflects the difficulty of representing steps in a complex reaction network by global "pseudo"-kinetic expressions. Values of reaction order ranging from 0.1 to 1.1 are reported. All investigators report metal removal rates lower than feed porphyrin disappearance rates, which is consistent with the sequential mechanisms discussed. Activation energies for vanadium removal are larger than for nickel. Hydrogen pressure dependence is typically greater than first order.

Rate coefficients reported in the literature indicate that pure metalloporphyrins in clean systems are up to 10 times more reactive than naturally

TABLE XXIV

SUMMARY OF PORPHYRIN HDM GLOBAL KINETIC STUDIES

Reference(s)	Catalyst	Porphyrin	Temperature, hydrogen pressure	Kinetic order for total metal removal	<i>E</i> (kcal/mole)	Order of hydrogen dependence	Metal removal rate/ porphyrin removal rate
Galiasso and Morales (1983)	CoMo/Al ₂ O ₃ sulfided	VO-TPP	380°C, 4 MPa H ₂	1.0	—	—	—
Hung and Wei (1980)	CoMo/Al ₂ O ₃ oxide	Ni-Etio	280–350°C, 4–12 MPa H ₂	0.1–1.0 (function of <i>T</i>) centered at 0.5	27.6	1.5	<1
Hung and Wei (1980)	CoMo/Al ₂ O ₃ oxide	Ni-TPP	280–350°C, 4–12 MPa H ₂	0.1–1.0 (function of <i>T</i>) centered at 0.5	34.0	2.2	<1
Hung and Wei (1980)	CoMo/Al ₂ O ₃ oxide	VO-Etio	280–350°C, 4–12 MPa H ₂	0.1–1.0 (function of <i>T</i>) centered at 0.5	37.0	1.2	<1
Kameyama <i>et al.</i> (1981, 1982, 1985)	CoMo/Al ₂ O ₃ sulfided	VO-TPP	350°C, tetralin used as H donor	1.0	39.5	—	<1
Morales <i>et al.</i> (1984a)	CoMo/Al ₂ O ₃ , Co/Al ₂ O ₃ Mo/Al ₂ O ₃ sulfided	VO-TPP	150–300°C, 1.4–7.4 MPaH ₂	1.0–1.1	13.9–14.3	1.1–1.9	<1
Rankel (1981, 1983)	CoMo/Al ₂ O ₃ sulfided	Ni-OEP, Ni-TPP, VO-TPP	315–400°C, 5–7 MPa H ₂	—	—	—	<1
Weitkamp <i>et al.</i> (1983, 1984)	CoMo/Al ₂ O ₃ sulfided	Ni-T3MPP	305°C, 5 MPa H ₂	—	—	—	<1
West (1984)	CoMo/Al ₂ O ₃ sulfided	VO-TPP	300–350°C, 5.6 MPa H ₂	1.0	32.0	—	<1

TABLE XXV

SUMMARY OF PORPHYRIN HDM REACTION NETWORK STUDIES

Reference(s)	Catalyst ^a	Porphyrin	Activation energy (kcal/mole)						Hydrogen pressure dependence						
			Hydrogenation	Dehydrogenation	Hydrogenolysis	Hydrogenation	Dehydrogenation	Hydrogenolysis	Hydrogenation	Dehydrogenation	Hydrogenolysis	Hydrogenation	Dehydrogenation	Hydrogenolysis	Hydrogenation
			k_1^b	k_2	k_3	k_4	k_5	k_6	k_7	k_1	k_2	k_3	k_4	k_5	k_6
Agrawal and Wei (1984)	CoMo/Al ₂ O ₃ (oxide)	Ni-Etio	17.1	22.9	32.6	1	0	2	3.7						
Agrawal and Wei (1984)	CoMo/Al ₂ O ₃ (oxide)	VO-Etio	18.3	16.5	24.9	1	0	2	1.5						
Webster (1984)	Group VIII/Al ₂ O ₃	Ni-Etio	4.6–21.5	—	3.2–15.8	—	—	—	0.43–40						
Reference(s)	Catalyst ^a	Porphyrin	k_1^b	k_3	k_2	k_4	k_5	k_6	k_7	k_1	k_3	k_2	k_4	k_5	k_6
Ware and Wei (1985a)	CoMo/Al ₂ O ₃ (oxide)	Ni-T3MPP	16.4	17.3	20.0	21.2	19.0	20.0	23.3	1	1	0	0	2	2
Ware and Wei (1985a)	CoMo/Al ₂ O ₃ (sulfided)	Ni-T3MPP	23.0	19.7	24.9	23.1	40.3	29.4	20.0	1	1	0	0	2	2
Webster (1984)	NiMo/Al ₂ O ₃ (oxide)	Ni-T3MPP	3.0	7.4	—	—	26.3	10.1	8.9	—	—	—	—	—	—

^a Reaction conditions for all runs: 280–345°C, 4.2–10.4 MPa H₂.^b Rate coefficients refer to reaction pathways in Fig. 20.^c Hydrogenolysis–hydrogenation reaction selectivity at 345°C, 6.99 MPa H₂.

occurring metalloporphyrins in petroleum resins (Galiasso *et al.*, 1985) and 100 to 500 times more reactive than nickel and vanadyl compounds in Kuwait atmospheric residuum (Hung and Wei, 1980).

Detailed reaction network studies are summarized in Table XXV. Rate parameters refer to first-order kinetic coefficients in the reaction networks for the respective metalloporphyrins in Fig. 20. These reaction networks successfully model the generation and removal of metal species in the demetallation of the porphyrins (Fig. 21). Activation energies for the three reaction types hydrogenation, dehydrogenation, and hydrogenolysis are consistent with similar reactions in HDS and HDN (Satterfield and Gultekin, 1981). Hydrogen pressure dependence reflects the nature of the reaction: hydrogenation steps are first order; dehydrogenation reactions are zero order, indicative of kinetic control; and the metal deposition steps are second order, suggestive of a sequence of rapid reactions lumped into the final hydrogenolysis step. Reaction of Ni-T3MPP on the sulfided catalyst is characterized by temperature and hydrogen pressure dependencies for the individual reaction steps similar to those on the oxide CoMo/Al₂O₃ catalyst.

Reaction selectivity in the bifunctional hydrodemetallation process can be defined as the ratio of the terminal metal deposition rate to the initial porphyrin hydrogenation rate: k'_3/k_1 for etioporphyrin and $(k_6 + k_7)/k_1$ for tetra(3-methylphenyl) porphyrin. This parameter characterizes the ability of the catalyst to conduct hydrogenolysis relative to hydrogenation. Under diffusion-limited conditions, metal deposition location is a strong function of this selectivity. As indicated in Table XXV, both Ni- and VO-etiochlorophyll demetallation on oxide CoMo/Al₂O₃ are characterized by a selectivity greater than unity, indicating that hydrogenation is rate limiting and that the concentration of intermediates is low. Metal deposition is rate controlling with Ni-tetra(3-methylphenyl)porphyrin (TPP types in general) on CoMo/Al₂O₃ and the selectivity is less than one. Consequently, intermediates accumulate in the oil. At equal conditions, overall metals removal from Ni-etiochlorophyll is faster than from Ni-T3MPP. This difference in reactivity reflects the porphyrin structural features previously discussed.

Higher HDM reaction selectivity is observed with Ni-T3MPP on CoMo/Al₂O₃ in the sulfided state, typical of industrial hydroprocessing conditions. Sulfiding increases the rate-limiting metal deposition activity relative to the hydrogenation activity (Ware and Wei, 1985a).

Modification of the hydrogenolysis (metal deposition)–hydrogenation selectivity in the demetallation of Ni-T3MPP has been achieved by chemically doping a CoMo/Al₂O₃ catalyst. Ware and Wei (1985b) demonstrated

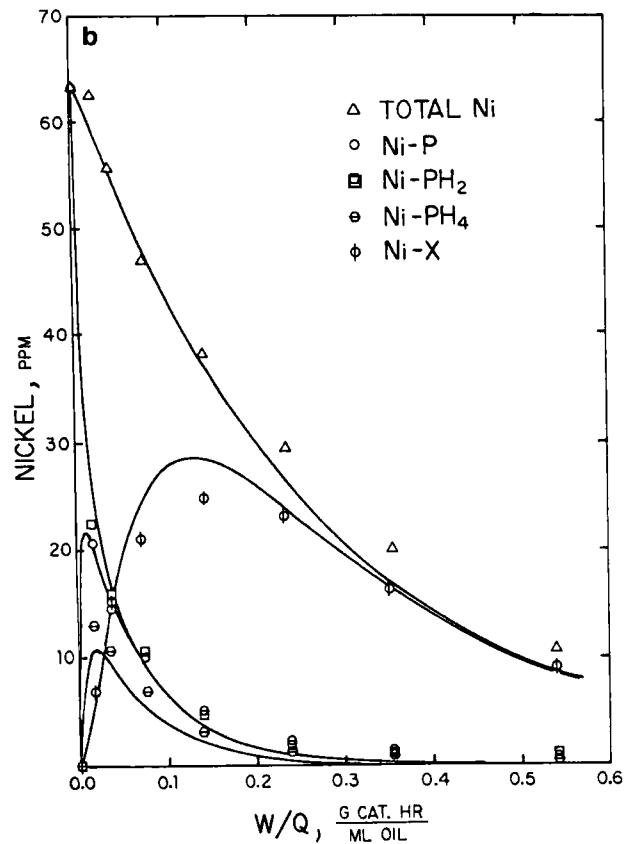
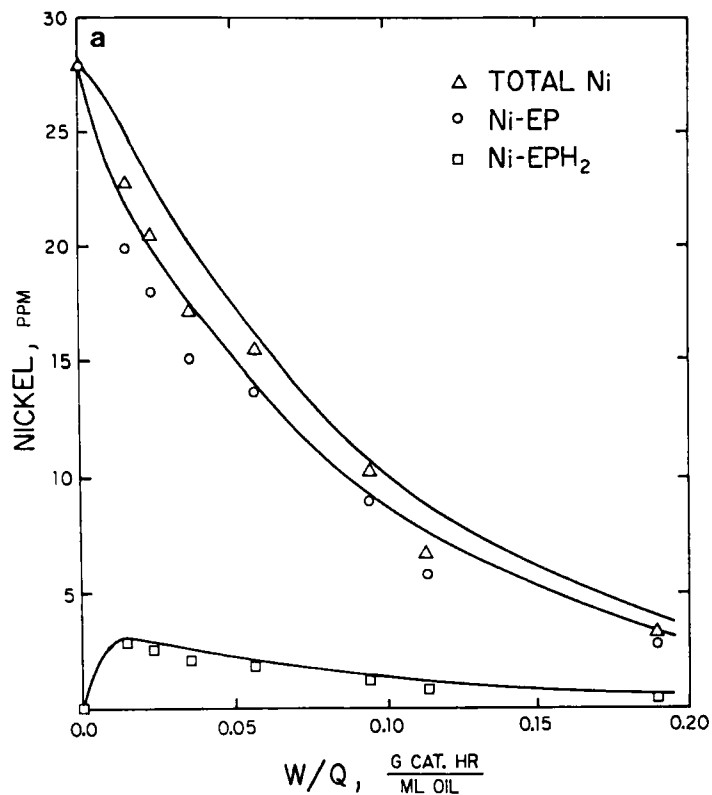


FIG. 21. Metal concentration versus contact time results for demetallation of (a) Ni-etioaporphyrin at 27 ppm Ni feed and (b) Ni-tetra(3-methylphenyl)porphyrin at 63 ppm Ni feed at 345°C and 6.99 MPa H₂ (1000 psig) on oxide CoMo/Al₂O₃ catalyst. Solid lines represent model calculations (Ware and Wei, 1985a).

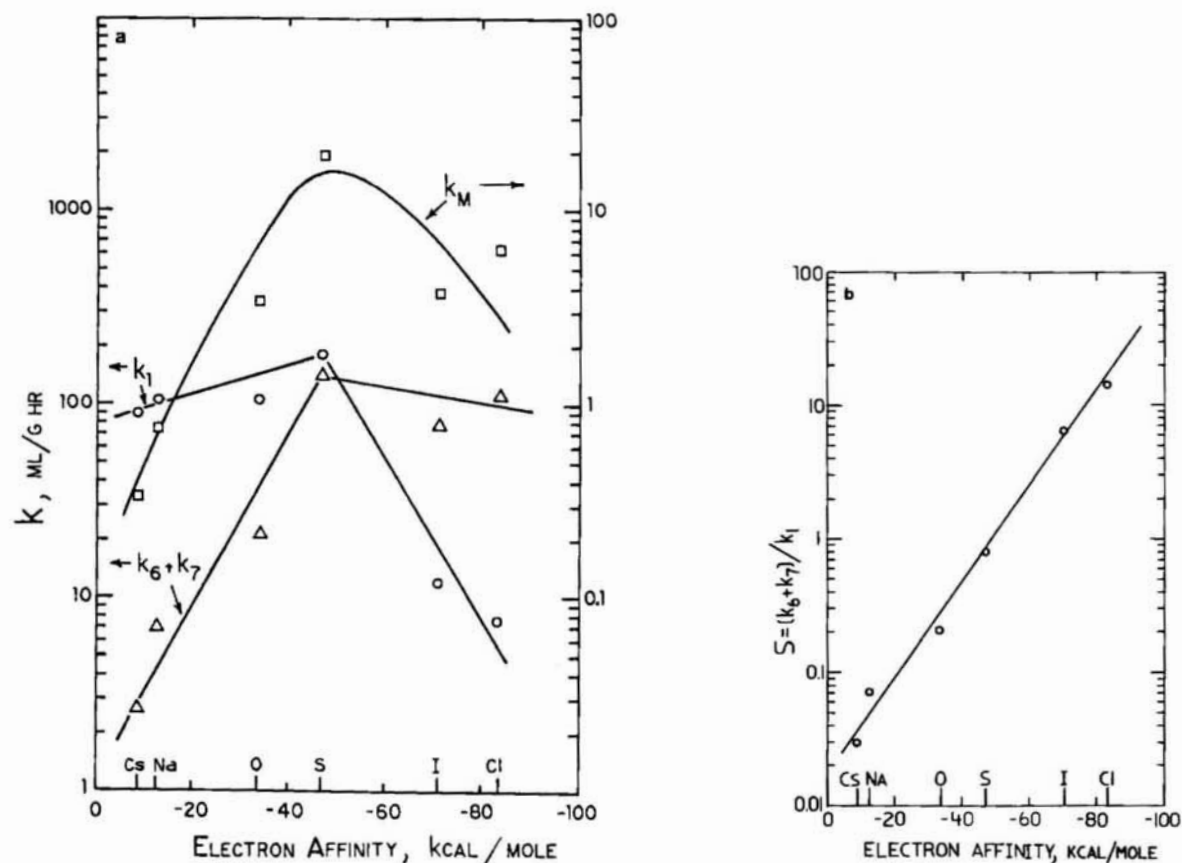


FIG. 22. (a) Ni-tetra(3-methylphenyl) porphyrin demetallation kinetic rate parameters and (b) reaction selectivity at 345°C and 6.99 MPa H_2 (1000 psig) versus electron affinity of dopant on modified CoMo/ Al_2O_3 catalysts (Ware and Wei, 1985b).

selectivity variations over three orders of magnitude including a shift in the rate-limiting step. As shown in Fig. 22, basic additives inhibit the terminal metal deposition activity relative to the base case oxide $\text{CoMo}/\text{A}_2\text{O}_3$ catalyst, whereas acidic additives enhance the hydrogenolysis steps. Catalysts with strong acidic components (halogens) also experienced an inhibition in hydrogenation activity attributed to site occupation by strong adsorption. The overall demetallation activity, represented by a pseudo-first-order rate coefficient k_M varies smoothly and displays a volcano-shaped curve with a maximum occurring on the sulfided catalyst. Variations in reaction selectivity $(k_6 + k_7)/k_1$ correlate with the electron affinity of the dopant, suggesting a strong dependence on catalyst acidity or electronic configuration of the surface metals.

Webster (1984) investigated the kinetics of Ni-etio porphyrin HDM reactions on alumina-supported group VIII metal catalysts and a group VIII-IB bimetallic catalyst, namely, $\text{Ru-Cu}/\text{A}_2\text{O}_3$. Group VIII_1 metals enhanced the hydrogenolysis step (k'_3), whereas group VIII_3 metals enhanced the initial hydrogenation step (k_1). The reaction selectivity (k'_3/k_1) varied by two orders of magnitude depending on the catalyst used (Fig. 23). Unlike all other catalysts, Pd shifted the rate-limiting step to hydrogenolysis ($k'_3/k_1 < 1$). The selectivity ratio correlated with group VIII metals percentage d-orbital character as Sinfelt (1969) had earlier demonstrated for hydrocarbon hydrogenation-hydrogenolysis reactions. The addition of copper to the ruthenium catalyst also achieved a predictable decrease in Ni-etio porphyrin demetallation selectivity. These results were interpreted on the basis of the "geometrical theory," with the hydrogenolysis step being structure sensitive and the hydrogenation step structure insensitive (Poniec, 1975).

All of these experiments have been conducted on catalysts considered to be in the fresh state. Deposited metal loadings were generally below 2 to 4 wt. %, whereas industrial hydrotreating catalysts may reach 50 to 65 wt. % metals. Webster (1984) reported declines in Ni-T3MPP demetallation activity on aged $\text{CoMo}/\text{Al}_2\text{O}_3$ catalysts containing up to 10 wt. % nickel. Activity declines of 50% for the HDM of VO-TPP were observed by West (1984) on catalysts with 30 wt. % vanadium. West interpreted the catalyst deactivation as the result of pore-mouth plugging. Metal profiles measured in the catalyst extrudates revealed a concentration of metal at the pellets' edge. Reaction selectivity on aged catalysts with high metals loading has not been carefully examined.

c. *VO-Porphyrin versus Ni-Porphyrin Reactivity.* The relative reactivity of vanadyl and nickel porphyrins has been examined in a limited

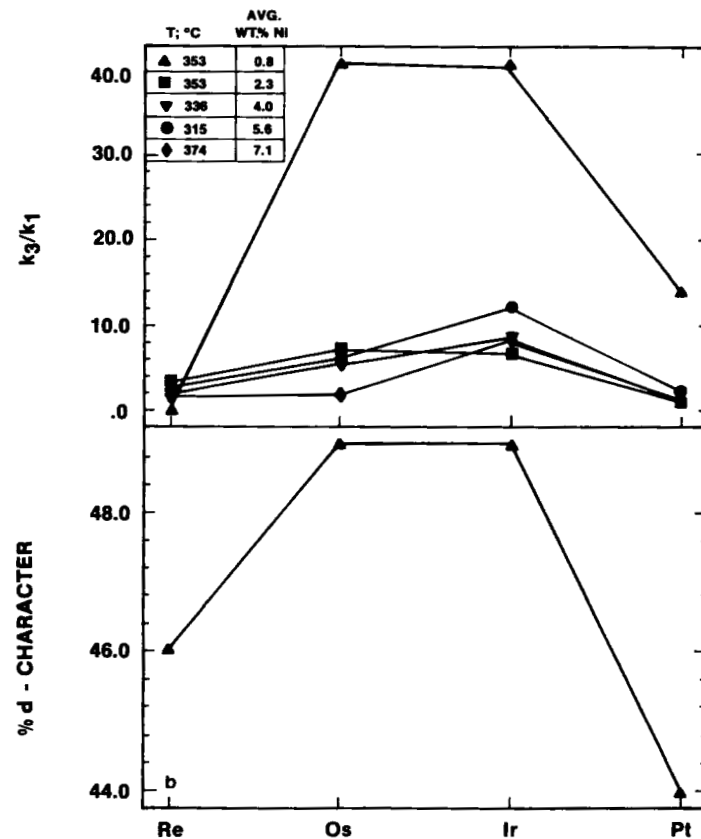
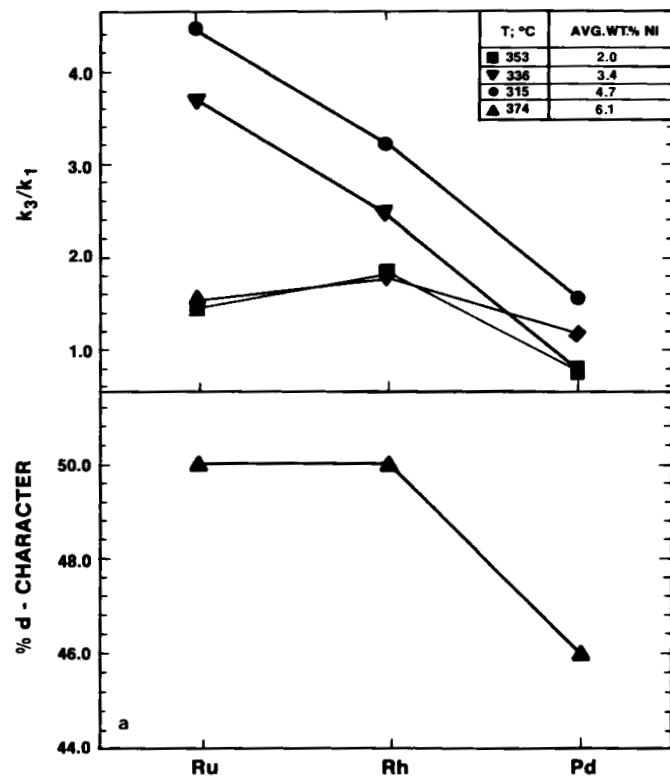


FIG. 23. Selectivity of Group VIII metals for Ni-etioporphyrin demetallation in relation to periodic position and percentage *d*-character of the metallic bond (Webster, 1984).

number of model compound studies. The results appear to be sensitive to the temperature and the presence of other porphyrins. In separate experiments, Hung and Wei (1980) demonstrated that nickel-etio porphyrin had a higher metal removal rate than the vanadyl analog only below 320°C. At higher temperatures VO-etio porphyrin is more reactive, apparently the consequence of higher activation energy. Agrawal and Wei (1984) also reported higher demetallation rates for VO-etio at elevated temperatures. Separate Ni-TTP and VO-TTP experiments by Rankel (1981) also indicate higher reactivity of vanadyl porphyrins at temperatures above 300°C.

In competitive demetallation experiments the same rates do not necessarily hold. Hung and Wei (1980) reported that with both Ni-etio and VO-etio in the feed, the vanadium removal rate was the same as in the individual vanadium run, whereas the nickel removal rate was suppressed to below that of vanadium removal. In a related study using a mixed Ni-T3MPP and VO-etio oil, Webster (1984) reported that VO-etio demetallated faster than Ni-TMPP and also suppressed the metal removal rate of the latter. This inhibition phenomenon offers a partial explanation as to why in most commercial operations with real feeds vanadium is more reactive than nickel.

An interpretation for the generally higher vanadium reactivity at typical hydrotreating conditions was first suggested by Beuther and Schmid (1963) and then restated by Shah and Paraskos (1975). The 4+ valance state of vanadium in porphyrins requires binding to oxygen, perpendicular to the porphyrin plane provides an enhanced site for adsorption and reaction on require an axial ligand since all valences are satisfied by planar coordination. The oxygen in the vanadyl group (VO^{2+}) protruding above the porphyrin plane provides an enhanced site for adsorption and reaction on the catalyst owing to the electron density associated with the oxygen. This strong adsorption may also inhibit the adsorption and subsequent reaction of nickel porphyrins in mixed Ni and VO experiments.

A factor contributing to the higher vanadyl reactivity in light of the reaction networks is the relative ease with which the porphyrin is reduced: VO^{2+} groups provide a stronger electron pull relative to Ni^{2+} resulting in a less basic, more readily reduced porphyrin macrocycle. Reduction potential measurements confirm this (Fuhrhop *et al.*, 1973). In the case of etio-type porphyrins which are rate limited by the initial hydrogenation, the enhanced reducibility translates into a higher overall demetallation rate for VO-etio porphyrin relative to Ni-etio porphyrin. Hydrogenation is not the rate-limiting step with tetraphenyl porphyrins on $\text{CoMo}/\text{Al}_2\text{O}_3$. In this case, overall rate enhancements due to ease of porphyrin reducibility alone may be less important.

2. Nonporphyrin Demetallation Studies

Demetallation studies with nonporphyrinic model compounds have been few. Those compounds that have been examined are depicted in Fig. 24.

Mitchell and Valero (1982, 1983) studied VO-phthalocyanine (VO-PC) and a Schiff base complex, VO-salen, as model vanadium compounds. The VO-PC provides a metal coordination environment comprised of four nitrogens, similar to the porphyrin. The benzo rings at the β -pyrrolic positions contribute to enhanced aromaticity in the metal ligand.

Vanadyl salen provides a model of mixed heteroatom metal coordination characteristic of Ni and VO in the maltenes and asphaltenes. Approximately 50–90% of the metals in petroleum are not contained in the free porphyrin fraction. Yen (1975, 1978) has postulated that these metals exist in a variety of environments such as highly aromatic bound porphyrins, complexed to tetradentates of mixed N, S, and O ligands, or defect sites in large aromatic sheets. Analytical work by Fish *et al.* (1984) has indicated the presence of metals complexed to salen-type ligands in petroleum.

Vanadyl salen is readily converted at 100°C with H₂S in the absence of a catalyst to a vanadium sulfide and a free organic ligand (or decomposition products). Vanadyl phthalocyanine is more stable with respect to ring attack and demetallation. Rates relative to catalytic reactions have not been measured. If VO-salen is an appropriate model of vanadium binding in asphaltenes, asphaltenic metals are more readily converted to sulfides under hydrotreating conditions than the porphyrinic metals. This suggests

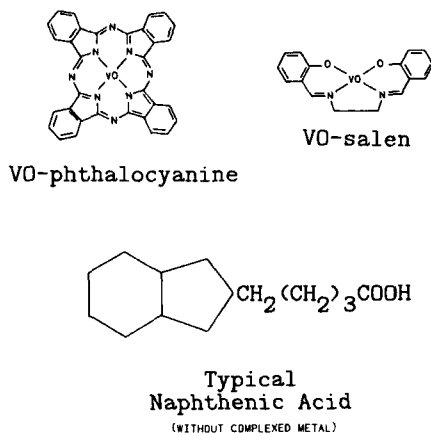


FIG. 24. Nonporphyrinic model compounds used in demetallation studies.

that in real oils where porphyrinic metals are observed to react more readily than the asphaltenic metals (Galiasso *et al.*, 1985), the depolymerization of asphaltene structures and the subsequent transport of metal species to active catalytic sites is rate controlling rather than the intrinsic demetallation chemistry.

Catalytic hydrodemetallation studies with vanadyl naphthenates have been reported by West (1984). The instability of these compounds makes them relatively poor models for mechanistic studies. At typical hydrotreating conditions, a homogeneous noncatalytic demetallation route and a heterogeneous catalytic route contribute to overall metal removal.

3. Model Compound Diffusion and Adsorption

Hydrodemetallation reactions require the diffusion of multiringed aromatic molecules into the pore structure of the catalyst prior to initiation of the sequential conversion mechanism. The observed diffusion rate may be influenced by adsorption interactions with the surface and a contribution from surface diffusion. Experiments with nickel and vanadyl porphyrins at typical hydroprocessing conditions have shown that the reaction rates are independent of particle diameter only for catalysts on the order of 100 μm and smaller ($R < 50\mu\text{m}$). Thus the kinetic-controlled regime, that is, where the diffusion rate D_{eff}/R^2 is larger than the intrinsic reaction rate k , is limited to small particles. This necessitates an understanding of the molecular diffusion process in porous material to interpret the diffusion-disguised kinetics observed with full-size ($\frac{1}{16}$ -in.) commercial catalysts.

When the effective molecular diameter of the diffusing species approaches that of the pore dimension, the diffusion rate drops dramatically owing to a reduction in solute mobility. This results from steric restriction and increased viscous drag within the pore and is termed restrictive or configurational diffusion. Molecular diameters for metalloporphyrins range from 12 to 15 Å for etio-type porphyrins and from 15 to 19 Å for the tetraphenyl-type porphyrins (Scheidt, 1978; Fleischer, 1963). The molecular size may even be larger if interactions between the porphyrin and oil components or impurities exist. Porphyrin-porphyrin interactions from van der Waal's attractions of the aromatic sheets or through the central metal axial ligand position are also possible. As such, a reduction in porphyrin mobility is to be expected for pore sizes on the order of 100 Å, at which the ratio of the porphyrin diameter to pore diameter exceeds 0.1.

Using concepts derived for transport of biological molecules in membranes, Spry and Sawyer (1975) proposed that the configurational

diffusivity drops as the fourth power of the molecular dimension ratio as given by

$$D_{\text{eff}} = \frac{D_{\infty}\epsilon}{\tau} (1 - \lambda)^4 \quad (1)$$

where D_{∞} is the bulk diffusivity and $\lambda = r_{\text{solute}}/r_{\text{pore}}$, the ratio of the two characteristic radii. The catalyst tortuosity and void fraction are τ and ϵ , respectively. (The derivation of Eq. (1) is developed in Section IV,B,5.) This equation predicts a 50% reduction in porphyrin diffusivity relative to the bulk in pores 100 Å in diameter.

The diffusion of metal-free octaethyl and tetraphenylporphyrin in alumina particles with average pore size ranging from 49 to 154 Å has been examined by Chantong and Massoth (1983). For values of λ between 0 and 0.4, the restrictive diffusivity to free solution diffusivity correlated with $(1 - \lambda)^n$, using $n = 3.5$ in near agreement with Spry and Sawyer. Values for porphyrin effective diffusivity in these materials are on the order of 10^{-6} cm²/sec at 25°C. Diffusion experiments at elevated temperature were not conducted, making extrapolation to hydroprocessing conditions difficult. The contribution of surface diffusion to the apparent porphyrin diffusion was negligible at room temperature, indicating that no effect is expected at higher temperatures.

Diffusion and adsorption studies with Boscan VO-porphyrin extracts and pure VO-TPP in CoMo/Al₂O₃ catalysts have been reported by Morales and co-workers (Galiasso and Morales, 1983; Morales and Galiasso, 1982; Andreu *et al.*, 1981; Morales *et al.*, 1984). The Boscan extract contained up to 30 wt. % vanadyl DPEP and vanadyl etioporphyrin. Effective diffusion coefficients at 300°C in a catalyst with an average pore diameter of 150 Å ($\lambda < 0.1$) are on the order of 10^{-5} cm²/sec. Configurational effects are minor for this system.

Vanadyl porphyrin interaction with the surface is a function of the catalyst. Adsorption through electron acceptor sites dominates on the oxide surface, whereas the sulfided catalyst interacts through electron donor sites (see Section IV,B,5). Heats of adsorption have been estimated to be 8 to 12 kcal/mole. Values in this range are indicative of weak adsorption interactions that are of reduced importance at hydroprocessing conditions.

Limited experimental data for nickel porphyrins indicate weaker adsorption than their vanadyl analogs, which is consistent with the oxygen ligand on vanadium playing an active role. With this difference it stands to reason that competitive adsorption contributes to the inhibition observed in nickel demetallation rates in the presence of vanadyl porphyrins. Therefore, the higher vanadium reactivity relative to nickel can be rationalized on the

basis of both intrinsic chemistry differences in the molecules and preferential catalyst site occupancy.

4. Intraparticle Metal Deposition Profiles from Diffusion-Limited Reactions

Scanning electron x-ray microanalysis techniques reveal that metal deposits are frequently nonuniform through the catalyst pellet cross section after demetallation reactions. Metal profiles measured after HDM studies with Ni and VO-etioporphyrin (Agrawal and Wei, 1984), Ni-tetra(3-methylphenyl)porphyrin (Ware and Wei 1985a), and VO-tetraphenyl porphyrin (West, 1984) demonstrate the inhomogeneity. Examples in

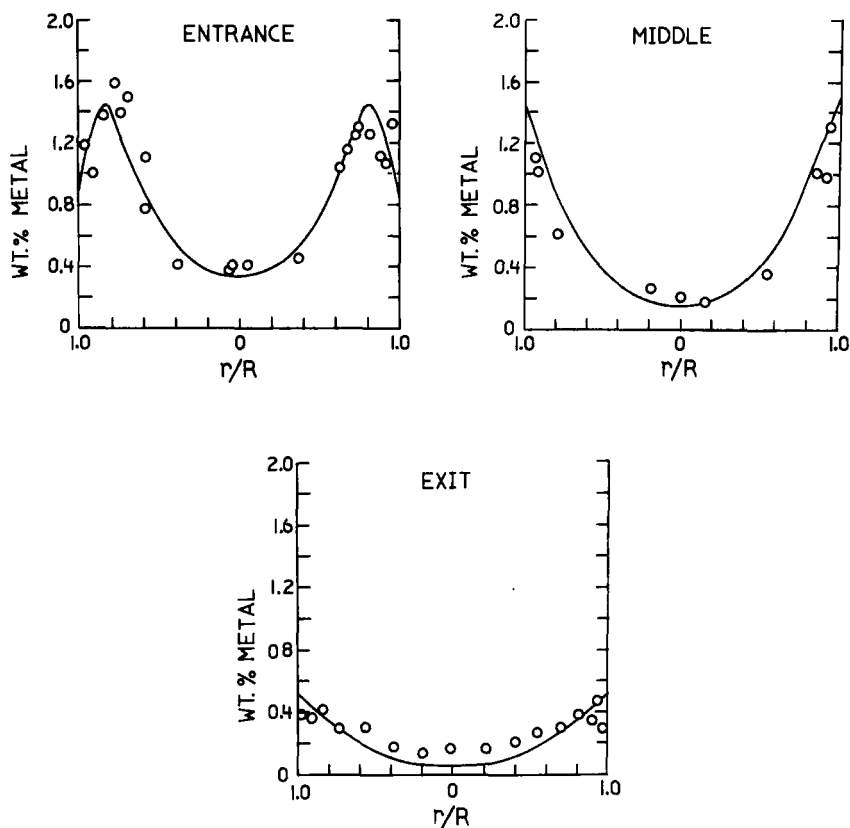


FIG. 25. Vanadium profiles in $\frac{1}{16}$ -in.-diameter aged catalysts at various reactor axial positions from VO-etioporphyrin demetallation at 343°C and 6.99 MPa H_2 (1000 psig) on oxide $CoMo/Al_2O_3$. Solid lines represent model calculations (Agrawal and Wei, 1984).

Figs. 25 to 28 show that the metal deposition in CoMo/Al₂O₃ hydrotreating catalysts is a function of the radial position within the catalyst and the axial location of the catalyst sample within the fixed-bed reactor. Nickel and vanadium both exhibit radial profiles with internal maxima, termed M-shaped profiles, at the reactor entrance. These maxima shift to the pellets' edge at the reactor outlet, generating the classic U-shaped profile.

These profiles are readily interpreted by a consecutive hydrodemetallation mechanism. The metalloporphyrins must first react to form the metal-depositing intermediates before metal accumulates on the catalyst. As feed porphyrin diffuses into the first catalyst particles and reacts, the concentration of intermediates rises and the M-shaped profiles appear. The maxima shifts to the pellets' edge as metal-depositing intermediates accumulate in the oil. The position of the internal maxima within the pellets is dependent on several factors, including the intrinsic reaction network, temperature, hydrogen pressure, and catalyst pore structure. Reaction kinetic studies reveal that increasing reactor temperature or hydrogen pressure accelerates the deposition reactions relative to diffusion processes, leading to higher Thiele moduli and sharper profiles. One possibility for obtaining more uniform profiles would be to increase the pore size to enhance diffusion.

Intrinsic reactivity patterns of the different porphyrins are reflected in their metal deposition profiles, which serve as "fingerprints" marking the reaction sequence. Vanadium profiles (Fig. 25) from pure VO-etio-porphyrin in oil demetallation experiments are steeper with less deposit in the pellets' center than the nickel profiles (Fig. 26) from the analogous experiment with pure nickel porphyrin. Pure compound intrinsic reactivity data revealed that vanadium was more reactive than nickel at most temperatures of interest. However, a reduction in VO-porphyrin diffusion by stronger adsorption interactions would also contribute to a steepening of the metal deposition profiles. Metal profiles have not been examined from demetallating model oils containing both Ni- and VO-porphyrins.

The additional reaction intermediates in the Ni-tetra(3-methylphenyl)-porphyrin network coupled with slower rates of metal deposition result in deeper penetration of the internal maxima and higher concentration of metals in the pellets' center compared to Ni-etio-porphyrin. Likewise, the selective enhancement in the metal deposition rates of Ni-T3MPP on the sulfided catalyst is apparent by the steeper profiles in Fig. 28 relative to the results in Fig. 27 on the oxide form of CoMo/Al₂O₃.

The theory of coupled multicomponent first-order reaction and diffusion given by Wei (1962) has been used to successfully model the metal deposition profiles (Agrawal and Wei, 1984; Ware and Wei, 1985a). The

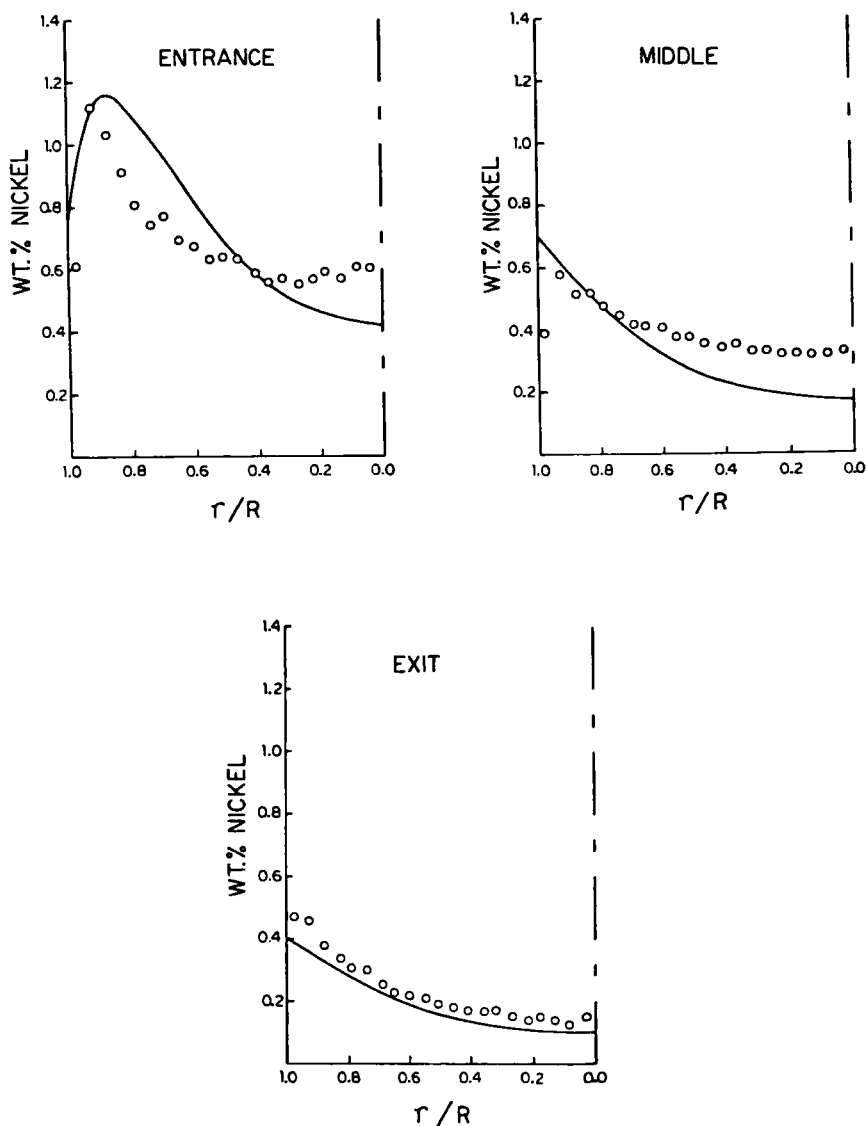


FIG. 26. Nickel profiles in $\frac{1}{16}$ -in.-diameter aged catalysts at various reactor axial positions from Ni-etiochlorophyll demetallation at 345°C and 6.99 MPa H_2 (1000 psig) on oxide $CoMo/Al_2O_3$. Solid lines represent model calculations (Ware and Wei, 1985a).

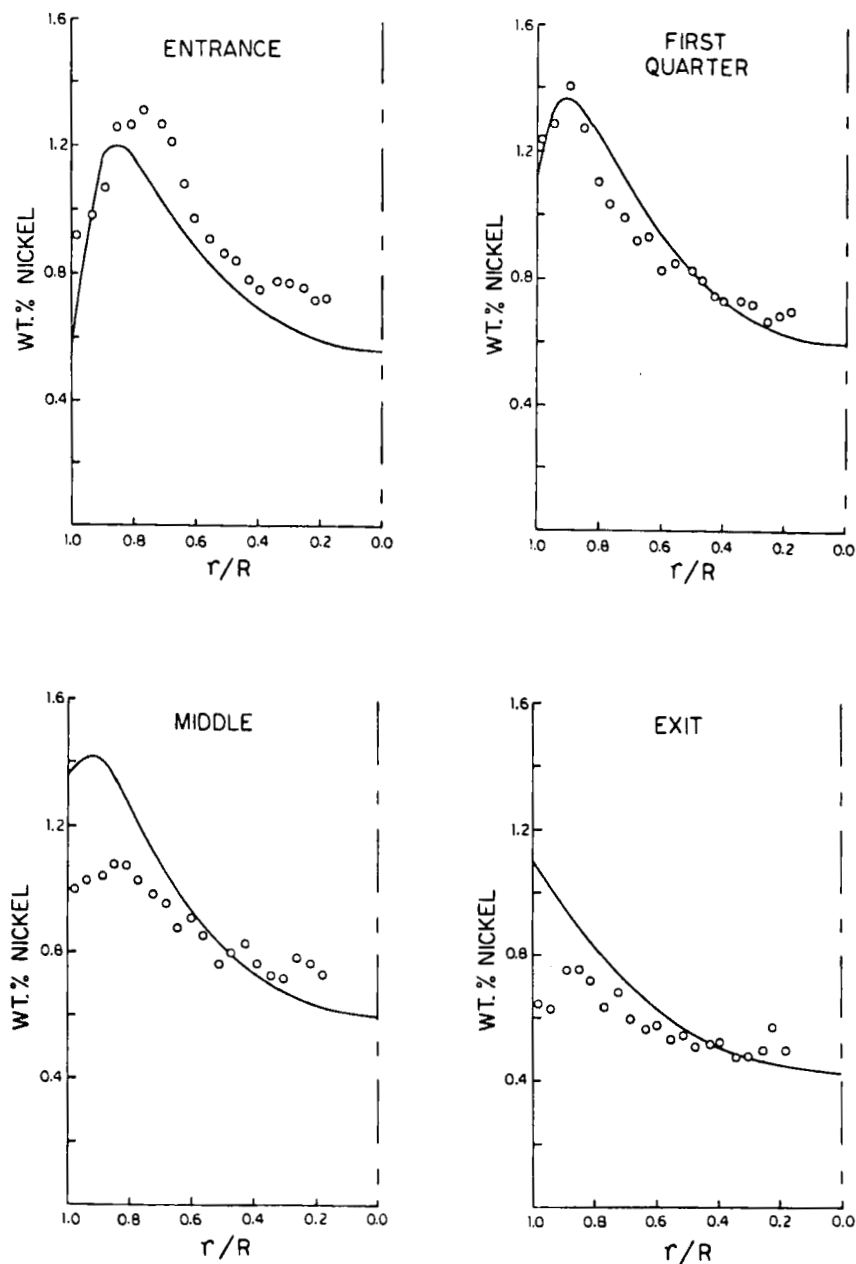


FIG. 27. Nickel profiles in $\frac{1}{16}$ -in.-diameter aged catalysts at various reactor axial positions from Ni-tetra(3-methylphenyl) porphyrin demetallation at 345°C and 6.99 MPa H_2 (1000 psig) on oxide $CoMo/Al_2O_3$. Solid lines represent model calculations (Ware and Wei, 1985a).

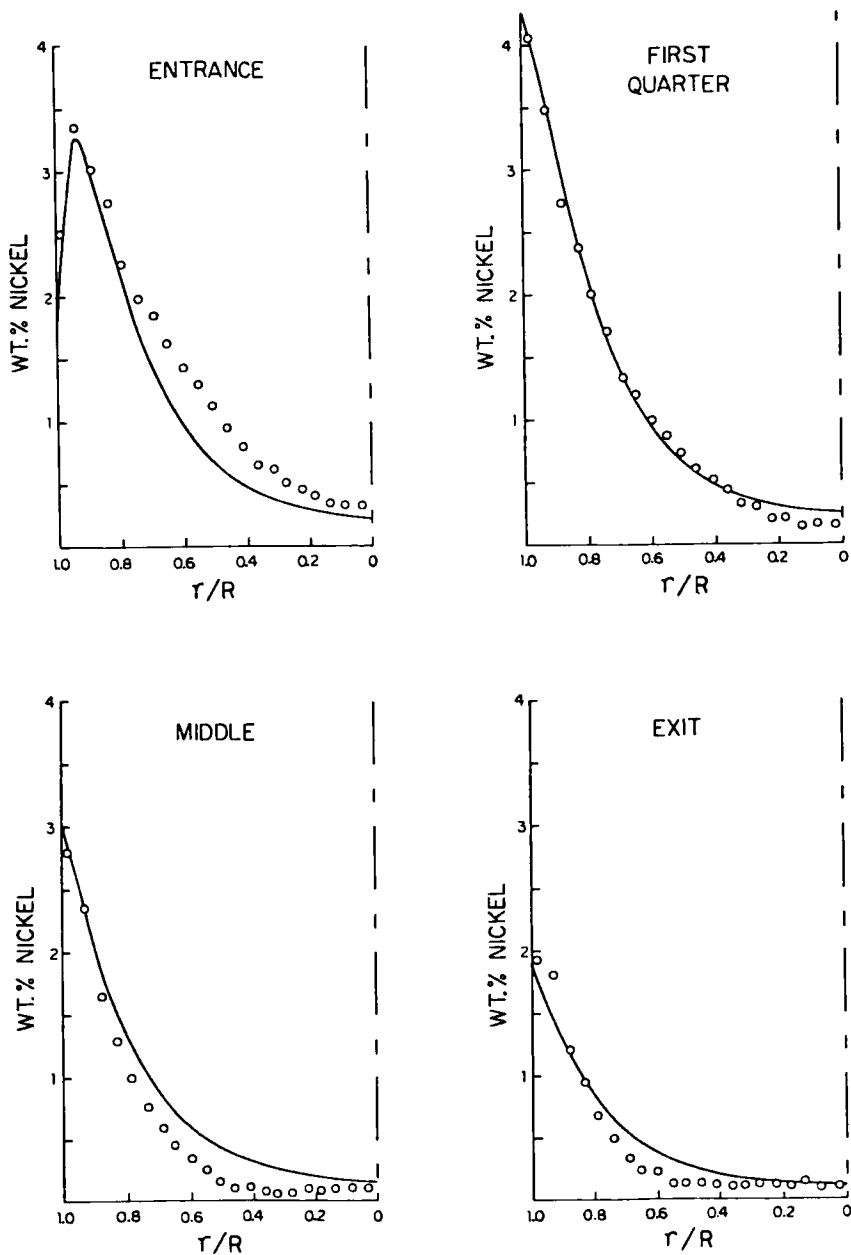


FIG. 28. Nickel profiles in $\frac{1}{16}$ -in.-diameter aged catalysts at various reactor axial positions from Ni-tetra(3-methylphenyl) porphyrin demetallation at 345°C and 6.99 MPa H_2 (1000 psig) on sulfided CoMo/ Al_2O_3 . Solid lines represent model calculations (Ware and Wei, 1985a).

generalized steady-state equation balancing diffusion and reaction rates in a catalyst is written as

$$\bar{D}\nabla^2\bar{a}(r) = \bar{K}\bar{a}(r) \quad (2)$$

where \bar{D} is the diagonal diffusion coefficient matrix, \bar{K} the reaction coefficient matrix, and $\bar{a}(r)$ the vector of metal species concentration. The matrix \bar{K} may take a variety of forms depending on the complexity of the demetallation network and the number of intermediates involved. Conversely, it may be reduced to a single element if the demetallation kinetics are simplified to a single first-order reaction. For Ni-etiochlorophyll demetallation by the network in Fig. 20, \bar{K} has the form

$$\begin{bmatrix} k_1 & -k_2 \\ -k_1 & k_2 + k_3 \end{bmatrix} \quad (3)$$

By defining the matrix $\bar{D}^{-1}\bar{K}$ to have eigenvectors \bar{Y}_i and eigenvalues μ_i and defining pseudoconcentrations as $\bar{b}(r) = \bar{Y}^{-1}\bar{a}(r)$, then

$$\nabla^2 \bar{Y}^{-1} \bar{a}(r) = \bar{\mu} \bar{Y}^{-1} \bar{a}(r) \quad (4)$$

which is equivalent to

$$\nabla^2 \bar{b}(r) = \bar{\mu} \bar{b}(r) \quad (5)$$

which has the solution in a cylindrical catalyst of radius R

$$\bar{b}(r) = \left\{ \frac{I_0(\sqrt{\mu_i} r)}{I_0(\sqrt{\mu_i} R)} \right\} \bar{b}(R) \quad (6)$$

where the braces denote the diagonal matrix and I_0 the modified Bessel function of the first kind of zero order.

Recalling the definition of b yields an expression for metal species in the catalyst given by

$$\bar{a}(r) = \bar{Y} \left\{ \frac{I_0(\phi_i r/R)}{I_0(\phi_i)} \right\} \bar{Y}^{-1} \bar{a}(R) \quad (7)$$

where $\phi_i = R\sqrt{\mu_i}$, the Thiele moduli. Using this expression, the metal profiles at a radial position r in a catalyst are calculated based on the concentration a_i of metal-depositing species in the oil. For the simple case of first-order kinetics, Eq. (7) reduces to

$$a(r) = \frac{I_0(\phi r/R)}{I_0(\phi)} a(R) \quad (8)$$

with the Thiele modulus, relating the characteristic reaction rate to diffusion rate, given by the familiar form $\phi = R\sqrt{k/D}$.

The solid lines in Figs. 25 to 28 are the result of model predictions of metal deposition based on porphyrin reaction pathways. Curves are generated using intrinsic kinetic rate parameters and effective diffusion coefficients for the metal species on the order of 10^{-6} cm²/sec. These values are similar to diffusion coefficients measured in the independent studies referenced.

The model predicts the metal deposition profiles inside the catalyst pellets at various bed locations and also predicts the average metal concentration in catalysts along the length of the bed. For a sequential hydrodemetallation scheme Agrawal and Wei (1984) have shown that along the reactor-bed length the average amount of metal deposited in a catalyst pellet passes through a maximum from reactor inlet to outlet as shown in Fig. 29. It is therefore possible for the reactor bed to first plug with accumulated metals at interior positions along the axis.

The bifunctional nature of the HDM mechanism (hydrogenation followed by hydrogenolysis) provides the potential for controlling the reaction selectivity and, consequently, the metal deposition site by judicious choice of catalyst. The consequences of the modifications in intrinsic demetallation selectivity of Ni-tetra(3-methylphenyl)porphyrin achieved by Ware and Wei (1985b) by acid-base doping of CoMo/Al₂O₃ are reflected in intrapellet metal profiles. Deposition profiles calculated from experimental kinetics are reproduced in Fig. 30. These profiles reflect changes in the reaction Thiele moduli resulting from changes in the intrinsic reaction chemistry. Diffusion coefficients are constant and independent of the catalyst used.

It is convenient to compare quantitatively the relative rates of the HDM reactions and the diffusion of metal species as revealed by the metal

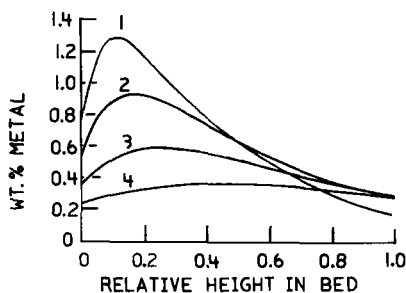


FIG. 29. Calculated averaged catalyst vanadium loading along the length of the reactor bed for demetallation of 28 ppm V as VO-etioporphyrin on oxide CoMo/Al₂O₃ after 68 hours on stream: (1) 343°C and 9.76 MPaH₂ (1400 psig), (2) 343°C and 6.99 MPa H₂ (1000 psig), (3) 315°C and 9.76 MPa H₂, (4) 288°C and 9.76 MPa H₂ (Agrawal and Wei, 1984).

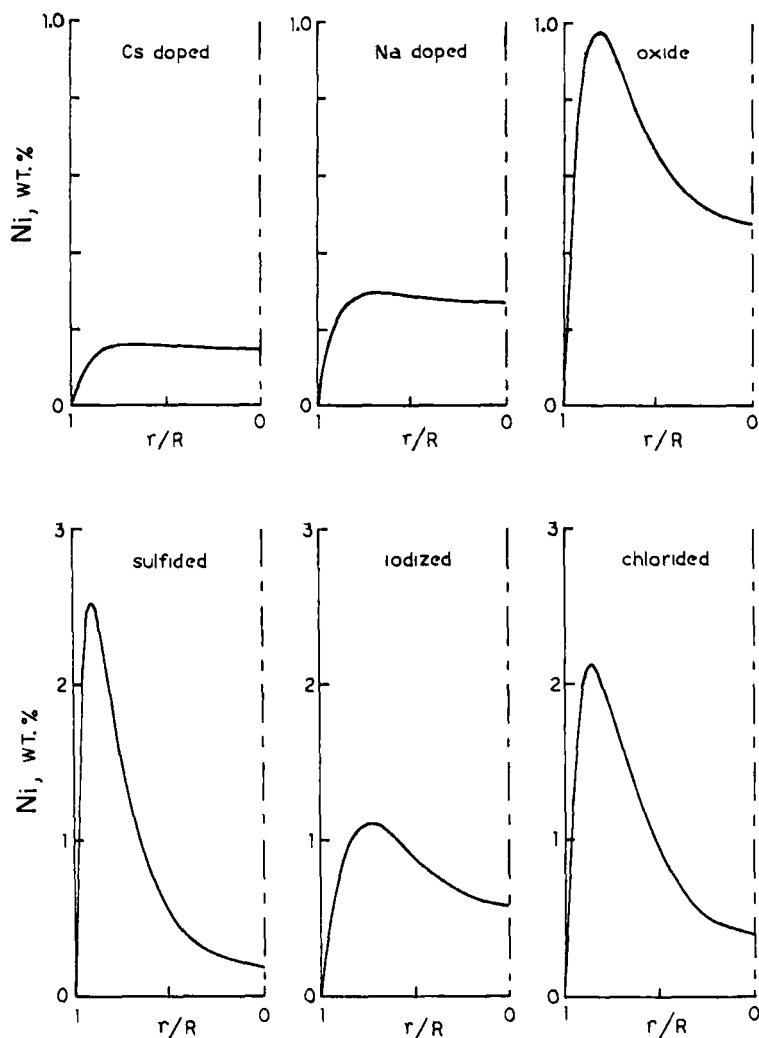


FIG. 30. Calculated nickel deposition profiles in $\frac{1}{16}$ -in.-diameter catalysts at reactor entrance for Ni-tetra (3-methylphenyl) porphyrin demetallation at 345°C and 6.99 MPa H_2 (1000 psig) on modified $\text{CoMo/Al}_2\text{O}_3$ catalysts (Ware and Wei, 1985b).

deposition patterns in aged catalyst extrudates. To facilitate this comparison, Tamm *et al.* (1981) define the metal distribution parameter θ_m by (for cylindrical shape):

$$\theta_m = \frac{\int_0^1 M(r)r \, dr}{M_{\max} \int_0^1 r \, dr} \quad (9)$$

where $M(r)$ is the local weight percent metal deposit, M_{\max} the maximum concentration across the radius, and r the fractional radius. This parameter is a ratio of the average metal concentration to the maximum concentration and therefore characterizes the effective utilization of the catalyst for metals deposits. A distribution parameter of unity corresponds to uniform profiles, whereas a value approaching zero would be characteristic of a sharp spike at the pellet's edge. The analogy is apparent between θ_m and the classic effectiveness factor, η , defined for a first-order reaction as

$$\eta = \frac{a(R) \int_0^1 I_0(\phi r/R)/I_0(\phi) r dr}{a(R) \int_0^1 r dr} = \frac{I_1(\phi)}{\phi I_0(\phi)} \quad (10)$$

If the maximum metal content occurs at the edge of the pellet, then the distribution parameter is equal to the reaction effectiveness factor.

The effect of HDM reaction selectivity variations on the metal distribution parameter at the reactor entrance for Ni-T3MPP follows.

METAL DISTRIBUTION
PARAMETERS FOR Ni-T3MPP
REACTION ON CoMo/Al₂O₃^a

Catalyst	θ_m
Cs doped	0.93
Na doped	0.92
Oxide form	0.66
Sulfided form	0.36
Iodized form	0.75
Chlorided form	0.50

^a Conditions: 345°C,
6.99 MPa H₂ (1000 psig).

As the table and Fig. 30 indicate, reaction of Ni-T3MPP in the presence of basic additives (Cs, Na) is characterized by small Thiele moduli and uniform profiles ($\theta_m \rightarrow 1$), indicative of kinetic-controlled reactions. Acidic components (S, I, Cl) result in larger Thiele moduli (smaller θ_m) and more sharp, U-shaped profiles, signaling strong diffusion-limited reactions.

Reaction selectivity variations achieved by Webster (1984) on group VIII metal-Al₂O₃ catalysts with Ni-etio porphyrin enable similar shifts in metal distribution parameters to be obtained.

A more attractive demetallation processing scheme may be one where the hydrogenolysis-hydrogenation selectivity is manipulated to a limiting case, enabling complete separation of the two reactions. The first catalyst would provide the necessary hydrogenation function to generate the hydrogenated metalloporphyrin intermediates. A second catalyst would

then be used to promote the final metal deposition step. In this configuration, poisoning of the precious hydrogenation catalyst would be avoided. The pore structure of the second catalyst could be constructed to accommodate a large quantity of metal prior to deactivation.

B. HYDRODEMETALLATION OF PETROLEUM OILS AND RESIDUUM

1. Kinetics and Mechanism of HDM Reactions

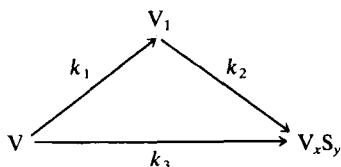
Studies undertaken with petroleum feedstocks to elucidate an understanding of hydrodemetallation reactions have yielded ambiguous and in some cases conflicting results. Comparison of kinetic phenomena from one study to the next is often complicated. Formulation of a generalized kinetic and mechanistic theory of residuum demetallation requires consideration of competitive rate processes which may be unique to a particular feedstock. Catalyst activity is affected by catalyst size, shape, and pore size distribution and intrinsic activity of the catalytic metals. Feedstock reactivity reflects the composition of the crude source and the molecular size distribution of the metal-bearing species.

Numerous investigators have examined the kinetics of metal removal from petroleum fractions. The majority of studies have used conventional hydrotreating catalysts, MoO_3 supported on $\gamma\text{-Al}_2\text{O}_3$ and promoted with CoO or NiO . Metal removal rates have generally been interpreted using simple mass action kinetic expressions of the form

$$\text{rate} = kp_{\text{H}_2}^m c^n \quad (11)$$

Kinetic models which consider demetallation as a complex reaction network of consecutive and parallel reactions taught by model compound studies have been recognized with real feedstocks. Tamm *et al.* (1981) suggest a sequential mechanism where the metal compounds are activated by H_2S . Model compound reaction pathway studies in the absence of H_2S , discussed in Section IV,A,1, and experiments in which H_2S was present in excess (Pazos *et al.*, 1983) indicate that sequential reactions are inherent to the chemistry of the metal compounds irrespective of the presence of H_2S . However, it is possible that both mechanisms contribute to metal removal.

Pazos *et al.* (1983) proposed a consecutive HDM reaction mechanism similar to the model compound studies in which part of the vanadium deposition occurs from species V_1 not originally present in the oil:



The molecular transformations required to generate V_1 were not speculated upon for real feedstocks. On the basis of model compound studies, it seems appropriate to postulate that k_1 is a hydrogenation step and k_2 and k_3 are hydrogenolysis steps. When the diffusion-free kinetic data of Pazos *et al.* (1983) are used, these definitions lead to a HDM reaction selectivity $(k_2 + k_3)/k_1 \cong 0.1$ for Bachaquero crude at 395°C, 1500 psig hydrogen, on sulfided CoMo/Al₂O₃. This value compares to $(k_6 + k_7)/k_1 \sim 2$ calculated from model compound Ni-T3MPP studies at equivalent operating conditions (Ware, 1983). The discrepancy may reflect Ni versus V reactivity or inhibition effects resulting from competitive adsorption of other heteroatom species with the real feedstock.

A summary of hydrodemetallation kinetic studies is presented in Table XXVI. The list is not exhaustive but does include a diversity of feedstocks and catalysts. It is apparent that a discrepancy in reaction order n with respect to total metal (Ni or V) concentration has been observed. Riley (1978) reported first-order kinetics for both nickel and vanadium removal when hydrotreating a Safaniya atmospheric residuum. Demetallation kinetic order of 1.0 to 1.5 depending on reactor configuration has been reported by van Dongen *et al.* (1980) for vanadium removal. Oleck and Sherry (1977) report a better description of the reaction system is obtained with second-order kinetics for nickel and vanadium removal from Lago-medio (Venezuelan) atmospheric residuum. All studies were conducted on CoMo/Al₂O₃ catalysts.

The apparent HDM reaction orders greater than unity have been attributed to the presence of more than one class of metal compounds reacting with different rates (Oleck and Sherry, 1977; Cecil *et al.*, 1968). Just as in hydrosulfurization, the simultaneous occurrence of several first-order reactions with different rates can lead to an apparent reaction order greater than unity (de Bruijn, 1976). Wei and Hung (1980) theoretically demonstrated conditions whereby two first-order reactions give rise to apparent second-order kinetics.

A spectrum of metal compound reactivities in petroleum could arise for several reasons. Nickel and vanadium exist in a diversity of chemical environments. These can be categorized into porphyrinic and non-porphyrinic species; vanadyl and nonvanadyl; or associated with large asphaltenic groups and small, isolated metal-containing molecules. Each can be characterized by unique intrinsic reactivity. Reaction inhibition which occurs between the asphaltenes and the nonasphaltenes, as well as between Ni and V species, can also contribute to reactivity distributions. The parallel reaction interpretation of the observed reaction order discrepancy is therefore compatible with the multicomponent nature of petroleum. Data obtained at low conversion could appear as first order and only at higher conversions would higher-order effects become obvious. The

TABLE XXVI

SUMMARY OF STUDIES ON KINETICS OF CATALYTIC HYDRODEMETALLATION

Reference(s)	Catalyst used	Oil	Kinetic order	Order of dependence on H ₂	E (kcal/g mole)	V removal rate/ Ni removal rate
Arey <i>et al.</i> (1967)	HDS catalyst	Kuwait atmospheric residual	—	—	—	>1
Audibert and Duhaut (1970)	HDS catalyst	Middle Eastern oils	—	1	—	>1
Beuther and Schmid (1963)	HDS catalyst	Kuwait reduced crude	2	—	—	>1
181 Dautzenberg <i>et al.</i> (1978)	CoMo/Al ₂ O ₃ , NiMo/Al ₂ O ₃	Caribbean and Middle East long residue	1	—	—	—
Gajardo <i>et al.</i> (1982)	CoMo/Al ₂ O ₃ , NiMo/Al ₂ O ₃	Boscan DAO Jobo DAO	— —	— —	— —	— —
Galiasso and Morales (1983)	CoMo/Al ₂ O ₃	Boscan and Jobo crudes	1	—	—	—
Inoguchi <i>et al.</i> (1971)	CoMo/Al ₂ O ₃	Khafji and Kuwait atmospheric residual	1 or 2	—	10	<1 below 400°C >1 above 400°C
Larson and Beuther (1966)	CoMo/Al ₂ O ₃	Kuwait atmospheric residual	1	—	—	>1
Ojima <i>et al.</i> (1978)	CoMo/Al ₂ O ₃	Gach Saran vacuum residuum	1	<1	—	>1
Oxenreiter <i>et al.</i> (1972)	CoMo/Al ₂ O ₃	Khafji and Gach Saran residual	—	—	—	>1

Pazos <i>et al.</i> (1981)	CoMo/Al ₂ O ₃	Tia Juana Pesado residuum	1	—	—	—
Riley (1978)	CoMo/Al ₂ O ₃	Safaniya atmospheric residuum	1	—	—	>1
Shah and Paraskos (1975)	HDS catalyst	Kuwait crude	—	—	—	>1
Chang and Silvestri (1976)	Manganese nodules, CoMo/Al ₂ O ₃ , Porocel	Kuwait residual, Agha Jari topped crude	1	>1 for CoMo/Al ₂ O ₃ (smaller for others)	—	>1
Chang and Silvestri (1974)	Manganese nodules	Agha Jari topped crude	1	—	—	>1
Dodet <i>et al.</i> (1984)	Manganese nodules, CoMo/Al ₂ O ₃	Gach Saran atmospheric residuum	1	0.7 for nodules 1.0 for CoMo	17.9 (nodule)	>1
Oleck and Sherry (1977)	Manganese nodules, CoMo/Al ₂ O ₃	Kuwait and Lagomedio atmospheric residual	2	>1 for CoMo/Al ₂ O ₃ , <1 for manganese nodule	38.2 (CoMo/Al ₂ O ₃), 26 (nodule)	>1
Galiasso <i>et al.</i> (1985)	Fe Mo/SiO ₂ -Al ₂ O ₃	Jobo crude: resin fraction asphaltene fraction	Ni 1 V 1 Ni 1 V 1	0.5 1.2 1.0 1.05	15 22 23 20	<1
Iannibello <i>et al.</i> (1982)	Ni, Co, Mo, W on bauxite	Adriatic Sea atmospheric resid	1	—	10-18	>1
Sasaki <i>et al.</i> (1982)	NiV/Al ₂ O ₃	Gach Saran vacuum residuum	—	—	—	>1
Van Dongen <i>et al.</i> (1980)	Proprietary demetallation catalyst	—	1-1.5 (function of reactor	—	—	—

apparent 1.5-order vanadium kinetics may reflect reaction orders of individual vanadium species less than 1.0. Van Dongen *et al.* (1980) interpreted this to indicate Langmuir–Hinshelwood metal removal kinetics with strong adsorption on the surface. Similarly, model compound studies have revealed that apparent half-order kinetics result from sequential HDM mechanisms (Hung and Wei, 1980).

Experimental evidence supports the notion of a distribution of metal compound reactivities dependent upon the molecular weight and the chemical environment of the metal-containing molecule. Galiasso *et al.* (1985) demonstrated with a resin and asphaltene fraction from Jobo crude that nickel and vanadyl compounds in the resin are 20 to 200 times more reactive for demetallation. Analysis revealed that the resin was made up primarily of porphyrinic metal, whereas the asphaltene metals were mostly nonporphyrinic. In addition to being more reactive, the Ni and V from the resin deposited uniformly across the Fe–Mo/silica–alumina hydrotreating catalyst (250- μm particles), whereas metals from the asphaltene fraction were concentrated in the outer regions of the catalyst. Not only are the asphaltene metals less reactive, this nonuniform deposition indicates a greater resistance to diffusion, consistent with larger molecules and the twofold higher average molecular weight of the asphaltene fraction. Within the resin fraction itself, reactivity distributions were detected as nonporphyrinic vanadyl compounds were converted preferentially to the vanadyl porphyrins.

Earlier investigators reported similar reactivity distributions. Kwan and Sato (1970) measured with electron spin resonance (ESR) a higher demetallation reactivity of nonvanadyl relative to vanadyl–vanadium in Khafji atmospheric residuum. Silbernagel and Riley (1980) studied three feeds prepared from the same source: a whole Venezuelan crude, its pentane extracted deasphalted oil, and the hydrofluoric acid-treated whole crude. Electron spin resonance measurements revealed that vanadium in the deasphalted oil (DAO) was present exclusively as vanadyl porphyrin. Hydrofluoric acid treatment of the crude removed the vanadyl porphyrin species, leaving nonporphyrinic metal compounds of diverse chemical types. Hydrotreating the separate fractions over CoMo/Al₂O₃ at equivalent conditions removed 90% of the Ni and V in the DAO, whereas the HF-treated oil, containing the more refractory metal compounds, was less than 35% demetallized. Metal removal from the whole crude was intermediate between that of the reactive porphyrinic and nonreactive nonporphyrinic fractions.

Oxenreiter *et al.* (1972) also demonstrated a range of metal reactivities depending upon the fraction of Khafji or Iranian Heavy (Gach Saran) crude. At similar desulfurization levels, the extent of demetallation of the

asphaltene fraction was 37% for V and 13% for Ni with Khafji residue and 46% for V and 33% for Ni from Iranian Heavy. In the less refractory resin fraction, demetallation was 80% for V and 70% for Ni in both feedstocks.

The relative ease of demetallating the resin fraction made up primarily of metalloporphyrins in free solution suggests that high overall metal conversion in petroleum is determined by the degree of asphaltene demetallation. The difficulty of asphaltene processing does not arise primarily because of stronger metal–ligand binding; in fact, the metal coordination chemistry is similar to that of porphyrins and may include porphyrin moieties. A hypothetical asphaltene “particle” was presented in Section II and showed metalloporphyrins laminated between aromatic sheets. The micellar nature of the asphaltenes, formed by association of condensed polyaromatic rings and heteroatom linkages, limits accessibility of metal compounds contained within these structures to the catalytic sites. Similarly, highly polar functional groups strengthen adsorption interactions with the catalyst reducing diffusion.

Mechanistic studies of asphaltene conversion indicate that metal removal is an integral part of a complex decomposition process. Asaoka *et al.* (1983) proposed a generalized sequential asphaltene conversion mechanism incorporating data obtained with asphaltenes derived from diverse sources: a Boscan crude, an Athabasca bitumen, and a Khafji vacuum residuum. As depicted in Fig. 31, the first stage of reaction involves conversion of the micelle structure (stacked polyaromatic sheets and naphthenic–aliphatic groups with molecular weights up to 13,000) into individual sheets and resin material (MW ~1000–3000). Dissociation occurs in part from depolymerization and thermal cleavage at reaction conditions of weak links formed by sulfur bridges between sheets and from weakening of π bond interactions between aromatic sheets. The removal of vanadium, and to a much lesser extent nickel, occurs simultaneously with the destruction of asphaltene micelles. Metal conversion activity

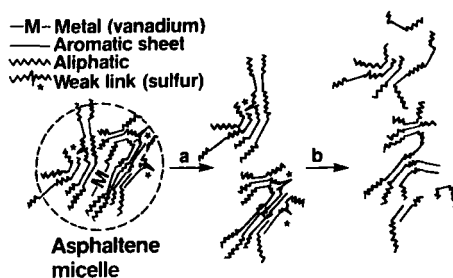


FIG. 31. Proposed mechanism for asphaltene conversion: (a) destruction of asphaltene micelle; (b) depolymerization due to heteroatom removal (Asaoka *et al.*, 1983).

results from the freeing of bound porphyrinic compounds layered between aromatic sheets. The depolymerization mechanism is consistent with earlier work by Richardson and Alley (1975) and Bridge and Green (1979), who reported conversion of asphaltenic material with molecular dimensions larger than the pore size of the catalyst.

Plumail *et al.* (1984) and Asoaka *et al.* (1983) postulate that the unit size of aromatic sheets making up asphaltenes undergoes little change, despite decreases in micelle molecular weight, indicating a decline in the number of unit sheets. As aliphatic and naphthenic linkages are removed, the aromatic centers are concentrated and asphaltene aromaticity increases. The nitrogen content in the asphaltenes and resins remains constant with hydrotreating conversion, whereas desulfurization occurs simultaneously with asphaltene conversion. It thus appears that nitrogen is a fundamental element of the asphaltene and resin molecular structure and is much more difficult to remove than either sulfur or nickel and vanadium.

Vanadium associated in partially converted asphaltenes exists in a more rigid structure but with lower dissociation energy than in the feed. The estimated dissociation energy for vanadyl species drops from 15 to 10 kcal/mole. These energy levels reflect the association between the porphyrinlike vanadium (IV) complexes containing the majority of the metal and the stacked aromatic sheets of the asphaltenes. Ligand coordination environment of the vanadyl, whether it be a four-nitrogen donor system (VON_4) as in porphyrins or a mixed ligand system (VON_2O_2 , VOS_2O_2 , VOS_4), exerts only minor differences in reaction chemistry. Hence the demetallation of vanadyl in petroleum asphaltenes is determined primarily by transport and active site accessibility restrictions imposed by the association of the vanadyl species with the aromatic planes (i.e., macrostructure) and to a lesser extent by the nature of the metal ligands. Under this premise, active site accessibility, not intrinsic reactivity, is rate controlling in the demetallation of petroleum residua.

Increasing temperature favorably affects the demetallation reaction rates. Apparent activation energies for global metal removal range from 10 to 38 kcal/mole depending on the kinetic order. For first-order kinetics these vary from 10 to 18 kcal/mole. Discrepancies in these lumped values may reflect differences in the crude source resulting in different rate-limiting steps or different adsorption energies. Diffusion-disguised first-order kinetics would also lead to an apparent activation energy one-half that of the intrinsic value. Metal removal reactions in conventional $\frac{1}{16}$ in. hydrotreating catalysts are generally diffusion limited (see Section IV,B,6).

Data in Table XXVI reveals that metal removal rates are enhanced ($m > 0$) by increases in hydrogen partial pressure in accord with model compound studies. Both feedstock and demetallation catalyst may in-

fluence the magnitude of the hydrogen response. Audibert and Duhaut (1970) observed first-order dependence on hydrogen when demetallating a Middle Eastern oil, whereas Chang and Silvestri (1976) and Oleck and Sherry (1977) observed higher-order dependence with Kuwait residuum on CoMo/Al₂O₃ catalysts. Hydroprocessing Kuwait residuum on nonconventional catalysts exhibits hydrogen dependence of less than one (Oleck and Sherry, 1977). The order of dependence is likely a function of the rate-limiting metal removal step. The reaction rate dependence on H₂S partial pressure is less understood. Evidence suggests that increasing the concentration of H₂S provides a rate enhancement at low H₂S concentrations.

Hydrogen consumption during hydrotreating (HDS, HDN, HDM) is dependent upon the feedstock and the degree of heteroatom removal. The heavier feedstocks require substantially more addition of hydrogen to attain a fixed level of upgrading, as shown in Fig. 32. Actual hydrogen consumption is greater than theoretical predictions estimated on the basis of metal content. Hydrogen requirements for simultaneous removal of other heteroatoms, aromatics saturation, and non selective hydrocracking

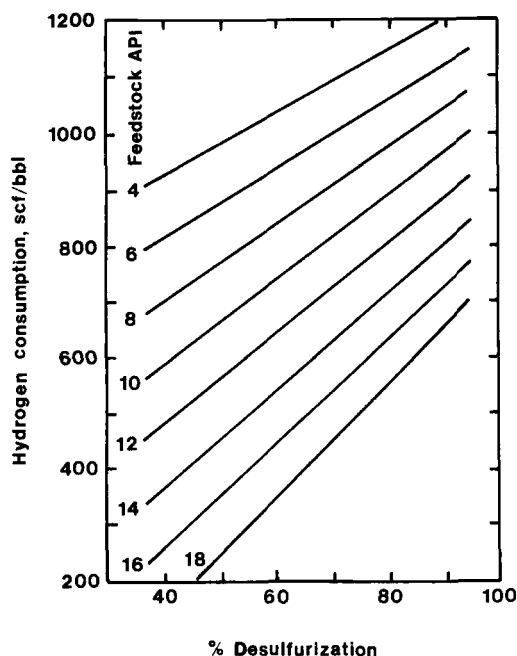


FIG. 32. Variation in hydrogen consumption with sulfur removal in relation to feedstock gravity (Speight, 1981).

of petroleum are responsible. For example, a Venezuelan atmospheric residuum containing 460 ppm Ni and V consumes 680 SCF H₂/BBL for 70% metals removal (80% desulfurization), whereas hydrogen consumption required for metal removal alone is estimated to be less than 10 SCF/BBL on the basis of model compound studies. Metals deposition on commercial catalysts may also increase hydrocracking activity relative to hydrotreating activity, thereby promoting higher hydrogen consumption. Feedstocks containing up to 1000 ppm Ni and V may increase hydrogen consumption by as much as 28% (Speight, 1981).

2. Vanadium versus Nickel Reactivity in Petroleum Oils

Most investigations have revealed that vanadium removal rates exceed those of nickel in petroleum residua. Results are summarized in Table XXVI. Cases of V/Ni activity ratios of less than one have been reported less frequently (Inoguchi *et al.*, 1971; Galiasso *et al.*, 1985). These have generally been due to a temperature phenomenon but may also result from unique feedstock or catalyst properties.

Data from Ohtsuka (1977) on the demetallation of a Khafji feedstock are shown in Fig. 33. The vanadium content is reduced simultaneously with an increase in desulfurization, but the nickel is not removed until 60% desulfurization. This behavior is observed for the full crude as well as for two atmospheric residua cuts (180°C+ and 310°C+) indicating consistently higher vanadium reactivity throughout the molecular weight distribution of metal-bearing compounds in the petroleum.

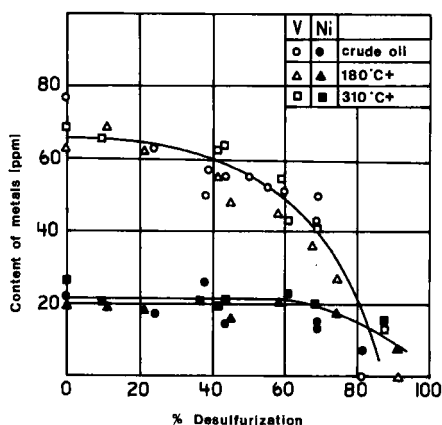


FIG. 33. Relationship between vanadium and nickel removal during desulfurization of petroleum oils (Ohtsuka, 1977).

Inoguchi *et al.* (1971) report that the vanadium removal rate exceeds that of nickel only at temperatures in excess of 400°C. Experiments with Khafji and Kuwait atmospheric residua revealed higher nickel removal rates below 400°C. Model compound porphyrin studies by Hung and Wei (1980) and Rankel (1981) also demonstrated a temperature dependence on the relative V/Ni removal rate. A higher apparent activation energy for vanadium removal observed by Hung and Wei (1980) could explain the reactivity ratio shift with increasing temperature. Catalyst properties and activity could also impact the V/Ni removal ratio. If vanadium were more diffusion limited than nickel, then a low-activity, large-pore catalyst would favor V removal, whereas a small-pore catalyst would favor Ni removal.

Vanadyl and nickel reactivity differences resulting from the chemistry of the oxygen ligand on vanadium were discussed in Section IV,A,1,c. Enhanced V reactivity could also arise from molecular size constraints. Beuther and co-workers (Beuther and Schmid, 1963; Larson and Beuther, 1966) speculate that nickel concentrates in the interior of asphaltene micelles while vanadium concentrates on the exterior. Thus a combination of stronger adsorption due to the oxygen ligand and inhibition of Ni reaction, coupled with the exposed position at the periphery of the asphaltene, may all contribute to the enhanced vanadium reactivity relative to nickel.

Model compound studies have shown the importance of porphyrin macrocycle basicity, resulting from electron-withdrawing substituents and metal ligands, on the reducibility and susceptibility of the central metal to reaction. Similar insight into the differences in relative basicity of vanadium- and nickel-containing complexes found in petroleum may therefore be valuable in rationalizing the observed effects and predicting demetallation activity.

3. *Reaction Selectivity during Hydroprocessing: HDM versus HDS and HDN*

The similarity of the reaction requirements for metal removal and sulfur and nitrogen removal leads to simultaneous reaction under typical hydrotreating conditions. Thiophenes are converted to olefins and paraffins, benzothiophenes are converted to alkylaromatics, while dibenzothiophenes are generally converted to biphenyls. The major reactions during HDS involve simple carbon-sulfur bond rupture and the capping of reactive fragments with hydrogen. Aromatic ring saturation is not usually a prerequisite for desulfurization. Nitrogen compounds which may be present include pyrroles, pyridines, indoles, quinolines, and carbazoles. Denitrogenation generally requires extensive hydrogenation of aromatic

structures prior to cleavage of the C–N bond. The simultaneous reaction of nitrogen compounds during demetallation may adversely affect catalyst performance by generation of basic nitrogen species which adsorb and poison sites with acidic character.

Riley (1978) reported that activity for hydroprocessing reactions decreased in the order $\text{HDS} > \text{HDM} > \text{HDN}$ when processing a Safaniya atmospheric residuum on $\text{CoMo}/\text{Al}_2\text{O}_3$ catalysts with pore size up to 150 Å. Only with large-pore catalysts did vanadium removal activity equal that of desulfurization. Pazos *et al.* (1981) report 40% higher desulfurization relative to vanadium demetallation of deasphalted Tia Juana residuum on a proprietary catalyst. Other investigators report similar trends in activity regardless of whether the feed is virgin crude oil (Radford and Rigg, 1970), atmospheric residuum (Kwan and Sato, 1970; Richardson and Alley, 1975), vacuum residuum (Radford and Rigg, 1970), or deasphalted oil (Howell *et al.*, 1985; Galiasso *et al.*, 1985). Thus within similar boiling fractions, the activity pattern remains $\text{HDS} > \text{HDM} > \text{HDN}$ even though there is a strong dependence of heteroatom reactivity on molecular weight.

A linear relationship is often observed between vanadium removal and sulfur removal, whereas the relationship between nickel and sulfur removal is linear but of smaller slope (Massagutov *et al.*, 1967). For asphaltene-containing stocks, this phenomenon is interpreted on the basis of heteroatom distribution within the asphaltene micelles (Beuther and Schmid, 1963). Sulfur and vanadium are concentrated on the exterior, whereas nickel is concentrated in the interior. Conversion of the asphaltene generally leads to simultaneous removal of sulfur and vanadium, whereas nickel removal is more difficult.

With deasphalted oils an alternative explanation is required to rationalize the linear relationships. Gajardo *et al.* (1982) postulate the linear relationships between HDM and HDS, and HDM and HDN are the result of similar active catalytic sites for each heteroatom species. This interpretation is compatible with model compound studies revealing similar sequential hydrogenation–hydrogenolysis reaction pathways for HDM, HDS, and HDN (see Section IV,A).

4. *Effect of Catalyst Properties on Activity*

a. *Catalytic Metals.* Some study has been made of the effect of catalyst composition on hydrodemetallation reactions. These results must be interpreted in context with catalyst pore size and age to be meaningful.

Riley (1978) reported that catalyst activity for vanadium removal from Safaniya atmospheric residuum is independent of the Co and Mo loading.

However, pore structure was small enough to have had an impact on the observed behavior. In an independent study Morales *et al.* (1983) reported that devanadiazation of Jobo Morichel DAO was insensitive to molybdenum loading above 5 wt. % even though this is well below monolayer coverage on Al_2O_3 . The promoter effect of cobalt was also claimed to be minimal for HDM. Catalyst aging by deposition of Ni and V may lead to monolayer coverage of active sites, potentially resulting in a "new" active catalyst surface independent of the original composition. Thus, initial activity data free from aging artifacts are necessary to substantiate these observations.

Plantenga *et al.* (1984) showed a linear increase in the initial HDM activity of Gach Saran atmospheric residuum with increasing levels of MoO_3 on alumina. However, the stability of the high- MoO_3 catalysts was lower than that of the low- MoO_3 catalysts, and after 20 days on stream the catalyst activity was independent of MoO_3 loading. Similar results were reported with $\text{NiO-MoO}_3/\text{Al}_2\text{O}_3$ catalysts. The activity pattern observed indicates that conversion is not solely limited by pore diffusion in these catalysts and that deactivation by metal deposits is resulting in the apparent independence of activity on "active" metal loading with mildly aged catalysts.

Sulfiding enhances the HDM activity of CoMo and NiMo/ Al_2O_3 catalysts relative to the performance of the oxide forms (Gajardo *et al.*, 1982). Similar results were reported in model compound studies (Ware and Wei, 1985b).

An examination of the activity of group I through VIII metal oxides supported on Al_2O_3 has been reported by Kushiyama *et al.* (1983) for demetallation of Khafji residuum. Average pore diameter of the Al_2O_3 carrier was between 200 and 300 Å, sufficiently large to minimize configurational diffusion effects. Initial activity results with catalysts which were not presulfided indicated that $\text{MoO}_3/\text{Al}_2\text{O}_3$ was the most active one-component catalyst for Ni and V removal. Marginal activity increases were observed with Co or Ni added as a promoter. However, catalysts composed of boron or phosphorus added to CoMo/ Al_2O_3 showed the highest activity for metals removal and sulfur and asphaltene conversion.

Webster (1984) reported an optimum Co/(Mo + Co) atomic ratio of 0.65 for HDM of Ni-porphyrins in model compound studies. A similar optimum ratio has been reported for HDS reactions (Wivel *et al.*, 1981). However, evidence supporting this optimum Co/Mo ratio for demetallation of real feedstocks is lacking. It is likely that this optimum is important only with clean catalysts in the initial stages of oil processing. Once Ni and V begin to accumulate on the surface, the original composition becomes less important.

Catalysts containing nonconventional active catalytic components have been considered for demetallation. Sasaki *et al.* (1982) report that NiV/Al₂O₃ catalysts have comparable activity as CoMo/Al₂O₃ for demetallation of Gach Saran vacuum residuum. This again is likely an artifact of deactivation of the fresh CoMo catalyst. Optimum Ni/V ratios range from 7/3 to 5/5. (These ratios are generally higher than the Ni/V ratio of most crudes.) One of the advantages of utilizing such a catalyst is that the active metal sites are continually regenerated *in situ* by deposition of Ni and V from the petroleum.

The suggestion that deposited Ni and V in the form of sulfides can themselves act as catalysts, in essence autocatalytic metal removal reactions, has been demonstrated by Sie (1980) and Devanneaux *et al.* (1985). Bare alumina carriers gradually acquired catalytic activity for HDM of residual feedstocks when exposed to the feedstock for prolonged periods under hydroprocessing conditions. Takeuchi *et al.* (1985) demonstrated that after accumulation of 10 wt. % vanadium on an alumina base, the *in situ* generated "catalyst" has essentially the same HDM activity as the Co-Mo-impregnated alumina. The HDS activity, however, is 35% lower for the alumina base covered with vanadium than the CoMo/Al₂O₃ catalyst. This reduced selectivity for sulfur removal relative to metals is typically observed with NiV/Al₂O₃ catalysts (Rankel and Rollmann, 1983; Toulhoat *et al.*, 1985).

Natural materials such as manganese nodules and bauxite have been considered as catalysts for demetallation. These materials are attractive for applications where the catalyst is disposed after deactivation since conventional CoMo/Al₂O₃ desulfurization catalysts may be too expensive. The nodules also have their metallurgical value increased after accumulating Ni and V.

Chang and Silvestri (1974, 1976) compared ocean nodule catalysts, rich in conventional hydrotreating metals (such as Ni, Mo, and Co) in addition to Mn, with freshwater nodules containing only trace levels of Ni, Mo, and Co. The freshwater nodules exhibited higher demetallation activity relative to the ocean nodules despite their lower "active" metal content. High iron concentration in the freshwater nodules relative to the ocean nodules (35 versus 12 wt. %) may have contributed to the observed behavior. Also, the freshwater nodules possessed a higher average pore diameter than the ocean nodules; the surface areas were similar. The most active manganese nodules are, however, less active than commercial CoMo/Al₂O₃ catalysts, an observation also confirmed by Dodet *et al.* (1984).

Chang and Silvestri (1976) determined that Porocel (activated bauxite) exhibited lower activity than that of the nodules for demetallation of Kuwait residuum. Transport limitations resulting from an average micro-

pore diameter of 20 Å and the absence of catalytic metals in the Porocel explain its poor activity. Bauxite-based catalysts with V and Ni removal activity similar to a commercial hydrotreating catalyst have been prepared by addition of 2.0 wt % NiO and 6.6 wt. % MoO₃ to bauxite support (Iannibello *et al.*, 1982).

The natural material catalysts exhibit similar metal removal selectivity patterns as conventional hydrotreating catalysts. Vanadium removal activity is higher than that of nickel and overall activity increases with hydrogen pressure. Thus little change in intrinsic demetallation pathways is indicated with these materials. However, in contrast to CoMo/Al₂O₃, the nodule catalysts are only moderately active for HDS and essentially inactive for HDN.

b. *Catalyst Pore Size Distribution.* Numerous studies have focused on the appropriate support pore size distribution for maximum demetallation activity. With hydrodemetallation reactions the problem is very complicated. The range of molecular weight and size of metal-bearing species in the oil influences the diffusivity through the pores and the range of reactivities of metal compounds influences the reaction kinetics. Since hydrotreating catalysts have pores ranging in size from 25 to more than 1000 Å and metal-bearing porphyrins and asphaltenes range in molecular diameter from 10 Å and up, intraparticle diffusion is generally important for demetallation. (See Section IV,B,5.) Microprobe profiles of Ni and V in aged catalysts do indeed reveal that the demetallation reactions are diffusion controlled. (See Section IV,B,6.)

Riley reported that pore structure controlled Ni and V removal in treating a Safaniya atmospheric residuum. Metals removal activity increased with increasing pore size from 100 to 150 Å in narrow-pore-size-distribution CoMo/Al₂O₃ catalysts. Larger-pore-size catalysts, typical of many of the newer HDM catalysts, were not examined.

An optimum pore size for maximum demetallation activity has been suggested by many investigators (Howell *et al.*, 1985; Hardin *et al.*, 1981; Inoguchi, 1976; Plumail *et al.*, 1983; Ruckenstein and Tsai, 1981). Catalysts prepared by Hardin *et al.*, (1981) contained two pore regimes: large interparticle pores corresponding to intergranular voids with diameters of 10,000 Å and larger and intragranular pores of 500 Å and smaller. Maximum activity for Ni and V removal from Athabasca bitumen occurred with catalysts characterized by median pore diameters of 200 Å. Increases in pore size above this resulted in a decrease in activity. This phenomenon is easily rationalized on the basis of catalyst surface area. As pore size increases, the catalyst surface area decreases and so does the number of reactive sites. Lowering the pore size increases the surface area

but also increases the diffusional resistance to the sites. There is a compromise between the increase in activity due to an increase in surface area and the decrease due to diffusional resistances; hence an optimum pore size is observed.

Plumail *et al.* (1983) determined an optimum pore diameter of 150 to 200 Å for demetallation of Boscan crude on unimodal catalysts, as shown in Fig. 34. Activity for vanadium removal parallels asphaltene conversion as a function of pore diameter. This similarity is not surprising considering that asphaltenes account for 75% of vanadium in Boscan crude and in light of the evidence for concurrent demetallation as asphaltenes are converted to resins. Hydrodesulfurization activity was highest on catalysts with pores of 100 Å, suggesting a difference in molecular size between the sulfur- and vanadium-bearing molecules. Bimodal catalysts having micropore diameters ranging from 100 to 320 Å and macropores of 1000 Å and greater also exhibit maxima in hydrodevanadiaization activity at 150 to 200 Å average pore diameter, similar to the monomodal catalysts. However, when macroporosity is incorporated into the catalyst, HDA and HDV activities are markedly enhanced, up to 50% higher than the unimodal catalysts. The introduction of macropores increases asphaltene accessibility to the micropores of the catalyst, enabling conversion by depolymeriza-

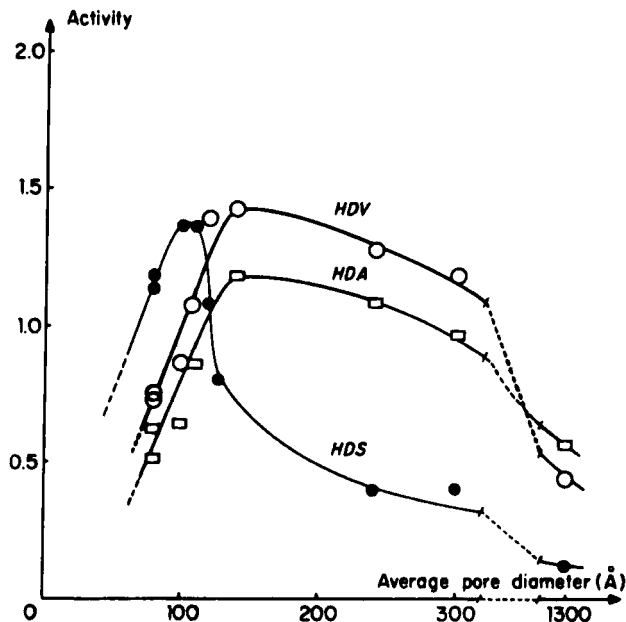


FIG. 34. Relationship between conversion activity and average catalyst pore diameter (Plumail *et al.*, 1983).

TABLE XXVII

VANADIUM AND NICKEL DISTRIBUTION FACTORS IN RESIDUUM HYDROPROCESSING CATALYSTS^{a,b}

Catalyst	Average pore diameter (relative scale)	Vanadium distribution factor		Nickel distribution factor	
		Arabian Heavy 455°C+	Maya 345°C+	Arabian Heavy 455°C+	Maya 345°C+
A	2.7	0.82	0.68	—	0.77
B	—	0.76	0.64	0.89	0.74
C	2.3	—	0.47	—	0.55
D	1.8	—	0.36	—	0.41
E	1.3	0.41	—	0.56	—
F	1	0.30	—	0.34	—
G	0.7	0.13	—	0.17	—

^a From Howell *et al.* (1985).^b All catalysts are either $\frac{1}{16}$ -in. cylinder or sphere. Catalyst B has a bimodal pore size distribution. The average pore diameter is defined as $40,000 \times$ pore volume (ml/g) divided by nitrogen surface area (m²/g).

tion and cracking and demetallation. Similar increases in HDS activity are not observed in the bimodal catalyst since 85% of the sulfur is contained in nonasphaltenic molecules characterized by smaller radii. Diffusional limitations in HDS generally appear only when the average micropore diameter is less than 100 Å with typical $\frac{1}{16}$ in.-diameter catalysts.

The appropriate choice of pore size for demetallation catalysts is not straightforward. Feed source can have a dramatic effect on the apparent activity and, consequently, the deposition profiles of Ni and V even when processing conditions are identical. This is illustrated by Howell *et al.* (1985) in Table XXVII, where metal distribution parameters θ_m (see Section IV,A,4) are compared for Arabian Heavy and Maya chargestock for a variety of catalysts. Metal compounds in Maya deposit unevenly, concentrating near the catalyst perimeter as indicated by the lower distribution parameters. This may be due to higher intrinsic reactivity or greater diffusional resistance (larger molecules, stronger adsorption) relative to Arab Heavy. Interestingly, Ni compounds in both feeds penetrate deeper and deposit more uniformly than the V counterparts.

Catalyst surface activity may be manipulated to alter the ratio of HDM activity to metal compound diffusivity with a predictable impact on optimum pore size (Howell *et al.*, 1985). Lowering the intrinsic surface activity by varying the quantity, chemical composition, or distribution of active catalytic metals will increase the Ni and V penetration into the catalyst. The lower surface activity catalysts may be able to tolerate a smaller pore size (higher total surface area) and still maintain an acceptable performance for the HDM reactions.

Tailoring the catalyst pore size distribution is one option available for altering the catalyst's selectivity for demetallation relative to other hydroprocessing reactions. Inoguchi (1976) and Plumail *et al.* (1983) have shown that specific desulfurization activity (activity per square meter of catalyst) remains constant down to pore sizes of 100 Å whereas maximum demetallation activity requires pores 50 to 100 Å larger. Therefore, selectivity for desulfurization increases with catalysts of relatively small pore diameters, whereas selectivity for demetallation reactions tends to increase in proportion to pore size. Figure 35 from Howell *et al.* (1985) clearly shows this effect for processing Arabian Heavy. The large pore catalyst A removes considerably more metals at a given HDS level than catalyst F. Similar shifts in HDS-HDM selectivity in response to catalyst pore size have been demonstrated by Fischer and Angevine (1986) processing Arabian Light and Kuwait atmospheric residua.

c. *Catalyst Size and Shape.* The diffusion-limited nature of HDM reactions makes catalyst size and shape an important consideration in the design to optimize catalyst performance. Bridge and Green (1979) demon-

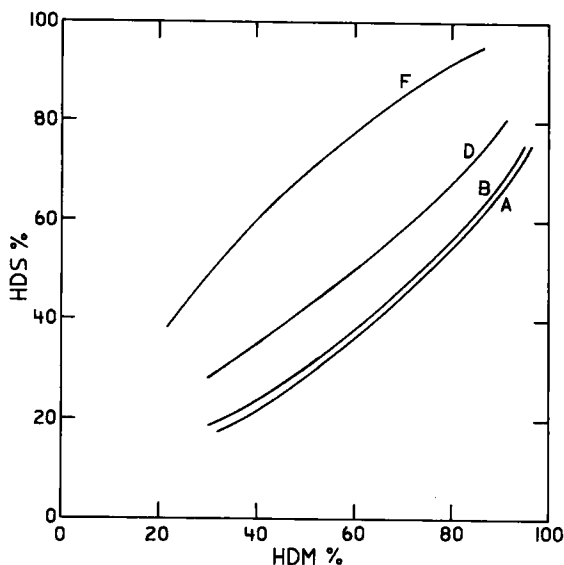


FIG. 35. Selectivity of HDM catalysts—percent HDM versus HDS of 405°C+ Arabian Heavy. See Table XXVII for catalyst identification (Howell *et al.*, 1985).

strated with demetallation of Boscan crude a decrease in the optimum pore size with reduction in catalyst particle size, as shown in Fig. 36. With smaller particles, higher intraparticle diffusion can be tolerated and catalysts with smaller pores and higher surface area are preferred. Decreasing the particle size increases the geometric surface area per unit reactor volume and shortens the diffusional distance, but this leads to

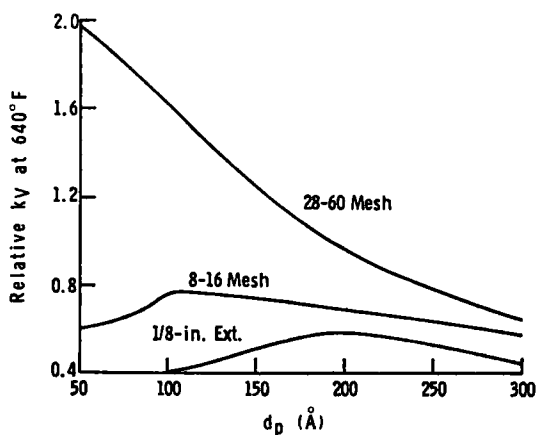


FIG. 36. Calculated effect of catalyst size and average pore diameter on Boscan demetallation kinetics (Bridge and Green, 1979).

increased pressure drop, which is often a constraint in fixed-bed hydro-processing reactors. Particles smaller than 0.8 mm ($\frac{1}{32}$ in.) are typically not used in commercial fixed-bed reactors because of excessive pressure drop or the potential for plugging of the catalyst bed with particulates common to residuum feeds.

Modification of the catalyst shape has been explored to reduce the diffusional resistance and yet maintain the hydraulic pressure drop characteristics of conventional 1.6-mm cylindrical extrudates or spheres. Included in this list of preparations with novel shapes are UNOCAL's cloverleaf-shaped extrudate developed jointly with American Cyanamid (Richardson *et al.*, 1979); W. R. Grace's Minilith (Pieria *et al.*, 1985); the chestnut bur catalyst developed by Institut Francais Du Petrole (Toulhoat *et al.*, 1985); a Chevron shaped-catalyst (Howell *et al.*, 1985); and Catalytica Associates' conceptual design of highly porous, micro-catalyst particles contained in a strong, attrition-resistant basket (Dautzenberg and De Deken, 1984, 1985). The impact of catalyst shape on metal penetration and aging characteristics is discussed in Section V.

5. *Diffusion and Adsorption Phenomena*

The consideration of parameters such as catalyst pore size distribution and the ratio of molecular size to pore size are especially pertinent in hydrotreating. Irrespective of the reaction chemistry, metal-bearing molecules must first reach the catalytic site within the support pore structure prior to conversion. Reactions involving metal compounds associated with large molecular clusters in petroleum are frequently diffusion limited in typical hydrotreating catalysts. The existence of diffusional phenomena is demonstrated by increases in conversion activity with increases in catalyst pore diameter and nonuniform Ni and V deposits in aged catalysts. Knowledge of the transport properties of these metal species is therefore necessary to allow rationale design of reaction processes for upgrading residuum. Of equal importance is an understanding of the diffusion process as related to the transient nature of the catalyst during deactivation resulting from accumulation of metal and coke deposits in aging catalysts. The transformation of catalyst pores during deactivation is discussed in Section V.

Studies of metal compound diffusion in porous media have consistently demonstrated that the rate of diffusion within the microporous material is less than would be observed in an unrestricted medium. This discrepancy, observed for all liquid diffusion processes in pores of small diameter is related to hydrodynamic phenomena. The proximity of the molecule to the pore wall increases the frictional drag on the diffusing species when the

ratio of the molecular size to pore size exceeds 0.1. Thus it is evident that most of the metal-containing asphaltenes (diameter 20–50 Å) and porphyrins (diameter ~10 Å) will encounter configurational diffusion in hydrotreating catalysts with pores of 100 to 200 Å in diameter.

Hydrodynamic theory for hindered diffusion developed for transport of biological molecules through porous membranes predicts that the diffusive transport is controlled by two phenomenon. First there is a steric partitioning K_p of the solute between the end of the pore and the bulk phase. In addition to this geometric effect, a second effect is increased viscous drag C_D on a solute molecule as it moves through the liquid-filled pore. The hindered or configurational diffusion in a single pore can be written as

$$D = D_\infty K_p C_D \quad (12)$$

where D_∞ is the unrestricted diffusivity. For a purely steric interaction between the solute and pore wall, Ferry (1936) proposed

$$K_p = (1 - \lambda)^2 \quad (13)$$

where λ equals the ratio of the molecular diameter to pore diameter or r_m/r_p . The chemical and electrical properties of the surface and solute are not considered in this geometrical approach. In reality, surface adsorption within the pore or repulsion between the molecule and surface may influence the equilibrium partition coefficient. Several functional forms for the dependence of C_D on λ have been proposed (Spry and Sawyer, 1975; Ma and Gabriel, 1978).

The simplest diffusion interpretation considers transport through straight channels, representative of idealized single pores in a catalyst support. Recent studies have measured diffusion of asphaltenes in well-defined porous membranes prepared from track-etched muscovite mica (Trash and Pildes, 1981; Baltus and Anderson, 1983). These experiments have been conducted in the absence of chemical reaction. Thrash and Pildes (1981) pioneered this asphaltene diffusion technique by measuring an average diffusivity of 4.5×10^{-6} cm²/sec for a sample of Middle East residuum asphaltenes in toluene at room temperature. Membrane pore diameters in excess of 100 Å were purposely chosen to minimize configurational effects enabling an average molecular diameter of 16 Å ($\lambda \approx 0.02$) to be calculated from the diffusion coefficient using the Stokes–Einstein equation. However, the lack of information concerning the molecular size distribution of the asphaltene sample makes interpretation of this average dimension and estimation of diffusivities in catalyst pores difficult.

Narrow cuts of asphaltenes from Kuwait atmospheric residuum with molecular radius ranging from 26 to 153 Å (based on size exclusion chromatography) were examined by Baltus and Anderson (1983) in pores

ranging from 70 to 500 Å. The use of narrow cuts minimized variations in diffusion coefficients due to the heterogeneous nature of petroleum asphaltenes. Bulk phase diffusivities for these fractions ranged from 16.1 to 2.71×10^{-7} cm²/sec at room temperature in tetrahydrofuran. Configurational diffusion was represented by

$$D/D_{\infty} = (1 - \lambda)^2(1 - 2.104\lambda + 2.089\lambda^3 - 0.948\lambda^5) \quad (14)$$

where the Renkin hydrodynamic drag equation was used for C_D (Renkin, 1954). At small λ (<0.25), Eq. (14) reduces to an empirical expression.

$$D/D_{\infty} = \exp(-b\lambda) \quad (15)$$

with $b = 4.6$. Baltus and Anderson proposed a value of $b = 3.69$ to account for larger values of λ encountered in their studies.

A major deficiency in the asphaltene diffusion studies results from the limitations of the experimental conditions employed. Measurements at room temperature and in clean solvents can potentially alter the effective size of the diffusing species relative to that in hydrotreating catalysts at reaction conditions.

Information relating to the diffusion of metal-bearing compounds in catalytic materials at reaction conditions has been obtained indirectly through classic diffusion and reaction theory. Shah and Paraskos (1975) calculated effective diffusivities of 7×10^{-8} and 3×10^{-8} cm²/sec for V and Ni compounds in reduced Kuwait crude at 760°F. These low values may be indicative of a small-pore HDS catalyst. In contrast, Sato *et al.* (1971) report that the effective diffusivity of vanadium compounds was one-tenth that of the nickel compounds on the basis of metal deposition profiles in aged catalysts. This large difference may be influenced by relative adsorption strengths not explicitly considered in their analysis.

Spry and Sawyer (1975) developed a model using the principles of configurational diffusion to describe the rates of demetallation of a Venezuelan heavy crude for a variety of CoMo/Al₂O₃ catalysts with pores up to 1000 Å. This model assumes that intraparticle diffusion is rate limiting. Catalyst performance was related through an effectiveness factor to the intrinsic activity. Asphaltene metal compound diffusivity as a function of pore size was represented by

$$D_{\text{eff}} = \frac{D_{\infty}^{\varepsilon}}{\tau} (1 - \lambda)^4 \quad (16)$$

where ε and τ are the catalyst void fraction and tortuosity, respectively. This expression assumes that the functional dependence of C_D on λ is equivalent to that of K_p . Bulk diffusivity for the asphaltene metal compounds estimated from correlations resulted in $D_{\infty}\varepsilon/\tau$ equal to

3×10^{-8} cm²/sec. Good agreement with HDM activity was claimed for asphaltene molecules up to 100 Å in diameter ($\lambda > 0.1$) with this configurational diffusion model.

Despite claims by Spry and Sawyer (1975) of analytical measurements verifying asphaltene molecular sizes in the 100 Å range at ambient conditions, it is unlikely that molecules this bulky exist at reaction conditions. The good predictive capability of the model may therefore result from a compensation effect. Electrostatic and adsorption interactions between solute molecules and the pore walls not explicitly accounted for with the purely geometric partition coefficient may result in the diffusing molecules appearing larger than they are at reaction conditions.

Direct diffusion measurements in catalytic materials under nonreacting conditions avoid complications associated with uncertainties in the reaction mechanism and distributions in reactivities resulting from the heterogeneity of metal compounds. Galiasso and Morales (1983) report that diffusion of Boscan porphyrin extracts in catalytic materials is strongly influenced by surface acidity and particle size, indicative of adsorption interference. Large particles and acidic surfaces exhibited the lowest diffusion rates and metal porphyrin adsorption capacities as a result of pore blockage. Increases in temperature and solvent polarity weaken these interactions and minimize the pore blockage effect. Polar solvents used in the experiment may, however, complicate the diffusion analysis by associating with the porphyrin molecule yielding a larger apparent critical diameter. Extrapolation of VO-porphyrin diffusivity data to hydroprocessing temperatures ($\sim 380^\circ\text{C}$) yielded an effective diffusivity ($D_{\infty}\epsilon/\tau$) on the order of 10^{-5} cm²/sec. This high value reflects the smaller size of the porphyrins relative to asphaltenic components and the large pore size (158-Å diameter) of the catalyst support which minimizes configurational effects ($\lambda < 0.1$).

A discussion of diffusion phenomena is not complete without mention of the importance of adsorption effects. Physical adsorption has a direct impact on the observed diffusion process. For example, diffusion of an organovanadium complex may be influenced by competitive adsorption with other vanadium species as well as by nickel compounds or other impurities in the oil. This competitive adsorption likely contributes to the large differences observed in the diffusion-limited reaction rates of nickel and vanadium compounds (Sato *et al.*, 1971).

Detailed adsorption studies by Morales and co-workers (Morales and Galiasso, 1982; Andreu *et al.*, 1981; Morales *et al.*, 1984) are unique in their examination of the interaction of VO-porphyrins extracted from Boscan crude on $\gamma\text{-Al}_2\text{O}_3$ -supported cobalt and molybdenum catalysts. Interaction with the oxide catalyst is primarily through the oxygen ligand of

the vanadyl group with electron acceptor sites on the surface (Al^{3+} , Mo^{6+} , Co^{2+} ions). These interactions are characterized by low heats of adsorption since polar solvents are able to desorb the porphyrins at room temperature. Adsorbed porphyrins do remain on the surface at temperatures as high as 500°C in streams of pure H_2 , but this environment is not representative of liquid-phase hydrotreating of heavy petroleum fractions. Reduced and sulfided catalysts exhibit stronger adsorption affinity, retaining porphyrins that would otherwise be desorbed in polar solvents on the oxide catalyst.

Diffuse reflectance spectroscopy (DRS) of VO-porphyrins on reduced and sulfided catalysts exhibit shifts in the porphyrinic electronic spectra (Soret, α , β bands) to higher frequencies. Adsorption results in modification of the delocalized electronic resonance structure not observed on the oxide form of the catalyst. X-ray photoelectron spectroscopy reveals shifts to higher Mo binding energies on reduced and sulfided catalysts following VO-porphyrin adsorption, consistent with transfer of electrons from Mo electron donor sites to the VO^{2+} ion. Interaction at the electron donor sites is stronger than interaction at electron acceptor sites typical of the oxide catalyst. This gives rise to the possibility of lower VO-porphyrin diffusion rates on sulfided catalysts, but this effect has not been experimentally demonstrated.

The adsorption interaction of Ni-porphyrin extracts from petroleum has been less thoroughly examined. Limited experimental evidence suggests that the adsorption is much weaker than typical for vanadyl porphyrins. This discrepancy may be further enhanced on reduced and sulfided catalysts where adsorption results from electron donation from the surface. The electron-withdrawing effect of the oxygen ligand creates a favorable environment for electron transfer to vanadium orbitals. Nickel is not similarly influenced by axial ligands since its coordination valences are satisfied by planar nitrogen atoms. Thus on sulfided catalysts, larger differences in vanadium and nickel species' apparent diffusivities may be present due in part to adsorption influences, whereas on oxide catalysts these differences may be less dramatic.

6. Metal Deposition Profiles in Aged Hydrotreating Catalysts

Hydrodemetallation reactions are revealed to be diffusion limited by examination of metal deposition profiles in catalysts obtained from commercial hydroprocessing reactors. Intrapellet radial metal profiles measured by scanning electron x-ray microanalysis show that vanadium tends to be deposited in sharp, U-shaped profiles (Inoguchi *et al.*, 1971; Oxenreiter *et al.*, 1972; Sato *et al.*, 1971; Todo *et al.*, 1971) whereas nickel has been observed in both U-shaped (Inoguchi *et al.*, 1971; Todo *et al.*, 1971) and

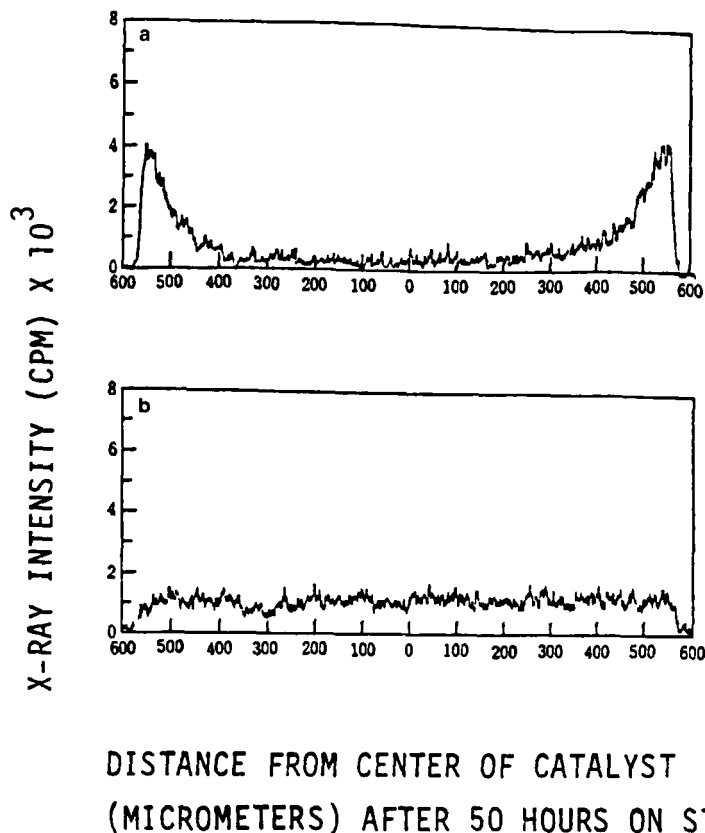


FIG. 37. Concentration profiles of (a) vanadium and (b) nickel within HDS catalyst after 50 hours on stream (Sato *et al.*, 1971).

uniform profiles (Oxenreiter *et al.*, 1972; Sato *et al.*, 1971). Examples of metal profiles in catalysts sampled from commercial reactors are shown in Fig. 37. The discrepancy between uniform and nonuniform nickel profiles may be due to reactivity differences in the nickel compounds from one feedstock to another or to a difference in pore size distribution between different catalysts.

Scrutiny of intrapellet metal concentration profiles reveals that the shapes of the profiles are a function of the axial position of the catalyst within a packed-bed reactor. Tamm *et al.* (1981) reported that nickel and vanadium profiles exhibit an internal maximum, termed M shaped, at the reactor inlet which shifts to the pellets' edge at the bed outlet, as shown in Fig. 38. Similar internal maxima in aged catalysts have been observed elsewhere (Pazos *et al.*, 1983; Oxenreiter *et al.*, 1972; Hardin *et al.*, 1978).

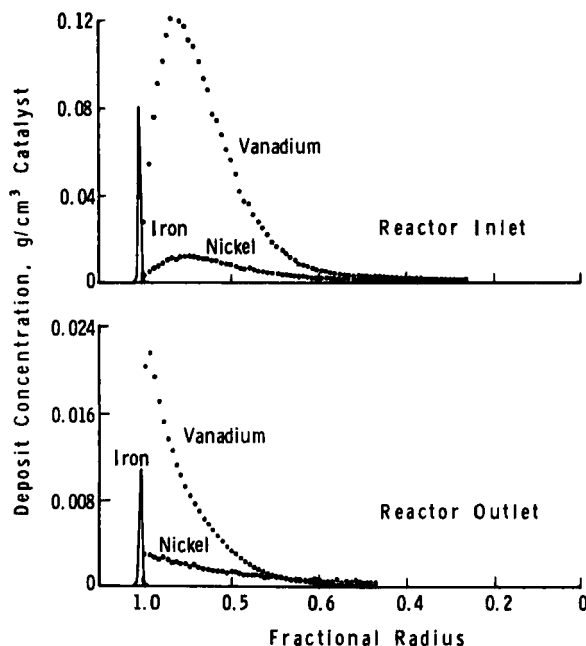


FIG. 38. Nickel, vanadium, and iron deposition profiles in aged $\frac{1}{16}$ -in. catalyst after processing Arabian Heavy atmospheric residuum at 370°C (700°F) and 12.59 MPa H_2 (1810 psig) (Tamm *et al.*, 1981).

The sharp iron profiles in Fig. 38 are thought to be due to deposits from rust and scale, not to organometallic compounds. Their removal likely occurs by a sieving process and thus delineates the edge of the pellet. The Ni and V internal maxima cannot be predicted by simple first- or second-order reaction kinetics. Rather, these profiles are a consequence of the consecutive HDM mechanism involving metal deposition from an intermediate not originally in the oil. This mechanism has been demonstrated in model oil systems (Section IV, A, 4) and now has evidence with real oils.

When metal compounds with a distribution of reactivities are lumped together, the overall metal removal kinetics may appear as second order even though individual classes of compounds may react as first order or through sequential pathways. Intrapellet metal profiles often provide evidence of a distribution of metal compound reactivities. Nickel profiles in Fig. 39 in catalyst aged with Gach Saran and Khafji residue can be interpreted as being made up of at least two components to the deposition pattern. Metal species, sometimes referred to as "easy" metals, are readily removed (low effectiveness factor), resulting in sharp metal gradients near

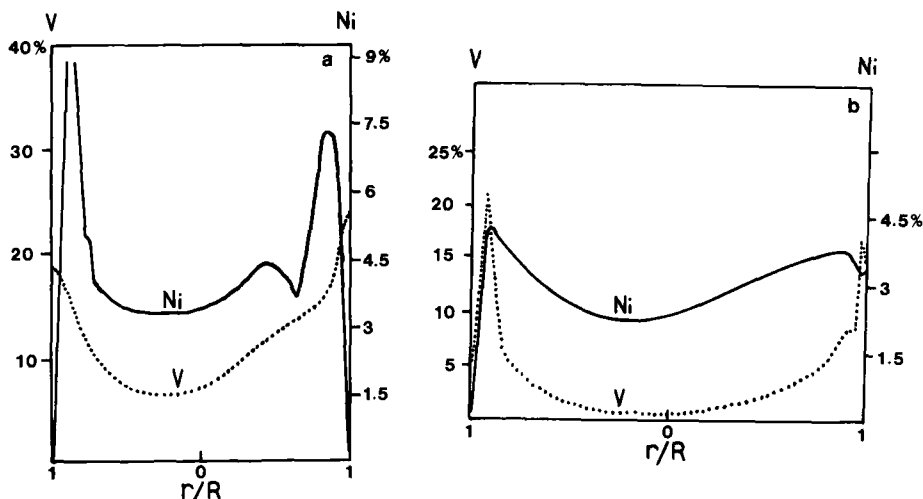


FIG. 39. Nickel and vanadium distributions throughout aged catalysts from (a) top of bed and (b) bottom of bed (Oxenreiter *et al.*, 1972).

the pellets' edge at the reactor entrance. Metalloporphyrins in the resin fraction may be typical of such species. The more refractory, "hard" compounds yield more uniform profiles (higher effectiveness factor). At the reactor outlet in Fig. 39 the "easy" Ni species is depleted and the relatively uniform profile reflects deposition from the remaining refractory Ni compounds. Metal profiles indicating the presence of "easy" and "hard" metal species have also been reported for V (Higashi *et al.*, 1985). The Ni and V profiles in Fig. 38 which fail to clearly show components from different reacting species may be a result of feed differences such as lower amounts of porphyrinic metals in free solution.

The chemical nature of the accumulating metals on the catalyst surface is primarily sulfides, independent of the feedstock and catalyst support (see discussion in Section V). Equilibrium constants for Ni and V sulfides are favorable for their presence at typical hydrotreating conditions (Bartholomew *et al.*, 1982). Vanadium may exist in a variety of states, including a vanadyl species, depending on the catalyst metal loading (Silbernagel, 1979). The vanadium-to-nickel weight ratio on spent catalysts is generally higher than that of the feed, signalling the ease of vanadium removal relative to nickel for most chargestocks.

Experimental variables which alter the shape of the metal profiles are a manifestation of the intrinsic reactivity and transport characteristics of the metal-bearing species. The extent to which the catalyst pore volume is utilized to accommodate metal deposits in response to these changes is

characterized by the metal distribution parameter θ_m defined by Tamm *et al.* (1981). (See Section IV, A, 4.) Catalysts with high intrinsic activity (for example, high active metal loadings) increase the ratio of chemical reaction to diffusion that is the Thiele modulus and concentrate metal deposits on the outer edge of the catalyst (low θ_m). Operating variables which increase the intrinsic activity, and hence the Thiele modulus, such as increasing temperature or hydrogen pressure, also result in poor distribution of metal within the catalysts. More uniform profiles (higher θ_m) are obtained in catalysts where diffusion resistance has been reduced either by incorporation of larger pores into the support or by reductions in catalyst particle size. A thorough examination of metal profile response to catalyst design variables and operating conditions has been given elsewhere (Howell *et al.*, 1985; Tamm *et al.*, 1981). The critical role these metal deposit distributions exert in catalyst deactivation and determining the ultimate catalyst lifetime is the subject of Section V.

The optimum catalyst and the optimum processing conditions for hydrodemetallation will depend upon the feedstock and the process application. To the extent that metal deposits determine the operating lifetime of the catalyst, knowledge of the intrinsic metal removal chemistry and molecular transport processes will enable prediction of metal deposition location within catalysts and will provide criteria for optimum catalyst design.

V. Catalyst Deactivation

While the heteroatoms S, N, and O are removed from the oil catalytically and from the reactor as gaseous products, the metals, because of their low volatility and insolubility in the oil after decomposition of the organometallic compounds, remain and accumulate in the reactor as solid deposits on the catalyst. Although demetallation of the oil is desirable to protect downstream processes or to prevent excessive corrosion in combustion equipment from a metal-laden fuel, it is recognized that catalytic hydrodemetallation of nickel and vanadium compounds in the oil, with their concurrent deposition on the catalyst throughout the catalytic reactor bed, is also the most important phenomenon causing catalyst deactivation in resid processing. A catalyst bed may accumulate nearly double its weight in feedstock contaminants. Obviously, deposits of this magnitude must severely affect the catalyst's ability to function.

Deactivation is brought about primarily by the continual and irreversible buildup of deposits within the catalyst pores. Loss of activity can be attributed to both the obstruction of catalyst pores by deposits and the chemical changes that occur when the deposited metal interacts with the original active sites on the catalyst. The former restricts the access of

residuum molecules to the catalytic site, while the latter cause of deactivation affects the intrinsic reactivity of the site itself. The economics of the process through catalyst costs, unit downtime, and feedstock flexibility are directly related to the ability of the residuum hydroprocessing catalyst to tolerate the deposition of nickel and vanadium. Increasing the tolerance of the catalyst or catalytic bed for metals accumulation without compromising on the activity required for conversion has been the major technical challenge of research in the area of residuum hydrodesulfurization. Continued progress in this area rests on the ability to develop novel catalyst systems through increased understanding of the physical and chemical processes that govern the activity and deactivation behavior of the catalyst.

The interrelationship among catalyst properties, operating strategy, residuum characteristics, and deactivation is a complex one. For residuum hydrodesulfurization, the operating strategy is to maintain constant catalyst activity and, therefore, constant sulfur level in the product by raising the temperature of the catalyst bed to compensate for deactivation. Catalyst in a fixed-bed processing residuum deactivates in a very characteristic fashion (Henke, 1970; Bridge *et al.*, 1979; Nitta *et al.*, 1979; Parkin *et al.*, 1979). Figure 40 from Tamm *et al.* (1981) illustrates a typical reactor average-temperature history that must be followed to maintain a constant sulfur level in the product. During the initial part of a run, the catalyst loses

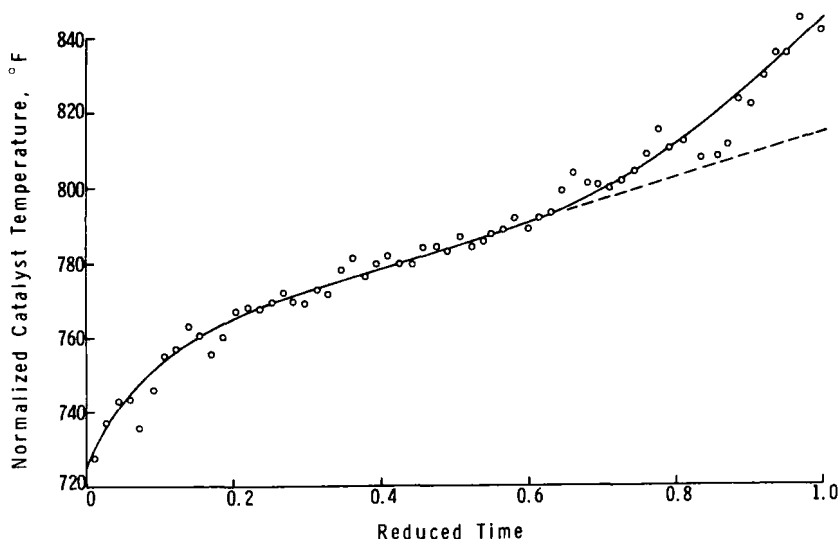


FIG. 40. Typical deactivation curve for residuum hydroprocessing catalyst. Arabian Heavy atmospheric residuum desulfurized to 1.10 wt. % product sulfur with a $\frac{1}{16}$ -in. extrudate catalyst (Tamm *et al.*, 1981).

activity rapidly and temperature must be increased rapidly to compensate. Some controversy remains regarding the cause of the deactivation during this initial period. Many researchers (Sie, 1980; Pazos *et al.*, 1983; Chang and Silvestri, 1976) speculate that this period corresponds to an initial buildup of a steady-state equilibrium coke level. Others (Tamm *et al.*, 1981) suspect that this period corresponds to an initial monolayer-type coverage of the surface by metal deposits which reduces the intrinsic reactivity of the catalyst. A period of slower, linear deactivation follows as a result of the continual buildup of metal deposits within the pore. The final period of rapid deactivation occurs when the deposit-laden pore mouths become constricted and eventually close, preventing access of reactants to internal catalytic sites. The deactivation rate during this pore mouth plugging phase is so rapid that temperature must be increased sharply to maintain product sulfur levels. The end-of-run temperature is usually determined by the metallurgical limits of the reactor.

This section will review the literature on the deactivation of residuum hydroprocessing catalysts from metal deposition. The first part will examine the two principal causes of catalyst deactivation resulting from the deposition of metals: (1) the loss of intrinsic catalytic activity of the catalytic sites and (2) the buildup of deposits affecting reactant diffusivity and ultimately resulting in the complete plugging of pore openings or pore mouths by deposit buildup. The second subsection reviews the dynamics of the deactivation process and how catalyst properties, process conditions, and feedstock characteristics determine the stability of a catalyst system. Unfortunately, this is an area where complete, detailed information is lacking in the published literature for several reasons. Although much information has been reported on the activity of various catalysts (Section IV) and on the kinetics of HDM and HDS, the stability aspect of catalysts and how this varies with catalyst properties remain rather proprietary. Furthermore, to conduct detailed research on stability or catalyst life is expensive because of the long duration of the tests, which last 2 months to 2 years. The last subject covered in this section is the modeling of the HDM process with catalyst deactivation. A successful model provides a design tool to predict catalyst performance, thereby reducing the need to conduct long-duration tests and increasing our ability to formulate new catalyst materials with better activity, selectivity, and stability.

A. MECHANISMS OF CATALYST DEACTIVATION

1. *Effects of Metal Deposits on Catalyst Intrinsic Activity*

Detailed examination of the chemical nature of the metal deposit on the catalyst has proved difficult because of the complexity and heterogeneity of

the deposit, particularly on the microscale. Consequently, little basic or correlative information is available on how feedback properties, operating conditions, or catalyst properties influence the chemical nature of the deposit.

Based on elemental analyses and microprobe tracing (Dautzenberg *et al.*, 1978), metal deposits appear to be present in sulfide forms and not as adsorbed porphyrin-type compounds or as metals in the elemental or metallic state. Takatsuka *et al.* (1979) and Rankel and Rollmann (1983) have reported direct linear correlations of the spent catalyst sulfur content with the deposited metal content. The sulfide forms of nickel and vanadium are consistent with expectations based on thermodynamics for the conditions typically encountered in residuum hydroprocessing units (600–800°F, 1000–2200 psig, H_2/H_2S environment).

Sophisticated spectroscopic methods, including NMR and EPR, were employed by Silbernagel (1979) to examine the State of metals on HDS catalysts. Three types of deposited vanadium were observed and related to the total metals content or age of the catalyst. At low (0.7 wt.%) or initial loadings of metals, a paramagnetic vanadyl (VO^{2+}) species involving sulfur was observed as the dominant form. This vanadium state did not correspond to the vanadyl present in the crude oil or on a vanadium-impregnated supports and did not increase with increased metal loading. The further accumulation of vanadium up to 10 wt.% resulted in the formation of diamagnetic vanadium existing in a number of chemically or physically different environments. Silbernagel (1979) suggested that this form may correspond to a monolayer of deposited metal in a sulfide or oxide phase. At still higher loadings above 10 wt.% V, the metal appears to be deposited as growing sulfide crystals with a stoichiometry close to that of V_2S_3 platelets.

Fleisch *et al.* (1984) employed x-ray photoelectron spectroscopy (XPS) on spent residuum HDS catalyst and also found the V_2S_3 sulfide phase. In addition, the XPS technique enabled the identification of Ni forms. Only sulfides in either the Ni_3S_2 or Ni_2S forms were observed. Nickel metal and NiS were not detected.

Takeuchi *et al.* (1985) have examined the HDS catalyst deposits in detail with XPS, ESR, x-ray diffraction, and electron microscopy. X-ray diffraction revealed the presence of the crystalline V_3S_4 phase, a nonstoichiometric, polycrystalline solid with sulfur-to-vanadium ratios of 1.2 to 1.5. This polycrystalline material was observed by microscopy as 10- μm -long, rod-shaped crystals on the outer surface of the catalyst and about 0.1 μm in length within the catalyst pores. The x-ray diffraction technique will not reveal any amorphous phases present. Electron spin resonance spectra revealed the presence of a vanadyl on the surface that was coordinated with 4S and distinctly different from the 4N coordination of the crude oil

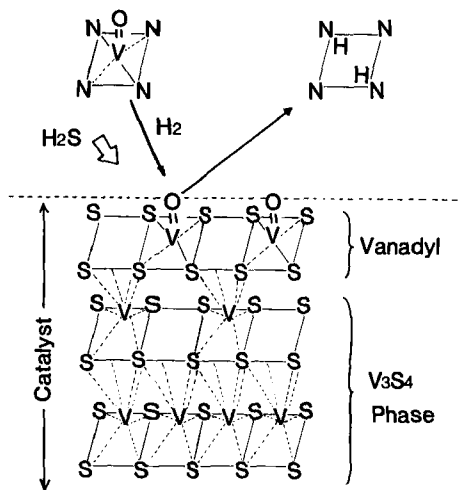


FIG. 41. Proposed reaction mechanism and model of a vanadium sulfide surface site for hydrodemetallation (Takeuchi *et al.*, 1985).

vanadyl. To account for the directionally oriented growth of the V_3S_4 phase, a reaction mechanism including a model of the active surface site was proposed and is shown in Fig. 41. A porphyrin-type molecule releases its vanadyl to the sulfur on the vanadium sulfide surface. The vanadyl is then deoxygenated with H_2S and forms a new sulfide surface to continue the growth process.

The presence of V_3S_4 crystals can only be attributed either to an autocatalytic mechanism of this type or the migration of the deposited metals. It is known that deposited Ni and V sulfides possess some catalytic activity (see Section IV). Slurry processes have been proposed which utilize Ni and V deposited from the oil onto a slurry material (Bearden and Aldridge, 1981). Studies have appeared in the literature demonstrating that nearly all of the transition metals are catalytically active for HDS reactions and presumably for HDM (Harris and Chianelli, 1984). Rankel and Rollmann (1983) impregnated an alumina catalyst base with Ni and V and concluded that these sulfides display an order of magnitude lower activity than the standard Co–Mo sulfide catalyst for HDS reactions, but exhibited similar activity for HDM reactions.

Takeuchi *et al.* (1985) tested the catalytic activity of deposited Ni and V by use of a catalytic metal-free alumina base. These interesting results are shown in Fig. 42. After accumulation of 10 wt.% vanadium on the catalyst, the alumina base, with little initial activity, has essentially the same activity for HDM and asphaltene cracking as the catalytic metal-

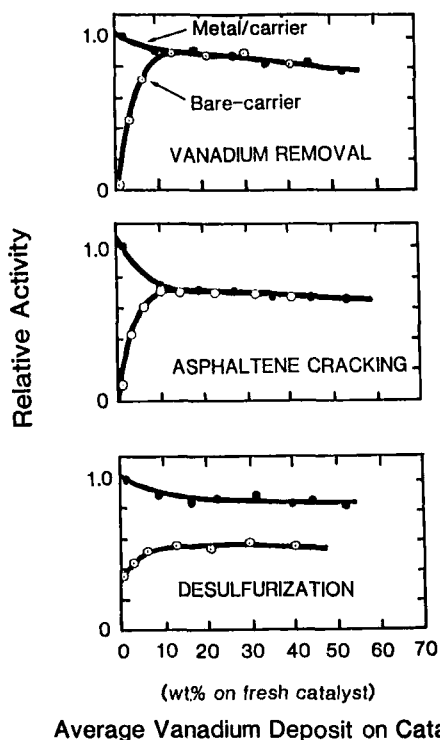


FIG. 42. Catalyst activity after vanadium deposition (Takeuchi *et al.*, 1985).

bearing catalyst. The activity for HDS, however, was appreciably lower for the alumina base with deposited vanadium than for the catalyst. Sie (1980) has also shown that the deposited metals can catalyze HDM.

In addition to metal sulfide deposits, the catalyst may accumulate up to 20 wt.% coke during the initial period, corresponding to several monolayers (Beuther *et al.*, 1980). The working catalyst surface would then contain several deposited layers of metal sulfides (Tamm *et al.*, 1981) and coke, as well as the original Co-Mo catalyst metals, at an early stage of the run. To what extent do these contaminants cover or interact with the catalytic metals and affect their activity? How these various components coexist on a working catalyst surface is not known precisely. Some physical evidence and suggestive data, however, reveal some of the important features. The microscopic examinations of Takeuchi *et al.* (1985) have shown that Ni and V sulfide deposits coagulate into bulk phases rather than as successive monolayers. Although well dispersed, coke deposits also apparently from discrete structures, as seen under similar microscopic

examination, with the majority of the alumina surface remaining exposed (Sanders *et al.*, 1983). This, however, does not preclude the possibility that coverage of catalytic metals has occurred.

Migration of catalytic metals or phases may occur in catalysis (Delmon and Grange, 1980). Fleisch *et al.* (1984), using the ESCA surface analysis method, found changes in the detected Mo/Al atomic ratio. These investigators speculated that Mo may migrate to the top of contaminant layers and remain exposed to reactants. Ramaswamy *et al.* (1985) observed structural changes of the alumina support as well as loss of active metals in aged Co-Mo-Al₂O₃ hydrodesulfurization catalysts that had undergone numerous oxidative regenerations.

One hypothetical model for the deposition is the purely random Poisson process (Wei, 1984) where any surface is equally likely to be the next deposition site, regardless of whether it is bare alumina or covered by previous depositions. For such a model, the probability of a surface covered with n number of deposits would be

$$P_n(m) = m^n e^{-m} / n! \quad (17)$$

where m is the average number of deposits on a surface site (Feller, 1957). Thus, the probability of a bare site is

$$P_0(m) = e^{-m} \quad (18)$$

and the probability of a site with a single deposit is

$$P_1(m) = m e^{-m} \quad (19)$$

If the catalyst activity is directly related to the probability of bare catalyst surfaces, then the activity after a single monolayer's worth of deposition would decline to 36.8% of its original value and to 13.5% of its original value after two monolayer's worth of deposition. This would agree very well with the observation of rapid temperature changes during the first period of catalyst aging (see Fig. 40) and an approximately linear temperature increase with time during the second period of aging to maintain conversion level. For the Poisson process,

$$k = b e^{-Q/RT} = b_0 e^{-m_e - Q/RT} = \text{const} \quad (20)$$

or

$$T = \frac{Q/R}{\ln(b_0/k) - m} \quad (21)$$

where m is roughly linear with time in constant conversion (HDS or HDM) operation.

We give here a timetable for the relation between $P_n(m)$, the probability that a surface has precisely n deposits upon it, and m , the average number of deposits on the entire surface.

P_n	m				
	0	1	2	3	4
0	1	0.368	0.135	0.050	0.018
1	0	0.368	0.271	0.149	0.073
2	0	0.184	0.271	0.224	0.146
3	0	0.061	0.180	0.224	0.195
4	0	0.015	0.090	0.168	0.195
5	0	0.003	0.036	0.101	0.156

It is seen that after the average coverage reaches two monolayers, the surface resembles the Grand Canyon, with a large number of hills of various heights, but very little of the original surface exposed. Smith and Wei (1985) used this approach to model the loss of catalyst activity in the HDM of a nickel porphyrin. With the assumption that the deposited Ni exhibits some activity, agreement between experiment and the Poisson model is very good, as shown in Fig. 43. We do not know how realistic this Poisson model is, since we do not know whether the next deposit is more likely to fall on a clean surface or on a pile. An equal deposition probability would imply that the final step is not surface specific, even though the overall rate is controlled by the amount of bare molybdenum left. The data of Webster (1984) and Fleisch *et al.* (1984) indicated that even at very high values of m , bare alumina and molybdenum signals can still be detected. Furthermore, metal profiles within the catalyst are not, under most conditions, uniform because of diffusion limitations, as discussed in Section IV. Thus, the extent of coverage of the original surface may be spatially dependent within the catalyst pellet. A more complicated model formulation would be required in this case to simulate the effect of deposition layers on catalyst activity.

Kinetic data also suggest that, despite the massive buildup of deposits, some of the catalytic sites maintain some degree of integrity. The data of Takeuchi *et al.* (1985) in Fig. 42 suggest that much of the CoMo remains exposed in order for the catalyst to exhibit HDS activity above that of the deposited metal sulfides. The working catalyst's specific activity probably results from the contributions of both that portion of the high-activity CoMo phases that remain uncovered and the lower activity Ni and V sulfides which coat the catalyst surface. Furthermore, coke deposits cannot

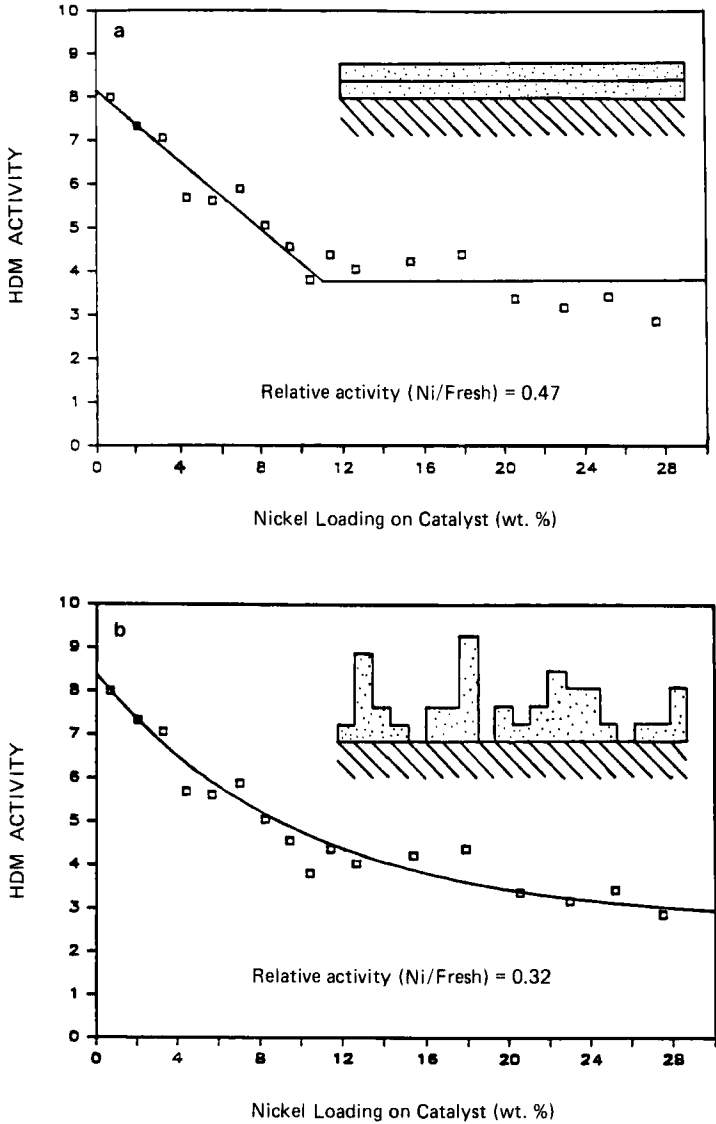


FIG. 43. Comparison of (a) monolayer and (b) Poisson deposition models of surface site deactivation with experimental aging data (Smith and Wei, 1985).

completely cover the active sites or there would be little activity remaining after a short period of contact with resid.

Obviously, the structure of a catalyst surface in any reaction system is important since it defines the catalyst itself. In residuum processing the pore structure is as critical. As shown in the following section, the pore structure influences the diffusion characteristics of metal-bearing molecules and thus the spatial distribution of metal deposits in catalyst pellets. The spatial distribution in turn affects the activity of the catalyst and the useful life of the reactor bed.

2. Deposit Obstruction of Catalyst Pores

As a heterogeneous catalytic reaction, HDM is unique and of interest from a theoretical standpoint in that it leaves an identifiable deposit in, more or less, the exact location where the catalytic reactions have occurred. Thus the spatial distribution of metal deposits in individual catalyst pellets and in the reactor bed is a reflection of the mechanism and kinetics of the HDM reaction and the impact that pore diffusion resistance has on this reaction. As discussed in Section IV, early investigations using electron microprobe analysis of pellet cross sections from aged catalyst revealed the characteristic spatial inhomogeneity of Ni and V sulfide deposits (Inoguchi *et al.*, 1971; Sato *et al.*, 1971; Scott and Bridge, 1971; Todo *et al.*, 1971). The deposits tended to concentrate in the pores near the external surface of the pellets, indicating that reactions were taking place before the metal-bearing compounds could diffuse deeper into the interior of the catalyst pellets.

During the course of operation, HDS or HDM catalysts processing residua may accumulate Ni and V deposits that reach up to 100% and higher of the initial catalyst weight. Obviously, such massive loadings must have a serious effect on the pore structure of the catalyst and the ability of large residuum molecules to diffuse freely through the pores. This phenomenon eventually leads to a sealing or plugging of the outer pores, resulting in complete deactivation with much of the catalyst still active but lost to inaccessibility.

The location of a metal sulfide deposit in a catalyst pellet is dependent on the relative rates of reaction and diffusion. The theory describing diffusion and reaction in catalysts was first developed by Thiele (1939) and extended by many others, including Wheeler (1955), Weisz (1962) and Satterfield (1970), and has been discussed in Section IV. Sato *et al.* (1971) and Tamm *et al.* (1981) have discussed metal deposit profiles in the context of the Thiele analysis.

An example of the distribution of Ni and V profiles in a HDS catalyst extrudate after an initial period of operation was shown in Fig. 38. The

steep profiles are typical of unimodal, microporous (average pore diameter usually in the range 40–100 Å) HDS catalysts processing residuum. Iron sulfide deposits are usually located outside the catalyst as a scale or as interstitial bulk matter with coke in the void space of the reactor bed. The source of the iron is probably reactive naphthenates, unique to certain crudes, or equipment corrosion. The buildup of external iron sulfide deposits does not contribute to catalyst deactivation inasmuch as it causes pressure drop problems in the reactor bed (Bridge, 1982). Nickel tends to penetrate the catalyst interior farther than vanadium since nickel has a higher effectiveness factor due to its higher diffusivity (smaller molecular size) or lower reactivity. The internal maxima or M-shaped profiles also observed by Hardin *et al.* (1978) and Oxenreiter *et al.* (1972) are a consequence of the sequential reaction path for HDM.

As discussed in Section IV, the metals distribution can be quantified with a distribution parameter θ_m (Tamm *et al.*, 1981) given by

$$\theta_m = \frac{\int_0^1 M(r)r \, dr}{M_{\max} \int_0^1 r \, dr} \quad (22)$$

where $M(r)$ is the concentration of metal as a function of normalized radial position r in a cylindrical catalyst and M_{\max} is the concentration at the maximum point. The distribution parameter is simply the ratio of the average concentration in the pellet to the maximum concentration, providing a convenient method of gauging the degree of catalyst utilization when it is spent and replaced. A high distribution parameter, like the effectiveness factor, implies that metal-bearing compounds penetrate deeper into the catalyst pore system before reacting. A more uniform deposit in this case reduces local deposit buildup, but coverage of catalytic sites for HDS

TABLE XXVIII
CHANGES OF SURFACE AREA AND PORE VOLUME THROUGH REACTOR BED^a

Bed section	Surface area (m ² /g)	Relative surface area	Relative pore volume
Fresh	188	100	100
4	64	34.0	17.9
5	70	37.2	23.8
6 ("top")	79	42.0	28.6
9 ("mild")	93	49.5	34.5
10	104	55.3	42.9
11	131	69.7	44.0
13 ("bot")	133	70.7	45.2
14	130	69.1	41.7

^a From Fleisch *et al.* (1984).

reactions extends farther into the catalyst. Conversely, a low distribution factor implies that reaction with metal deposition is occurring predominantly in the outer pores, a situation which leads to rapid plugging of the pore mouths, but leaving the deeper internal pores and catalytic sites less affected. When the maximum in the profile occurs at the edge of the particle, the catalyst effectiveness factor is equivalent to the distribution parameter for the HDM reaction.

Fleisch *et al.* (1984) measured the catalyst surface area and pore volume changes that occurred after severe deactivation of a 100- to 150-Å pore catalyst. The results of these measurements are shown in Table XXVIII for various positions in the reactor bed. Catalyst surface area and pore volume are substantially reduced in the top of the bed due to the concentrated buildup of metals in this region. The pore volume distribution of Fig. 44 reveals the selective loss of the larger pores and an actual increase in smaller (<50-Å) pores due to the buildup of deposits and constriction of the larger pores. Fleisch *et al.* (1984) also observed an increase in the hysteresis loop of the nitrogen adsorption-desorption isotherms between fresh and spent catalysts, which reflects the constrictions caused by pore

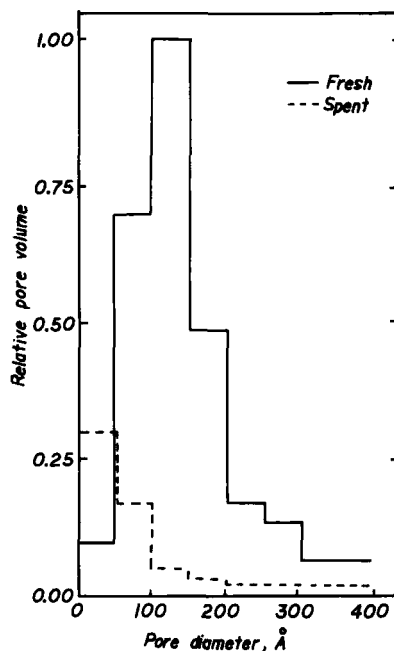


FIG. 44. Pore volume distribution of fresh and spent catalyst after processing residuum (Fleisch *et al.*, 1984).

mouth plugging. Inoguchi *et al.* (1971) observed substantial decreases (by 40%) in surface area and pore volume after a long-duration activity test. However, only slight decreases in the mean pore diameter were observed.

Any process variable which increases the HDM reaction rate will decrease the effectiveness factor and hence the distribution parameter. Effects of hydrogen partial pressure and reaction temperature on the deposited metal profiles were obtained by Tamm *et al.* (1981) and are shown in Figs. 45 and 46. Consistent with the HDM reaction mechanism, both higher temperature and hydrogen enhance the reaction rate (see Section IV) and, therefore, decrease the distribution parameter.

Feed source may also have a substantial effect on the distribution parameter (Tamm *et al.*, 1981). Given the complexity of crude oil with reference to residuum properties, it is not surprising that differences in metal distribution parameters are observed. This finding suggests that optimal catalyst properties may vary with the residuum source. Galliasso *et al.* (1985) have compared the HDM kinetics of porphyrins and non-porphyrin compounds in both resins and asphaltenes. The individual

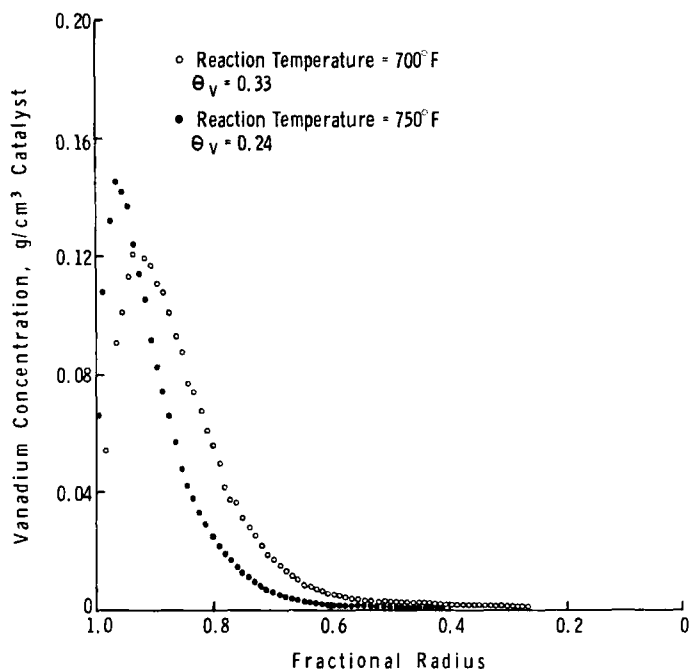


FIG. 45. Effect of hydrogen partial pressure on vanadium deposition for an Arabian Heavy atmospheric residuum at a reaction temperature of 371°C (700°F) using a $\frac{1}{16}$ -in. extrudate catalyst (Tamm *et al.*, 1981).

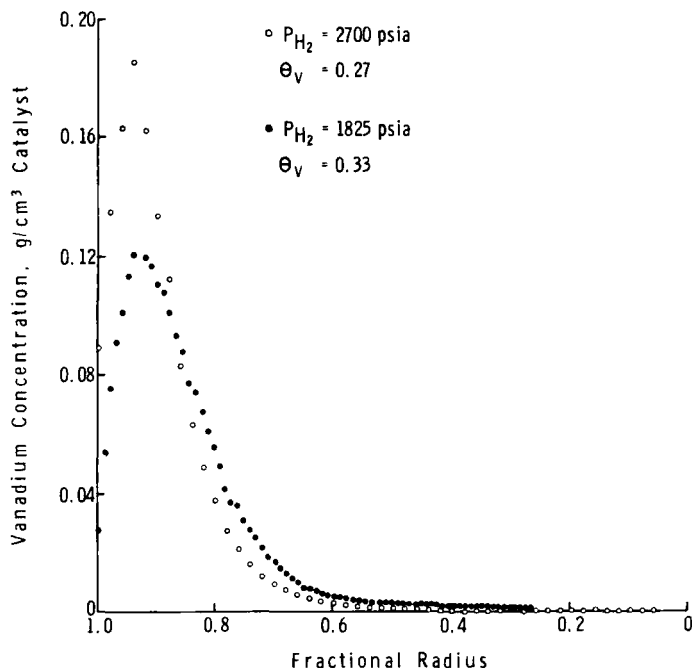


FIG. 46. Effect of reaction temperature on vanadium deposition for an Arabian Heavy atmospheric residuum using a $\frac{1}{16}$ -in. extrudate catalyst at a hydrogen partial pressure of 12.59 MPa (1825 psia) (Tamm *et al.*, 1981).

groups followed first-order kinetics. Vanadium and nickel from the resins deposited uniformly in the catalyst, while those of the asphaltene deposited in the outer regions of the catalyst.

Coke deposition may also affect the stability of residuum-processing catalysts. Galiasso *et al.* (1980) sampled and analyzed catalyst properties at successive stages of deactivation over a 6-month period in a fixed-bed pilot plant run with a heavy oil containing 338 ppm V. The catalyst deactivated in the characteristic manner, similar to that shown in Fig. 40. After a 10 day initial deactivation period, the bimodal catalyst accumulated 18 wt. % coke but only 1.2 wt % V. During this period the catalyst's surface area decreased from a fresh value of 170 m²/g to only 80 m²/g. Clearly, coke deposits had the major effect on the condition of the pores. Nearly all of the 60% loss in pore volume was in the micropore range (<100 Å). Despite these major changes, HDM activity only decreased by 10%, which suggests that the small pore microstructure does not contribute significantly to the HDM rate in this catalyst. After 5 months on stream and just before the final period of accelerated deactivation, the surface area

had declined to $30 \text{ m}^2/\text{g}$ and the pore volume was only 30% of its initial value. Catalyst activity declined slowly during this period to 70% of its initial HDM value. Coke deposition apparently does not increase deactivation during this period. After the final period of accelerated deactivation, the catalyst accumulated still more vanadium. The pore mouths, however, were nearly plugged. In separate absorption experiments, asphaltene uptake by the same catalyst was measured. After the first initial period of coke deactivation, the catalyst had nearly 95% of the capacity of the fresh catalyst for adsorbing asphaltenes in this test. The deactivated catalyst had less than 10% of its original capacity for adsorbing asphaltenes.

Prasher *et al.* (1978) observed a substantial loss in the intraparticle diffusion characteristics of an alumina-based catalyst in hydrocracking a residuum after several days on stream. By using selected compounds for the measurements, reductions in diffusivities were observed in comparison to the fresh catalyst, even though pore sizes did not change significantly. These investigators speculated that this was due to changes in the tortuosity from the blocking of pore interconnections or to increased constriction. The short exposure time in this case suggests that coke buildup is primarily responsible for the changes in catalyst properties.

Since HDM is a diffusion-limited reaction in most cases, catalyst properties—including pore structure and pellet shape and size—can be tailored to influence the effectiveness factor, the activity for both HDM and HDS, and the stability. Catalysts designed for maximum desulfurization activity usually have a sharp unimodal pore size distribution with median pore diameters on the order of 50 \AA and a large surface area. Because activity is high but diffusion is relatively slow, these catalysts are susceptible to rapid poisoning from the plugging of the pore mouths. High-activity HDS catalysts will only have satisfactory stability if the feedstock has less than about 100 ppm metals. Increasing the pore size with a corresponding decrease in surface area will increase the tolerance for high-metal feedstocks, but with a sacrifice in activity for HDS. Large-pore catalysts with a unimodal pore size distribution and a lower surface area are selective for HDM. Pore plugging will occur less rapidly with large pores due to the higher effectiveness factor. Catalysts of this type generally do not have sufficient activity for the HDS reactions but find service in a guard bed, demetallizing high-metal feedstocks upstream of the more active but less stable HDS catalyst. This will be discussed in more detail in Section V,B.

Bimodal catalysts were designed as a compromise between the important features of both HDS and HDM catalysts. The bimodal catalyst has micropores ($<50 \text{ \AA}$) and mesopores in the 50- to $100\text{-}\text{\AA}$ pore diameter range which provide the high surface area and large macropores

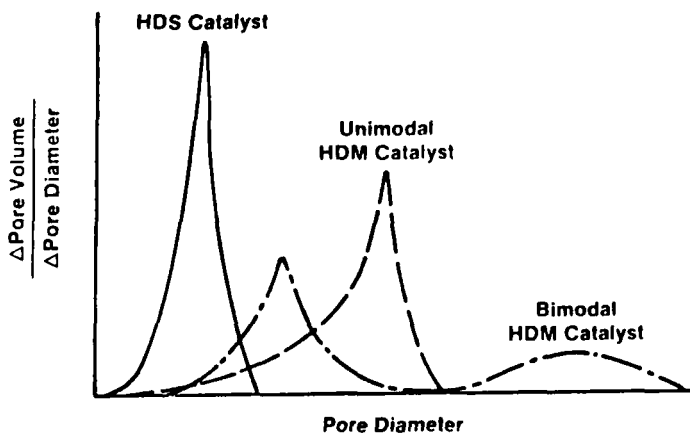


FIG. 47. Pore size distribution characteristics of typical residuum hydroprocessing catalysts (Howell *et al.*, 1985).

(>1000 Å) for access of large molecules to the catalyst interior. The bimodal catalysts have high effectiveness factors because of the macropores and high activity because of the high surface area micropore-mesopore structure. The geometry of the pore arrangement, that is interconnectivity in amorphous catalyst, is generally not known. Bimodal catalyst can be constructed as an agglomeration of microparticles. The mesopores or micropores are contained within the microparticles. The macropores are formed by the void spaces between the compacted microparticles. A comparison of pore size distribution for these types of catalyst is shown in Fig. 47. The effect that the pore structure can have on the distribution of deposited vanadium is shown in Fig. 48 for a microporous catalyst, a macroporous catalyst, and a bimodal catalyst. The difference in the distributions between the microporous and bimodal catalyst is significant even though micropore diameters and surface areas (SA) are comparable.

In addition to catalyst pore structure, catalytic metals content can also influence the distribution of deposited metals. Vanadium radial profile comparisons of aged catalysts demonstrated that a high concentration of Co + Mo increases the reaction rate relative to diffusion, lowering the effectiveness factor and the distribution parameter (Pazos *et al.*, 1983). While minimizing the content of Co and Mo on the catalyst is effective for increasing the effectiveness factor for HDM, it may also reduce the reaction rate for the HDS reactions. Lower space velocity or larger reactors would then be needed to attain the same desulfurization severity.

Catalyst particle size also influences the deposition pattern as a consequence of the characteristic diffusion length parameter in the Thiele

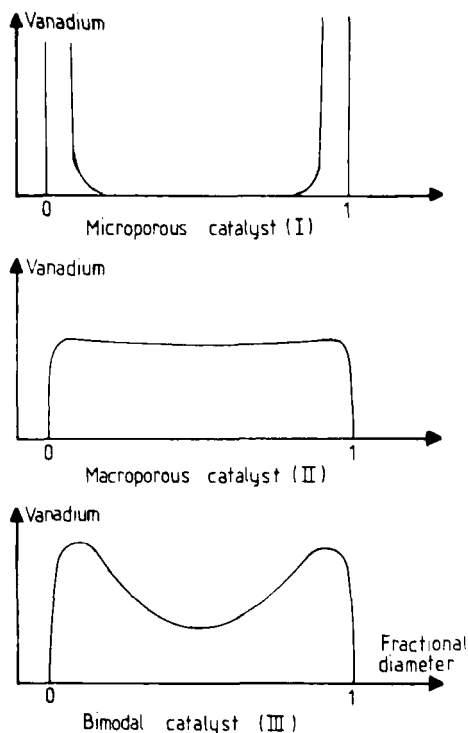


FIG. 48. Experimental vanadium deposit distributions in a microporous catalyst (100 Å micropore diameter/204 m²/g SA); macroporous catalyst (1300 Å pore diameter/14.5 m²/g SA); and bimodal catalyst (120 Å micropore, 25,000 Å macropore diameters/200 m²/g SA) (Plumail *et al.*, 1983).

modulus. The deposit profiles of Tamm *et al.* (1981) in Fig. 49 show that penetration depth is independent of catalyst diameter, so that the pore volume of the smaller $\frac{1}{32}$ -in. catalyst is more effectively used. This is a direct consequence of the Thiele modulus. If a dimensionless variable normalized to the extrudate radius were used, the profiles would be significantly different. Smaller catalyst pellets are definitely an effective approach to increasing the metals capacity and life of catalysts. There is a limit, however, based on reactor hydrodynamics. Pressure drop down the reactor may become impractical if the catalyst size is smaller than $\frac{1}{32}$ -in. Bridge and Green (1979) have shown that the optimal pore diameter decreases with decreasing particle size as a consequence of the Thiele modulus.

Another approach to improving access to the catalyst interior and, therefore, the metal uptake capacity is to modify the catalyst shape, which can decrease the effective diffusion length without compromise on reactor

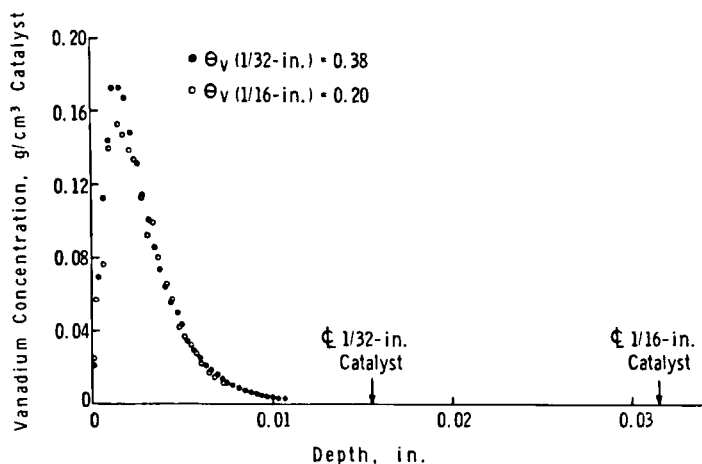


FIG. 49. Effect of catalyst particle size on vanadium deposition for an Arabian Heavy atmospheric residuum processed at 370° (700°F) under 12.59 MPa (1825 psia) of hydrogen (Tamm *et al.*, 1981).

pressure drop or the physical strength of the catalyst. This is a very active area of research with many imaginative proprietary shapes appearing in the patent literature. Novel catalyst shapes of the types shown in Fig. 50 offer potential for increasing catalyst tolerance for contaminants through greater access to internal surface without sacrifice of activity or reactor pressure drop limitations. Pereira *et al.* (1987) have recently reviewed the design philosophy for HDM catalyst with respect to the impact of catalyst pore size and shape on activity, stability, physical strength, and reactor pressure drop.

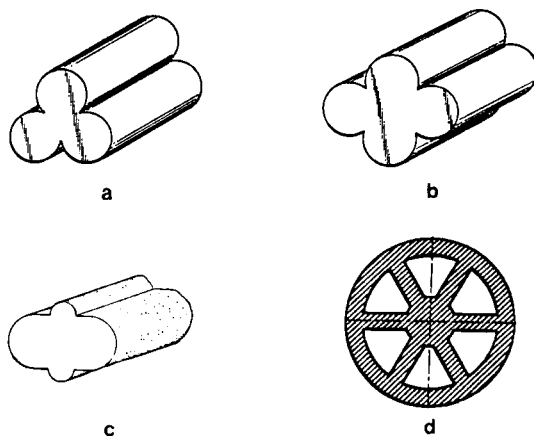


FIG. 50. Novel catalyst shapes for residuum processing. (a) UNOCAL's cloverleaf shape, (b) AKZO Chemie/Ketjen's asymmetric quadralobe, (c) Chevron's Bumpy Oval, (d) W. R. Grace's Minilith.

B. DYNAMICS OF REACTOR-BED DEACTIVATION

The manner in which Ni and V sulfide deposits accumulate on individual catalyst pellets depends on the kinetics of the HDM reactions as influenced by catalyst properties, feed characteristics, and operating conditions. The dynamic course of deactivation of catalytic reactor beds is also determined by the kinetics of the HDM reaction. The lifetime and activity of a reactor bed are directly related to the details of the metal deposit distribution within individual pellets. This section will review deactivation behavior of reactor beds in light of our understanding of the reaction and diffusion phenomena occurring in independent catalyst pellets. Unfortunately, this is an area of research which remains mostly proprietary with too little information published. What has been published is generally lacking in detail for the same reason.

The two leading theories concerning the cause of the first rapid deactivation period (up to 0.2 reduced time in Fig. 40) include coke deposition and monolayer coverage by deposited metal. Pazos *et al.* (1983) found a direct relationship between the coke content of the catalyst and catalyst activity during the initial deactivation period. At the end of this period, roughly 100 hours, both activity and coke level simultaneously stabilized. Sie (1980) observed similar phenomena but also reported that coke level was inversely related to hydrogen pressure. Beuther *et al.* (1980) found that the equilibrium coke level on the catalyst increases with average pore radius, as might be expected if the source of coke were large, hydrogen deficient molecules. In contrast, Inoguchi *et al.* (1971) observed that the coke level remained constant after 100 hours on stream but occupied primarily the micropore volume in the 50 Å range. This would affect the less diffusion-limited but more kinetically sensitive HDS reaction. However, HDS and HDM have concurrent initial deactivation periods. Kwan and Sato (1970) were able to correlate catalyst HDS activities with coke content after the first 50 hours on stream. There obviously remains some controversy regarding the role of coke in the overall deactivation. In any case, the useful lifetime of a catalytic bed apparently does not correlate with the amount of coke on the catalyst support (Hannerup and Jacobsen, 1983; Jacobsen *et al.*, 1983).

Tamm *et al.* (1981) have suggested that metals are primarily responsible for the initial deactivation. They report that the length of the initial deactivation period is directly related to the concentration of metals in the feedstock and the total run length or catalyst lifetime. Tamm *et al.* (1981) also observed that the initial deactivation period responds to process variables that influence the metal deposition pattern in catalysts. Lower hydrogen pressure and smaller catalyst size result in a greater loss of initial

activity owing to the more even distribution of deposits through the catalyst volume with greater contamination of the active surface. However, hydrogen pressure also influences the equilibrium level of coke on the catalyst. Furthermore, the precursors of coke, in some instances, may exhibit diffusion-limited behavior, possibly because they are associated with the asphaltenes or metal compounds in the oil. Nielsen *et al.* (1981) and Tamm *et al.* (1981) observed carbon deposition profiles with maximums in the outer region of the pellet. Undoubtedly, both metals and coke contribute to the initial deactivation period in a complex manner.

The second period of slow linear deactivation is brought about by the continual buildup of metal sulfide deposits within the catalyst pores, concentrating in the outer region of the catalyst and increasing the diffusion resistance of molecules. The length of this second deactivation stage is determined by those variables which influence the Thiele modulus, including catalyst intrinsic activity, pore structure, metal compound size (diffusivity) and reactivity, process temperature, and hydrogen pressure. With a more even distribution of metal deposit in the catalyst, the lower the maximum concentration will be after a given time on stream and the longer this intermediate stage of deactivation will last.

The final period of deactivation begins with the complete obstruction of the pores. This phenomenon occurs in a wave form, starting at the reactor inlet, where deposit concentrations are at a maximum, and traveling through the reactor as each successive bed increment become deactivated. The pore-plugging wave accelerates because reactor temperature must be raised rapidly to maintain desired conversions. Increasing concentrations of metals pass through the upper deactivated layers and reach the lower portion of the reactor bed. The onset of a pore-plugging wave will occur sooner with a low distribution parameter. With a high distribution parameter, however, the pore-plugging wave, once started, will traverse the reactor at a higher rate. Figure 51 illustrates the effect of the Thiele modulus on the shape of the deactivation curve. The smaller catalyst—with a lower Thiele modulus, a higher effectiveness factor, and a higher distribution parameter (Fig. 49)—has a longer intermediate deactivation period because of its greater capacity for metals, but a more rapid final pore-plugging phase. The larger catalyst with a less effective distribution within the catalyst pellets has a very short intermediate deactivation period, but a relatively long pore-plugging phase. Nielsen *et al.* (1981) observed similar effects with catalyst size and higher pressure, as shown in Fig. 52. Lower hydrogen pressure improves the metals distribution parameter (Tamm *et al.*, 1981), but not necessarily the catalyst life in this case. For the large-pore catalyst (A), lower hydrogen pressure resulted in such severe coke deactivation that an equilibrium coke level could not be

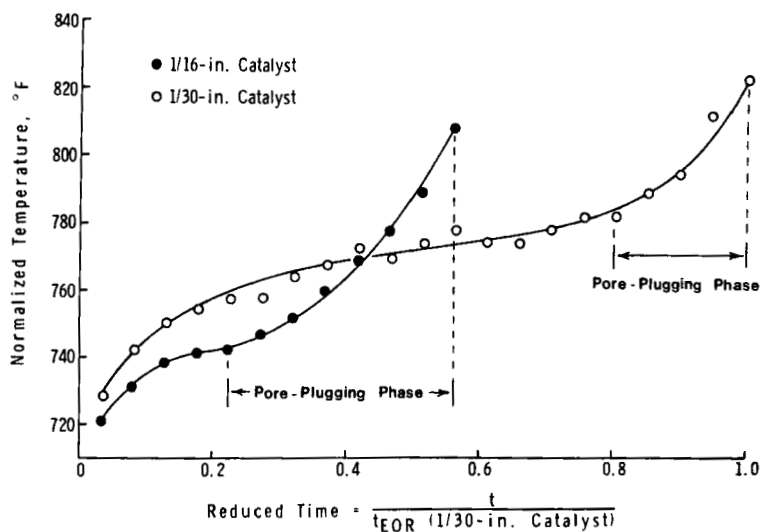


FIG. 51. Effect of catalyst pellet size on deactivation behavior for an Iranian Heavy atmospheric residuum desulfurized to 0.5 wt. % product sulfur (Tamm *et al.*, 1981).

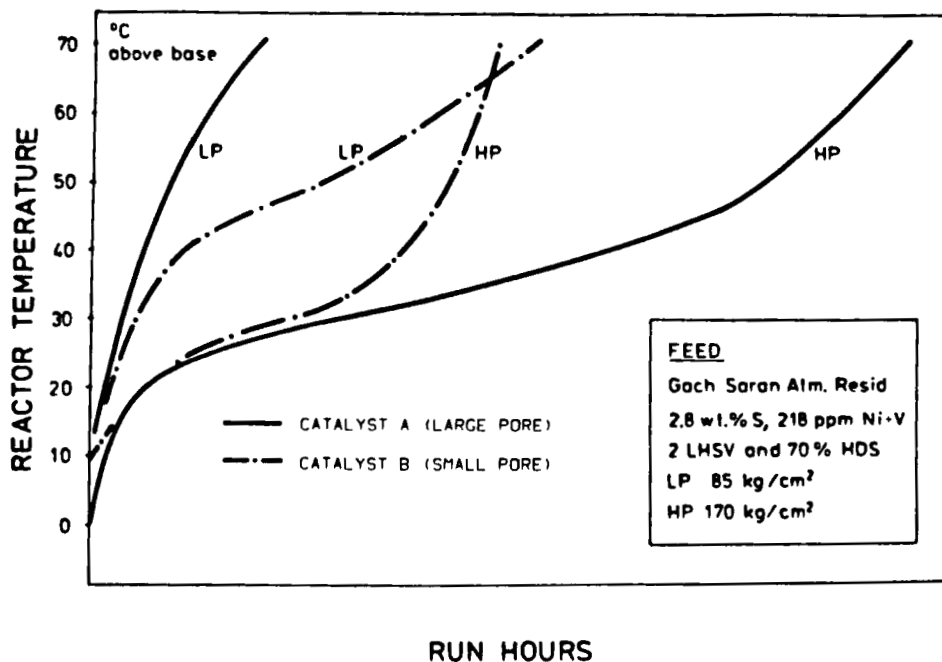


FIG. 52. Pore size and hydrogen partial pressure effects on residuum catalyst stability (Nielsen *et al.*, 1981).

established with the increasing temperatures required to maintain constant HDS. Tamm *et al.* (1981) also considered the effect of hydrogen pressure. Higher hydrogen pressure shortened the intermediate deactivation period but lengthened the pore-plugging phase.

The spatial distribution of deposited Ni and V in the reactor bed is determined by the activity of the catalyst and phenomenologically parallels that for profiles in individual pellets. Metals will tend to deposit near the reactor inlet with a highly active catalyst. A more even distribution or one skewed toward the reactor outlet is obtained for catalyst with less activity, as shown by Pazos *et al.* (1983). Generally with a typical small-pore (60-Å), high-surface-area desulfurization catalyst, metals will concentrate near the inlet (Sato *et al.*, 1971; Tamm *et al.*, 1981). Fleisch *et al.* (1984) observed concentration maximums a short distance into the catalyst bed, as a probable consequence of the consecutive reaction path.

Residuum properties may also influence the distribution of deposits in reactor beds owing to reactivity differences of different organometallic compounds. A Boscan crude reportedly (Pazos *et al.*, 1983) has a steeper reactor deposit profile than Bachaquero, possible as a consequence of its higher metal porphyrin content (Dean and Whitehead, 1963). Silbernagel and Riley (1980) examined the distribution of deposited V and Ni in a reactor bed processing a deasphalted oil fraction containing only vanadyl porphyrins and an HF-treated crude containing vanadium but not in the porphyrin form. The more reactive porphyrins were found to deposit more at the reactor inlet region compared to nonporphyrinic compounds.

The concentration of metals in the feedstock can also have a major impact on catalyst life. Figure 53 compares the relative catalyst lifetimes for a typical HDS catalyst processing the high-metals Maya residuum and an Arabian Heavy residuum. As is evident, a higher concentration of metals in the feedstock increases the rate of deactivation of both the intermediate period and the final pore-plugging phase. New catalyst systems are required to handle heavy feeds that have metal concentrations of this magnitude.

Tamm *et al.* (1981) measured the maximum concentration of vanadium buildup in the catalyst at various reactor positions and times on stream. Near the reactor inlet, maximum vanadium concentrations increased rapidly with time before leveling off. The catalyst in this portion of the bed has apparently reached its capacity and lost nearly all activity for HDM at about 80% of the run length. The catalysts in the reactors midsection and at the outlet have lower maximum concentrations, which increase more slowly with time. The lower zones of the catalyst bed are protected somewhat from metals deposition by the catalyst in the inlet region. This phenomenon continues until the catalyst bed does not have enough activity

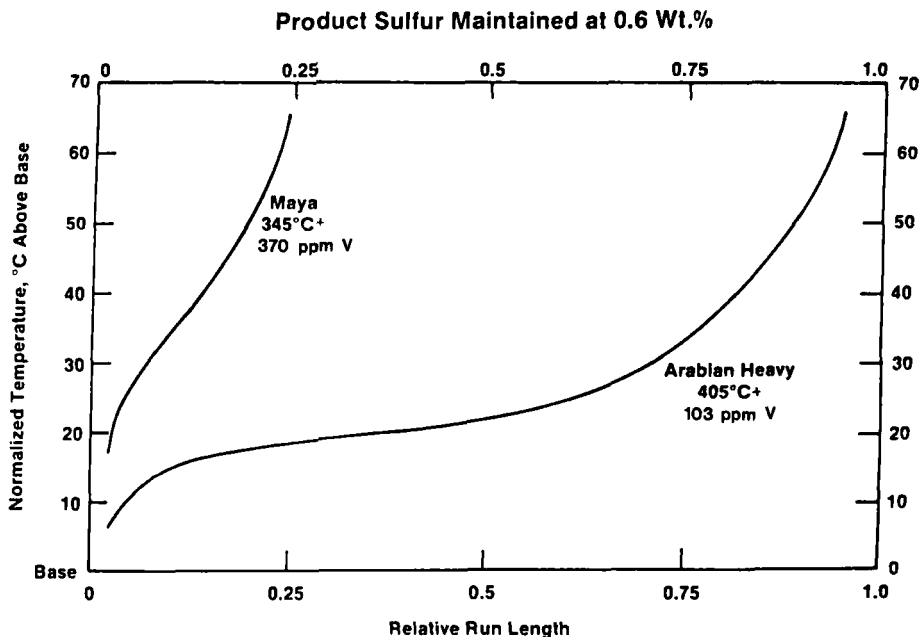


FIG. 53. Comparison of residuum processing catalyst stability for high-(Maya) and low-(Arabian Heavy) metal-content feeds (Howell *et al.*, 1985).

to sustain the desired conversions. The relative HDS activity of the catalyst at different bed positions was tested. The inlet had only one-tenth the activity of the reactor outlet for HDS as expected from a pore-plugging wave phenomenon. Ozaki *et al.* (1975) observed a similar activity profile from deactivation in a commercial unit based on the exotherms across individual reactor sections. Coke concentration on the catalyst is also generally observed to increase from inlet to outlet (Fleisch *et al.*, 1984; Sato *et al.*, 1971). This is often explained in terms of the reactor temperature profile. An increase in the temperature, causing an increase in the equilibrium coke level on the catalyst from inlet to outlet, results from the exothermicity of the reactions.

The severity of the conditions can also influence the catalyst deactivation rate. Higher severity or deeper desulfurization can be obtained by operation at higher temperatures for more catalyst activity. As shown in Fig. 54, however, this higher activity is at the expense of useful catalyst life. At higher temperature the metals distribution parameter is lower and coke formation is more rapid because of increased catalyst activity.

The conflicting requirements of high activity for HDS and high capacity for metals accumulation for long life suggest that an optimum in catalyst

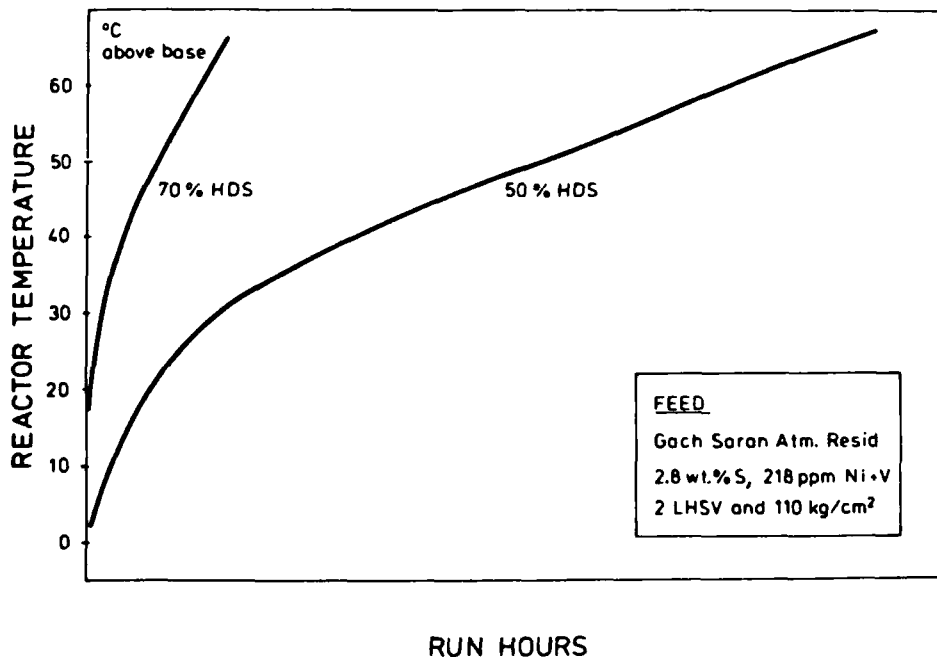


FIG. 54. Effect of operating at higher temperature for higher process severity and conversion on catalyst stability (Nielsen *et al.*, 1981).

properties and/or operating conditions exists. A large-pore catalyst or low hydrogen pressure enhances the metals capacity by increasing the distribution parameter. The activity in this case maybe too low for the required degree of HDS with the result that the end-of-run temperature is reached before the catalyst has reached its potential metals capacity. Conversely, a small-pore and high-activity catalyst has sufficient activity to reach a stable equilibrium coke level, but the earlier onset of pore plugging due to a low distribution parameter limits catalyst life. For feedstocks that contain less than 200 ppm metals, satisfactory performance or catalyst life is obtained by optimization of catalyst properties, including pore size distribution, catalytic metals content, pellet size, and pellet shape (Howell *et al.*, 1985). For more difficult feedstocks, composite catalyst beds or graded catalyst systems using more than one type of catalyst have been developed (Fischer and Milstein, 1977).

Graded catalyst systems employ two or more catalysts to combine both high metal capacity and high activity. A larger-pore catalyst, designed to maximize metals removal and to provide capacity for metals accumulation, is used in the first reactor bed. This, in effect, provides a metals removal

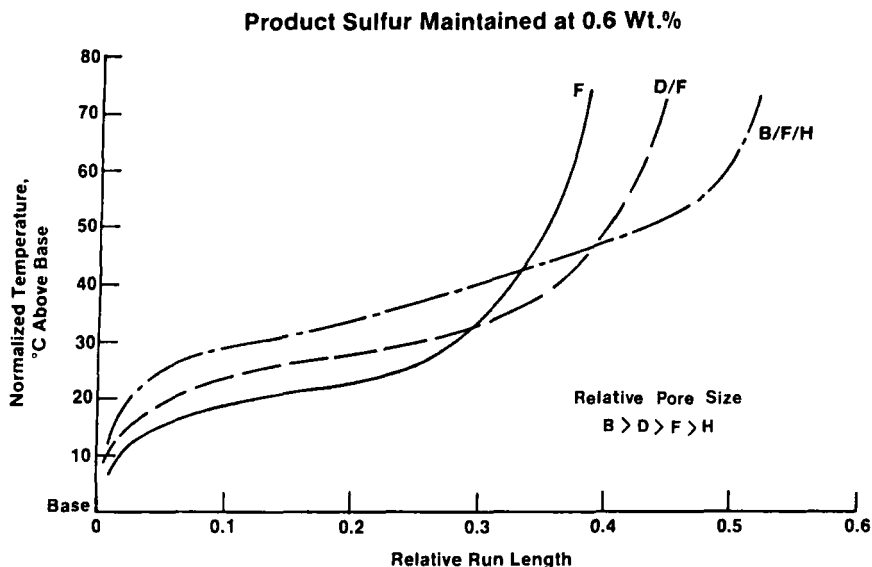


FIG. 55. Effect of graded catalysts systems on initial activity and extended run lengths (Howell *et al.*, 1985).

pretreatment step for more active small-pore, high-surface-area HDS catalyst(s) that follows in second and possibly third reactor beds. Fischer and Milstein (1977), Howell *et al.* (1985), and Nielsen *et al.* (1981) have demonstrated increased catalyst lifetimes with graded catalyst systems compared to single catalyst beds. Jacobsen and Hannerup (1983) demonstrated that a composite bed with a large-pore catalyst followed by a smaller-pore catalyst can nearly double the useful life of a reactor bed for HDS. Howell *et al.* (1985) reported an extension of catalyst life using a three-catalyst system (Fig. 55) with increasing specialization of catalyst function. Incorporation of lower-activity (larger-pore) but more tolerant catalyst in the first reactor bed results in a higher loss of initial activity for HDS but a longer run length for the bed because of greater metals capacity and HDM activity. This filtering effect protects the higher-HDS-activity but less tolerant catalyst in the subsequent beds.

C. MODELING OF CATALYST DEACTIVATION

The selection of a catalyst or the design of a new catalyst for a particular purpose will depend on activity, selectivity, and stability requirements. These requirements are generally related but not necessarily compatible in

the case of HDM. In many catalytic processes deactivation is brought about by some undesirable side reactions, coke formation being a common example. Improved stability may, therefore, be obtained by improved selectivity. For the HDM process, however, catalyst deactivation is a direct, stoichiometric consequence of the desired main reaction. Maximum catalyst activity for metals removal would not appear to be consistent with maximum catalyst stability. Catalysts designed for desulfurization also have high activity but not necessarily high stability.

Modeling of the HDM reaction and the catalyst deactivation that results from metal deposition can sort out the number of complicated factors that influence the performance of a catalyst and provide a better understanding of the process. It is the purpose of modeling to enable a rational approach to the design and use of catalysts based on activity, selectivity, and stability considerations. Although catalyst activity and selectivity are easily evaluated by screening tests, routine catalyst stability determinations are often too time-consuming to be practical for hydroprocessing applications. Modeling of the deactivation process provides a powerful tool for exploring the various catalyst design options. One notable example of this is a patent by Jaffe (1981) for predicting the optimum catalyst pore size distribution for HDM and HDS. The optimum catalyst for a specific crude oil is determined from the measured size distributions of S, Ni, and V molecules in the chargestock and the desired level of these impurities in the product.

In modeling the deactivation of catalysts by metal deposits, many aspects of the phenomenon must be considered. Reaction and diffusion in catalysts are influenced by the size and reactivity of large metal-bearing oil compounds, the pore structure of the catalyst, the intrinsic activity of the catalyst for HDM and HDS and the effects of metal deposits thereon, and the manner in which deposits obstruct pores. The modeling effort in this area has been relatively weak, however, especially with respect to theoretical studies having corroborating experimental data. Most experimental information has been obtained from fixed-bed reactors whose dynamics of deactivation under continual temperature adjustments can obscure the behavior of single pellets and complicate the mathematical analysis of single-pellet deactivation. Consequently, models that have been developed from catalyst life tests are more correlative. On the other hand, the more rigorous theoretical approaches to catalyst deactivation of single pellets lack supporting experimental studies. Nevertheless, the theoretical approaches provide useful insights into the deactivation process and the design criteria for new catalyst formulations.

Modeling of reaction and diffusion in heterogeneous catalysis begins with a definition of the structure or geometry of the internal porous media.

The mathematical description of the pore structure provides the basis not only for the conservation equations and their boundary conditions, but also for the approach taken in the treatment of catalyst deactivation by pore plugging. In the case of an amorphous heterogeneous catalyst, the complexities of the fine structure of porous media limit the accuracy with which mass transport phenomena can be modeled or even visualized. Experimental techniques that have the capability of revealing fine structural features such as dead-end pores and interconnectivity are not yet available. Some recent experimental and theoretical progress in the area of pore interconnectivity and narrow-neck distributions has been reported (Conner and Lane, 1984; Mann *et al.*, 1981; Mann and Golshan, 1981). Pore structural models of varying complexity and sophistication have been proposed and adopted for the simulation of reaction and diffusion in catalysts. These extend from simplistic parallel bundles of nonintersecting pores (Johnson and Stewart, 1965) to complex random networks of pores using statistical or stochastic models to describe the size distribution, orientation, and interconnectivity of pores (Broadbent and Hammersley, 1957; Pismen, 1974; Gonzalez and Galiasso, 1983; Reyes and Jensen, 1985). Local mass flux relationships are evaluated and integrated over the pore space to obtain effective diffusivity properties. Generally, the topological complexities of the pore structure are reduced to a single parameter such as the tortuosity factor. A detailed discussion of this active area of experimental and theoretical research is beyond the scope of this review. Reyes and Jensen (1985) have published a brief review of the state of this art.

Even if a complex mathematical description of the fine structure of pores were available, the use of such a model for the deactivation problem would encounter further difficulties. Detailed information on the nature of the deposit distribution in the fine structure would be required. This is currently beyond analytical capabilities.

In addition to the simplification of pore structure, assumptions are needed regarding the effects of contaminant metals on the intrinsic activity of the surface. For HDM it appears that the catalyst's intrinsic activity is not significantly affected (see Fig. 42). This is not the case for the HDS reaction, however. Most model formulations also neglect the effects of surface coke on activity since it does not have an impact on long-term stability unless conditions are too severe.

This review will only focus on the modeling efforts in pore diffusion and reaction in single-catalyst pellets which have incorporated pore plugging as a deactivation mechanism. A broad literature exists on the deactivation of catalysts by active site poisoning, and it has been reviewed by Froment and Bischoff (1979). The behavior of catalytic beds undergoing deactivation is

also an important aspect in the design and operation of processes. This area has been reviewed extensively by Kavarik and Butt (1982) and Hughes (1984).

Newson (1975) was among the first to develop a pore plugging model of demetallation to predict catalyst life. By using the pore structure model of Wheeler (1951), the pellet was assumed to have N pores of identical length but with a specified distribution of pore radii. Metal deposition was assumed to be a first-order reaction over an outer fraction of the pore length and to have a uniform thickness. This model showed that the broadness of the size distribution had little effect on the catalyst life for the same average radii, but that increasing the radii from 45 to 65 Å more than doubled the catalyst life. The restricted form of the diffusivity (see Section IV,B,5) was not employed in this model.

Hannerup and Jacobsen (1983) were able to correlate fixed-bed experimental data on the decay of a global second-order HDS reaction rate constant k_N as a function of metals uptake by using an empirically obtained expression of the form

$$k_N(t) = k_{N0}[1 - (\mu_v(t)/\mu_{v0})^2] \quad (23)$$

where μ_v and μ_{v0} are, respectively, the weight of metals accumulated on the catalyst at some time on stream and at the end of run, where constant HDS operation is not possible. The HDS rate constant k_{N0} is the start-of-run activity when the initial period of deactivation is neglected. The values of k_{N0} and μ_{v0} , determined experimentally, are influenced by catalyst properties and process conditions. The agreement with experimental data on the variation of activity with time was surprisingly good even though a mechanism or model for deactivation was not incorporated.

Dautzenberg *et al.* (1978) considered a pore mouth plugging model in which the local pore radius (initially uniform) changes with time according to

$$\partial r / \partial t = k \cdot C \cdot V_{\text{dep}} \quad (24)$$

where k , C , and V_{dep} are, respectively, the rate constants for vanadium removal, molar concentration of vanadium, and deposit volume per mole of vanadium. A variable ϕ defined as the relative catalyst age, equivalent to the fraction of the pore mouth blocked, was given by

$$\phi = 1 - \frac{r_0}{r_i} = \frac{kV_{\text{dep}}}{r_i} \int_0^t C_0 dt \quad (25)$$

with r_0 , r_i , and C_0 defined, respectively, as the pore mouth radius after some time on stream, the initial pore radius, and the concentration of vanadium outside the particle. When the single-pore balance for the

diffusion and first-order reaction of metal-bearing compounds were used, derived expressions for HDM and HDS activity in terms of the relative catalyst age correlated deactivation data over a wide range of temperatures, pressures, and space velocities and for two feedstocks. Although this model accounted for the changes in pore radius and the effect of this on the local reaction rate, it did not consider configurational diffusion effects (see Section IV,B,5) and the corresponding changes in diffusivity of metal-bearing molecules with pore diameter.

Kodama *et al.* (1980) developed a detailed HDS and HDM model for deactivation of pellets and reactor beds. The model included reversible kinetics for coke formation, which contributed to loss of porosity. Second-order kinetics were used to describe both HDM and HDS reaction rates, and diffusivities were adjusted on the basis of contaminant volume in the pores. The model accurately traced the history of a reactor undergoing deactivation. This model, however, contains many parameters and is thus more correlative than theoretical or discriminating.

Rajagopalan and Luss (1979) developed a theoretical model to predict the influence of pore properties on the demetallation activity and on the deactivation behavior. In this model the change in restricted diffusion with decreasing pore size was included. Catalysts with slab and spherical geometry composed of nonintersecting pores with uniform radius but variable pore lengths were assumed. The conservation equation for diffusion and first-order reaction in a single pore of radius r_p is

$$r_p^{-2} \frac{d}{dz} \left(r_p^2 D_p \frac{dC}{dz} \right) - \frac{2kC}{r_p} = 0 \quad (26)$$

where k is the rate constant, C is the concentration of metal-bearing compound, z is the distance into the pore, and the diffusivity D_p for restricted transport is given by (Spry and Sawyer, 1975)

$$D_p = D_\infty \left(1 - \frac{r_m}{r_p} \right)^4 \quad (27)$$

with D_∞ as the bulk diffusivity and r_m as the radius of the metal-bearing molecule. The metal was assumed to deposit in the pores at a rate determined by the local concentration of metal-bearing molecules:

$$dM(z)/dt = \delta 2\pi r_p k C M \quad (28)$$

The terms δ and M are, respectively, the number of metal sulfide molecules per organometallic compound and the molecular weight of the deposit. The rate of deposit formation is highest at the pore entrance where C is largest. The intrinsic activity of the surface was assumed to be unaffected

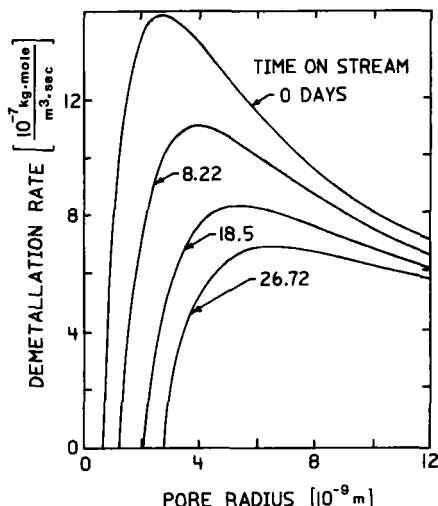


FIG. 56. Model computation for the demetallation rate as a function of pore size and time on stream for first-order kinetics and configurational diffusion of a 12.5-Å-diameter metal-bearing molecule (Rajagopalan and Luss, 1979).

by the deposit. Only surface area and pore radius change with time. This seems to be a valid assumption for HDM but would probably not apply to the more sensitive HDS reaction. The predicted effects of pore size and time on stream for this model are shown in Fig. 56 for a resid metal-bearing molecule of 12.5-Å diameter. Initial activity is very sensitive to pore radius due to the strong influence of restricted diffusion. Optimum activity occurs at a pore radius of roughly five times the diameter of the compound. This is in general agreement with the experimental observation reviewed in Section IV. It is also evident in Fig. 57 that larger pores sustain higher activity at longer times on stream. Rajagopalan and Luss (1979) also computed the optimum lifetime activity over the life of the catalyst. Optimal pore size was found to be larger than that for optimum activity. The effect of pore structure was also examined with a comparison of the uniform pore structure with that of a catalyst having the same surface area but with a Maxwellian pore size distribution. While the initial activity of the uniform pore catalyst was higher, the Maxwellian distribution was more stable because a certain percentage of the pores were larger.

The model formulated by Ahn and Smith (1984) considered partial surface poisoning for HDS and pore mouth plugging for HDM reactions. The conservation equations with first-order reactions for metal-bearing and sulfur-bearing species were based on spherical pellet geometry rather than on single pores. Hence, a restricted effective diffusivity was employed

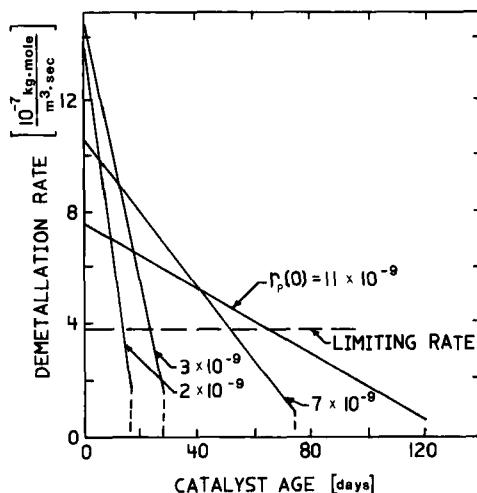


FIG. 57. Model computation of the effect of pore size on catalyst stability using first-order kinetics and configurational diffusion for a 12.5-Å-diameter metal-bearing molecule (Rajagopalan and Luss, 1979).

for metal-bearing compounds:

$$D_{\text{eff}} = \frac{\varepsilon D_{\infty}}{\tau} \left(1 - \frac{r_m}{r_p}\right)^4 \quad (29)$$

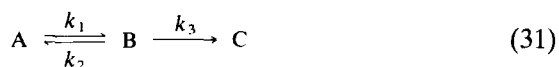
where ε and τ are the porosity and tortuosity, respectively, and with r_m and r_p defined as before. Activity loss for HDS was accounted for by the decrease in surface area from pore shrinkage and a lower intrinsic activity of the contaminated portion of the catalyst surface. The model was used to evaluate how Thiele modulus parameters determine the degree of deactivation by pore plugging versus that from surface poisoning. It was not extended to predict optimum catalyst properties.

Haynes and Leung (1983) formulated a similar configurational diffusion model combining the effects of active site poisoning as well as pore plugging on the HDM reaction. In this case the reaction form in the conservation equation is multiplied by a deactivation function which accounts for the loss of intrinsic activity, $(1 - \chi)$ is frequently chosen, where χ is the fractional coverage of the sites. Other forms of the site deactivation function have been discussed by Froment and Bischoff (1979). The deactivation was found to depend on a dimensionless parameter given by

$$\delta = 2W_s / \rho_p r_0 \quad (30)$$

with W_s , ρ_p , and r_0 defined, respectively, as the mass of adsorbed poison at complete site coverage, poison density, and initial pore radius. When $\delta < 0.99$, the pores become constricted but do not plug. Phenomenologically, this result is obtained because of the decrease in intrinsic activity where deposition has occurred. This approach may represent a diffusion-limited coke type of deactivation but does not seem to be realistic for metal deactivation.

Laboratory studies on both model compounds and real residuum feedstocks under commercial conditions have shown that the metal deposit profile on aged catalyst pellets is often M shaped, having a concentration maximum at some internal radial position. The simple first- or second-order kinetics employed by the models discussed cannot predict such a profile. This profile is a consequence of the sequential path for HDM where the hydrogenated intermediate B must first be formed from the original oil compound A prior to forming the deposit C:



As discussed in Section IV, Agrawal and Wei (1984) and Ware and Wei (1985b) have successfully modeled experimental deposit profiles by using the theory of coupled, multicomponent first-order reaction and diffusion. Wei and Wei (1982) employed this theory to evaluate the influence of catalyst properties on the shape of the deposit profile. Agrawal (1980) developed a model for the deactivation of unimodal and bimodal catalysts based on the consecutive reaction path. These approaches represent a more realistic consideration of the HDM reaction mechanism than first-order kinetics and will, accordingly, be discussed in more detail.

By using the theory of multicomponent first-order reaction and diffusion (Wei, 1962), the specific conservation equation for A and B in the catalyst pellet is expressed as

$$\begin{bmatrix} D_A & 0 \\ 0 & D_B \end{bmatrix} \nabla^2 \begin{bmatrix} A \\ B \end{bmatrix} = \begin{bmatrix} k_1 & -k_2 \\ -k_1 & k_2 + k_3 \end{bmatrix} \begin{bmatrix} A \\ B \end{bmatrix} \quad (32)$$

with boundary conditions of

$$r = 0, \quad \nabla \begin{bmatrix} A \\ B \end{bmatrix} = \begin{bmatrix} 0 \\ 0 \end{bmatrix} \quad (33)$$

$$r = R, \quad \begin{bmatrix} A \\ B \end{bmatrix} = \begin{bmatrix} A_R \\ B_R \end{bmatrix} \quad (34)$$

where r is the pellet coordinate (spherical, cylindrical, or one-dimensional infinite slab), R is the surface, and A_R and B_R are the external concentrations. The effective diffusivities D_A and D_B were assumed to be independent of pore size, that is, nonrestricted diffusion, by Wei and Wei (1982).

For a one-dimensional slab, the solution to Eq. (26) is of the form

$$\begin{bmatrix} A(r) \\ B(r) \end{bmatrix} = \mathbf{X} \begin{bmatrix} \frac{\cosh \phi_1(r/R)}{\cosh \phi_1} & 0 \\ 0 & \frac{\cosh \phi_2(r/R)}{\cosh \phi_2} \end{bmatrix} \mathbf{X}^{-1} \begin{bmatrix} A_R \\ B_R \end{bmatrix} \quad (35)$$

where \mathbf{X} and \mathbf{X}^{-1} are, respectively, the eigenvector and corresponding inverse matrix of the rate constant matrix \mathbf{K} . The Thiele moduli are given by

$$\phi_i = R \sqrt{\lambda_i/D_i} \quad (36)$$

where λ_i are the eigenvalues of \mathbf{K} . Using the rate constant data of Agrawal (1980) to determine the eigenvalues and the relationship between the Thiele moduli assuming equal diffusivities for A and B,

$$\phi_2/\phi_1 = \sqrt{\lambda_2/\lambda_1} \quad (37)$$

The metal deposition pattern after equal time on stream computed for various values of the Thiele modulus ϕ_2 is shown in Fig. 58. Since deactivation was not incorporated into this model, the absolute values for the concentration of the deposit C are arbitrary and depend on time on stream. The deposit profiles have shapes identical to the profile of intermediate B since C is derived from B as a first-order rate process. A factor of 3 to 10 difference in the Thiele modulus can result in a shift from center maximum to near edge maximum-type profiles. Comparison with experimental data can illustrate the difficulty in directly modeling data on real feedstocks and catalysts. Pazos *et al.* (1983) obtained an M-shaped profile for a catalyst with 23.4 wt. % CoO + MoO₃ and a center maximum profile for the same catalyst base with 12.5 wt. % CoO + MoO₃. According to the model a factor of 10 difference in the Thiele modulus, or a factor of 100 in the rate constants, would appear to best simulate the results. Yet there is only a factor of 2 difference in the catalytic metals (Co + Mo) content, which leads to significantly different deposit profiles in practice. The proper trend, however, is demonstrated. Accurate modeling of the deposition process not only requires an adequate model of the pore structure and the correct reaction path, but also an understanding of what factors influence the intrinsic activity of the catalytic surface.

The effects of metal deposition on catalyst pore plugging were not included in this computation of Wei and Wei (1982). Rather, this model

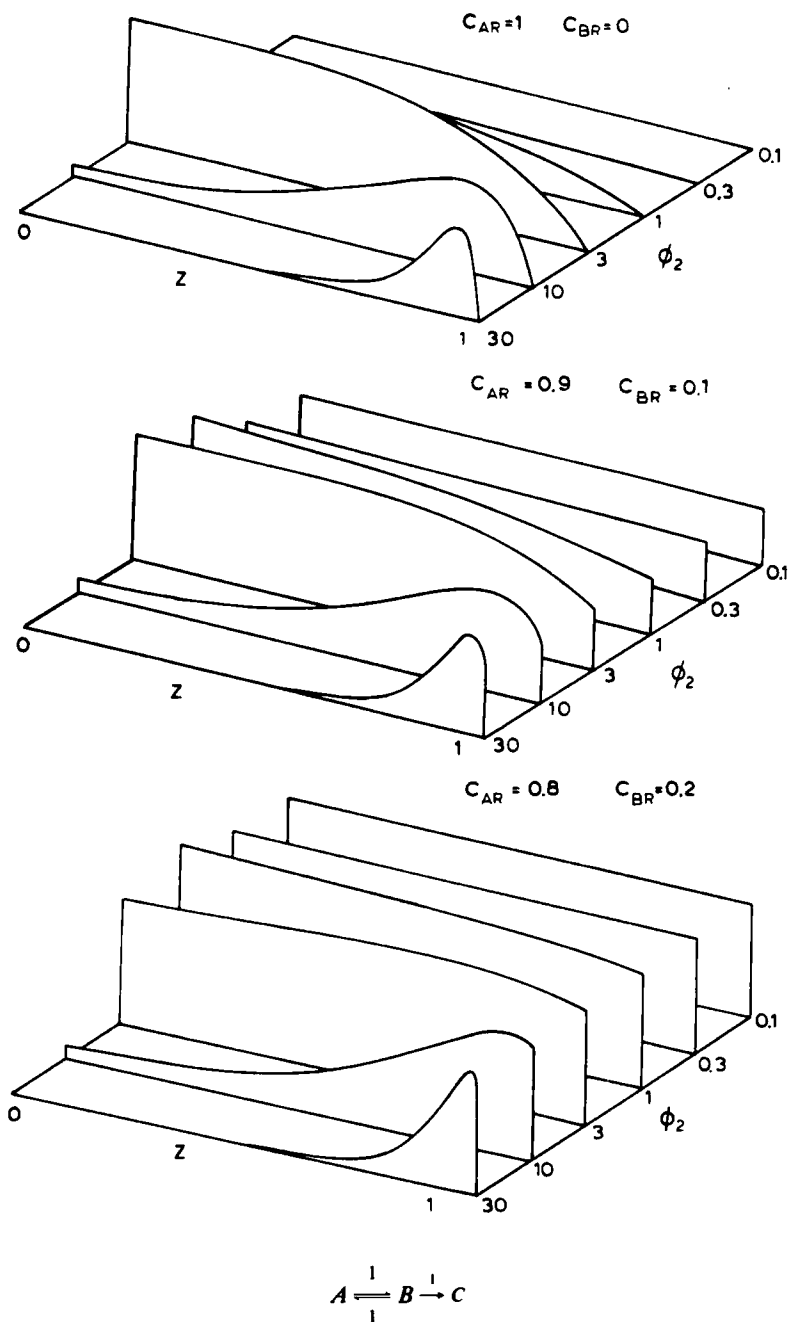


FIG. 58. Computed metal deposit profiles based on a sequential reaction mechanism (Wei and Wei, 1982).

serves to illustrate that catalyst properties can determine the extent of deposition and the type of profile obtained. The sequential mechanism appears to be a more realistic approach based on metal deposit distribution. The four types of profiles predicted by the model—including the M-shaped or shell maximum, the U-shaped or edge maximum, the center maximum, and the uniform deposit—have been observed experimentally.

Agrawal (1980) adopted the grain model of Sohn and Szekely (1972) to model the deactivation of a bimodal catalyst for the HDM reaction. The schematic in Fig. 59 illustrates the proposed physical structure of the catalyst pellet. The macrospherical pellet of radius R_a is composed of numerous microspheres of radius R_i , where the number of microspheres per unit volume is given by

$$N = 3(1 - \epsilon)/4\pi R_i^3 \quad (38)$$

and ϵ_a is the porosity of the macrospherical pellet. The void space between the microspheres constitutes the macropores with an equivalent macropore radius given by (Wheeler, 1951)

$$R_m = \frac{2}{3} \left(\frac{\epsilon_a}{1 - \epsilon_a} \right) R_i \quad (39)$$

for hexagonal close packing. This approach leads to unrealistically small macropores in some cases owing to the inadequacy of the idealized model of packed spheres in representing a macroporous structure. Agrawal (1980) was forced to use macropore diffusivities from the literature.

The micropores are contained within the microspheres as a set of parallel cylindrical pores of equal length L and radius R_p (Wheeler, 1951) with

$$L = (R_i \sqrt{\tau_i})/3 \quad (40)$$

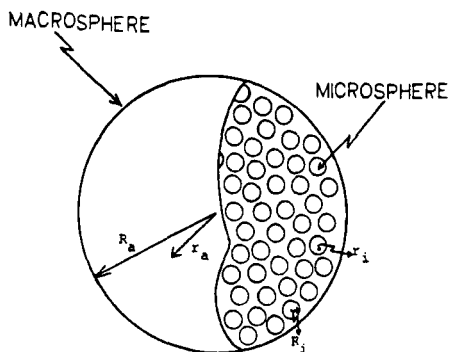


FIG. 59. Schematic of the Sohn and Szekely (1972) grain model for a macroporous catalyst (Agrawal, 1980).

where τ_i is the tortuosity of the micropores. The number of micropores in a single microsphere is

$$N_p = 4\varepsilon_i R_i^2 / R_p^2 \tau_i \quad (41)$$

Agrawal (1980) assumed that since the surface area of the macropores was significantly less than that of the micropores, the reaction in the macropores could be neglected. The conservation equations in the macropores for A_a and B_a , for the consecutive reaction path of Eq. (31), are expressed as

$$D_a \cdot \nabla^2 A_a = n4\pi R_i^2 D_i \left(\frac{\partial A_i}{\partial r_i} \right)_{r_i=R_i} \quad (42)$$

$$D_a \cdot \nabla^2 B_a = n4\pi R_i^2 D_i \left(\frac{\partial B_i}{\partial r_i} \right)_{r_i=R_i} \quad (43)$$

The microporous diffusivity D_i in the constricted form and assumed equal for A and B is given by

$$D_i = \frac{\varepsilon_i D_\infty}{\tau_i} \left(1 - \frac{r_m}{R_p} \right)^4 \quad (44)$$

where r_m is the radius of the molecules.

The conservation equations for the micropore, taking the reaction sequence of Eq. (31) into account, are given by the coupled multicomponent form of Eq. (32) for a cylindrical pore:

$$\frac{\partial}{\partial x} R_p^2 D_i \frac{\partial}{\partial x} \begin{bmatrix} A_i \\ B_i \end{bmatrix} = \begin{bmatrix} k_1 & -k_2 \\ -k_1 & k_2 + k_3 \end{bmatrix} \begin{bmatrix} A \\ B \end{bmatrix} \quad (45)$$

where x is the distance from the micropore dead end. At the mouth of the micropore ($x = L$),

$$A_i = A_a \quad (46)$$

$$B_i = B_a \quad (47)$$

and at $x = 0$,

$$\frac{\partial A_i}{\partial x} = \frac{\partial B_i}{\partial x} = 0 \quad (48)$$

The radius in the micropore and hence the constricted diffusivity in the micropore are functions of position in the micropore x , location of the microsphere in the pellet r_a , and time due to the deposition of the metal sulfide. The micropore radius R at time t is determined by the deposition

rate expressed as

$$\frac{dR(x, r_a, t)}{dt} = -\frac{k_3 B_i(x, r_a, t)}{\rho_m} \quad (49)$$

where ρ_m is the density of the deposit. The deposit is assumed to affect only diffusion and active surface area, but not intrinsic HDM activity.

Using this model, Agrawal (1980) computed the initial demetallation rate as a function of micropore radius and microsphere radius (grain size) for the bimodal catalyst. The results are shown in Fig. 60 for a typical set of

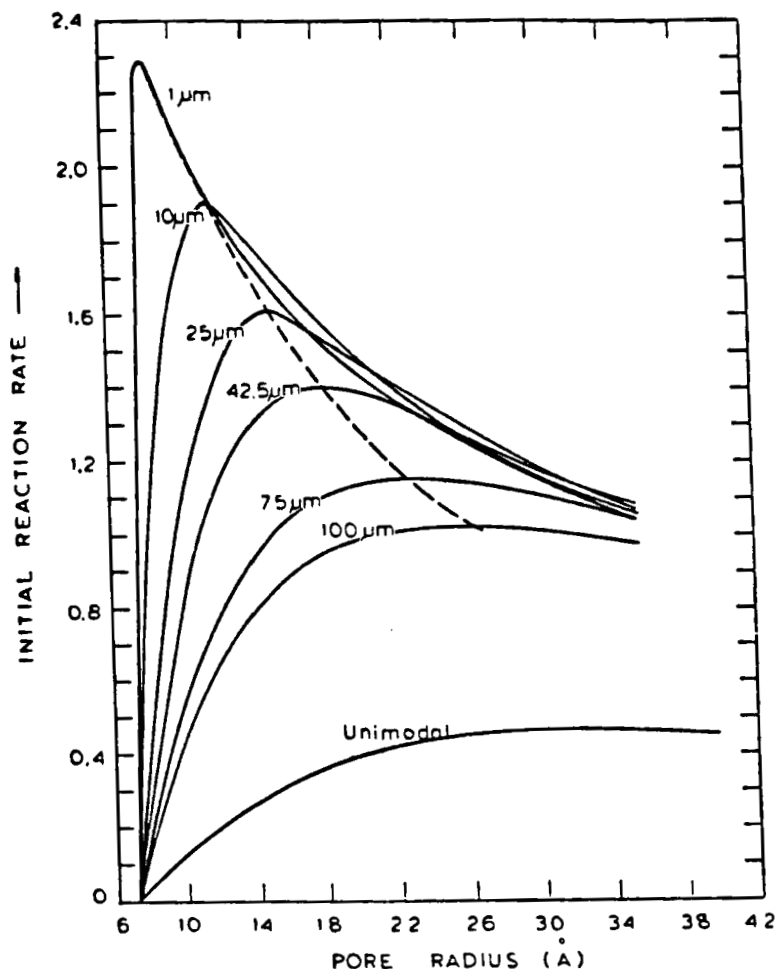


FIG. 60. Initial HDM reaction rate versus micropore radius and grain size at a fixed porosity for the macroporous catalyst (Agrawal, 1980).

catalyst parameters and a metal-bearing molecule radius of 7.1 \AA . For grain size, the HDM rate first increases with pore radius because of the functional dependence of diffusivity on pore radius in the restricted diffusion regime. After a maximum, the HDM rate decreases with increasing micropore radius due to the decrease in active surface area. Decreasing the grain size for a given pore radius increases the HDM rate in the restricted regime because of the greater access to the micropore surface area within the microspheres. The unimodal catalyst in this model is simply a scale-up of a single microsphere to the size of the catalyst pellet. Bimodal

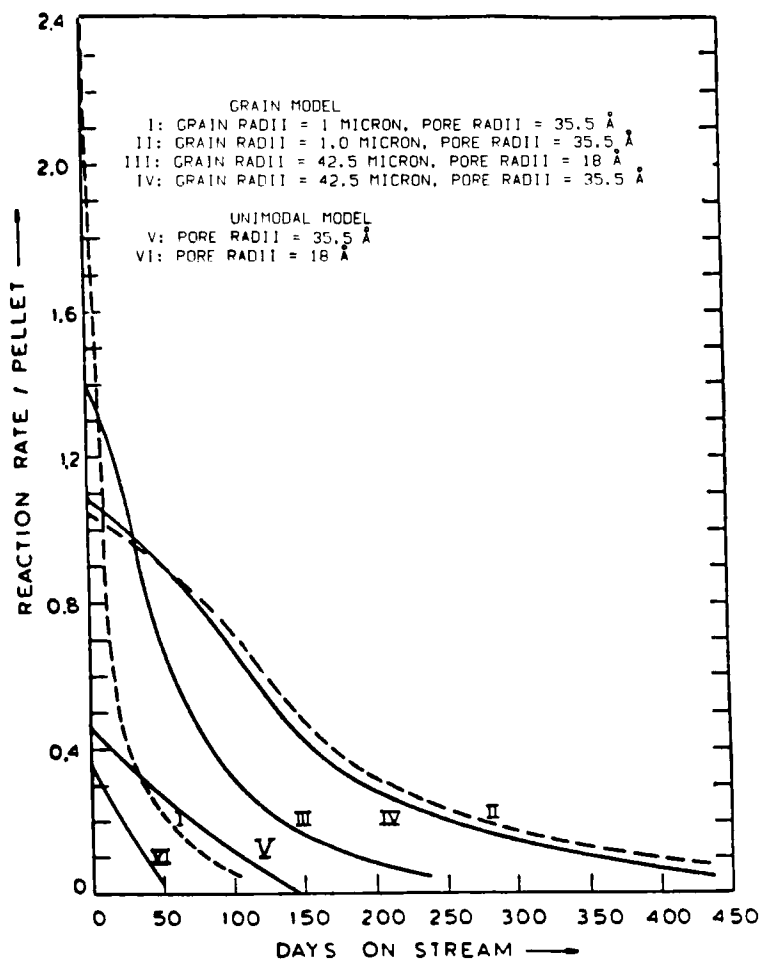


FIG. 61. Effect of pore size and grain radius on the stability of the macroporous catalyst activity for HDM (Agrawal, 1980).

catalysts appear to have far greater HDM activity because of the greater accessibility of the micropore volume than the unimodal catalyst.

Agrawal (1980) computed the deposit concentration in the microspheres as a function of position in the pellet and time. Initially, the deposit concentrates in the microspheres near the outer region of the pellet. With the outer region deactivated, deposit formation progresses inward because of access to the inner microspheres through the unobstructed macropores. The profiles in the microspheres are more or less uniform because of the low Thiele modulus. In the case of the unimodal catalyst without macropores, the buildup of deposit in the outer region of the pellet would seal the outer pores and prevent access to internal sites.

Agrawal (1980) also computed the effect of time on stream on the HDM reaction rate for various cases of bimodal and unimodal catalysts. These comparisons are shown in Fig. 61. As is evident, improvements in stability and overall activity rather than initial activity are gained, whether unimodal or bimodal catalysts are used, by increasing the micropore size. The relative capacity of the catalysts can be visualized as the area under the curves in Fig. 61.

At present it cannot be ascertained whether the use of more sophisticated models accounting for the fine structure of pores would provide better insight or predictions for new catalyst designs. Models with this degree of complexity have not been applied to the pore plugging problem. The inclusion of foulant deposition within a fine structure model would render an intractable mathematical problem. Furthermore, the present ability to control and analyze the details of the pore structure of materials is rather limited, making it difficult to evaluate various theoretical approaches and to design novel catalysts. This is an area where a significant research effort may provide valuable returns.

VI. Conclusions

Despite cyclic economic conditions involving worldwide oil production and highly effective energy conservation measures, the capability of the modern oil refinery to convert low-quality, heavy crudes to needed transportation fuels will be a necessity eventually. Upgrading the residuum from the heavy crudes must accomplish two tasks: (1) reduction of hydrocarbon molecular weight and (2) removal of detrimental non-hydrocarbon impurities including the heteroatoms N and S and the metals Ni and V that are dissolved in the oil as organometallic complexes. The technology for upgrading residuum exists today in various forms, with

hydroprocessing as the method of choice for maximizing the yield and quality of distillate range products. A major obstacle hindering the widespread utilization of residuum hydroprocessing technology, however, has been the economic penalty imposed by the presence of Ni and V. The deposition of these metals on the hydroprocessing catalyst from hydrodemetallation (HDM) reactions, although desirable from the standpoint of product quality, accelerates the deactivation of the catalyst, particularly with residua containing more than 200 ppmw metals.

The research efforts of many investigators over the past several decades have contributed to the current understanding of the basic phenomena in HDM as well as in the development of technology for utilizing heavy oils. As is often the case in a chemical engineering application, many diverse disciplines of science and engineering have been involved.

Analytical chemists have learned much about the composition and chemical structure of metalloporphyrin compounds in oil and, to a lesser extent, the nonporphyrinic metal compounds. Only in recent years, however, has the complex structure of the physicochemical system that characterizes the entire oil been recognized. Native petroleum is a system in which the solubility behavior of its molecules is determined by a delicate balance of strong intermolecular forces. The properties of residuum, including Ni and V metal compounds, are governed primarily by these intermolecular associations. Asphaltenes, in which the majority of petroleum metals tend to concentrate, were previously thought to be the highest-molecular-weight components of petroleum, existing as large, observable micellar entities with dimensions on the order of the pore size of catalysts (50–100 Å). This interpretation was based on the analyses of asphaltenes precipitated from the petroleum with solvents, rather than in their native solution environment. Furthermore, much of the process and catalyst development efforts in residuum HDM were based on these concepts. It is now recognized that the molecules, including metal-bearing porphyrins and nonporphyrins, which comprise asphaltenes are much lower in molecular weight but highly polar. Relatively little is known about the chemical structure of the nonporphyrin metal compounds and their intermolecular associations with other highly polar residuum molecules which comprise the asphaltenes upon precipitation by solvents. Furthermore, the state of intermolecular associations at the high temperatures and pressures encountered in hydroprocessing is unclear. This should be a fruitful area of research for providing guidance in the design and development of HDM technology.

The use of model compounds in reaction kinetic studies has provided valuable insight into the fundamental processes occurring in residuum hydroprocessing. The reaction of Ni and V porphyrins under commercial

HDM conditions involves a sequential mechanism on two distinct types of catalytic sites. The porphyrins are initially hydrogenated, forming precursor species which subsequently undergo ring cleavage reactions, depositing the metal on the catalyst surface. This sequential network results in unique radial metal deposition profiles in aged catalyst pellets under diffusion-limited conditions. Metal profiles in catalysts sampled from commercial residuum hydroprocessing reactors are compatible with this mechanism. The bifunctional nature of the catalytic requirements suggests that the reactivity of metal compounds in residuum oils may be manipulated to control the location at which metals deposit within the catalyst during hydroprocessing.

The incentive to explore the intrinsic phenomenon with probe molecules and model feeds remains. The choice of a suitable Ni or V model compound to supplement the porphyrin studies is limited only by the capabilities of the analytical chemist to scrutinize the residuum. Studies with real feedstocks are necessary and remain the preferred option when information for specific processing applications is required. The risk associated with such a large capital investment as hydroprocessing is too great to justify a design based on anything but the anticipated feedstock. Predicting the behavior of one stock based on experience with another is difficult due to the complexity of petroleum. However, for this same reason, sole reliance on real feeds heightens the challenge to understand the common fundamental processes in HDM. Ideally, the level of fundamental understanding will be balanced with its utilization when model compound studies are constantly referenced to the requirements of hydroprocessing petroleum residuum.

While catalytic HDM results in a desirable, nearly metal-free product, the catalyst in the reactor is laden with metal sulfide deposits that eventually result in deactivation. Loss of catalyst activity is attributed to both the physical obstruction of the catalyst pellets' pores by deposits and to the chemical contamination of the active catalytic sites by deposits. The radial metal deposit distribution in catalyst pellets is easily observed and understood in terms of the classic theory of diffusion and reaction in porous media. Application of the theory for the design and development of HDM and HDS catalysts has proved useful. Novel concepts and approaches to upgrading metal-laden heavy residua will require more information. However, detailed examination of the chemical and physical structure of the metal deposits is not possible because of current analytical limitations for microscopically complex and heterogeneous materials. Similarly, experimental methods that reveal the complexities of the fine structure of porous materials and theoretical methods to describe them are not yet

available. Basic research in these areas should provide the means for developing novel catalysts with sufficiently improved tolerance for economically upgrading high-metal-content residua.

ACKNOWLEDGMENTS

The authors are grateful to P. J. Angevine of Mobil Research and Development Corporation and R. L. Howell and J. G. Reynolds of Chevron Research Company for their careful review of the manuscript. Their comments and suggestions provided valuable guidance.

References

- Agrawal, R., "Kinetics & Diffusion in Hydrodemetallation of Nickel and Vanadium Porphyrins." Sc.D. thesis, MIT, 1980.
- Agrawal, R., and Wei, J., *Ind. Eng. Chem. Process Des. Dev.* **23**, 505, 515 (1984).
- Ahn, B., and Smith, J. M., *A.I.Ch.E. J.* **30**, 739 (1984).
- Altgelt, K. H., *J. Appl. Polymer Sci.* **9**, 3389 (1965).
- Altgelt, K. H., *ACS Prepr. Div. Petrol. Chem.* **13**, 37 (1968).
- Anderson, R. F., Olson, R. K., Hutchings, L. E., and Penning, R. T., *Future Heavy Crude Oils Tar Sands, Int. Conf., 2nd, Caracas*, p. 1189 (1982).
- Andreu, P., Galiasso, R., Morales, A., Abrams, D., Katan, L., Pantoja, L., Sojo P., and Vergara, E., In "Studies in Surface Science and Catalysis" (T. Seiyama and K. Tanabe, eds.), Vol. 7 Part B, p. 877. Elsevier, Amsterdam, 1981.
- Angst, C., Kratky, C., and Eschenmoser, A., *Angew. Chem. Int. Ed. Engl.* **20**, 263 (1981).
- Arey, W. F., Jr., Blackwell, N. E., III, and Reichle, A. D., *World Petrol. Congr., 7th*, Vol. 4, p. 167 (1967).
- Asaoka, S., Nakata, S., Shiroto, Y., and Takeuchi, C., *Ind. Eng. Chem. Process Des. Dev.* **22**, 242 (1983).
- Audibert, F., and Duhaut, P., *Midyear Meet. Am. Petrol. Inst., Div. Refining, 35th, Houston*, May 13-15 (1970).
- Baker, E. W., *J. Am. Chem. Soc.* **88**, 2311 (1966).
- Baker, E. W., and Palmer, S. E., In "The Porphyrins" (D. Dolphin, ed.), Vol. 1, Chap. 11. Academic Press, New York, 1978.
- Baker, E. W., Yen, T. F., Dickie, J. P., Rhodes, R. E., and Clark, L. F., *J. Am. Chem. Soc.* **89**, 3631 (1967).
- Baltus, R. E., and Anderson, J. L., *Chem. Eng. Sci.* **38**, 1959 (1983).
- Barbour, R. V., and Petersen, J. C., *Anal. Chem.* **46**, 273 (1974).
- Bartholomew, C. H., Agrawal, P. K., and Katzer, J. R., *Adv. Catal.* **31**, 135 (1982).
- Barton, S. S., Kraft, J. P., Owens, T. R., and Skinner, L. J., *J. Chem. Soc.* **3**, 339 (1972).
- Barwise, A. J. G., and Whitehead, E. V., *ACS Prepr. Div. Petrol. Chem.* **25**, 268-279 (1980).
- Bearden, R., and Aldridge, C. L., *Energy Prog.* **1**, 44 (1981).
- Beaton, W. I., McDaniel, N. K., McWhirter, W. E., Petersen, R. D., and Van Driesen, R. P., *Oil Gas J.* **84**(27), 47 (1986).
- Berthe, C., Muller, J.-F., Cagniant, D., Grimblot, J., and Bonnelle, J. P., *Charact. Heavy Crude Oils Petrol. Resid Int. Symp., Lyon* 164-168 (1984).
- Beuther, H., and Schmid, B. K., *Proc. World Petrol. Congr., 6th Sect. III, Pap. 20* (1963).

- Beuther, H., Larsen, O. A., and Perrotta, A. J., In "Catalyst Deactivation" (B. Delmon and G. F. Froment, eds.), Elsevier, Amsterdam, 1980.
- Biggs, W. R., Fetzer, J. C. Brown, R. J., and Reynolds, J. G., *Liquid Fuel Technol.* **3**, 397 (1985).
- Boduszynski, M. M., *ACS Prepr. Div. Petrol. Chem.* **24**, 935 (1979).
- Boduszynski, M. M., *ACS Prepr. Div. Petrol. Chem.* **27**, 1367 (1983).
- Boduszynski, M. M., *ACS Prepr. Div. Petrol. Chem.* **30**, 625 (1985).
- Boduszynski, M. M., Chadha, B. R., and Szkuta-Pochopien, T., *Fuel* **56**, 432 (1977).
- Boduszynski, M. M., McKay, J. F., and Latham, D. R., *Proc. Assoc. Asphalt Paving Technol., Louisville* **49**, 123-143 (1980).
- Bridge, A. G., *Adv. Catal. Chem. Symp., Salt Lake City May* (1982).
- Bridge, A. G., and Green, D. C., *ACS Prepr. Div. Petrol. Chem.* **24**, 791 (1979).
- Bridge, A. G., Scott, J. W., and Reed, E. M., *Oil Gas J.* **73**(20), 94 (1975).
- Bridge, A. G., Reed, E. M., Tamm, P. W., and Cash, D. R., *A.I.Ch.E. Symp. Ser.* **148**, 225 (1979).
- Broadbent, S. R., and Hammersley, J. M., *Proc. Cambridge Philos. Soc.* **53**, 629 (1957).
- Brown, J. K., and Ladner, W. R., *Fuel* **39**, 87 (1960).
- Buchler, J. W., In "Porphyrins and Metalloporphyrins" (K. M. Smith, ed.), Chap. 5. Elsevier, Amsterdam, 1975.
- Busch, D. H., Pillsbury, D. G., Lovecchio, F. V., Tait, A. M., Hung, Y., Jackels, S., Rakowski, M. C., Schammel, W. P., and Martin, L. Y., In "Electrochemical Studies of Biological Systems" (D. T. Sawyer, ed.), *ACS Symp. Ser.* **38**, Chap. 3 (1977).
- Campagna, R. J., Frayer, J. A., and Sebelsky, R. T., *Encycl. Chem. Process. Des.* **15**, 216 (1982).
- Cecil, R. R., Mayer, F. Z., and Cart, E. N., *AIChE Meet., Los Angeles* (1968).
- Chang, C. D., and Silvestri, A. J., *Ind. Eng. Chem. Process Des. Dev.* **13**, 315 (1974).
- Chang, C. D., and Silvestri, A. J., *Ind. Eng. Chem. Process Des. Dev.* **15**, 161 (1976).
- Chantong, A., and Massoth, F. E., *AIChE J.* **29**, 725 (1983).
- Chelton, H. M., and Traxler, R. N., *World Petrol. Congr., 5th Sect. V*, p. 247 (1959).
- Clerc, R. J., and O'Neal, M. J., Jr., *Anal. Chem.* **33**, 1587. (1961).
- Conner, W. C., and Lane, A. M., *J. Catal.* **89**, 217 (1984).
- Copelin, E. C., *Anal. Chem.* **36**, 2274 (1964).
- Corbett, L. W., *Anal. Chem.* **41**, 576 (1969).
- Corbett, R. A., *Oil Gas J.* **83**(41), 73 (1985).
- Costantinides, G., and Arich, G., *World Petrol. Congr. 6th, Frankfurt Pap. V-11* (1963).
- Dautzenberg, F. M., and DeDeken, J. C., *Cat. Rev. Sci. Eng.* **26**, 421 (1984).
- Dautzenberg, F. M., and DeDeken, J. C., *ACS Prepr. Div. Petrol. Chem.* **30**, 8 (1985).
- Dautzenberg, F. M., Klinken, J. V., Pronk, K. M. A., Sie, S. T., and Wijffels, J. B., *ACS Symp. Ser.* (65), 254 (1978).
- Dean, R. A., and Whitehead, E. V., *Proc. World Petrol. Congr., 6th Pap. V-9* (1963).
- de Bruijn, A., *Proc. Int. Congr. Catal., 6th* **2**, 951 (1976).
- Delmon, B., and Grange, P., In "Catalyst Deactivation" (B. Delmon and G. F. Froment, ed.), Elsevier, Amsterdam, 1980.
- Dereppe, J., Moreaux, C., and Castex, H., *Fuel* **57**, 435 (1978).
- Devanneaux, J., Gallex, J. P., and Engelhard, P. A., *ACS Prepr. Div. Petrol. Chem.* **30**, 84 (1985).
- Dickie, J. P., and Yen, T. F., *Anal. Chem.* **39**, 1847 (1967).
- Dickie, J. P., Haller, M. W., and Yen, T. F., *J. Colloid Interface Sci.* **29**, 475 (1969).
- Dickson, F. E., and Petrakis, L., *J. Phys. Chem.* **74**, 2850 (1970).
- Dickson, F. E., and Petrakis, L., *Anal. Chem.* **46**, 1129 (1974).

- Dickson, F. E., Davis, B. E., and Wirkkala, R. A., *Anal. Chem.* **41**, 1335 (1969).
- Dickson, F. E., Kunesch, C. J., McGinnis, E. L., and Petrakis, L., *Anal. Chem.* **44**, 978 (1972).
- Dodet, C., Noville, F., Crine, M., Marchot, P., and Pirard, J. P., *Appl. Catal.* **11**, 251 (1984).
- Dolphin, D., ed., "The Porphyrins." Academic Press, New York, 1978.
- Douwes, C. Th., van Klinken, J., Wijffels, J. B., and van Zijll Langhout, W. C., *Proc. World Petrol. Congr., 10th* **4**, 175 (1980).
- Drushel, H. V., *Adv. Catal. Chem. Conf., Snowbird, Utah Oct. 3-5* (1979).
- Dwiggins, C. W., Jr., *J. Phys. Chem.* **69**, 3500 (1965).
- Ebert, L. B., Scanlon, J. C., and Mills, D. R., *ACS Symp. Ser.* **169**, 73 (1982).
- Ebert, L. B., Scanlon, J. C., and Mills, D. R., *ACS Prepr. Div. Petrol. Chem.* **30**, 636 (1985).
- Eccles, R. M., Gray, A. M., and Livingston, W. B., *Oil Gas J.* **80**(15) 121 (1982).
- Erdman, J. G., and Harju, J. G., *ACS Prepr. Div. Petrol. Chem.* **8**, 252 (1963).
- Erdman, J. G., and Ramsey, V. G., *Geochim. Cosmochim. Acta* **25**, 175 (1961).
- Erdman, J. G., Ramsey, V. G., and Hanson, W. E., *ACS Prepr. Symp.* **3**, A73 (1958).
- Erickson, R. L., Myers, A. T., and Horr, C. A., *Bull. Am. Assoc. Petrol. Geol.* **38**, 2200 (1954).
- Feller, W., "An Introduction to Probability Theory and Its Applications," Vol. 1, 2nd Ed. Wiley, New York, 1957.
- Ferris, S. W., Black, E. P., and Clelland, *Ind. Eng. Chem., Prod. Res. Dev.* **6**, 127 (1967).
- Ferry, J. D., *J. Gen. Physiol.* **20**, 95 (1936).
- Filby, R. H., In "The Role of Trace Metals in Petroleum" (T. F. Yen, ed.). Ann Arbor Science, Ann Arbor, Mich., 1975.
- Fischer, K. A., and Schram, A., *World Petrol. Congr., 5th Sect. V*, Pap. 20 (1959).
- Fischer, R. H., and Angevine, P. J., *Appl. Catal.* **27**, 275 (1986).
- Fischer, R. H., and Milstein, D., U.S. Patent 4,016,067 to Mobil Oil Corp, 1977.
- Fish, R. H., and Komlenic, J. J., *J. Anal. Chem.* **56**, 510 (1984).
- Fish, R. H., and Komlenic, J. J., and Wines, B. K., *Anal. Chem.* **56**, 2452 (1984).
- Fisher, L. R., and Dunning, H. N., *Bur. Mines Rep. Invest.* (5844) (1961).
- Fitz, C. W., and Rase, H. F., *Ind. Eng. Chem. Prod. Res. Dev.* **22**, 40 (1983).
- Fleisch, T. H., Meyers, B. L., Hall, J. B., and Ott, G. L., *J. Catal.* **86**, 147 (1984).
- Fleischer, E. B., *J. Am. Chem. Soc.* **85**, 146 (1963).
- Froment, G. F., and Bischoff, K. B., "Chemical Reactor Analysis and Design." Wiley, New York, 1979.
- Fuhrhop, J. H., In "The Porphyrins" (D. Dolphin, ed.), Vol. II, Chap. 5. Academic Press, New York, 1978.
- Fuhrhop, J. H., Kadish, K. M., and Davis, D. G., *J. Am. Chem. Soc.* **95**, 5140 (1973).
- Furimsky, E., *Catal. Rev. Sci. Eng.* **25**, 421 (1983).
- Gajardo, P., Pazos, J. M., and Salazar-Guillen, A., *Appl. Catal.* **2**, 303 (1982).
- Galiasso, R., and Morales, A., *Appl. Catal.* **7**, 57 (1983).
- Galiasso, R., Blanco, R., Gonzalez, C., and Quinteros, N., *Fuel* **62**, 817 (1983).
- Galiasso, R., Garcia, J., Caprioli, L., Pazos, J. M., and Soto, A., *ACS Prepr. Div. Petrol. Chem.* **30**, 50 (1985).
- Gallegos, E. J., *World Petrol. Congr., 7th* **4**, 249 (1967).
- Gary, J. H., and Handwerk, G. E., "Petroleum Refining, Technology and Economics." Dekker, New York, 1975.
- Gates, B. C., Katzer, J. R., and Schuit, G. C. A., "Chemistry of Catalytic Processes." McGraw-Hill, New York, 1979.
- Gibson, K. R., Green, D. C., and Teichmann, D. P., *Chem. Eng. Prog.* **79**, 93 (1983).
- Girdler, R. B., *Proc. Assoc. Asphalt Paving Technol.* **34**, 45 (1965).

- Gonzalez, C., and Galiasso, R. E., *Rev. Tec. Intevep.* **3**, 3 (1983).
- Goulon, J., Retournard, A., Friant, P., Goulon-Ginet, C., Berthe, C., Muller, J., Poncet, J., Guillard, R., Escalier, J., and Neff, B., *J. Chem. Soc. Dalton Trans.* (6), 1095 (1984).
- Graeser, U., and Niemann, K., *Oil Gas J.* **80**(12), 121 (1982).
- Graeser, U., Escher, G., Holighaus, R., and Wenzel, F., *Proc. Midyear API Refining Meet.*, 51st, May **65**, 169 (1986).
- Griffin, R. L., Simpson, W. C., and Miles, T. K., *ACS Prepr. Div. Petrol. Chem.* **3**, A13 (1958).
- Grizzle, P. L., Green, J. B., Sanchez, V., Murgia, E., and Lubkowitz, J., *ACS Prepr. Div. Petrol. Chem.* **26**, 839 (1981).
- Hall, G., and Herron, S. P., *ACS Prepr. Div. Petrol. Chem.* **24**, 924 (1979).
- Hannerup, P. N., and Jacobsen, A. C., *ACS Prepr. Div. Petrol. Chem.* **28**, 576 (1983).
- Hardin, A. H., Ternan, M., and Packwood, R. H., "The Effects of Pore Size in $\text{MoO}_3\text{-CoO-Al}_2\text{O}_3$ Hydroprocessing Catalysts," CANMET Report 81-4E, Energy, Mines and Resources, Canada, 1981; see also *ACS Prepr. Div. Petrol. Chem.* **23**, 1450 (1978).
- Harris, S., and Chianelli, R. R., *J. Catal.* **86**, 400 (1984).
- Haynes, H. W., Jr., and Leung, K., *Chem. Eng. Commun.* **23**, 161 (1983).
- Henke, A. M., *Oil Gas J.* **68**(14), 97 (1970).
- Higashi, H., Shirono, K., Sato, G., Nishimura, Y., and Egashira, S., *ACS Prepr. Div. Petrol. Chem.* **30**, 111 (1985).
- Ho, T. C., *Catal. Rev. Sci. Eng.* **30**, 117 (1988).
- Hohnholt, J. F., and Fausto, C. Y., *Chem. Eng. Prog.* **81**(6), 47 (1985).
- Hohnholt, J. F., and Fausto, C. Y., *Oil Gas J.* **84**(1), 63 (1986).
- Howell, R. L., Hung, C. W., Gibson, K. R., and Chen, H. C., *Oil Gas J.* **83**(30), 121 (1985).
- Hughes, C. C., and Mann, R., *ACS Symp. Ser.* **65**, 201 (1978).
- Hughes, R., "Deactivation of Catalysts," Academic Press, New York, 1984.
- Hung, C. W., and Wei, J., *Ind. Eng. Chem. Process Des. Dev.* **19**, 250, 257 (1980).
- Hung, C. W., Howell, R. L., and Johnson, D. R., *Chem. Eng. Prog.* **82**(3), 57 (1986a).
- Hung, C. W., Olbrich, H. C., Howell, R. L., and Heyse, J. V., *AIChE Nat. Meet., New Orleans, April*, Pap. 12b (1986b).
- Hydrocarbon Process.* **65**(9), 83 (1986).
- Iannibello, A., Marengo, S., and Girelli, A., *Appl. Catal.* **3**, 261 (1982).
- Ignasiak, T., Kemp-Jones, A. V., and Strausz, O. P., *J. Org. Chem.* **42**, 312 (1977).
- Inoguchi, M., *Shokubai* **18**, 78 (1976).
- Inoguchi, M., Kagaya, H., Daigo, K., Sakurada, S., Satomi, Y., Inaba, K., Tate, K., Nishiyama, R., Onishi, S., and Nagai, T., *Bull. Jpn. Petrol. Inst.* **13**, 153 (1971).
- Jacobsen, A. C., Hannerup, P. N., Cooper, B. H., Bartholdy, J., and Nielsen, A., *A.I.Ch.E. Spring Nat. Meet., Houston* (1983).
- Jaffe, S. B., U.S. Patents 4,267,071 to Mobil Oil Corp. (1981) and 4,351,717 (1982).
- Johnson, M. F. L., and Stewart, W. E., *J. Catal.* **4**, 248 (1965).
- Kameyama, H., and Amano, A., *J. Jpn. Petrol. Inst.* **25**, 118 (1982).
- Kameyama, H., Sugishima, M., Yamada, M., and Amano, A., *J. Jpn. Petrol. Inst.* **24**, 317 (1981).
- Kameyama, H., Shibuya, M., Teshigahara, I., and Amano, A., *J. Jpn. Petrol. Inst.* **28**, 83 (1985).
- Kanazawa, H., and Reynolds, B. E., *NPRA Annu. Meet., San Antonio, March* (1984).
- Kaparakos, N. E., Lasher, J. S., Sato, S., and Seno, K., *Jpn. Petrol. Inst., Tokyo, October* (1984).
- Katz, J. R., and Sivasubramanian, R., *Catal. Rev. Sci. Eng.* **20**, 155 (1979).
- Kavarik, F. S., and Butt, J. B., *Catal. Rev. Sci. Eng.* **24**, 441 (1982).

- Kodama, S., Nitta, H., Takatsuka, T., and Yokoyama, T., *J. Jpn. Petrol. Inst.* **23**, 310 (1980).
- Komatsu, S., Hori, Y., and Shimizu, S., *Proc. Midyear API Refining Meet.*, 51st, May **65**, 299 (1986).
- Koots, J. A., and Speight, J. G., *Fuel* **54**, 179 (1975).
- Kushiyaama, S., Kobayashi, S., Aizawa, R., Koinuma, Y., Inoue, K., and Shimizu, Y., *J. Jpn. Petrol. Inst.* **26**, 404 (1983).
- Kwan, T., and Sato, M., *Nippon Kagaku Zasshi* **91**, 1103 (1970).
- Larson, O. A., and Beuther, H., *ACS Prepr. Div. Petrol. Chem.* **11**, B95 (1966).
- Lasher, J. S., and Lasher, A. G., Chevron Research Co., private communication.
- Long, R. B., *ACS Prepr. Div. Petrol. Chem.* **24**, 891 (1979).
- Lorenz, D. B., Bolen, R. J., Dunning, H. N., and Eldib, I. A., *J. Colloid. Sci.* **16**, 493 (1961).
- Ma, Y. H., and Gabriel, G. A., *ACS Prepr. Div. Petrol. Chem.* **23**, 1437 (1978).
- Mack, C., *ACS Prepr. Div. Petrol. Chem.* **5**, A39 (1960).
- McKay, J. F., and Latham, D. R., *ACS Prepr. Div. Petrol. Chem.* **26**, 831 (1981).
- McKay, J. F., Amend, P. J., Cogswell, T. E., Harnsberger, P. M., Erickson, R. B., and Latham, D. R., "Analytical Chemistry of Liquid Fuel Sources, Tar Sands, Oil Shale, Coal and Petroleum." *Adv. Chem. Ser.* **170**, Chap. 9 (1978).
- McKay, J. F., Amend, P. J., Harnsberger, P. M., Cogswell, T. E., and Latham, D. R., *Fuel* **60**, 14 (1981a).
- McKay, J. F., Harnsberger, P. M., Erickson, R. B., Cogswell, T. E., and Latham, D. R., *Fuel* **60**, 17 (1981b).
- McKay, J. F., Latham, D. R., and Haines, W. E., *Fuel* **60**, 27 (1981c).
- Maier, C. A., Peries, J. P., and Quignard, A., *NPRA Annu. Meet.*, Los Angeles, March Pap. AM-86-56 (1986).
- Mann, R., and Golshan, H., *Chem. Eng. Commun.* **12**, 377 (1981).
- Mann, R., Androutsopoulos, G. P., and Golshan, H., *Chem. Eng. Sci.* **36**, 337 (1981).
- Massagutov, R. M., Berg, G. A., Kulinich, G. M., and Kirillov, T. S., *Proc. World Petrol. Congr.*, 7th p. 177 (1967).
- Menzies, M. A., Silva, A. E., and Denis, J. M., *Chem. Eng.* **88**(4), 46 (1981).
- Miller, J. W., Skipek, M., Baron, K., and Lindsay, D. A., *Proc. API Refining Mid-Year Meet.*, 48th **62**, 163 (1983).
- Mitchell, P. C. H., In "Catalysis" (C. Kemball and D. A. Dowden, eds.), Vol. 4, Chap. 7. Royal Society of Chemistry, London, 1980.
- Mitchell, P. C. H., and Valero, J. A., *React. Kinet. Catal. Lett.* **20**, 219 (1982).
- Mitchell, P. C. H., and Valero, J. A., *Inorg. Chim. Acta* **71**, 179 (1983).
- Morales, A., and Galiasso, R., *Fuel* **61**, 13 (1982).
- Morales, A., Martinez, N. P., Laine, J., Payen, E., and Grimblot, J., *Appl. Catal.* **6**, 329 (1983).
- Morales, A., Garcia, J. J., and Prada, R., *Proc. Int. Congr. Catal.*, 8th **2**, 341 (1984a).
- Morales, A., Marrero, C., and Galisso, R., *Proc. Int. Congr. Catal.*, 8th **2**, 329 (1984b).
- Moschopedis, S. E., Fryer, J. F., and Speight, J. G., *Fuel* **55**, 227 (1976).
- Nelson, W. L., *Oil Gas J.* **74**(46), 72 (1976).
- Nelson, W. L., *Oil Gas J.* **75**(9), 126 (1977).
- Newson, E., *Ind. Eng. Chem., Proc. Des. Dev.* **14**, 27 (1975).
- Nielsen, A., Cooper, B. H., and Jacobsen, A. C., *ACS Prepr. Div. Petrol. Chem.* **26**, 440 (1981).
- Nitta, H., Takatsuka, T., Kodama, S., and Yokoyama, T., *AIChE Nat. Meet.*, 86th, Houston (1979).
- Nollensteyn, F. J., *J. Inst. Petrol. Technol.* **10**, 311 (1924).

- Nongbri, G., and Tasker, K. G., *ACS Prepr. Div. Petrol. Chem.* **30**, 110 (1985).
- Ohtsuka, T., *Catal. Rev. Sci. Eng.* **16**, 291 (1977).
- Ojima, Y., Shimizu, Y., Kondo, T., Ukegawa, K., Matsumura, A., Sakabe, T., Yagi, T., Yamada, T., and Hamada, S., *J. Jpn. Petrol. Inst.* **21**, 372 (1978).
- Oleck, S. M., and Sherry, H. S., *Ind. Eng. Chem. Process Des. Dev.* **16**, 525 (1977).
- Osawa, E. Kato, T. and Yoshida, Z. *J. Org. Chem.* **32**, 2803 (1967).
- Oxenreiter, M. F., Frye, C. G., Hoekstra, G. B., and Sroka, J. M., *Jpn. Petrol. Inst.*, Nov. 30 (1972).
- Ozaki, H., Satomi, Y., and Hisamitsu, T., *World Petrol. Congr.*, 9th, Tokyo, Vol. 6, p. 97 (1975).
- Paraskos, J. A., Montagna, A. A., and Brunn, L. W., *Annu. AIChE Meet.*, 67th, Washington, D. C., Dec. (1974).
- Parkin, E. S., Paraskos, J. S., and Frayer, J. A., *Nat. AIChE Meet.*, 74th, New Orleans March (1979).
- Pazos, J. M., Aquino, L., and Pachano, J., *ACS Prepr. Div. Petrol. Chem.* **26**, 456 (1981).
- Pazos, J. M., Gonzalez, J. C., and Salazar-Guillen, A. J., *Ind. Eng. Chem. Process Des. Dev.* **22**, 653 (1983).
- Periera, C. J., Beeckman, J. W., Cheng, W. C., Donnelly, R. G., and Hegedus, L. L., *ACS Prepr. Div. Petrol. Chem.* **30**, 74 (1985).
- Periera, C. J., Donnelly, R. G., and Hegedus, L. L., in "Catalyst Deactivation" (E. E. Petersen and A. T. Bell, eds.), p. 315. Marcel Dekkar, New York, 1987.
- Petersen, J. C., *Fuel* **46**, 295 (1967).
- Petersen, R. C., and Alexander, L. E., *J. Am. Chem. Soc.* **90**, 3873 (1968).
- Petersen, J. C., Barbour, R. V., Dorrence, S. M., Barbour, F. A., and Helm, R. W., *Anal. Chem.* **43**, 1941 (1971).
- Pismen, L. M., *Chem. Eng. Sci.* **29**, 1227 (1974).
- Plantenga, F. L., Sonnemans, J. W. M., Desai, P. H., and Suzuki, T., *Proc. Midyear API Refining Meet.*, 49th, May 14-17 **63**, 221 (1984).
- Plumail, J. C., Jacquin, Y., Martino, G., and Toulhoat, H., *ACS Prepr. Div. Petrol. Chem.* **28**, 562 (1983).
- Plumail, J. C., Toulhoat, H., Jacquin, Y., and Martino, G., *Proc. Int. Congr. Catal.*, 8th **2**, 317 (1984).
- Ponec, V., *Catal. Rev. Sci. Eng.* **11**, 41 (1975).
- Prasher, B. D., Gabriel, G. A., and Ma, Y. H., *Ind. Eng. Chem. Process Des. Dev.* **17**, 266 (1978).
- Radford, H. D., and Rigg, R. G., *ACS Prepr. Div. Petrol. Chem.* **15**, A131 (1970).
- Rajagopalan, K., and Luss, D., *Ind. Eng. Chem. Proc. Des. Dev.* **18**, 459 (1979).
- Rakow, M. S., and Calderon, M., *Chem. Eng. Prog.* **77**(2), 31 (1981).
- Ramaswamy, A. V., Sharma, L. D., Singh, A., Singhal, M. L., and Sivasanker, S., *Appl. Catal.* **13**, 311 (1985).
- Rankel, L. A., *ACS Prepr. Div. Petrol. Chem.* **26**, 689 (1981).
- Rankel, L. A., and Rollmann, L. D., *Fuel* **62**, 44 (1983).
- Ray, B. R., Witherspoon, P. A., and Grim, R. E., *J. Phys. Chem.* **61**, 1296 (1957).
- Renkin, E. M., *J. Gen. Physiol.* **38**, 225 (1954).
- Reyes, S., and Jensen, K. F., *Chem. Eng. Sci.* **40**, 1723 (1985).
- Reynolds, J. G., *Liquid Fuels Technol.* **3**, 73 (1985).
- Reynolds, J. G., Biggs, W. R., Fetzer, J. C., Gallegos, E. J., Fish, R. H., Komlenic, J. J., and Wines, B. K., *Collect. Collog. Semin. (Inst. Fr. Petrol.)* **40**, 153 (1984).
- Reynolds, J. G., Biggs, W. R., and Fetzer, J. C., *Liquid Fuels Technol.* **33**, 423 (1985).
- Reynolds, J. G., Gallegos, E. J., Fish, R. H., and Komlenic, J. J., *Energy and Fuels* **1**, 36 (1987).

- Richardson, R. L., and Alley, S. K., *ACS Prepr. Div. Petrol. Chem.* **20**, 554 (1975).
- Richardson, R. L., Riddick, F. C., and Ishikawa, M., *Proc. Midyear API Refining Meet.*, 44th, May 14-17 **58**, 21 (1979).
- Riley, K. L., *ACS Prepr. Div. Petrol. Chem.* **23**, 1104 (1978).
- Ruckenstein, E., and Tsai, M. C., *AIChE J.* **27**, 697 (1981).
- Sasaki, Y., Ojima, Y., Kondo, T., Ukegawa, K., Matsumura, A., and Sakabe, T., *J. Jpn. Petrol. Inst.* **25**, 27 (1982).
- Sanders, J. V., Spink, J. A., and Pollack, S. S., *Appl. Catal.* **5**, 65 (1983).
- Sato, M., Takayama, N., Kurita, S., and Kwan, T., *Nippon Kagaku Zasshi* **92**, 834 (1971).
- Satterfield, C. N., "Mass Transfer in Heterogeneous Catalysis." MIT Press, Cambridge, Massachusetts, 1970.
- Satterfield, C. N., and Gultekin, S., *Ind. Eng. Chem. Process Des. Dev.* **20**, 62 (1981).
- Satterfield, C. N., and Yang, S. H., *J. Catal.* **81**, 335 (1983).
- Satterfield, C. N., and Yang, S. H., *Ind. Eng. Chem. Process Des. Dev.* **23**, 11 (1984).
- Scheer, H., In "The Porphyrins" (D. Dolphin, ed.), Vol. II, Chap. 1. Academic Press, New York, 1978.
- Scheidt, W. R., In "The Porphyrins" (D. Dolphin, ed.), Vol. III, Chap. 10. Academic Press, New York, 1978.
- Schuetze, B., and Hofmann, H., *Hydrocarbon Process.* **63**(2), 75 (1984).
- Scott, J. W., and Bridge, A. G., *Adv. Chem. Ser.* **103**, 113 (1971).
- Shah, Y. T., and Paraskos, J. A., *Ind. Eng. Chem. Process Des. Dev.* **14**, 368 (1975).
- Shibita, K., Kajiyama, H., Sanada, Y., and Sohma, J., *Fuel* **58**, 888 (1979).
- Sie, S. T., "Catalyst Deactivation: Studies in Surface Science and Catalysis" (B. Delmon and G. F. Froment, eds.), Vol. 6, p. 545. Elsevier, Amsterdam, 1980.
- Siewert, H. R., Koenig, A. H., and Ring, T. A., *Hydrocarbon Process.* **64**(3), 61 (1985).
- Sikonia, J. G., *Hydrocarbon Process.* **59**(6), 73 (1980).
- Silbernagel, B. G., *J. Catal.* **56**, 315 (1979).
- Silbernagel, B. G., and Riley, K. L., "Catalyst Deactivation: Studies in Surface Science and Catalysis" (B. Delmon and G. F. Froment, eds.), Vol. 6, p. 313. Elsevier, Amsterdam, 1980.
- Sinfelt, J. H., *Catal. Rev. Sci. Eng.* **3**, 175 (1969).
- Smith, K. M., In "Porphyrins and Metallo-porphyrins" (K. M. Smith, ed.), Chap. 1. Elsevier, Amsterdam, 1975.
- Smith, B. J., and Wei, J., *AIChE Nat. Meet. Nov. 10-15, Chicago* (1985).
- Snyder, L. R., Buell, B. E., and Howard, H. C., *Anal. Chem.* **40**, 1303 (1968).
- Sohn, H. Y., and Szekeley, J., *Chem. Eng. Sci.* **27**, 763 (1972).
- Sosnowski, J., Turner, D. W., and Eng, J., *Chem. Eng. Prog.* **77**(2), 51 (1981).
- Speight, J. G., *Fuel* **49**, 76 (1970).
- Speight, J. G., *Fuel* **50**, 102 (1971).
- Speight, J. G., "The Chemistry and Technology of Petroleum." Dekker, New York, 1980.
- Speight, J. G., "The Desulfurization of Heavy Oils and Residua." Dekker, New York, 1981.
- Speight, J. G., and Moschopedis, S. E., *ACS Prepr. Div. Petrol. Chem.* **24**, 910 (1979).
- Spencer, W. A., Galobardes, J. F., Curtis, M. A., and Rogers, L. B., *Sep. Sci. Technol.* **17**, 797 (1982).
- Spry, J. C., and Sawyer, W. H., *Annu. AIChE Meet.*, 68th Los Angeles, Nov. (1975).
- Subramanian, J., and Fuhrhop, J. H., In "The Porphyrins" (D. Dolphin, ed.), Vol. II, Chap. 8. Academic Press, New York, 1978.
- Sue, H., and Fujita, M., *Oil Gas J.* **84**(21), 51 (1986).
- Sugihara, J. M., Branthaver, G. Y., Wu, G. Y., and Weatherbee, C., *ACS Prepr. Div. Petrol. Chem.* **15**, C5 (1970).

- Sundararaman, P., *Anal. Chem.* **57**, 2204 (1985).
- Takatsuka, T., Nitta, H., Kodama, S., and Yokoyama, T., *ACS Prepr. Div. Petrol. Chem.* **24**, 730 (1979).
- Takeuchi, C., Fukui, Y., Nakamura, M., and Shioto, Y., *Ind. Eng. Chem. Proc. Des. Dev.* **22**, 236 (1983).
- Takeuchi, C., Asaoka, S., Nakata, S., and Shioto, Y., *ACS Prepr. Div. Petrol. Chem.* **30**, 96 (1985).
- Tamm, P. W., Harnsberger, H. F., and Bridge, A. G., *Ind. Eng. Chem. Process Des. Dev.* **20**, 262 (1981).
- Teichman, D. P., Bridge, A. G., and Reed, E. M., *NPRA Annu. Meet., San Antonio March* (1982).
- Thiele, E. W., *Ind. Eng. Chem.* **31**, 916 (1939).
- Thrash, R. J., and Pildes, R. H., *ACS Prepr. Div. Petrol. Chem.* **26**, 515 (1981).
- Todo, N., Kabe, T., Ogawa, K., Kurita, M., Sato, T., Sihmada, K., Kuriki, Y., Oshima, T., Takematsu, T., and Kotera, Y., *Kogyo Kagaku Zasshi* **74**, 563 (1971).
- Toulhoat, H., Plumail, J. C., Martino, G., and Jacquin, Y., *ACS Prepr. Div. Petrol. Chem.* **30**, 85 (1985).
- Treibs, A., *Angew. Chem.* **49**, 682 (1936).
- Tynan, E. C., and Yen, T. F., *Fuel* **48**, 191 (1969).
- van Dongen, R. H., Bode, D., van der Eijk, H., and van Klinken, J., *Ind. Eng. Chem. Process Des. Dev.* **19**, 630 (1980).
- Van Driesen, R. P., and Fornoff, L. L., *Hydrocarbon Process.* **64**(9), 91 (1985).
- Vanik, S. J., Frayer, J. A., Huling, G. P., and Somers, A. E., *Proc. API Refining Midyear Meet., 42nd* **56**, 384 (1977).
- van Zijll Langhout, W. C., Ouwkerk, C., and Pronk, K. M. A., *Oil Gas J.* **78**(48), 120 (1980).
- Vaughan, G. B., Tynan, E. C., and Yen, T. F., *Chem. Geol.* **6**, 203 (1970).
- Venuto, P. B., and Habib, E. T., Jr., *Catal. Rev. Sci. Eng.* **18**, 1 (1978).
- Vercier, P., Thiault, B., Mouton, M., Colin, J. M., Doligez, Ph., and Allain, A., *ACS Prepr. Div. Petrol. Chem.* **26**, 882 (1981).
- Vrinat, M. L., *Appl. Catal.* **6**, 137 (1983).
- Wales, M., and Van der Waarden, M., *ACS Prepr. Div. Petrol. Chem.* **9**, B-21 (1964).
- Ware, R. A., "Reactivity of Nickel Porphyrins in Catalytic Hydrodemetallation." Sc.D. thesis, M.I.T., 1983.
- Ware, R. A., and Wei, J., *J. Catal.* **93**, 100, 122 (1985a).
- Ware, R. A., and Wei, J., *J. Catal.* **93**, 135 (1985b).
- Webster, I. A., "Catalytic Hydrodemetallation of Nickel Porphyrins: Reactivity and Catalyst Surface Studies." Sc.D. thesis, M.I.T., 1984.
- Wei, J., *J. Catal.* **1**, 526, 538 (1962).
- Wei, J., *AIChE Annu. Meet., San Francisco Pap. No. 28a.* (1984).
- Wei, J., and Hung, C. W., *Ind. Eng. Chem. Process Des. Dev.* **19**, 197 (1980).
- Wei, J., and Wei, R. G., *Chem. Eng. Commun.* **13**, 251 (1982).
- Weisz, P. B., *Adv. Catal.* **8**, 137 (1962).
- Weitkamp, J., Gerhardt, W., Rigoni, R., and Dauns, H., *Erdöl Kohle Erdgas Petrochem.* **36**, 569 (1983).
- Weitkamp, J., Gerhardt, W., and Scholl, D., *Proc. Int. Congr. Catal., 8th* **2**, 269 (1984).
- West, M., Ph.D. thesis, University of California, Berkeley (1984); see also West, M., and Petersen, E. E., *Annu. AIChE Meet., San Francisco, Nov. Pap. No. 109* (1984).
- Wheeler, A., *Adv. Catal.* **3**, 249 (1951).
- Wheeler, A., "Catalysis," Vol. 2. van Nostrand-Reinhold, Princeton, New Jersey, 1955.

- Whetsel, K. B., *Appl. Spectrosc. Rev.* **2**, 51 (1968).
- Williams, R. B., *Am. Soc. Test. Materials, Spec. Tech. Publ.* (224), 168 (1957).
- Wilson, R., and Kivelson, D., *J. Chem. Phys.* **44**, 154 (1966).
- Winniford, R. S., *J. Inst. Petrol.* **49**, 215 (1963).
- Wivel, C., Candia, R., Clausen, B. S., Morup, S., and Topsøe, H., *J. Catal.* **68**, 453 (1981).
- Yamamoto, M. D., *Oil Gas J.* **75**(20), 146 (1977).
- Yen, T. F., *ACS Prepr. Div. Fuel Chem.* **15**, 93 (1971).
- Yen, T. F., *ACS Prepr. Div. Petrol. Chem.* **17**, F102 (1972).
- Yen, T. F., *ACS Prepr. Div. Petrol. Chem.* **18**, 648 (1973a).
- Yen, T. F., In "Trace Substances in Environmental Health" (D. D. Hemphill, ed.), Vol. 6. Univ. of Missouri Press, Columbia, 1973b.
- Yen, T. F., *Energy Sources*, **1**, 447 (1974).
- Yen, T. F., "The role of Trace Metals in Petroleum." Ann Arbor Science Publ., Ann Arbor, Michigan, 1975.
- Yen, T. F., *Energy Sources* **3**, 339 (1978).
- Yen, T. F., and Erdman, J. G., *ACS Prepr. Div. Petrol. Chem.* **7**, 5 (1962).
- Yen, T. F., and Silverman, S. R., *ACS Prepr. Div. Petrol. Chem.* **14**, E32-E39 (1969).
- Yen, T. F., Erdman, J. G., and Pollack, S. S., *Anal. Chem.* **33**, 1587 (1961).
- Yen, T. F., Boucher, L. J., Dickie, J. P., Tynan, E. C., and Vaughan, G. B., *J. Inst. Petrol.* **55**, 87 (1969).
- Yen, T. F., Tynan, C., Vaughan, G. B., and Boucher, L. J., In "Spectrometry of Fuels" (R. A. Fiedel, ed.), pp. 187-201. Plenum, New York, 1970.
- Young, B. J., and Richardson, R. L., *Hydrocarbon Process.* **56**(9), 103 (1977).

This Page Intentionally Left Blank

THE SAFETY MATRIX: PEOPLE APPLYING TECHNOLOGY TO YIELD SAFE CHEMICAL PLANTS AND PRODUCTS

Kent Davis

Director of Personnel and Safety
Dow Chemical U.S.A. Operations
2020 Willard H. Dow Center
Midland, Michigan 48674

I. Introduction	262
A. Failure Modes	265
B. Intellectual Approach to Problem Solving	266
C. Voluntary Standards	268
D. Application to Chemical Engineering Education	270
II. Organization	271
A. Establishing Policy	271
B. Allocating Resources	272
C. Role of Line Management	272
III. Functional Roles	274
A. The Research Role	274
B. The Engineering Role	276
C. The Operations Role	279
D. The Marketing Role	281
IV. Programs and Procedures	281
A. Minimum Requirements	282
B. The Fire and Explosion Index	285
C. Reactive Chemicals	292
D. Loss Prevention Principles	296
E. Operating Discipline	297
F. Technology Centers	299
G. Critical Instruments	303
H. Safety Training	306
I. Audits	310
V. Society's Role	312
A. Legislation	312
B. Judgment of Products	314
C. The Chemical Engineer's Changing Role	315
VI. Summary and Conclusions	316
References	318

I. Introduction

The function of the chemical industry is to turn scientific knowledge into useful products. Like all other human activity, discharging this function requires that companies and people in the industry deal successfully with a wide range of risks. Most of these risks are common to nearly all production activities; some are unique to the chemical industry. The successful chemical plant or laboratory safety program must address both the common risks and those which are unique to it, such as ones which arise out of the reactivity, toxicity, or other hazards inherent in many of the industry's processes and products.

The chemical industry has an excellent record of meeting that challenge. In 1985, the latest year for which national statistics are available, chemical companies reporting to the National Safety Council had a lost-time injury rate of 0.52 injuries per 200,000 hours worked, compared to a rate of 1.98, nearly four times higher, for all U.S. industry (1).

The Dow Chemical Company is an industry leader in safety performance and has been recognized appropriately by its peers with the Lammot DuPont Safety Award four times in the 1980's for its outstanding safety record. This award is presented annually by The Chemical Manufacturers Association to the member companies (grouped by size) with the most improvement in reducing their injury rate compared to the previous three years. The accompanying graphs (Figs. 1 and 2) depict the significant reduction in both serious injuries (DAW injuries) and medical treatment cases (OSHA recordables) over the past ten years for DOW. The reductions are by factors of 4–5 in the time period for both types of injuries.

What are the factors which contribute to this success story? That really is the subject of this chapter and is of importance to both the practicing chemical engineer and the student engineer who is considering a career in the chemical industry.

The Dow Chemical Company believes strongly that the factors are best described by a three-dimensional matrix (Fig. 3) which has as its elements (1) the organization or management; (2) the individual functions such as manufacturing, engineering, research, and marketing; and (3) the safety programs and procedures. The interrelationships and interworkings of the matrix elements are the key factors that drive the process toward improvement. Thus it becomes apparent that what is at work is not a proprietary or unique technology but rather a system which is adaptable to anyone who chooses to apply the necessary discipline continuously and consistently.

Improvement does not come instantaneously as a result of a new insight or design improvement or even an improved procedure or new policy.

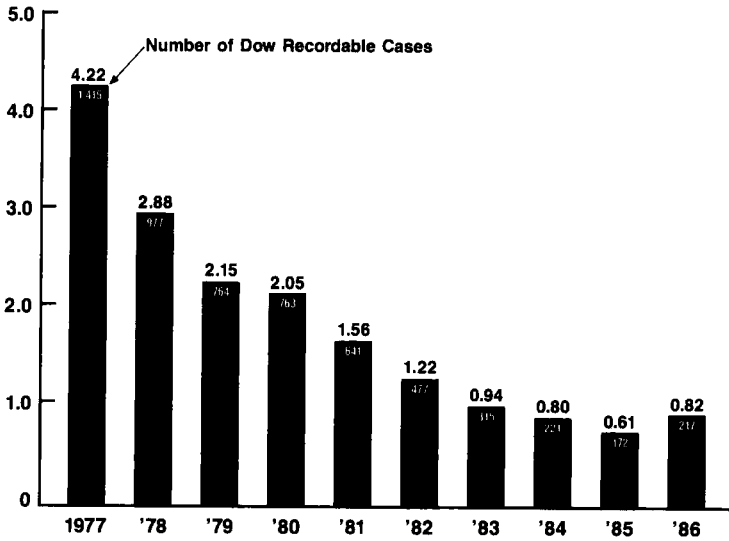


FIG. 1. United State Area Dow recordable case incident rates per 200,000 hours worked.

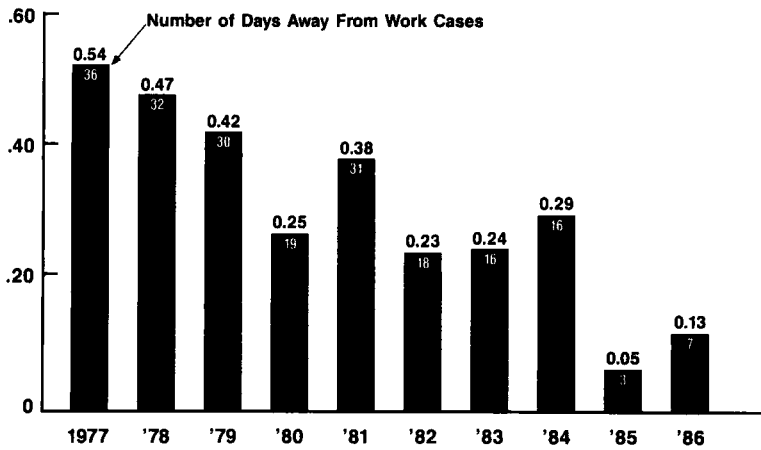


FIG. 2. United States Area days away from work frequency rates per 1 million hours worked.



FIG. 3. Dow safety matrix.

Rather it is the result of a process which starts with any of the above factors, such as a design improvement, which then must be communicated and implemented over a period of time throughout the organization. Dow assures this continuous emphasis through a multifaceted audit program which covers every facility in the company. Several of these audits are described in detail in this chapter.

Most injuries in the chemical industry are similar to those found in other industries and are not uniquely chemically related.

For the year 1986, Dow Chemical U.S.A. experienced 217 OSHA recordable incidents (those involving physical injury which require medical care beyond first aid or work restrictions including lost time) which were classified as follows.

Type	Number	Percentage
Caught in, under, or between	50	23
Falls	26	12
Thermal burns (other than fire and explosion or electrical)	13	6
Sprains, strains, overexertion, or bodily reaction	24	11
Chemical contact	2	1
Struck against or by	80	37
Miscellaneous	22	10
Total	217	100

Physical activities of people in and around plant equipment resulted in most of the injury categories (such as falls, sprains, strains, and so on) and the actual chemical contact is very small (1%)

In spite of the low level of chemical-related incidents, it also must be remembered that incidents involving chemicals potentially could be the most catastrophic in terms of human injury and property damage. The industry prepares for this potential by careful design and with proper procedures for safe operations.

The data presented above are based on criteria established by OSHA and kept by all employers. Dow has long had extensive reporting of its safety performance to all levels of management and employees. Continuous improvement is both a hallmark as well as a company expectation.

Society's expectations play a growing role as an outside influence on the safety matrix. Those expectations are expressed in laws and regulations which affect how and where the chemical industry will produce and market its products, as well as in the reception its products receive in the marketplace.

A. FAILURE MODES

Safety and loss performance in the chemical industry is the result of the interaction of plant design, construction and maintenance with production processes, and trained people applying a well-developed operating discipline. An accident leading to personal injury, property damage, or product loss invariably is the result of the failure of one or more of these elements. Each factor involved in chemical production—equipment, process, product, and people—may be subject to a variety of failure modes which may lead to accidents.

Typical failure modes for a pump (equipment) might include failure to stop or start on command, seal rupture or leak due to corrosion, bearing failure, or loss of electrical power. Process failures might include loss of pressure or vacuum, utilities (electric power, for example), or loss of control resulting in excessive heat or cooling. Failure mode for personnel can encompass the entire range of human reactions, from lack of knowledge to incorrect response, inattention, failing to lock out equipment, or using the wrong tools.

The challenge to the chemical engineer is to identify the failure modes, assess their possible effects, and then take action to prevent or mitigate those effects.

The novice may see the chemical engineer's responsibility as being limited to nonhuman failures. However, most nonhuman failures have their origin in human action, inaction, or misaction, and their effects are mitigated or magnified by human reactions. As Fig. 4 shows, unsafe conditions are present in only half of the accidents resulting in lost-time

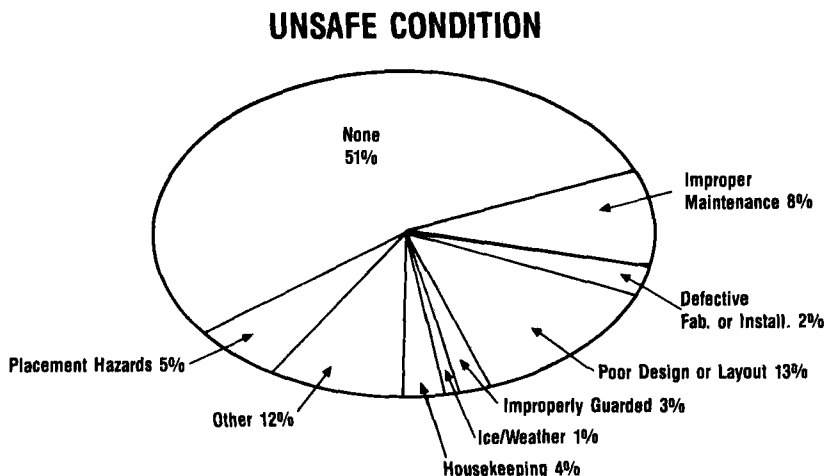


FIG. 4. Presence of unsafe conditions in Dow recordable incidents in 1986.

injuries, and it is possible that human failures could have contributed to those unsafe conditions.

In addition to the need to consider human reactions in designing plants, processes, and equipment, the chemical engineer always will be dealing with people in plant operations. In the chemical industry, most chemical engineers apply their skills in operations, management, safety, loss prevention, and other related activities.

B. INTELLECTUAL APPROACH TO PROBLEM SOLVING

Students of management have developed a variety of standard techniques for problem solving. In general, they are variations on a theme of understanding the problem as completely as possible, identifying possible solutions, evaluating those solutions against previously established criteria, and then adopting the solution which best meets the criteria.

Chemical industry hazards may arise out of the toxicity or reactivity of the chemicals being processed or produced, the plant and equipment design, the process being used, operating and maintenance procedures, or management practices and controls.

Several methods of evaluating chemical industry hazards are summarized in "Guidelines for Hazard Evaluation Procedures," published by The Center for Chemical Plant Safety of the American Institute of Chemical Engineers. Figure 5 outlines the general procedures to be followed.

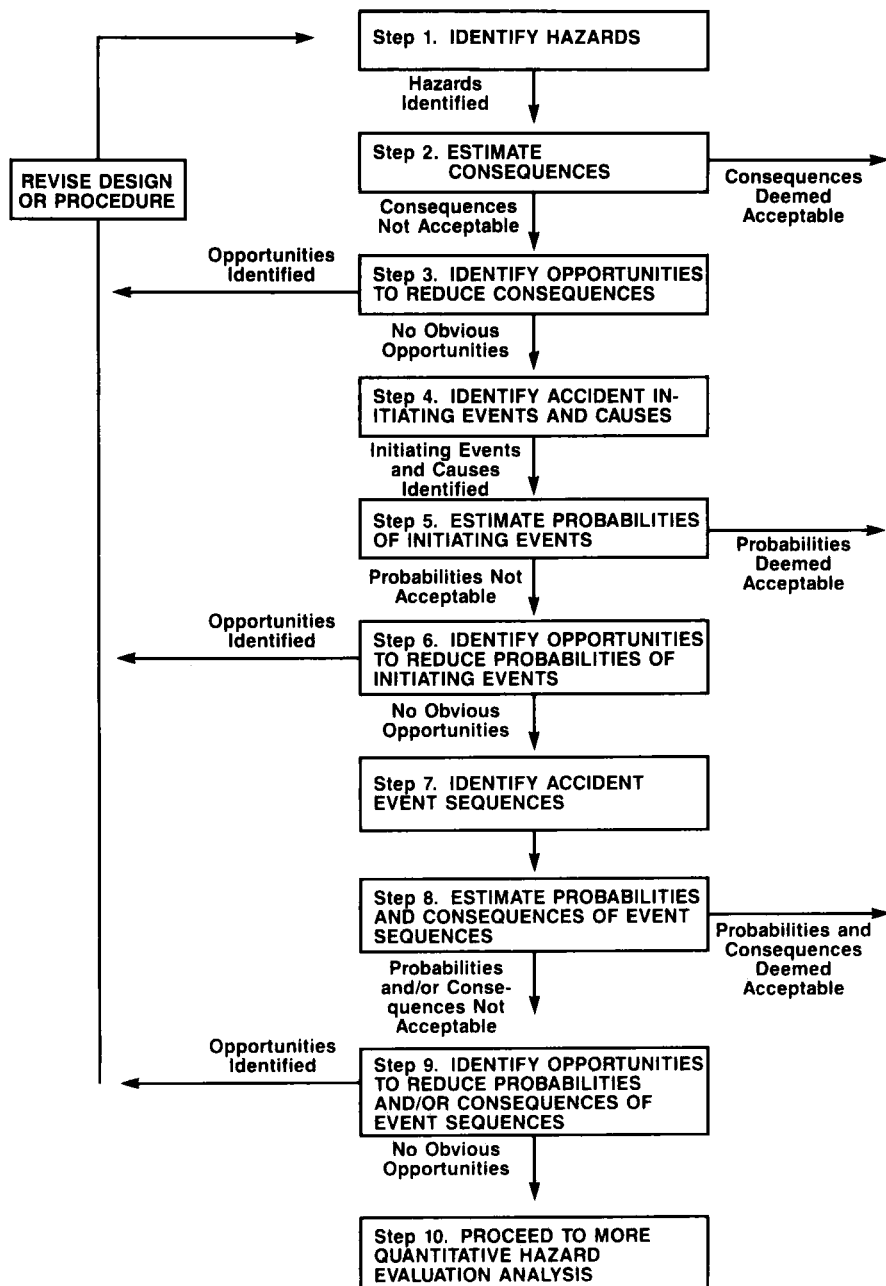


FIG. 5. Steps in a predictive hazard evaluation. (From "Guidelines for Hazard Evaluation Procedures." Copyright © 1985 American Institute of Chemical Engineers.)

The major effort is to identify all hazards in relative terms so that various solutions may be assessed. Accepted solutions are then reflected in design to achieve acceptable levels of exposure or risk.

Several methods are available and in general use such as fault tree analysis (2) and logic diagrams. These procedures require detailed, step-by-step analysis of processes with decision points at appropriate steps such that proper consideration can be given to safety and loss prevention factors. An example of a logic diagram for deciding the necessity of a fire protection deluge sprinkler system is shown as Table I.

The owner of an operation uses "worst case" thinking in evaluating the safety of the operation. At every point where an exothermic reaction may take place, consideration should be given to the worst possible combination of conditions which realistically could exist. This may include such conditions as loss of cooling water, wrong combination of reactants, wrong position of valves, plugged lines, instrument failure, air leakage, loss of agitation, dead-headed pump, mishandled catalyst, and so on. An engineering evaluation is then made of the consequences of worst case conditions.

Potentially serious consequences of a worst case situation may rule out conducting the operation. Usually, adequate means of avoiding the situation and coping with the consequences can be devised. These start with preventive measures, followed by corrective measures, then containment measures and, as a last resort, isolation techniques. Redundancy is essential for protection against reactive chemicals accidents.

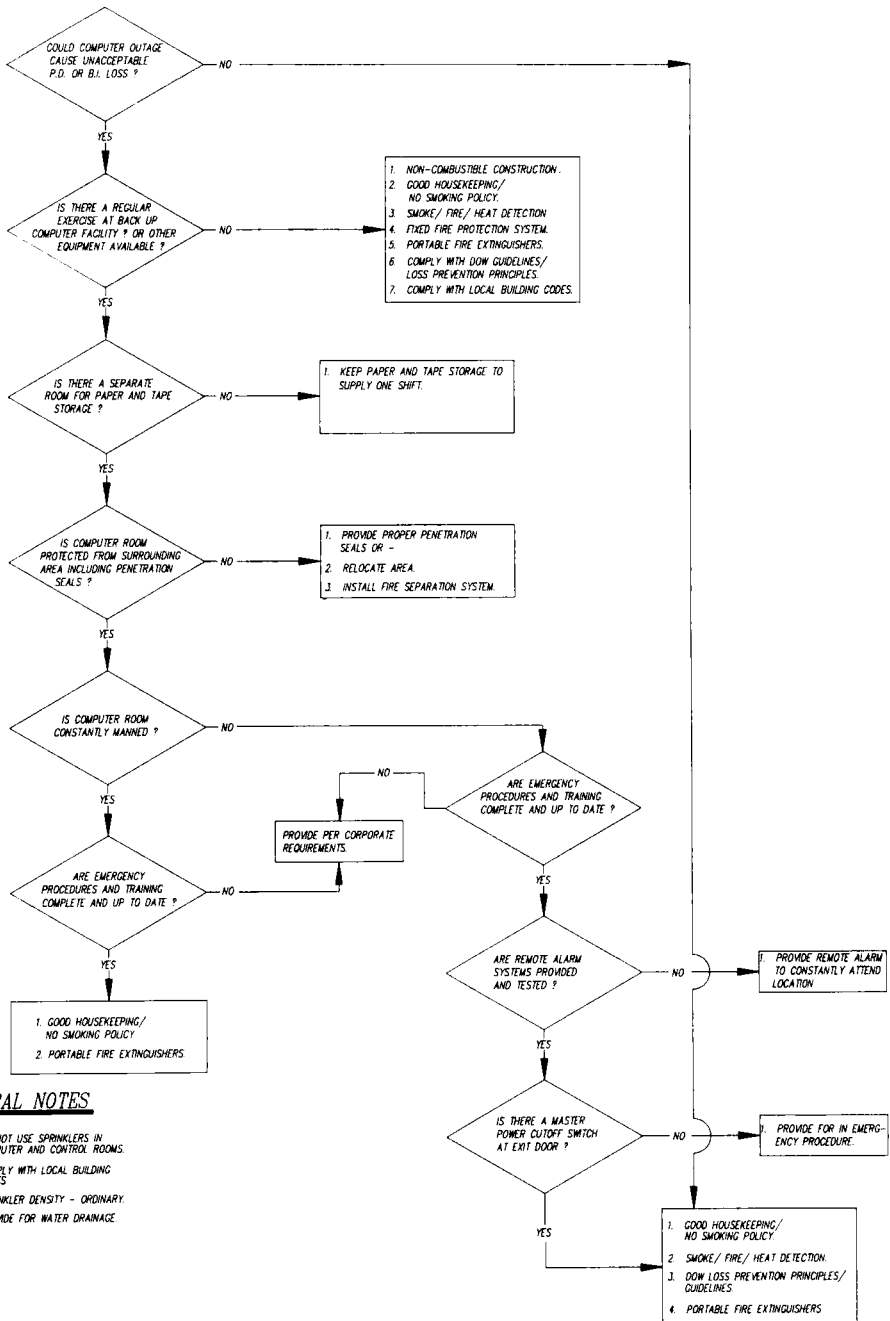
C. VOLUNTARY STANDARDS

Standard setting traditionally has been a function of professional and engineering societies and insurance companies which are in the business of making judgments on the risk being contemplated. Among these groups are:

1. American Society of Mechanical Engineers (ASME)
2. American Petroleum Institute (API)
3. Instrument Society of America (ISA)
4. National Electrical Code (NEC)
5. National Fire Protection Association (NFPA)
6. Associated Factory Mutual Fire Insurance Companies (Factory Mutual)
7. American Society for Testing Materials (ASTM)

TABLE I

LOGIC DIAGRAM TO EVALUATE FIRE PROTECTION NEEDS FOR AN ELECTRONIC COMPUTER SYSTEM



State and local building codes, often based on standards set by one or more of the above groups, have the force of law and must be followed where applicable. While API has published standards covering some storage tanks, the U.S. Environmental Protection Agency is developing standards for underground storage of petroleum and chemical products. This is just one example of the developing societal role in effecting human and environmental health standards. Where EPA or OSHA standards have not yet been developed, the Association of Government Industrial Hygienists sets recommended levels for workplace exposure to hazardous materials.

D. APPLICATION TO CHEMICAL ENGINEERING EDUCATION

Since the chemical industry operates by handling potentially hazardous materials safely, safety has always been an important consideration for chemical engineers. Engineers have never been able to discharge their professional responsibility only by designing efficient equipment or developing efficient processes. Today society has expanded that traditional responsibility to include environmental and community protection. The chemical industry's operations and products should not have an unacceptable impact upon its neighbors, its customers, or the environment.

Just as safety, loss prevention, and environmental protection cannot be separated from other essential chemical plant activities, the practical application to the chemical engineering curriculum could be explained by emphasizing the consequences of poor design which could lead to injury or property damage.

For example, chemical engineering students studying corrosion to learn how various materials of construction may be affected by acids, alkalis, or process conditions in order to select the most economic materials for a particular use would be impacting the safety and loss prevention performance of that equipment because a vessel or pipeline leaking due to corrosion is a hazard to workers in the area. The spilled material may create an environmental hazard as well as a hazardous waste problem requiring special precautions for cleanup and disposal.

The public has a growing interest in the results of the chemical engineer's efforts, such as the safety of chemical plants and chemical processes. Today's chemical engineer might be called upon to explain, in formal testimony and to general audiences, what is needed to assure chemical safety and what is being done to assure it. Such explanations may come in testimony before legislative and regulatory bodies or in talks before community groups. The chemical engineer who is dedicated to designing

and operating safer plants and processes is an asset to the community as well as to the employer and the profession.

The challenge to chemical education is to make it clear that safety and loss prevention are integral considerations in every part of the curriculum.

II. Organization

A. ESTABLISHING POLICY

The Dow Chemical company has developed a formal statement of goals and has identified four core values which guide the company and its employees in achieving those goals. One of these core values states:

Our conduct demonstrates a deep concern for ethics, citizenship, safety, health and the environment.

This concern is confirmed and assured by the role of Dow's board of directors' Committee on Environment, Health and Safety. Established by amendment to the company's bylaws in 1979, the committee consists of four directors (two inside and two outside directors), the Vice President of Health and Environment Services and the Director for Corporate Safety and Services.

Dow's corporate bylaws provide:

The Environment, Health and Safety Committee shall have the authority and the responsibility to assess any and all aspects of the company's decisions that pertain to operating policies and practices at its facilities to determine their impact on worker safety and health and on the environment in and around its facilities and to make recommendations to the board of directors and the management of the company.

The chairman of the committee also has the responsibility and authority to assure that, where Dow products are involved, immediate action is taken anywhere in the world when necessary to protect employees, customers, the public, and the environment.

Dow's safety program had its origins in the 1930s, when Dow had a single manufacturing location in Midland, Michigan. It continues to develop to meet the changing needs of a global company and the changing expectations of society. Today's corporate safety policy is both comprehensive and succinct. It says in part:

Employees of The Dow Chemical Company must perform in such a manner as to prevent accidents which can cause personal injury, illness or loss of proprietary information and Dow facilities must be designed and operated to prevent property loss and interruption to our business.

Every employee is expected to comply with established rules and procedures as a condition of employment and to participate in the Safety, Loss Prevention and Security program. Safety performance and attitude shall be considered major and essential employee job performance measurement criteria.

B. ALLOCATING RESOURCES

Since safety is an integral part of all Dow operations, there is no specific allocation of "resources," that is no specific budget item, for safety programs. Safety expenditures are not defined by the pairs of safety goggles or rubber gloves distributed, nor even the hours spent in safety meetings. The engineer at the drawing board designing a new plant, or in research developing a new process, is working toward safety in chemical operations. A leaking pipeline incurs costs through loss of production efficiency and an increase in maintenance. It also presents a risk to people and the environment. Its repair restores production efficiency and eliminates safety and environmental hazards. Similarly, worker training, which includes working safely, is an operating cost, not a safety cost. It is, therefore, difficult and not productive to attempt to identify one portion of a cost as safety and another portion as something else. Suffice it to say that where safety is a consideration in allocating funds or people, the commitment must be made.

C. ROLE OF LINE MANAGEMENT

Central to Dow's safety policy—and its success—is the principle that safety performance and attitude are major and essential job performance criteria for every job from senior executive to the newest worker in the most remote plant.

However, the policy assigns ultimate responsibility for safety to line management. Even the chairman of the board of directors' Environment, Health and Safety Committee is a line manager as vice president for manufacturing.

Dow's safety policy states:

Safety, Loss Prevention and Security are the direct responsibility of line management and are important measures of managerial performance. In order to insure that every employee is prepared to work safely, every supervisor has the responsibility to provide a safe work environment with proper equipment and adequate training. Each supervisor also has the responsibility, through personal example and the involvement of all employees, to create a climate in which everyone shares concern for the safety and security of their fellow workers and for the prevention of losses.

Line management has a responsibility to monitor and assess all changes in process

technology and work procedures in order to continue to provide a safe, secure work environment.

A Safety, Loss Prevention and Security function is provided by the Company, on a Corporate, Area and location basis, to assist line management in implementing these responsibilities.

In addition to the Safety, Loss Prevention and Security (SLPS) function mentioned in the policy statement above, line management draws on industrial hygiene, medical and environmental management personnel to ensure that operations meet company standards, as well as all legal requirements. Line management also is supported by the activities, programs and procedures described below. However, in each case, the "owner"—the manager or superintendent responsible for the process unit, location, function, or area—is responsible for seeing that staff and program support is used in the manner best suited to the local operation.

It is because of this principle of management responsibility that Dow's "Minimum Requirements" simply specify the elements a safety, loss prevention, and security program must contain, rather than addressing details which may not be relevant to every situation. Other SLPS documents and programs are advisory, except where government laws and regulations are concerned, with final decisions left to the line manager concerned. As an example, managers often find it necessary to review the chemical processes in their units with a Reactive Chemicals Committee. However, the committee's conclusion is a recommendation to the responsible manager, not an order.

Each of the broad, functional areas described later has its own safety responsibilities and is organized to meet those responsibilities. For example, the research function is responsible for safety and loss prevention in research laboratories and pilot plants. However, research also has the duty of identifying potential hazards in the products and processes it develops. The research "owner" must then assure that those hazards are communicated effectively to the engineering, operating, and marketing people who must deal with them.

Since line management carries the responsibility for safety, loss prevention, and security, job performance ratings reflect managerial performance in these matters.

Safety performance also can affect other elements in periodic job performance ratings. Corporate insurance policies in the chemical industry typically include large self-insurance factors—"deductibles"—which are in the millions of dollars. Any losses which fall within this self-insurance limit are charged to the unit involved. This affects the unit's costs and profitability, also major factors in evaluating the manager's job performance.

III. Functional Roles

The separate functions of research, engineering, operations, and marketing are described briefly in this section. The purpose is to provide an overview which helps to explain their relationships within the matrix as opposed to delineating the distinctive aspects of each.

The impact of the matrix on safety in industry shows up most clearly in an examination of the roles of the basic industrial functions: research, engineering and operations, and marketing. The effective interaction of these functions is absolutely essential to chemical plant safety and loss prevention.

Research provides the basic information needed for safe manufacture and marketing of products, especially of potentially hazardous products from chemical and other industries. Engineering designs the plants in which those products can be produced safely. Operations brings research and engineering together with plant operators and supervisors to assure safe manufacturing of chemicals. Marketing extends that knowledge to help customers use potentially hazardous products safely.

A. THE RESEARCH ROLE

Research is the orderly search for knowledge aimed at the discovery and interpretation of facts. It is, of course, the traditional source of new chemical products.

Chemical engineers look to research for information on the characteristics of chemicals and materials that affect process and plant design. For example, viscosity is one determinant of pumping capacity and pipeline dimensions. Laboratory-determined corrosivity of a product and corrosion-resistance of materials help the designer select materials to be used in process equipment. Research also is called upon to determine the temperatures and pressures of reactions, which are factors in materials selection and equipment and plant design. Finally, research must provide the knowledge of toxicity and other hazards essential to producing and handling chemicals safely.

Much of the role assigned to applied research is the result of experience. This is particularly true of the research role in safety and loss prevention. Experience has shown that we must have certain knowledge in order to produce a chemical safely; research is assigned to develop that knowledge before the chemical goes into production.

The matrix is truly interfunctional; manufacturing and marketing provide the real-world experience to help determine exactly what knowledge research should investigate and how engineering should design for it. The environment, health, safety, and loss prevention performance of the chemical industry reflects the effectiveness with which the functional elements of the matrix interact.

The early chemical industry was concerned with acute hazards that were readily identified: If a liquid burned the skin or if fumes caused choking and gasping, the effect quickly became obvious and rubber gloves or respirators were used. The next step, which began at Dow in the mid-1930s, was to ask research to determine safe levels of exposure for workers in chemical plants, before a new chemical or process was put into production. Experience has taught the industry to be concerned with the possibility of less obvious adverse effects, including effects not detectable through casual observation.

Some of that experience has been enacted into laws and regulations. For example, today the law requires that many chemicals be proven "safe" for their proposed use before they can be marketed. Thus the research organization may be asked to develop information on acute, subacute, and chronic effects of human exposure to a new or old chemical product. Data also frequently are called for on the effects of exposure on wildlife and the environment and on the routes and metabolism of a chemical in the environment.

The research role in safety and loss prevention goes far beyond identifying hazards. Research is instrumental in the discovery of less hazardous materials and in the development of less hazardous processes. For example, research at Dow led to a new processing technique which reduced the hazard of a process by reducing the maximum inventory of instantaneously hazardous materials. (See more detailed description in Ref. 3.) While inventory itself is rarely the source of an accident, the severity of human injury and property damage is largely determined by the quantity of hazardous materials released by the incident.

The development of the new process also affirms Dow's position that safety is inseparable from other elements of chemical operations. The new process provides increased productivity and quality as well as safety.

An important, safety-related role of research is reactive chemicals testing (4). At Dow, Research and Development has the responsibility of determining the potential hazards of chemicals and mixtures. (See further discussion in Ref. 3.)

B. THE ENGINEERING ROLE¹

The purpose of this discussion is to highlight areas of chemical plant design and engineering which experience has shown are most vulnerable to safety and loss incidents and to suggest some factors the designer should consider to reduce that vulnerability. Future experience, as well as the experience of others, may identify other areas of vulnerability. The reader should not assume that addressing the concerns raised here discharges the engineer's responsibility for the inherently safer chemical plant.

It has become popular in the past few years to talk about the "inherently safe" chemical plant. Using the dictionary definition of "inherent," such a plant would be safe regardless of other forces, including the actions of humans.

A far more realistic goal is the "inherently safer" plant. Such a plant is designed to assure that it can be operated safely and so as to minimize the effects of any accidents which do occur. The object is to design a plant which *can* be safe; the people who will operate and maintain it largely determine whether it *will* be safe.

Design techniques for an inherently safer plant include improved layouts, inventory reduction, and process improvements.

Layout improvements include separation of hazardous areas to eliminate a potential "domino effect" in fires and explosions; separation of hazardous materials processing, storage, and handling from control rooms and offices to minimize the exposure of people to safety and loss incidents; and provision of adequate access for emergency vehicles and personnel evacuation. They also encompass long-term planning so that process and storage areas are not likely to be near areas where the public will congregate or live.

Inventory reduction may involve simply reducing the quantity of hazardous materials on hand at any time, including producing hazardous materials as needed rather than storing them against future need.

Process improvements may reduce hazards in a number of ways. Improvements including altering process pressure or temperature, changing materials handling methods and instrumentation, and so on.

Computer-controlled operation is becoming the standard in the chemical industry. Computer control makes it possible to measure more variables and get more process information than ever before. When necessary, the computer also can react more quickly and precisely to change process variables. Computer operation, with adequate redundancy, makes a major contribution to the inherently safer chemical plant.

¹ Much of the material in this section is based on Ref. 3.

In summary, the inherently safer plant is user-friendly. Its design takes maximum advantage of the accumulated experience of the chemical industry and takes into consideration the fact that people must operate and maintain it. It is built so that opportunities for plant and people failures are minimized, so that the effects of those failures which do occur are minimized, and so that the effects of failures can be mitigated readily through adequate facilities and access for emergency response.

All projects must be reviewed in the beginning as well as at various stages of preliminary design so that process alternatives and emergency planning become part of the design process. Reviewers should include people knowledgeable about manufacturing, reactive chemicals, process safety, and loss prevention. Dow achieves this multidisciplinary approach through the use of project teams whose members have the appropriate skills and backgrounds.

1. *General Design Factors*

Englund (Table II) has identified the major general opportunities in the design of inherently safer chemical plants. (See more detailed explanation in Ref. 3.) Many of these factors are addressed in Ref. 5. Other Dow programs, including "Minimum Requirements," are as essential to plant design and construction as to operations.

Spacing between plant units is important in limiting damage from fires, explosions and gaseous or liquid releases. Proper spacing also provides adequate access for repair and emergency equipment as well as for evacuation in the case of accidents.

TABLE II

GENERAL DESIGN OPPORTUNITIES FOR INHERENTLY SAFER CHEMICAL PLANTS^a

Clear responsibility for safety in design and operation
Critically review alternatives early in design
Incorporate emergency planning into original plant design
Provide adequate spacing of process plants, tanks, and roads
Use minimum storage inventory of hazardous materials
Design liquid storage so leaks and spills do not accumulate under tanks or process equipment
Use open structures for plants using flammable or combustible materials
Avoid buried tanks
Construct process and storage areas so they are not close to residential areas or potential residential areas
Design for total containment
Redesign obsolete plants before accidents occur
Store liquefied gases at low temperatures and pressures

^a Source: Englund (3).

Buffer zones separating relatively hazardous operations from neighboring residential, commercial, or industrial properties also are important. The human toll in the Bhopal disaster was magnified by the fact that a town had been allowed to grow up at the plant's boundary.

Various standard-setting groups, including NFPA and Factory Mutual, provide guidance for separation of potentially hazardous equipment and processes. Dow achieves adequate spacing between critical process units, and between Dow installations and neighboring properties, by applying the Dow Fire and Explosion Index and a Chemical Exposure Index.

2. *Process Design Factors*

Process design, the primary province of the chemical engineer, is the heart of the inherently safer chemical plant. Englund has listed the major considerations in process design in Table III and discusses them in more detail in Ref. 3.

3. *Equipment Design Factors*

Numerous developments in mechanical equipment, piping, control systems, and electrical systems have contributed to the design of safer chemical plants. However, they also have made the designer's job more difficult. With so many choices, how is the designer to choose the best one?

It is not possible for today's designer to be an expert in every field. Making the right choice among a myriad of options requires recourse to plant experience, technical experts, literature, laboratory testing, and judicious evaluation of vendor information.

Key guidelines for equipment design are shown in Table IV and are discussed in more detail in Ref. 3.

TABLE III

PROCESS DESIGN OPPORTUNITIES FOR INHERENTLY SAFER CHEMICAL PLANTS^a

Understand the reactive chemicals and reactive chemicals system involved
Minimum inventory by changes in chemistry
Minimum inventory by changes in mixing intensity
Low inventory distillation processes
Minimize inventory in heat exchangers
Reduce the possibility of losses from dust explosions
Substitute less hazardous materials in processes, transportation, and storage
In <i>situ</i> production and consumption of hazardous materials
Incineration to dispose of hazardous materials

^a Source: Englund (3).

TABLE IV

EQUIPMENT DESIGN OPPORTUNITIES FOR INHERENTLY SAFER CHEMICAL PLANTS

Avoid catastrophic failure of engineering materials
Adequate redundancy of instrumentation and control systems
Properly designed relief systems, taking into account two phase flow and reactions if appropriate
Provisions for safe and rapid isolation of piping systems and equipment
Use piping, gaskets, and valves that take advantage of modern technology
Use strong vessels to withstand maximum pressure of process upsets
Avoid inherently unsafe equipment
Use pumps suitable for hazardous service

C. THE OPERATIONS ROLE

Operations is the term used at Dow to describe all the activities involved in manufacture and distribution of chemicals. The wide-ranging scope of activities from raw materials acquisition and handling, through chemical processing and finally to making delivery to the user encompasses most of the facilities as well as the people in the chemical industry. Operations bears the responsibility for implementing the product and process developments conceived in research and making them into materials which can be economically delivered. Similarly, operations is called on to respond to an everchanging competitive marketplace and be able to produce the quality and quantity of goods which meet the customers needs.

The combination of a large percentage of company assets (people and process facilities) required for the operations function necessitates a correspondingly significant expenditure of effort toward the safe use of these assets. All the programs and procedures described in the next section (e.g. reactive chemicals, critical instruments, loss prevention principles) have been developed through experience gained from operations over many decades. Research, engineering, and marketing are all called on to participate in developing the programs as experience dictates need, but the actual implementation ultimately occurs in operations.

Some examples of the variety of activities which operations oversees can be helpful in understanding this multifaceted role and some of the safety and loss prevention considerations. A magnesium producing facility has been in operation for over 20 years reacting lime with magnesium in seawater to precipitate magnesium hydroxide which is subsequently reacted with HCl to produce magnesium chloride. Finally, a purified MgCl_2 is fed to an electrolytic cell to produce the magnesium metal. Economic considerations dictate a change to dolomite (equimolar CaCO_3 – MgCO_3) as a raw material. Operations will be required to work closely

with process research to understand the differences required to process an alternate raw material. In addition, the engineering staff will incorporate process equipment changes to accommodate the new raw material, and operations personnel will train the plant operators and revise the procedures which must be changed.

This example illustrates the broad role which is part and parcel to the operations function in the matrix. It is not possible to overemphasize the interconnection between elements of the matrix in achieving the desired results of safe production and handling of chemicals.

At the same time it would not be useful to attempt to define a functional role which is exclusively operations or research or engineering. The success of the system lies in making the matrix work by coordinating the functional expertise of each area.

In addition to the training and implementation roles described in Section IV, line management has the following safety-related responsibilities.

1. Assure that environment installations, including air and water pollution control devices, waste treatment plants, and waste disposal facilities are properly installed, maintained, and operated so that the conditions of federal and state operating permits are met.

2. Assure that plant equipment is properly maintained so that it can be operated safely.

3. Assure that firefighters and other emergency response personnel are trained, equipped, and available to react promptly and correctly to emergency incidents arising in the plant.

4. Communicate information on safety and loss-related incidents promptly to others within Dow who need to know about the incident or who can benefit from learning about its causes.

5. Work with emergency response personnel and the public in plant communities to assure preparedness in the event of a chemical-related emergency.

6. Provide trained, equipped emergency response personnel to assist in dealing with transportation incidents involving the plant's product.

7. Work with marketing, customers, warehousemen, truckers, and other carriers to help assure that hazardous materials are stored, transported, used, and disposed of safely.

Unique, though not exclusive, to the operations function is the concept called *operating discipline* (see Section IV, E). Incorporated in this idea is the systematic accumulation of all operating experience such that mistakes will not be repeated. Any change, no matter how small, requires reassessment of its impact on the operating discipline.

In summarizing the operations role in the safety matrix, the elements of organization, function, and programs come together to manufacture and transport the chemicals which are the reason for the industry's existence.

D. THE MARKETING ROLE

The concept that chemical marketers have a role in chemical safety and loss prevention may seem remote. However, as pointed out above, some chemical products may present hazards which are not obvious to those who may handle, use, or otherwise be exposed to such products. Marketers are the link between the producers and users of chemicals. Thus they are the logical channel between those who know the hazards of individual chemicals and the users who need to know in order to handle them safely.

In some cases, product labels and hazards to consumers. Warning statements may be indicated by prudence or required by law. For example, agencies such as the U. S. Food and Drug Administration or the Environmental Protection Agency may require that detailed instructions and warnings accompany products which they regulate.

In other cases, products may be restricted for sale only to (or at the request of) those who are trained to use them properly. Thus consumers can purchase some medicines only when the medicines are prescribed by a physician. Some agricultural chemicals are classified as "restricted" pesticides because of the hazards they pose. These products can be sold and used only under the direction of a certified pesticide applicator, a person who is certified as trained and knowledgeable about hazardous pesticides.

Other chemicals, too, should be sold to or handled only by people who are trained and equipped to handle and use them safely. Dow's Product Stewardship Program works to assure that handlers and users of Dow products are aware of specific hazards and are trained and equipped to handle them.

IV. Programs and Procedures

Programs and procedures were defined earlier as one element of the matrix which underlies safety in the chemical industry. The terminology used to describe programs will vary from company to company throughout industry. In this chapter, the programs are designated as they known in The Dow Chemical Company. Experienced engineers will be able to identify comparable programs from the text. Dow's programs and procedures are experience-driven. They are synthesized from knowledge

developed and experience gained within Dow and outside of it (both within the chemical industry and outside of it). All of Dow's safety and loss prevention related programs are subject to revision when new experience makes it desirable. For example the "Fire and Explosion Index" is now in its sixth edition.

The Dow Chemical Company is engaged in research and development, manufacture, and distribution of thousands of chemical products. Production takes place in more than 330 process units at 118 locations in 30 countries. Distribution takes place through dozens of warehouses and via thousands of miles of railroad, highways, and sea lanes. Hazards vary from site to site, process unit to process unit, and even carrier to carrier. People differ even more widely. Vulnerability to injury—human, property, and environment—truly is infinitely variable.

It is impossible to write programs or procedures which are appropriate for universal application in such a diverse environment. Ultimately, the detailed decisions about safety and loss prevention have to be made by the responsible person on the scene—the person Dow refers to as the "owner."

In most cases, Dow's corporate programs and procedures achieve universal application within the Dow environment by being guidelines not directives. They call attention to the need to comply with pertinent laws, regulations, and standards where such criteria exist.

But they go much further to synthesize experience throughout Dow, the rest of the chemical industry, and wherever relevant experiences may be found. This synthesis helps managers identify elements which must be addressed to achieve the Dow core value:

Our conduct demonstrates a deep concern for ethics, citizenship, safety, health and the environment.

Each line manager, whether president of the U. S. Area or superintendent of a Chlor-Alkali plant in Brazil, adapts these corporate guidelines appropriately for his or her responsibility. Corporate programs and procedures do not relieve line management of responsibility, but help line management meet it.

A. MINIMUM REQUIREMENTS

The heart of Dow's safety and loss prevention program is summarized in "Minimum Requirements for Safety, Loss Prevention and Security." Like other elements of safety and loss prevention, "Minimum Requirements" is revised as experience indicates revision is desirable.

“Minimum Requirements” is presented as the basis upon which areas and their respective units can build their own specific programs. The 20-page document is published over the signatures of corporate management and the presidents of the six geographic areas into which Dow is organized.

It bears the message:

We believe these *Minimum Requirements* are important, and we expect compliance as a way of life to assist in achieving the Company’s goals of providing a safe workplace for each of its employees and of protecting its plants and property.

Where existing facilities do not meet these requirements, it is expected that a plan for compliance will be developed and implemented with a firm time commitment to Management.

“Minimum Requirements” contains a statement of policy and a list of specific requirements in three sections, “Safety,” “Loss Prevention,” and “Security,” plus a section on “Other Related Safety, Loss Prevention and Security Requirements.” The latter section addresses distribution emergency response, industrial hygiene and medical programs, material hazard identification, and product stewardship.

The “Minimum Requirements” are supported by guidelines which address individual topics and by reference to appropriate standard-setting and regulatory organizations.

1. *Safety*

Each location is required to establish a safety program designed to maintain a safe and healthy work environment for employees. This safety program must incorporate the following elements.

1. Accident/incident investigation and reporting
2. Regular internal and external safety audits
3. Employee training and job operating instructions
4. Compliance with government regulations
5. Personal protective clothing and equipment
6. Safe operation of motor vehicles and motorized handling equipment
7. Testing of emergency alarms and protective devices
8. Safety standards for contractors and subcontractors
9. Written job and process operating procedures
10. Safe entry into tanks, vessels, and other confined spaces
11. De-energizing, lockout, and red tag procedures for work on power driven equipment
12. Guarding and interlocking of mechanical and other equipment where appropriate

13. Rules controlling smoking and hot work
14. Rules covering safe use of ladders, scaffolding and so on
15. Safe line and equipment opening operations

2. *Loss Prevention*

Each Dow location is required to establish a loss prevention program base on hazard evaluation and designed to reduce the probability and magnitude of incidents. Programs must include the following elements, based on criteria and guidelines contained in Dow's "Loss Prevention Principles."

1. Building and structure design and separation
2. Capital project review for safety, loss prevention, and security, including reactive chemicals and industrial hygiene
3. Handling of combustible dusts
4. Electrical installations
5. Emergency planning, including coordination with local community and industrial neighbors
6. Equipment and piping conformity with standards and Dow and governmental requirements
7. Adequate burner management and combustion control systems
8. Fire protection systems and firefighting capability
9. Handling of flammable liquids and gases
10. Instrumentation, including redundancy and failsafe and emergency controls
11. Leak and spill control/containment
12. Control of flexible joints and fragile devices in hazardous service
13. Adequate means of emergency exit with regular drills to assure prompt escape of occupants in case of an emergency
14. Pressure vessel design
15. Protection of process computers and data handling equipment
16. Monitoring of rotating equipment
17. Storage of flammable, toxic, combustible, or corrosive materials

In addition, the "Minimum Requirements" mandate that each location have an appropriate Reactive Chemicals Program, and apply "Fire and Explosion Index" guidelines to evaluate the hazard potential of all processes. Each production unit also is required to use the minimum safety and loss prevention guidelines as developed by the Technology Center for its particular process. Where no technology center exists for the subject plant, process technology guidelines or the best available Dow technology are used.

B THE FIRE AND EXPLOSION INDEX

Dow's Fire and Explosion Risk Analysis Program provides a step-by-step, objective evaluation of the realistic fire, explosion, and reactivity potential of process equipment and its contents. The procedure allows calculation of the damage that would probably result from, and the areas which could be exposed to, fire or explosion generated in the process unit being evaluated. Management can then decide unit spacing needed to protect people from injury and to keep potential property and equipment damage to acceptable levels.

The first edition of Dow's "Fire and Explosion Index (F&EI) Guide," published in 1964, was based on the Factory Mutual "Chemical Occupation Classification Guide." As experience has been accumulated and evaluated, the Dow guide has gone through several revised and expanded editions. The current sixth edition was published in May 1987. It draws on NFPA 325M and 49.

The F&EI program is a step-by-step objective evaluation of the realistic fire, explosion, and reactivity potential of process equipment and its contents. The quantitative measures employed in the analysis are based on historic loss data, the energy potential of the material under study, and the extent to which loss prevention measures are currently applied. A toxicity factor is included to recognize the presence of toxic materials which can complicate the response of emergency personnel, thereby reducing their ability to investigate or mitigate damage during an incident. Figure 6 is an outline of the F&EI calculation procedure.

1. *Pertinent Process Units*

For the purposes of the "F&EI Guide" a process unit is defined as any primary item of process equipment. For example, in the process area of a styrene/butadiene latex plant, process units could include monomer mix feed preparation, reactors, strippers, monomer recovery, aqueous room, and styrene scrubber. A warehouse also may be treated as a process unit. In particular, materials stored within a fire-walled area, or within the total storage area where fire walls are not provided, would constitute such a process unit.

The F&EI assumes that a process unit handles a minimum of 5,000 lb or about 600 gal of a flammable, combustible, or reactive material. If less materials is involved (in a pilot plant, for example), the risk will be overstated.

Most plants have many process units. However, only those units that could have an impact upon the process from a loss prevention standpoint should be evaluated.

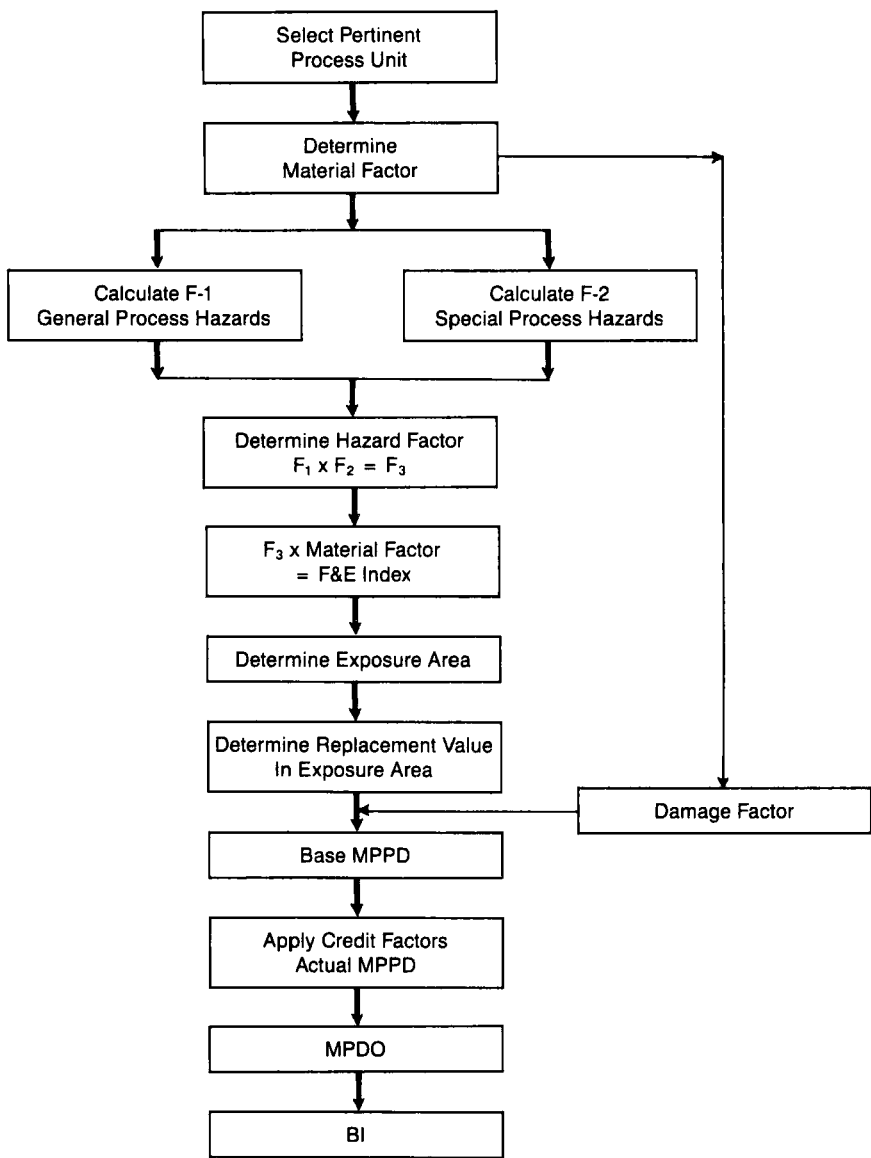


FIG. 6. Procedure for calculating unit hazard factor F&E index.

Important factors for selecting these pertinent process units include:

1. Chemical energy potential (material factor)
2. Quantity of hazardous material in the unit
3. Capital density (dollars per square foot)
4. Process pressure and process temperature
5. Past history of problems that could be conducive to a fire or explosion incident

The destruction of scarce, critical, or one-of-a-kind equipment in or near a process unit could create many days of downtime, even with minimal fire or explosion damage. This potential for high losses due to business interruption might qualify such equipment as a pertinent process unit for evaluation.

Careful consideration is needed when equipment is arranged in series and the items are not effectively isolated from each other. An example would be a reaction train without an intermediate pump. In such situations, the type of process determines whether the whole train or just a single vessel should be considered as the process unit.

It is also important to give careful consideration to the state or stage of the operation. Normal stages, such as start-up, steady-state operation, shutdown, filling, emptying, adding catalyst, and so on, often create unique conditions that have an impact on the F&EI. Occasionally more than one stage will have to be studied in determining the significant risk.

2. *The Material Factor*

The material factor (MF) is the basic starting value in computation of the F&EI and other risk analysis values. It is a measure of the intrinsic rate of potential energy release from fire or explosion produced by combustion or other chemical reaction. The MF is obtained from N_f and N_r , NFPA "signals" expressing flammability and reactivity (or instability), respectively. The values for many materials are found in NFPA 325M or NFPA 49. Dow has developed values for additional materials and published them as an appendix of the "F&EI Guide."

Where published values are not available, the N_f of liquids and gases is developed from flash point data and the St of dusts or mists is determined by dust explosion testing. The N_f combustible solids depends upon the nature of the material as described in the left column of Table V.

The reactivity value is obtained by using the peak temperature of the lowest differential thermal analysis (DTA) or differential scanning calorimeter (DSC) exotherm value as shown in column 2 of Table VI. Alternatively, it can be obtained from a qualitative description of the instability (or

TABLE V
MATERIAL FACTOR DETERMINATION GUIDE

Liquids and gases flammability or combustibility ^a	NFPA 325 m or 49	Reactivity or instability				
		$N_r = 0$	$N_r = 1$	$N_r = 2$	$N_r = 3$	$N_r = 4$
Noncombustible ^b	$N_f = 0$	1	14	24	29	40
F.P. > 200°F	$N_f = 1$	4	14	24	29	40
200°F > F.P. \geq 100°F	$N_f = 2$	10	14	24	29	40
F.P. < 100°F, B.P. \geq 100°F	$N_f = 3$	16	16	24	29	40
F.P. < 73°F, B.P. < 100°F	$N_f = 4$	21	21	24	29	40
Combustible dust or mist ^c						
St-1($K_{St} \leq 200$ bar m/sec)		16	16	24	29	40
St-2($K_{St} = 201-300$ bar m/sec)		21	21	24	29	40
St-3($K_{St} > 300$ bar m/sec)		24	24	24	29	40
Combustible solids						
Dense, ^d > 40 mm thick	$N_f = 1$	4	14	24	29	40
Open, ^e < 40 mm thick	$N_f = 2$	10	14	24	29	40
Foam, fiber, powder, etc. ^f	$N_f = 3$	16	16	24	29	40

^a Includes volatile solids.

^b Will not burn in air when exposed to a temperature of 1500°F for a period of 5 min. F.P. = flash point, closed cup; B.P. = boiling point at standard temperatures and pressure (STP).

^c K_{St} values are for a 16 liter or larger closed test vessel with strong ignition source. See NFPA 68, "Guide for Venting of Deflagrations."

^d Includes wood 2-in. nominal thickness, magnesium ingots, tight stacks of solids, and tight rolls of paper or plastic film. Example: Saran Wrap.

^e Includes coarse granular material such as plastic pellets, rack storage, wood pallets, and nondusting ground material such as polystyrene.

^f Includes rubber goods such as tires and boots. Styrofoam brand plastic foam and fine material such as Methocel cellulose ethers in dust/leak-free packages.

TABLE VI
DETERMINING REACTIVITY FOR CHEMICALS NOT LISTED IN NFPA 325M OR NFPA 49^{a,b}

N_r	Exotherm (°C)	Qualitative description
0	400	Substance is completely stable, even when heated under pressure
1	305-400	Mild reactivity upon heating with pressure
2	215-305	Significant reactivity, even without heating or pressure
3	125-215	Detonation possible with confinement
4	125	Detonation possible without confinement

^a Exotherm is the peak temperature of the lowest differential thermal analysis or differential scanning calorimeter exotherm value.

^b Exceptions: (1) If the exotherm peak results in $N_r = 4$, but the substance, mixture, or compound is not shock-sensitive, make $N_r = 3$. (2) If the substance or compound is an oxidizer, increase N_r by one (but not over $N_r = 4$). (3) Any shock-sensitive material must be $N_r = 3$ or $N_r = 4$, depending on exotherm temperature. (4) If the N_r obtained seems inconsistent with known properties of the substance, mixture, or compound, additional reactive chemicals testing should be done.

reactivity with water) of the substance, mixture, or compound at ambient temperatures as shown in column 3 of the table.

Mixtures can be troublesome under certain conditions. Normally, the material factor should be based on the initial reactive mixture which fits the description of "most hazardous material present during a realistic operating scenario."

Mixtures of solvents or of a solvent with a reactive material can also create troublesome situations. Generally, the MF for such mixtures should be obtained from reactive chemical testing data. However, if reactive chemical testing data is not available, a satisfactory approximation can be obtained by using the MF of the component with the highest MF value.

A particularly troublesome mixture is the "hybrid," a mixture of combustible dust and flammable gas which can form an explosive mixture in air. Dow requires that reactive chemical testing be employed to determine the proper MF in this unique situation.

It is important to recognize that the MF represents the hazard of the selected material at ambient temperature and pressure. The effects of temperature and pressure above ambient may require adjustment of the material factor.

3. *The Unit Hazard Factor*

The unit hazard factor is the product of the general process hazards factor and the special process hazards factor. It is a penalty determined by reviewing values assigned to each of the contributing hazards identified in Table VII. Each item listed is considered to be a factor contributing to the development or escalation of an incident which could cause a fire or explosion. General process hazards are factors that play a primary role in determining the magnitude of a loss incident. Special process hazards are factors that contribute primarily to the probability of a loss incident. They

TABLE VII

PROCESS HAZARDS CONTRIBUTING TO FIRE AND EXPLOSION INCIDENTS

General process hazards	Special process hazards
Exothermic chemical reactions	Toxic materials
Endothermic processes pressure	Sub-atmospheric
Material handling and transfer	Operation in or near flammable range
Enclosed or indoor process units	Dust explosion
Access relief pressure	
Drainage and spill control	

consist of specific process conditions that experience has shown to be major causes of fire or explosion incidents.

The penalties comprising the unit hazard factor are calculated based on a single, specific instant in time during which the material represented by the MF is associated with the process unit in the most hazardous state of operation. Start up, general operation, and shut down are among the operational states that should be considered.

4. Area of Exposure

The area or radius of exposure to damage from a loss incident can be calculated by multiplying the F&EI by 0.84 or by using Fig. 7. People and

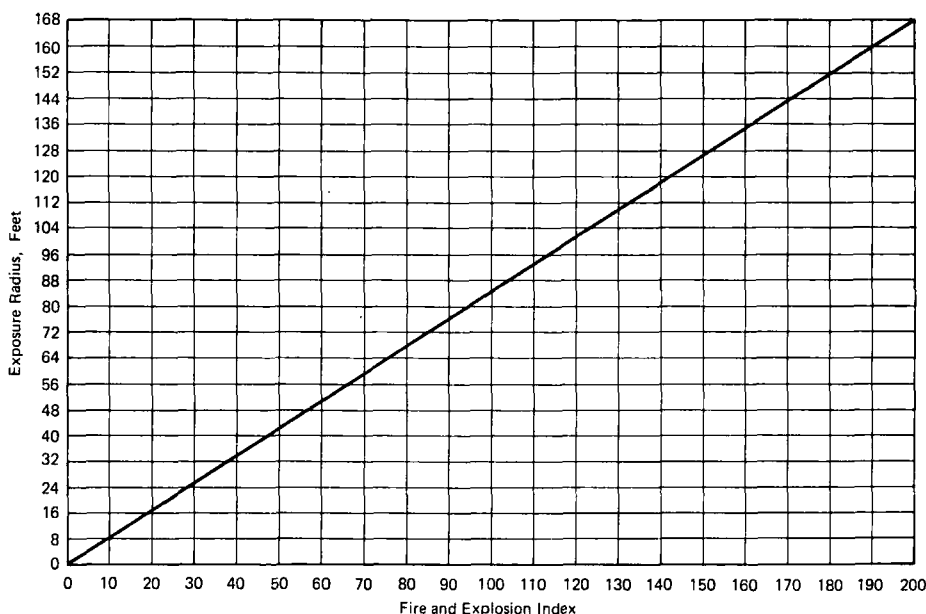


FIG. 7. Relationship of area(radius) of exposure to F&E index. The exposure radius represents an area of exposure—the area containing equipment that could be exposed to a fire or to a fuel–air explosion generated in the process unit being evaluated. It is typically a cylindrical volume of plant area surrounding the process unit. This volume is expected to be the amount of plant at risk in the event of a fire or explosion caused by an incident in the process unit under study. It is recognized that a fire and/or explosion incident does not spread out into a perfect circle producing equal damage in all directions. The actual damage can be affected by positioning of the equipment, wind direction, and drainage layout, all of which are important factors influencing loss prevention designs. However, the circle affords a good basis for later calculations of values.

property within this radius are considered to be at risk. However, the area of exposure may be modified by certain considerations.

If the area of exposure is external to but includes walls or buildings that are resistant to fire or explosion or both, the building may not be at risk. In general, the risk of explosion may exist when a significant quantity of material is being processed above its flash point.

The entire area of a single building containing a process unit is considered to be an exposure area unless various parts of the building are separated from each other by vertical fire walls. If the risk of explosion exists, the entire building is considered to be an exposure area, even if its parts are separated by fire walls.

A multistory building containing fire-resistant floors would be divided into exposure areas by floor levels.

Fire-resistant walls are an adequate barrier to exclude a building from fire exposure penalties if the fire source is external. However, a fire-resistant wall is not an adequate barrier where an explosion hazard exists.

Blast resistant walls are adequate for establishing the boundary of an area of exposure provided the protection from blasts is oriented in the correct direction.

The replacement value of the property within the area of exposure represents the maximum probable property damage resulting from a fire or explosion in the process unit being evaluated.

The following example illustrates the results of two F&EI calculations.

	Process unit A	Process unit B
Unit hazard factor	4.0	4.0
Material factor	16	24
Damage factor	0.45	0.45
F&E index	64	96
Exposure radius	54 ft (16.4 m)	81 ft (24.6 m)

Although both process units have a unit hazard factor (F_3) of 4.0, the final measurement of their probable loss exposure must include the hazard of the material being processed or handled.

The conditions in process unit A represent 45% damage to 9,156 ft² (851 m²) of surrounding area. The conditions in process unit B represent 74% damage to 20,600 ft² (1914 m²) of surrounding area.

If process unit B had a unit hazard factor of 2.7 instead of 4.0, the F&EI would be the same as that of process unit A, 64. However, the damage factor for process unit B would be 0.64 (based on a material factor of 24), compared to a damage factor of 0.45 (based on a material factor of 16) for process unit A.

C. REACTIVE CHEMICALS

In a drug manufacturing pilot plant, a flammable solvent was replaced by trichloroethylene, which generally is not considered flammable or explosive at room temperature. The residue to be extracted was made alkaline with strong caustic soda, and two gallons of trichloroethylene were added. Immediately, an emulsion was formed and began to decompose. For a period of five hours, gases bubbled to the surface and ignited spontaneously. Fortunately no one was injured. Subsequent investigation showed that caustic and trichloroethylene are stable by themselves, but when mixed they react to form dichloroacetylene, a poisonous gas that is spontaneously flammable and explosive in air.

That was a reactive chemical incident, fortunately a minor one. Dow defines a reactive chemical incident as a chemical reaction which produces the conditions for or causes an uncontrolled or dangerous energy release which may result in or has the potential for resulting in injury or property damage. Some of the worst disasters in chemical history have resulted from uncontrolled chemical reactions.

The control of chemical reactions is fundamental to the manufacture of nearly all chemical products. Chemical reactions may get out of control because the wrong raw material is used, operating conditions are changed, equipment failures or time delays occur, or because the chemistry of the process is not completely understood.

In most cases, the chemistry of the process is well understood. In Dow's experience, the major factors in reactive chemicals incidents (multiple factors are involved in some incidents) are:

1. Errors in operating procedure (85%)
2. Lack of positive identification of a material (37%)
3. Critical instruments and devices (11%)
4. Materials of construction (10%)

Dow's Reactive Chemicals Program is intended to forestall such failures. The program includes the following guidelines.

1. The owner of a material or process is responsible for obtaining sufficient information for safe operation.
2. Location managers should establish a knowledgeable working committee at the site to assist the owner in evaluating potential reaction hazards.
3. Screening tests should be performed to provide data on the reactivity of compounds and mixtures.
4. Additional tests, calculations, and evaluations should be performed

to obtain other relevant information whenever screening tests indicate a potential hazard or whenever experience indicates the desirability.

5. All chemical processes should be reviewed periodically.

6. New plant superintendents should review their processes with the local reactive chemicals committee within 90 days of assuming responsibility.

7. Manufacturing and research people should be trained in the concept and execution of the Reactive Chemicals Program.

8. Data on potential reaction hazards should be gathered and disseminated throughout Dow.

9. Every incident and potential incident involving reactive chemicals will be investigated and reported, including causes and corrective actions.

10. All reactive chemicals incidents are to be reported to site management and to the local Reactive Chemicals Committee as soon as possible, but in no case later than 48 hours after the incident.

In addition to the general responsibilities listed above, owners in functions have specific responsibilities appropriate to their function. These include securing appropriate process reviews and assuring that reactive chemicals information is made available to those both inside and outside of Dow who need it.

Figure 8 outlines factors to be considered in determining a potentially hazardous operation.

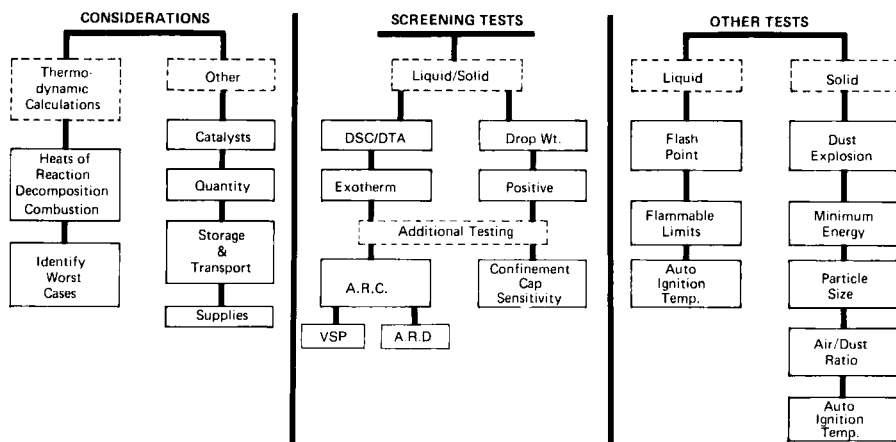


FIG. 8. Considerations and testing diagrams. This outline is the owner's general guide for determining a potentially hazardous operation. Interpretation of results and need for additional testing should be determined in consultation with analytical personnel and the Reactive Chemicals Committee.

1. *Reactive Chemicals Committees*

A Reactive Chemical Committee in each division, site, location, or organization coordinates all reactive chemicals functions at the location. The committee consists of qualified technical personnel including, where possible, representatives from research, engineering, production, safety and loss prevention, testing and any other appropriate function. The responsibilities of the committee are to:

1. Establish the program in its organizational group within the framework of Dow's "Guidelines for a Reactive Chemicals Program."
2. Collect and distribute hazard data from sources outside its organizational group.
3. Forward hazard data generated in its organizational group to other Reactive Chemicals Committees.
4. Train people in the use of the reactive chemicals program.
5. Provide data and consultation to owners and management concerning hazard evaluation of materials and processes.
6. Coordinate programs for hazard review of existing materials and processes within its organizational group.
7. Investigate and report all reactive chemicals incidents.

A corporate Reactive Chemicals Advisory Board includes representatives from several groups and disciplines in the company. This advisory board:

1. Determines company planning for the program.
2. Approves equipment and procedures for standardizing basic hazard evaluation tests.
3. Coordinates and directs the efforts of all organizational groups in establishing their reactive chemicals programs.

2. *Process Review*

A process review is a formal procedure in which all factors that could lead to a reactive chemicals incident are investigated and lines of defense are identified and implemented. Process reviews are conducted on new processes and on changes in existing processes before they are put into operation. They also are conducted upon changes in supervision and periodically on existing processes. In addition, a reactive chemicals incident may trigger a process review.

Each process review will vary with the nature of the operation. In general the process review will include the following actions.

1. Review the process chemistry, including principal reactions and expected side reactions along with the heat of reactions and pressure build up potential.
2. Review the reactive chemicals test data for evidence of exotherms, shock sensitivity, or other evidence of instability or energy release potential.
3. Examine the process in detail with the aid of appropriate flow diagrams, looking at upset conditions, delays which can occur, modes of failure, worst case situations, and other ways of abusing the chemical, with particular attention to redundancy and critical controls.
4. Probe each phase of the operation from raw material receipts through product distribution for any point where a reactive chemicals accident could take place.
5. Consider the consequences of not following procedures (i.e., incorrect order of addition or stoichiometry, no agitation, and so on.)
6. Review start up and shut down procedures and the consequence of a time delay in any step of the process.
7. Identify the line of defense which will be employed to avoid reactive chemicals accidents at each point.

3. *Data Handling*

The owner of a material or process must obtain, maintain, and update the reactive chemicals data needed for safe operation of the process. Information is available from several sources.

Technology centers (see Section IV,F) maintain central files containing the reactive chemicals data pertaining to their technology. Dow also maintains a computerized data base of reactive chemicals information on its Midland Scientific Data Center computer in Midland, Michigan. For many materials, data may be obtained from the technical literature and from suppliers' literature.

Because of the complexity of reactive chemicals testing, not all laboratories, are equipped or qualified to conduct the tests required. However, many Dow laboratories can perform several of the needed tests. The local Reactive Chemicals Committee identifies and arranges for needed testing.

4. *Reactive Chemicals in the Matrix*

The Reactive Chemicals Program is an important element in Dow's safety matrix. The research role includes support of the Reactive Chemicals Program, as well as maintaining location reactive chemicals programs within the research organization. The engineer selecting equipment and

designing plants and processes must take into consideration many of the factors contained in the Reactive Chemicals Program. The Reactive Chemicals Program applies wherever Dow people investigate, design for, produce, or handle reactive chemicals.

D. LOSS PREVENTION PRINCIPLES

Dow's "Loss Prevention Principles" (LPPs) are a collection of design and installation practices which experience has shown to result in safer and more reliable operations (5). They constitute recommendations to be followed, where appropriate, in plant design and modifications.

LPPs are developed through the combined efforts of process engineering groups, technology centers, manufacturing, and loss prevention representatives. They also include appropriate references to external standards, such as those established in the National Electrical Code, by such groups as the American Petroleum Institute and by regulatory agencies like OSHA, the Occupational Safety and Health Administration.

Loss prevention principles are dynamic tools, changing as needed to keep up with improving methods. A new edition of the LPP manual, containing several hundred pages, is published every two years. Part of the safety and loss prevention responsibility of Dow employees is to make certain that improved methods appear in the next edition of the LPP manual. The current (1986) edition contains 94 loss protection principles addressing 17 major elements of plant design.

A typical loss prevention principle, LPP 7.1, deals with the storage of flammable liquids. It defines flammable liquids, then discusses eight factors to be considered in storing such chemicals. The major factors, each with several subdivisions, are:

1. Vapor space and vapor recovery
2. Buried tanks above and below ground
3. Floating roof tanks
4. Diking of tanks
5. Location of pumps
6. Fire protection
7. General, including various specifications and standards not covered above

Each LPP may also discuss information which should be included in the operating discipline and maintenance procedures for the process activity covered. Appropriate references to other LPPs are provided, as are references to applicable industry and government standards.

E. OPERATING DISCIPLINE

In 1974, a fire and explosion at a chemical plant in Flixborough, England killed 28 employees and injured 36. Property damage included more than 1,800 houses and 167 shops and factories. The incident began when the plant jerry-rigged a system to bypass a disabled reactor. Workers erected temporary scaffolding to support a 20-in. pipe and violated industry and manufacturer's recommendations in assembling and testing the bypass piping. They tested for leaks but not for the strength of the assembly (6).

Several years later, an explosion occurred at a plant producing trichlorophenol in Seveso, Italy. The production run itself ended at 6:00 a.m. Saturday morning, when the plant closed for the weekend.

Because of this closing schedule the following occurred.

1. Instead of distilling off 50% of the solvent after the end of the batch, as required by the operating procedure, the operators distilled off only 15%.
2. Instead of adding 3,000 liters of water to cool the reaction mixture to 50–60°C, as required by the operating procedure, the operators added none.
3. Instead of continuing to stir until fully cooled, as required by the operating procedure, the operators stopped the stirring after 15 min.
4. Instead of remaining with the unit until the mixture had cooled, as required by the operating procedure, the operators left at 6:00 a.m.

Exothermic decomposition of the mixture caused the rupture disk on the vessel to break $6\frac{1}{2}$ hours later, venting material containing dioxin over a wide area (7).

One team investigating the 1983 disaster at Bhopal, India, reported that the scrubbing system which should have absorbed the vapor discharged from the relief valves, the flare system which should have burned any vapor which got past the scrubbing system, and the cooling system for the tank were not in operation or not in full working order.

In each of these cases technology was not lacking, but the discipline required to follow procedures and good operating practices—operating discipline—was lacking.

There is no definition or checklist which will tell you, “now you have an operating discipline.” It is several different things. It is all the knowledge needed to operate a plant to produce a quality product safely, efficiently, and without insult to the environment. It also is the training required to equip the entire work force to achieve that goal. And it is the orderly conduct and self-control which leads to that achievement.

In "computerese," operating discipline is the software—standards, written procedures, operating instructions, guidelines, training, supervision, and conduct—needed to operate a plant successfully.

At Dow, the operating discipline in a typical production unit will include:

1. The operations book, which contains detailed instructions for starting up, operating, and both routine and emergency shutdown of the process
2. The applicable operating computer program(s)
3. The Critical Instruments Program (see Section IV,G)
4. Support publications, including such material as safety, health and environmental standards, quality control and cost data, and so on
5. Equipment data materials, including specifications, maintenance and lubrication schedules and records, critical instrument records, and so on
6. Training program information, including manuals and aids, documentation and records
7. Research back-up data

Operating discipline forces thinking things through ahead of time. It provides for initial and follow-up training of all personnel involved in operating and maintaining the plant.

Operating discipline also provides an "institutional memory" for the plant it covers. It assures information transfer to new employees and to all employees in the event changes are made, and it assures that company and legal requirements are met.

The accidents described above are dramatic examples of failure of operating discipline. Experience teaches that some similar failure underlies every adverse incident in a chemical plant.

A young chemical engineer may be assigned to initiate the operating discipline for a new process unit. The effort will involve searching all the files relating to the specific unit, then seeking information on comparable units elsewhere within the company and outside it. At Dow, the technology center is a primary contributor, but the search for experience with similar technology extends as far as the data can be found.

Research and engineering make vital contributions to the initial operating discipline, as to manufacturing people with experience in similar technology. Dow has found that plant operators can contribute valuable experience to the development of the discipline.

Once this initial operating discipline is put into usable form, it must be communicated to the people who will use it. This means a series of training sessions before plant start up, training that continues through the start up period.

But the operating discipline is never complete. It is a dynamic effort, changing as operating mistakes are made and corrected, as process or materials changes are implemented, or other improvements made in any aspect of the operation. The operating discipline also will be reviewed and, if necessary, changed when incidents occur which cause or could cause human injury, property or product loss, or environmental damage. It will be reviewed whenever a new plant superintendent is assigned and at other appropriate intervals.

At any time, the operating discipline provides extensive documentation of the plant's history.

Others may create, implement, and update the operating discipline. However, the plant manager or superintendent bears the responsibility for establishing and maintaining it. At Dow, this responsibility is formally spelled out in the company's "Minimum Requirements for Safety, Loss Prevention and Security."

Line management has a responsibility to monitor and assess all changes in process technology and work procedures in order to continue to provide a safe, secure work environment.

F. TECHNOLOGY CENTERS

A major challenge facing a multilocation company is assuring that the best product, specific or process-specific knowledge reaches the people who must put it into practice. There are times, for example, when a plant superintendent in Thailand has more in common with a counterpart in Stade, Germany than with his neighbor in the office next door.

One Dow agricultural chemical is manufactured in 12 plants in 11 different countries, from Indonesia to The Netherlands. Although their plants are scattered around the globe, the superintendents share the same problems related to operations, quality control, reactive chemicals, safety and loss performance, and other factors which, while common to the chemical industry, are also unique to their specific process. Thus each plant superintendent needs to share experiences regularly with others who face the same operating requirements.

Dow meets this multilocation challenge through a network of Technology Centers. Each Technology Center is the central repository of knowledge encompassing all aspects of plant design and operation for a specific product or process which is found in more than one Dow location. In addition to those which are product- or process-specific, Technology Centers have been established to promote expertise in the environmentally significant areas, solid waste treatment and incineration and water treatment.

Other organizational groups are essential to safe and efficient operations. However, except for line management, other functional groups are assigned specific areas of responsibility such as product or process research, engineering, technical service, industrial health, environmental services, analytical development, safety and loss prevention, security, and so on.

Each Technology Center interacts with all these functions to become the central library of knowledge, including safety and loss prevention knowledge, for its technology. It also acts as a coordinator of knowledge generated by line operations as well as that generated by sources outside of Dow.

The Technology Center also develops programs addressing such concerns as quality assurance, energy utilization, yield improvement, and safety performance. These programs then are used as the basis for plant design and for measuring plant performance. Technology center personnel also act as consultants to those responsible for plant operations.

1. Design and Other Guidelines

Technology Centers ordinarily will develop design guidelines for use in designing or modifying plants, collect and publish process-specific reactive chemicals and critical instruments recommendations, and so on. The guidelines expressly reflect "knowledge to data." Reports of safety or loss incidents, process problems, material of construction problems, or equipment failures all trigger a review of the design guidelines to assure that they contain the latest and best knowledge.

Centers usually adapt company-wide guidelines to activities within their scope. For example, the S/B (styrene/butadiene) Latex Technology Center has developed a Critical Instruments Program specifically for Dow's latex plants around the world. It identifies typical latex production equipment likely to be controlled by critical instruments. The program then draws upon Dow (and non-Dow) latex and other plant and research knowledge and experience to propose test procedures and test intervals for such instruments.

2. Organization

No two Technology Centers (see Fig. 9) are organized exactly the same way, but the general organizations are similar. Each center is located at a site which employs the technology it covers. Since all action in Dow takes place through the line organization, each technology center is headed by a manager who also has line manufacturing responsibilities. A full-time technical manager with years of manufacturing experience oversees the day-to-day operation of the center.

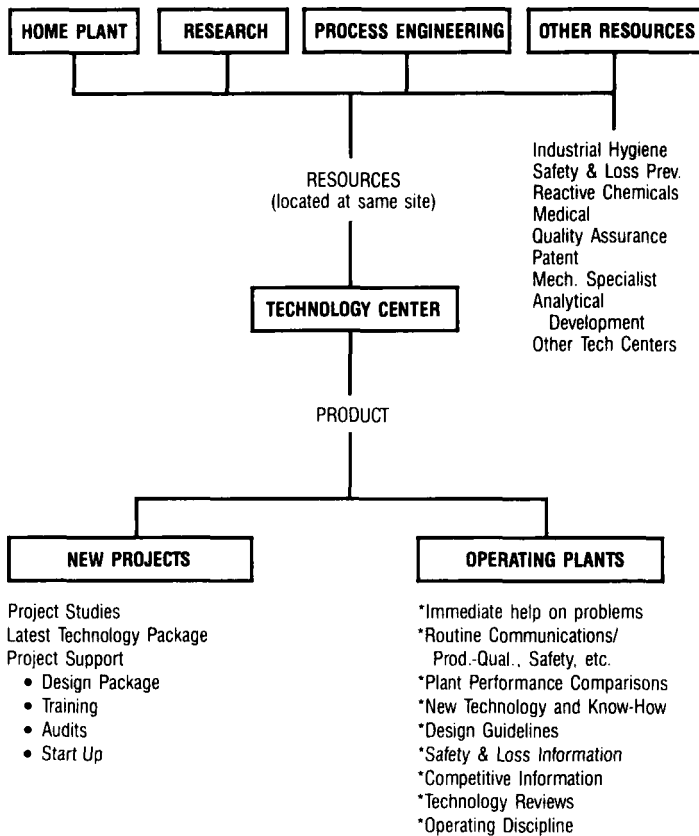


FIG. 9. One possible organization of a technology center.

Depending upon the scope of the technology, additional technical people may also be assigned full time to the center. Technology Centers also draw on other Dow specialists as needed. Specialists are assigned to support each center in engineering, safety and loss prevention, industrial hygiene, and quality assurance. Experts in economic evaluation, patents, medical matters, and legal matters also can be called on when needed.

3. Operations Interface

Because the Technology Center is the central repository of knowledge for its technology, it interacts continuously with line management as well as research, engineering, marketing, and other functional groups. This interaction keeps the center aware of the current knowledge and experience gained by those groups which affect its technology.

Written, monthly reports from each plant cover performance, safety and loss incidents, and the status of plant projects and developments. Statistics are supported by narratives describing product and process problems and solutions, equipment problems and changes, capital projects, and other information. These reports, shared with other plants within the Technology Center's scope, are an important resource for people responsible for production performance, quality, and safety.

4. *Safety Role*

Technology Centers develop and maintain safety and loss prevention guidelines for their particular process, as well as process technology and plant design standards.

Technology Centers also collect information about safety and loss-related incidents and quickly communicate it to other plants within the center's scope so that action can be taken to prevent similar incidents elsewhere. As a result of this "safety alert" procedure, complete information on a safety-related incident in a polystyrene plant in Australia can reach a similar unit in Ohio or California within 48 hours. At the same time the incident would be reported to other Dow locations in Australia, to Dow's Pacific Area headquarters, and to the corporate safety and loss prevention group for dissemination through their respective channels.

Technology center specialists frequently will be involved in investigating major safety and loss incidents.

5. *Reviews and Audits*

The Technology Center provides expert counsel in the process and safety reviews which precede and accompany the construction or modification of plants and processes within its scope.

Global technology reviews, held approximately every two years, bring production managers together with research and technology center personnel for face-to-face discussions. In addition, every 18 to 24 months the center conducts a technology audit—an operating and technology review—at each of its plants.

The technology audit brings together technology center and research personnel, operating managers from another plant in the same technology area, and the management of the plant being audited. This team reviews such areas as quality assurance, yield performance and improvement, and energy utilization.

The Technology Center audit team also addresses safety, reactive chemicals and critical instruments programs, and industrial hygiene and environmental quality efforts and performance which are specific to the technology.

During the audit, the team is alert to new technology, good operating practices, new equipment, and operating disciplines which can be communicated to other plants within the Technology Center's scope.

G. CRITICAL INSTRUMENTS

A Critical instrument is a device and its accompanying system whose proper functioning is necessary to prevent a serious incident. The system that reads the signal, interprets it, and displays it is as critical as the device that generates the signal.

A serious incident is one in which serious personal injury or serious health, environmental, or economic damage could occur. Some examples of critical instruments and instrument systems are:

1. Vibration monitor and overspeed trip on large-scale rotating equipment
2. Limit switch system which stops moving machinery if a door is opened for access
3. Interlock system which stops feed to a reactor if the agitator is not turning and where continued feed could result in a reactive chemical hazard
4. High-level switch on storage tank which shuts off transfer system

Dow's Critical Instruments Program describes identification of critical instruments, and provides guidelines for their design, installation, testing, maintenance, and documentation.

1. *Identifying Critical Instruments*

Identification of critical instruments is the responsibility of the "owner" of the process and usually is a part of process research and design. In addition to recognizing critical instruments, the operation must be reviewed to make certain that instrumentation is adequate to prevent a serious incident.

In a typical plant, instruments may be classified in three levels of criticality.

1. Level 1 instruments are those whose failure probably will cause personnel to be exposed to injury and also cause equipment damage.
2. Level 2 instruments are those whose failure probably will cause equipment damage but should not expose personnel to injury.
3. Level 3 instruments are those whose failure probably will not cause personal injury or equipment damage.

2. *Testing Critical Instruments*

Once a critical instrument loop is identified, a procedure for testing the entire loop must be written. The test procedure will influence the design of the new system, since, if possible, the test should be an actual performance test. For example, if a high temperature should close a valve, the ideal test would consist of raising the temperature to see if the valve closes. Efforts should be made to avoid test procedures which require temporary wiring disconnects, valve closures, and so on, which might not be returned properly to operating condition.

Test procedures preferably are designed to be performed by the plant operator. This practice is desirable because:

1. It reinforces the operator's awareness and knowledge of the importance of the loop.
2. The operator is available to perform the test when the unit is ready for test.
3. The operator has the knowledge to create any control situations required for realistic performance tests.

The operating computer can be programmed to do the performance test. It can be relied upon to test exactly as instructed and to test at frequencies impractical for human operators. However, computer-performed tests should be monitored and documented by an operator.

A minimum interval of three months between tests of each critical instrument loop is recommended; in no case should the interval exceed 12 months. However, frequency of testing should be based on plant judgment and experience, as well as on Technology Center information.

Figure 10 was prepared by a Dow technology center as a logic diagram to illustrate an approach to be taken to determine how often a critical instrument loop should be tested.

The owner first decides what failures could lead to an unwanted result, in this case overfilling a storage tank.

The next step is to estimate the probable frequency of each failure. The failure rates chosen for the example are empirical [e.g., chemical plant experience indicates that an operator failure (checking the level indicator) will occur one out of every 100 operations in a relatively stress-free situation]. The estimated failure rates will be replaced with actual rates when accumulated experience permits.

Note that two of the four possible critical failures are human. The operator fails to check the level indicator before unloading, or the purchasing department orders a new supply before the reorder level is reached.

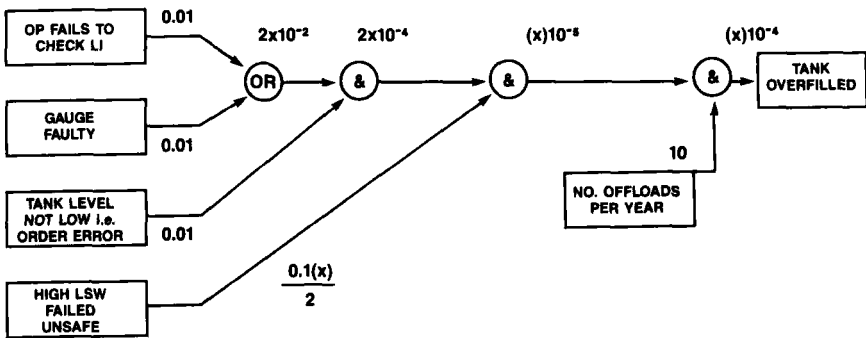


FIG. 10. Determining test interval for critical instruments. Example of tanker off loading which is operator supervised. The tank has a local level indicator (LI) and separate level alarm (LA) and level switch (LSW). Offloading is performed 10 times per year. (x) is the number of operations per year. Probability of overfill equals $10^{-4}(x)$. Proposed target is less than or equal to 3×10^{-5} . Testing interval: $10^{-4}(x) \leq 3 \times 10^{-5}(x) \leq 3 \times 10^{-1} = 4$ months. Note that if only one tanker is offloaded per year, it is better to check LSW prior to offloading.

3. Engineering and Design Considerations

As described above, performance testing is an important consideration in the design of a critical instrument loop. Components of the system must be selected for ease of testing, as well as for their ruggedness and reliability.

While redundancy—backing up one system with another just like it—is a logical way to protect against instrument failure, diversity may be a better choice in many cases. For example, dual thermocouples in the same well could corrode out at the same time. It might be better to have two different types of measurement, one a thermocouple in a thermowell and the other possibly a resistance thermal detector.

In general, redundancy or other backup is required for level 1 instruments. Level 2 instruments may require redundancy if the equipment which it protects is critical to the process. Level 3 instruments ordinarily do not require redundancy.

Individual routing duplication of control cables can increase the reliability of redundant loops. Cable and instrument piping, routing, and protection must take into account potential damage from chemical spills, fire, lightning, and other hazards. Instrument cables should be routed through the least hazardous areas, and should be in separate cable trays and trenches from electrical wiring. In addition, critical instruments normally are independent of regular control loops.

The designer must also consider the failsafe condition of loop components: control valves must fail in the safe mode. Reliability may be

improved by providing backup electrical power and air supplies. However, the failure mode cannot always be guaranteed on electrical and pneumatic components.

In computer systems, program logic is an important component of the critical instrument loop. Security precautions must be taken to prevent inadvertent changes in programming. In addition, manual overrides are discouraged. For example, if it is critical to shut down a pump during an emergency situation, a manual "on" switch may not be desirable.

4. *Auditing the Program*

Dow's Critical Instruments Program requires that written records of critical instrument tests, with the name of the tester and information on any unsatisfactory performance, be kept for the current and preceding year. In addition, the Critical Instruments Program is included in the plant's program of safety audit and is audited on an annual basis.

H. SAFETY TRAINING

Most safety, loss prevention, and security (S/LP/S) incidents result from or are intensified by some kind of human failure. Training reduces the risk of injury to people and the loss of property and technology.

At Dow, training begins before an employee goes on the job and continues throughout the working career. Each supervisor bears primary responsibility for training and motivating workers under his or her supervision. Success in meeting that responsibility is a major factor in evaluating the supervisor's performance. Safety attitude and motivation also are major factors in evaluating the performance of each worker.

1. *The Dowville Workshop*

Dowville is a fictitious, small formulations plant located in western Nebraska. An incident at Dowville resulted in two injuries and an unexpected runaway reaction during the first run of a new product.

That imaginary incident is the subject of a case study presented several times each year to groups of Dow supervisors and managers. The students represent a cross section of both experience and line and staff responsibilities. During a 2½-day Safety, Loss Prevention and Security Workshop, they will investigate the Dowville incident.

Workshop participants are provided with notebooks containing all the safety, loss prevention, and security related data that exists at Dowville. The notebooks include personnel files, safety meeting minutes, and reac-

tive chemicals and industrial hygiene data. The participants are divided into teams of five or six people to investigate the incident and search out root causes.

During the workshop, participants spend half of each day in classes on major factors in safety, loss prevention, and security. The schedule includes classes on:

1. Operating discipline,
2. Reactive chemicals and process change,
3. Critical instruments,
4. Attitudes and safety,
5. Accident investigation,
6. Industrial hygiene/protective equipment,
7. Training methods, and
8. Security.

The balance of participants' time is spent studying the Dowville case and preparing team reports to be delivered at the end of the workshop. In the reports, the team identifies the root causes of the Dowville incident, identifies deficiencies in Dowville's S/LP/S programs that allowed the root causes to exist, and recommend actions to correct those deficiencies. The team presentations are judged by a panel of managers with one report selected as the winner.

a. *Workshop goals.* The Dowville Workshop teaches participants:

1. That S/LP/S matters are line responsibilities that cannot be delegated to staff functions.
2. That S/LP/S risks can be managed like any other part of Dow's business.
3. That S/LP/S performance is a measure of managerial performance just as surely as are cost control, quality, or anything else.
4. That top management has endorsed certain minimum S/LP/S requirements for all Dow locations and expects compliance from all Dow employees.

Workshop sessions are designed to stress the contents of the "Minimum Requirements" and their application to each participant's operation. They stress that learning experiences can be shared with other Dow employees to minimize relearning. The success of the Workshop depends on the sharing of experiences, both among participants during the workshop and among participants and co-workers after the workshop ends.

Workshop objectives are met only when measurable improvements in safety, loss prevention, and security programs have been made in participants' own areas as a result of attending the workshop.

b. *Post-Workshop Assignments.* Following their attendance at the Dowville Workshop, participants are required to share what they have learned with others in their own operations.

A second assignment requires a presentation on the workshop, with emphasis on solutions to the most significant problem in the attendees' own operations, at their next safety meeting.

Each year, 800 to 1000 Dow supervisors, superintendents, and managers take part in Dowville workshops.

2. *Supervisor Training*

Supervisor safety training applies to all levels of Dow management and is tailored to the individual's responsibility. For example, a manager with global responsibilities for reactive chemical products which are new to him may be required to conduct a reactive chemicals review for the products and then pass a written examination.

All supervisors receive basic training in industrial and chemical plant safety, including training and motivation of their workers for safety on the job. They also receive specialized training appropriate to their responsibilities. Formal training courses, held annually with documentation of the training, focus on some phase of the safety and loss prevention program. In addition, specialized courses address specific operational problems.

3. *Worker Training*

The new employee receives both basic and job-specific orientation before entering the plant. The experienced worker receives appropriate training before undertaking a new position or whenever changes in the workplace or in job content make it desirable. Checklists assure that safety and other aspects of the job are covered. Written tests make certain the employee understands the safety and other important aspects of the job.

Ongoing training takes place in regular safety meetings; in *ad hoc* meetings held whenever a safety-or loss-related incident occurs; in job performance reviews; and in frequent, informal personal contact with supervisors.

Since 85–95 % of chemical plant accidents are not chemical-related, much of the safety training is similar to that provided in effective safety programs in all kinds of industry. Of course, chemical safety is not neglected.

Employee training includes:

1. The operating discipline for the job the employee holds or is about to begin

2. Safe work habits
3. Housekeeping
4. Proper use of tools
5. Lockout and red tag procedures
6. Safe use of ladders, work platforms, and so on
7. Purpose and use of personal protective equipment
8. Emergency procedures
9. Safe operation of motorized equipment as appropriate
10. Safety, loss prevention, and security rules applying to the plant, department, and process

4. *Industrial Hygiene*

Safety training also includes training in industrial hygiene for employees who potentially are exposed to chemical, physical, or biological agents. Employees of outside contractors also are given the same training as Dow workers when the training is appropriate to their involvement with Dow products or processes.

This training is part of the initial, new job orientation for all employees and is repeated at least annually. The training includes:

1. Identity and potential consequences of potential exposure to toxic amounts of hazardous agents present
2. Acceptable levels of exposure
3. Most recently measured levels of exposure
4. Engineering and operating measures used to control exposure
5. Personal protective equipment and employee conduct required to control exposure

The training program also includes a provision for timely feedback of new measurements of exposure levels, with additional control information where needed.

Contractors working in Dow sites are required to provide equivalent, appropriate training for their own employees on Dow premises.

5. *Safety Meetings*

On-the-job safety meetings with written agenda are held on a regular basis for all workers by each supervisor. The program may draw on the plant safety and loss prevention department, or other sources, for training and review appropriate to the unit situation. Even if the primary program is prepared by others, the agenda always provides for a free discussion of worker concerns and suggestions about safety in the local unit.

In addition to the scheduled meetings, *ad hoc* meetings are held when a personal injury or property damage incident or “near miss” occurs in the unit. Such meetings usually are limited to the specific incident. Supervisors will review the incident with workers and discuss ways in which a recurrence can be avoided.

I. AUDITS

Audits are an important part of safety and loss prevention. Ideally, they are educational for the plant being audited. In addition, well-planned and well-executed audits will detect deficiencies in the program and point out situations where performance deviates from accepted standards.

Members of the audit team must be familiar with safe work and loss prevention practices and with the site’s and Dow’s standards of performance.

Safety audits are evolutionary—details change as knowledge is gained. In addition, special sections may be added to the basic audit to cover unique differences of location, type of operation, product, and equipment. Dow safety and loss prevention people have a slogan: “You get what you *inspect*, not what you *expect*.”

Specifically, a safety and loss prevention audit should be designed and conducted to:

1. Review the entire safety and/or loss prevention program to determine if it contains all the essential elements.
2. Determine if the site, location, or department has appropriate written standards of performance opposite each important program element.
3. Determine that the standards of performance have been communicated to all site people and are known and accepted. In many cases, specific training will be required.
4. Establish that a program of regular internal audits exists for each important program element, to assess actual field performance as compared to written standards of performance.
5. Provide meaningful and practical recommendations to improve the ineffective elements of the program.
6. Assess the attitude of management, supervision, and other employees regarding their acceptance of, motivation towards, and involvement in all elements of the program.
7. Establish that specific objectives, goals and plans exist to reach the next stage of program development.
8. Assess the rate of progress toward these goals.

A well-conducted program of internal self-audits is important to a site's overall safety and loss prevention efforts. The discussion in this section is applicable to internal audits as well as to external audits conducted by audit teams from other Dow units.

1. *The Audit Team*

People selected for the audit team must know safety and loss prevention standards and terminology. In addition, they must be familiar with Dow's "Minimum Requirements" and with management's expectations for safety and loss prevention performance.

The team's expertise should be compatible with the kind of audit to be conducted. Audits of certain programs may require the selection of specialists in electrical equipment, pressure vessels, maintenance, motor fleet activities, and other fields. Line managers of other units are excellent members of audit teams. They bring a different background to spot weaknesses. In addition, participation is a learning experience for the manager and increases the involvement of those responsible for results. It may also be helpful to have a previous auditor of the unit as one member of the audit team.

Auditors also should be skilled in spotting potential accident-producing situations, whether from unsafe practices, conditions, or design criteria. duPont's Safety Training Observation Program (S.T.O.P.)² is helpful in developing these skills. The program provides clues on how, what, and where to observe by building a pattern of observation for auditors to follow.

2. *The Audit Process*

The complete safety and/or loss prevention audit encompasses four phases.

1. A Pre-Audit Safety Awareness Survey, distributed through line management, asks employees about their knowledge of and attitude toward the location's safety and loss prevention programs.

2. Management interviews and the examination of program documents and records reveal whether the safety and loss prevention program contains essential elements with written standards of performance based on Dow's best global know-how.

² E. I. duPont de Nemours, "Safety Training Course for Supervision," Library No. AA523.

3. Interviews with and observation of employees on the job to assess their knowledge, involvement in, perception of, and compliance with the program.

4. Inspection and observation of the work environment enables the auditor to help local management identify work hazards resulting from unsafe design, lack of protective features, or exposure to materials in or evolving from the process. It also provides an opportunity to observe work practices and equipment operations.

3. *The Audit Report*

A supervisor of the unit being observed normally accompanies the auditor. During the inspection, the supervisor is informed of practices, equipment, or devices needing correction. This enables the supervisor to take or consider corrective measures before the audit report is presented to management.

A verbal report is given to management before the audit team departs. This procedure allows the managers to ask questions about any portion of the report and to point out areas where the audit team could have misjudged or been misled.

A detailed written Audit Report is sent to management of the unit audited within two weeks. This allows management to develop a course of action to meet the auditors' recommendations.

V. **Society's Role**

Society is playing a growing role in determining the conditions under which the chemical industry will operate its plants; transport, store, and market its products; and handle its wastes. This role is expressed in legislation, in product judgment, and in the sheer weight of public pressure which can affect the chemical plant's ability to function.

A. **LEGISLATION**

A wide range of legislation from every level of government can affect every phase of chemical production and marketing.

1. *Municipal Legislation*

Local zoning laws affect plant location and the kind of operations which can be conducted in various areas of a town, city, or county. Other local

laws affect transportation routes for hazardous materials and prescribe conditions under which waste must be disposed.

A growing number of communities are enacting "right to know" laws. These laws require that public officials, health workers, plant workers, and in some cases the general public, be kept informed of hazardous materials produced, used, or stored within the community. In addition, state and federal laws often give local citizens an effective voice in how those laws will be applied within their community.

2. *State Legislation*

State laws may prescribe safe working conditions in chemical and other plants. They also may prescribe environmental standards which must be met in plant operations. States also have or may enact "right to know" laws as well as legislation governing transportation, storage, marketing, or disposal of hazardous materials.

State agencies have significant roles in the administration of federal environmental and safety laws and regulations. Thus, the state may issue operating permits and monitor compliance under, for example, the Clean Air Act, etc.

3. *Federal Legislation*

A growing number of federal laws affect the chemical industry's operations and its products. In general, these laws require that some federal regulatory agency establish detailed regulations to implement the law and then enforce those regulations.

In broad terms, the regulations require operations, products, or activities which conform to the regulation. They also may demand monitoring, recordkeeping, and reporting to document compliance.

Penalties for violations can be severe. In some cases, violation can lead to banning a product or shutting down a plant or operation. In other cases, civil penalties may run as high as \$50,000 for each day a violation continues. Criminal penalties, including jail sentences, are also possible. Citizen suits to force compliance or for damages may also be permitted. In addition, knowingly submitting a false or inaccurate report is a felony punishable by imprisonment for up to five years or a \$10,000 fine or both.

Table VIII summarizes major legislation which impacts the chemical industry with society's expectations for safe materials and a clean environment. The chemical engineer has a vital role to play in assuring that products meet these requirements.

TABLE VIII

MAJOR FEDERAL ENVIRONMENT AND SAFETY LEGISLATION

Title	Enacted	Summary
Federal Insecticide, Fungicide and Rodenticide Act (FIFRA)	1947, amended in 1972	Regulates production, marketing, and use of pesticides
Federal Water Pollution Control Act (Water Quality Act)	1961, amended in 1987	EPA establishes standards for release of contaminants to waterways
Occupational Safety and Health Act (OSHA) ^a	1970	Mandates health and safety standards in the workplace
Clean Air Act	1963, amended in 1967, 1970, 1977	Governs airborne emissions
Toxic Substances Control Act (TSCA)	1976	EPA may require testing and restrict or ban production and sale of hazardous chemicals
Clean Water Act	1977	Governs discharge of pollutants into waterways
Safe Drinking Water Act	1974, amended in 1986	Prohibits contamination of drinking water supplies
Resource Conservation and Recovery Act (RCRA)	1965 as Solid Waste Disposal Act, 1970 as Resource Recovery Act, 1976 as RCRA	Regulates disposal of hazardous solid wastes
Comprehensive Environmental Response, Compensation and Liability Act (CERCLA) or Superfund	1980, amended in 1986	Provides for clean up of existing hazardous waste sites; imposes "superfund" tax on production of petroleum and other chemicals

^aAdministered by OSHA; all others administered by EPA.

B. JUDGMENT OF PRODUCTS

Public opinion also regulates products through the marketplace. Products may have to be modified because the risk to plant workers' health is unacceptable. Consumers may switch to what they perceive as less hazardous products. Either worker or public reaction can make a product unmarketable.

The fate of the urea formaldehyde foam industry is a classic example of the power of public reaction. Urea formaldehyde foam insulation which was not installed properly emitted formaldehyde fumes which caused discomfort and, in some cases, allergic reactions. Formaldehyde also was identified as a suspect carcinogen. The product became unmarketable long

before the industry could establish installation standards or the government could impose regulations.

Chlorofluorocarbons (CFCs) are widely used in refrigeration and air conditioning, insulation, and plastic foams. Although nontoxic and nonflammable, they are believed to deplete the ozone layer in the atmosphere which shields the earth from the sun's ultraviolet radiation. While action to control the production and use of CFCs was still being debated, McDonald's Corporation announced it would no longer use foam food containers produced with the aid of CFC in its fast food outlets.

These and other examples reinforce the increasing role which chemical engineers have in meeting society's expectations for safe products and a clean environment.

C. THE CHEMICAL ENGINEER'S CHANGING ROLE

Society's growing role in matters affecting the chemical industry has brought about corresponding changes in the chemical engineer's role, particularly in process and plant design and operations.

The need to design inherently safer plants has been expanded to encompass designing environmentally acceptable plants. Environmentally acceptable plants generate minimum quantities of potentially hazardous wastes either as potential emissions to the environment or as materials requiring disposal. Wastes are recycled and reused where possible. If this is not possible, they may be treated to reduce or eliminate the hazard or destroyed through incineration. Disposal in a secure landfill is the final option.

At Dow, all four options are employed. First, processes are designed or changed so that waste generation is minimized or so that wastes are recycled or reused. Second, liquid wastes including, in some cases, rainwater runoff are collected and sent to a water treatment plant where biological methods destroy the hazardous elements. Other wastes, including sludge from the water treatment plants, go to high-temperature incinerators for destruction. The incinerators may also generate steam or power for use in the manufacturing process.

Finally, incinerator ash and other hazardous wastes go to a secure landfill. Figure 11 is a cross section of Dow's Salzburg landfill in Midland, Michigan. Plastic and clay linings prevent contaminants from leaching into groundwater. Monitoring wells assure that any leaching will be detected so that leachate can be collected and returned to the treatment system.

The chemical engineer also has another important role. As a trained professional, the chemical engineer is in a unique position to help society

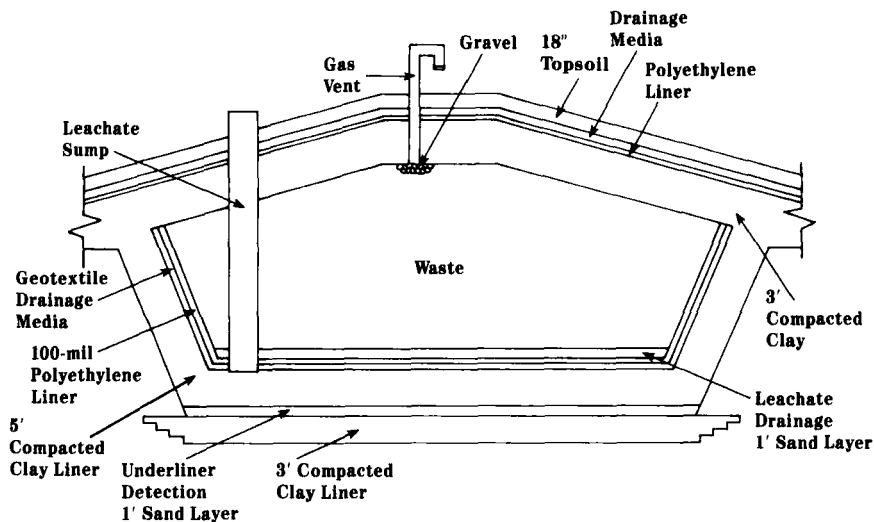


FIG. 11. Landfill cell construction detail, longitudinal section.

arrive at decisions and judgments based on knowledge rather than on fear and false or incomplete information.

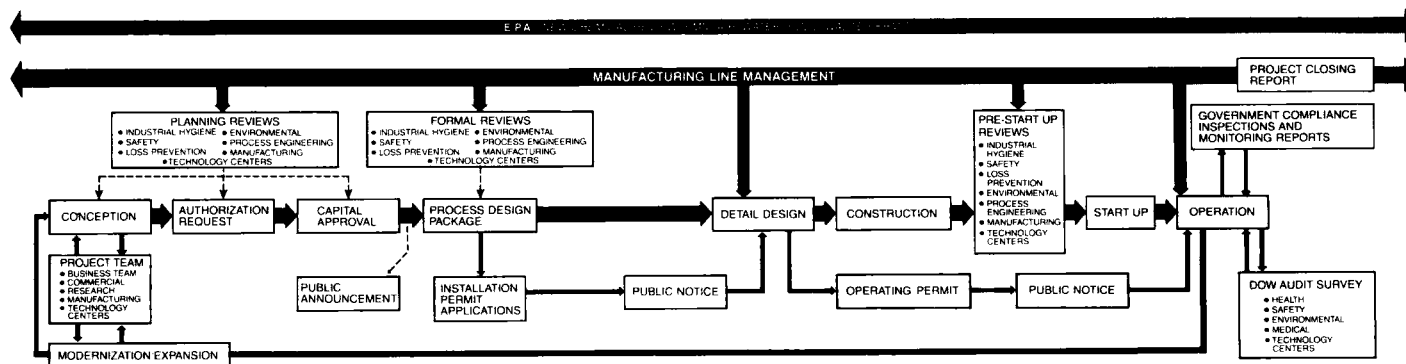
An engineer may be called upon to provide comments and testimony in hearings leading up to legislation, regulation, or the granting of permits. Important contributions also can be made through active participation in public discussion of questions relating to the chemical industry.

VI. Summary and Conclusions

Safety, loss prevention, security, and environmental protection are basic responsibilities of the chemical engineer both as an engineer and as a supervisor or manager of chemical operations and marketing. The engineering student and professional must make them primary considerations in both study and practice of the profession. Figure 12 summarizes the elements the chemical engineer must address in discharging his or her professional duties.

ACKNOWLEDGMENTS

Thanks to William E. Stephenson, APR, Ketchum Public Relations, for research and writing; Cindy C. Newman, Communications Department, The Dow Chemical Company, for project coordination and editing; Stanley M. Englund, Process Engineering, The Dow Chemical



MAJOR CONSIDERATIONS

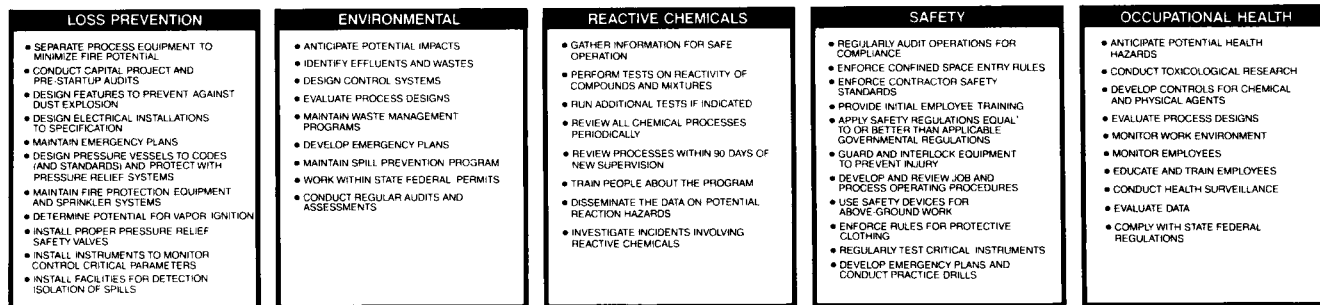


FIG. 12. Typical considerations of health, safety, and environment in safe plant operations.

Company, for project review and research; and Marcia M. Bussa, Communications Department, The Dow Chemical Company, for typing and proofing.

Resources Available from Dow:

- "Guidelines for Safety & Loss Prevention Audits"
- "Guidelines for Emergency Planning"
- "Fire and Explosion Index, 6th Edition"
- "Guidelines for A Reactive Chemicals Program"
- "Fundamentals of Fire and Explosion"—by Daniel R. Stull

Publications available from: Corporate Safety, Loss Prevention, and Security, 2030 Dow Center, Midland, Michigan 48674.

References

1. "*Accident Facts 1986 Edition*." National Safety Council, Chicago, 1986.
2. Fault tree analysis, "*Guidelines for Hazard Evaluation Procedures*," Section 2.8 p. 2-18, AIChE, 1985.
3. Englund, S., Opportunities in the design of inherently safer chemical plants, in "*Advances in Chemical Engineering*" (J. Wei, J. L. Anderson, K. B. Bischoff, and J. H. Seinfeld, eds.), Vol. 15. Academic Press, San Diego, in press.
4. Liening G., The Dow Chemical Company, Midland, Michigan, personal communication, 1986.
5. "Loss Prevention Principles," The Dow Chemical Company, Midland, Michigan, February 1986.
6. Report of the Court of Inquiry, "The Flixborough Disaster," London, June 27, 1974.
7. Howard, W. B., Seveso: Cause: Prevention, Loss Prevention Symposium, AIChE, August 1984.

INDEX

A

Active constraint strategy, 49–59
 constraint functions, 55, 57
 feasibility measure calculation, 51–52
 Kuhn-Tucker conditions, 50, 54
 mixed-integer nonlinear program, 56
 resilience analysis, 50–51
 resilience test, 49–50
 summary, 55–56
 Al_2O_3 catalysts, 195
 Arylporphyrins, structure, 106
 Asphaltenes, 99, 110, 115, 249
 amount of precipitate from crude oil, 111
 aromatic sheets
 defect site, 129–130
 unit size, 190
 C_7 fraction, 114
 chemical structure, 115–121
 aromaticity, 116
 degree of substitution, 117
 early spectroscopic studies, 115–116
 heteroatom concentration, 119–120
 model, 116–117
 molecular formula, 117–118
 naphthenic portion, 118
 conversion, mechanistic studies, 189
 definition, 111
 diffusion, 203
 metal porphyrin and nonporphyrin
 association
 isotropic to anisotropic vanadium ratio,
 133
 vanadium elution profiles, 130–131
 vanadyl compound molecular weight,
 132–133
 molecular weight and size, 121–127
 apparent VPO, 122
 definable average macrostructure, 122
 field ionization mass spectrometry,
 125–126

narrow cuts, 203–204
 partially converted, associated vanadium,
 190
 properties, residuum fraction, polar
 fractions, 123–125
 ASTM D2007, 110–111
 Audits, safety and loss prevention, 310–312

B

Bimodal catalysts, 224–225

C

Catalyst
 aged, metal deposition profiles, 206–210
 metals accumulating on surface, 209
 novel shapes, 227
 pore diameter and conversion activity,
 198
 pore size distribution, 197–200
 size and shape, 200–202
 Catalyst deactivation, 210–212
 core values, 271
 deposit obstruction of catalyst pores,
 219–227
 bimodal catalysts, 224–225
 coke deposition, 223–224
 distribution parameter, 220
 feed source effect, 222
 high-activity catalysts, 224
 hydrogen partial pressure effect, 222
 metal sulfide deposit location, 219–220
 particle size effect, 226–227
 pore structure effect, 225–226
 pore volume distribution, 221
 shapes, 226–227
 effects of metal deposits on catalyst
 intrinsic activity 212–219

- after vanadium deposition, 214–215
 - coke deposits, 215
 - metal migration, 216
 - Poisson model, 216–218
 - vanadium state, 213
 - vanadium sulfide, 214
 - modeling, 234–248
 - assumptions, 236
 - conservation equation, 238, 241, 245
 - demetallation rate as function of pore size and age, 239
 - deposit profiles, 241–243
 - grain model, 244–246
 - HDS reaction rate constant as function of metals uptake, 237
 - microspheres, 244–245
 - partial surface poisoning, 239–240
 - pellets and reactor beds, 238
 - pore mouth plugging, 239–240
 - pore plugging, 237
 - pore size effect on catalyst stability, 239–240, 247–248
 - pore structure, 236
 - purpose, 235
 - reaction and diffusion in heterogenous catalysts, 235–236
 - reaction rate versus micropore radius and grain size, 246
 - relative catalyst age, 237
 - Thiele modulus, 242
 - reactor-bed, 228–234
 - coke level, 228
 - feedstock metal concentration effects, 231–232
 - final period, 229
 - graded catalyst systems, 233–234
 - maximum vanadium concentration, 231
 - pellet size effect, 229–230
 - pore-plugging wave, 229
 - pore size and hydrogen partial pressure effects on stability, 229–230
 - rapid deactivation period, 228
 - severity of conditions, 232–233
 - slow linear deactivation period, 229
 - spatial distribution of deposition, 231
 - reactor curve, 211
 - safety policy, 271–273
 - Catalytic cracking, 141–142
 - Catalytic hydrodemetallation, petroleum, 96–98
 - model compound studies, 158–184
 - diffusion and adsorption, 173–175
 - intraparticle metal deposition profiles, 175–184
 - metalloporphyrins, *see* Metalloporphyrins
 - nonporphyrins, 172–173
 - operations role, 279–280
 - Catalytic metals, HDM, 194–197
 - Chemical engineer, safety
 - education, 270–271
 - role, 315–316
 - Chemical industry
 - lost time injury rate, 262–263
 - presence of unsafe conditions in recordable incidents, 265–266
 - recordable case injury rates, 262–263
 - Chlorofluorocarbons, 315
 - Chlorophylls, transformation to petroporphyrins, 101
 - Class 1 target, 85–86
 - Coke, deposition, 223–224
 - Critical instruments, 303–306
 - auditing program, 306
 - engineering and design, 305–306
 - identification, 303
 - testing, 304–305
 - Crude oil
 - amount of asphaltene precipitate, 111
 - distillation, 135
 - hydrocarbon classes, 98
 - properties of atmospheric residua, 100
 - reserves, 96
 - trace elements, 96
 - vanadium
 - complex concentrations, 112
 - elution profiles, 130–131
- D**
- Deasphalted oil hydrocracker, feed and product properties, 144
 - Delayed coking, residuum hydrotreating, 141, 143
 - Design
 - guidelines, 300
 - safety factors, 277–278
 - Desulfurization
 - conditions, feedstock type effects, 136–137
 - yields and properties, 136, 138
 - Diffusion-limited reactions, intraparticle metal deposition profiles, 175–184

Dow Chemical Company
 minimum requirements for safety, loss
 prevention and security, 282-284
 safety performance, 262-263
 Downstream paths, resilient heat exchanger
 networks, synthesis, 82-85, 87-88
 Dowville Workshop, 306-308
 Dynacracking process, 152-153

E

Ebullated-bed reactors, RDS-HDM
 hydroprocessing technology, 148-151
 Electron spin resonance, nonporphyrin
 metal compounds, 107
 Engineering, safety role, 276-279
 Equipment design, safety factors, 278-279
 Expanded-bed reactors, RDS-HDM
 hydroprocessing technology, 148-151

F

Feasibility test, 10, 11-13
 resilient heat exchanger networks
 with piecewise constant heat capacities,
 36-38
 with stream splits, 42-43
 Federal legislation, safety role, 313-314
 Field ionization mass spectroscopy,
 petroleum, 125-126
 Fire and explosion index, 285-291
 area of exposure, 290-291
 material factor, 287-289
 pertinent process units, 285, 287
 procedure for calculating, 286
 unit hazard factor, 289-290
 Fixed-bed reactors, residuum hydrotreating,
 147-148
 Flammability, materials, 287-289
 Flexibility index, 18-23, 62-63
 calculation, 20
 class 1 FI target, 85-86
 compared with resilience index, 27
 definition, 19
 at stage of structure, 77-82
 critical point, 78
 general form, 77
 heat transfer coefficients and cost data,
 80

multiperiod MILP transshipment
 model, 79
 target, resilient heat exchanger network
 synthesis, 65-72
 composite temperature-enthalpy curves,
 69
 definition, 66
 lack of practicality, 66
 pinch behavior diagram, 67
 uncertainty range, 70
 use of class 1 target, 69-72

G

Grain model, 244

H

Hazard evaluation
 logic diagram, 269
 operation, 293
 predictive, 267
 Heat exchanger networks, 1-3, *see also*
 Resilient heat exchanger networks
 Heat transfer coefficients, 80
 Heavy oil, blending, 99
 Heteroatom compounds, petroleum,
 combustion emissions, 135
 Hydrodemetallation
 adsorption, 205-206
 aged catalysts
 intrapellet metal concentration profile,
 207-208
 metal deposition profiles, 206-210
 bifunctional nature, 181
 catalyst
 loss of activity, 250
 pore size distribution, 197-200
 size and shape, 200-202
 catalytic metals, 194-197
 ocean nodule catalysts, 196
 optimum Co/Mo ratio, 195
 optimum Ni/V ratio, 196
 Porocel, 196-197
 sulfiding effects, 195
 diffusion, 202-205
 diffusivity as function of pore size, 204
 hydrodynamic theory, 203
 porous media, 202-203

effect of pore size and grain radius on
 stability of macroporous catalyst,
 247-248
 kinetics and mechanism of reactions,
 184-192
 catalyst size and pore diameter effects,
 201
 first-order kinetics, 190
 hydrogen consumption, 191-192
 metal removal rates, 184
 reaction orders, 185, 188
 resin fraction, 189
 summary, 186-187
 mechanisms, 97
 porphyrin
 global kinetic studies, 163-164
 reaction network studies, 165-166
 reaction rate versus micropore radius and
 grain size, 246
 reaction selectivity, 193-194
 vanadium sulfide surface site, 214
 vanadium versus nickel reactivity, 192-193
 Hydrodenitrogenation, reaction selectivity,
 193-194
 Hydrodesulfurization
 aged catalysts, V and Ni concentration
 profiles, 207
 high-activity catalysts, 224
 low-sulfur fuel oil, 136
 reaction rate constant as function of
 metals uptake, 237
 reaction selectivity, 193-194
 Hydrogen, consumption variation with
 sulfur removal, 191-192
 Hydorphyrins, structure, 106
 Hydroprocessing, 135-145
 Hydrotreating, residuum, 96

I

Industrial hygiene, 309
 Inherently safer plant, 276-277

L

Landfill cell construction, 316
 LC-fining, high-conversion, yield and
 product quality, 150
 Line management
 role in safety, 272-273

safety-related responsibilities, 280
 Loss prevention
 minimum requirements, 284
 principles, 296
 Low-sulfur fuel oil
 cut point, 140
 HDS, 136

M

Marketing, safety role, 281
 Material factor, fire and explosion index,
 287-289
 Metalloporphyrin
 association with asphaltenes, *see*
 Asphaltenes
 composition and chemical structure, 249
 demetallation studies
 configurational diffusivity, 173-174
 effectiveness factor, 183
 hydrogenated intermediates, 162
 intrinsic reaction kinetic studies,
 163-169
 metal concentration versus contact
 time, 166-167
 metal distribution parameter, 182-183
 reaction pathways, 159-163
 reaction selectivity, 166, 168
 temperature sensitivity, 171
 vanadium reactivity, 171
 VO-porphyrin versus Ni-porphyrin
 reactivity, 169-172
 VO-tetraphenylporphyrins, 162-163
 formation, 101
 molecular size, 105, 173
 nickel analogs, 159
 precipitation, 112
 structure, 102
 MoO₃ catalysts, 195
 Moving-bed reactor, RDS-HDM
 hydroprocessing technology, 151-152
 Multiperiod HEN, synthesis using structural
 optimization, 72, 74-82
 flexibility index, 77-82
 multiperiod synthesis-analysis-resynthesis
 algorithm, 74-76, 88
 operability test, 76-77
 Multiperiod MILP transshipment model, 79
 Multiperiod synthesis-analysis-resynthesis
 algorithm, 74-76, 88
 Municipal legislation, safety role, 312-313

N

- Naphthenic acid, 172
- Nickel
 - nonporphyrin metal compounds, 105–107
 - petroporphyrins, 101, 103
 - versus vanadium reactivity, 192–193
- Ni-etio porphyrin
 - demetallation reaction pathway, 160–161
 - HDM reaction kinetics, 169
 - reaction selectivity, 169–170
- Ni-tetra(3-methylphenyl) porphyrin
 - catalytic demetallation studies, 162
 - demetallation
 - kinetic rate parameters and reaction selectivity, 166, 168–169
 - metal distribution parameters, 183
 - nickel profiles, 176, 178–179, 181–182
 - reaction pathway, 160–162
- Nitrogen, distribution in petroleum, 114
- NiV/Al₂O₃ catalysts, 196
- Nonporphyrin demetallation studies, 172–173

O

- Ocean nodule catalysts, 196
- Octaethylporphyrin, diffusion, 174
- Oil, physicochemical system, 249
- Operability test, 76–77
- Operating discipline, 280, 297–299
- Operations, safety role, 279–280

P

- Petroleum, *see also* Catalytic
 - hydrodemetallation, petroleum;
 - Residuum
 - composition, 98–100
 - distribution of nickel and vanadium
 - asphaltene, *see* Asphaltenes
 - ASTM D2007 separation procedure, 110–111
 - atmospheric residuum fractions, 112–114
 - by boiling point, 109–110
 - lower-molecular-weight fractions, 115
 - solubility classes, 110–115
 - vanadium complex concentrations, 112
 - DPEP series, 103–104, 129
 - etio series, 104, 129

- field ionization mass spectroscopy
 - envelopes, 125
- heteroatom concentration, 119–120
- metalloporphyrin content, 103
- metal porphyrin and nonporphyrin
 - association, 127–134
- nickel in, 99
- nonporphyrin metal compounds, 105–109
 - arylporphyrins, 106
 - EPR, 107–108
 - hydroporphyrins, 106
 - nonlinear analysis and V complexes of
 - tetradentate-mixed ligands, 107
 - SEC-HPLC, 107–108
- porphyrin metal compounds, 101–105
- vacuum residuum, 99
- vanadium in, 99
- vanadyl nonporphyrin fraction
 - coordination spheres, 107–108
- Petroleum oils, vanadium versus nickel
 - reactivity, 192–193
- Petroporphyrins
 - molecular weight calculation, 104
 - nickel and vanadium in, 101, 103
 - rhodo-type, 104–105
- Pinch design method, 88
- Poisson deposition models, 216–218
- Polar compounds, petroleum
 - concentrations, 119–120
- Pore plugging model, 237
- Pore structural models, 236
- Porocel, 196–197
- Porphyrin
 - etio-type, 161
 - hydrogenation, 161
 - metal compounds, petroleum, 101–105
 - skeletal structure, 101–102
- Porphyrin-degraded product, 106
- Process design, safety factors, 278
- Process unit
 - fire and explosion index, 285, 287
 - hazard factor, 289–290
- Pyrrole ring, hydrogenation, 161

R

- Ramsbottom carbon, 141
- RDS-HDM hydroprocessing technology, 145–153
 - ebullated, expanded, and slurry-bed
 - reactor, 151–152

- miscellaneous reactor configurations, 152–153
- moving-bed reactor, 151–152
- summary, 146
- Reactive chemicals
 - data handling, 295
 - Dow's program, 292–293
 - incident, 292
 - safety matrix, 292–296
- Reactivity, materials, 287–289
- Research, safety role, 274–275
- Residuum, conversion alternatives, 135
- Residuum hydrodesulfurization
 - catalysts, 136
 - feedstock and products prior to cooking, 143
 - feedstocks and products prior to catalytic cracking, 141–142
 - high-severity, yields and properties, 140
 - hydroprocessing unit, 139
 - multiple fixed-bed reactor, 139
- Residuum fraction
 - atmospheric, Ni, V, N and S distributions, 112–114
 - separation procedures, 123
- Residuum hydroprocessing
 - catalysts
 - pore size distribution characteristics, 225
 - vanadium and nickel distribution factors, 199
 - model compounds, 248–249
 - obstacle to, 249
- Residuum hydrotreating, 96, 134–135, *see also* Heat exchanger networks
 - catalysts, 153–158
 - metal oxides in, 153
 - physical properties, 153–154
 - selection, 154
 - summary, 155–157
 - combined with catalytic cracking, 141
 - commercial operating capacity, 145
 - delayed coking, 141, 143
 - development, 136
 - elevated temperature and pressure, 136
 - feedstock type effect on desulfurization conditions, 136–137
 - fixed-bed reactors, 147–148
 - single fixed-bed reactor, 136, 138
 - solvent deasphalting, 143–145
- Resilience index, 10, 23–28, 62–63
 - advantage, 25
 - compared with flexibility index, 27
 - definition, 23–24
 - uncertainties, 25
- Resilience test, 10, 13–18, 62–63
 - active constraint strategy, 49–50
 - critical points, 16
 - feasibility constraints, 15
 - feasible region, 14
 - resilient heat exchanger networks
 - with flow rate uncertainties, 48
 - with piecewise constant heat capacities, 38–40
 - with stream splits, 43–47
 - constraints, 43–44
 - feasible region, 45
 - supply temperatures, 17
 - uncertainty range, 14–15
- Resilient heat exchanger networks
 - analysis, 2–3
 - energy balances, 12, 15, 17, 21, 26
 - energy recovery, 13, 15, 21, 26
 - exchanger and cooler loads, 13, 16, 21, 26
 - feasibility test, 11–13
 - flexibility index, 18–23
 - heater loads, 13, 16, 21, 26
 - minimax problem, 12
 - resilience index, 23–28
 - resilience test, *see* Resilience test
 - areas for future research, 62–64
 - assumed, 2
 - class 2 problems, 59–62
 - disadvantage, 60
 - minimum heating requirement, 61
 - target temperatures, 60
 - constraints, 11
 - corner point theorem, 28–29
 - empirical methods, 3–8
 - drawbacks, 4
 - interaction effects, 7–8
 - stream inlet and outlet temperatures, 4
 - energy recovery constraint, 32
 - linear analyses
 - definition of class 1 and 2 problems, 29–33
 - sufficient conditions for, 28–29
 - nonconvex feasible region, class 2 problem, 33
 - nonlinear analysis
 - active constraint strategy, *see* Active constraint strategy
 - ΔT_m constraints, 35–26
 - energy balance constraints, 34–35

- feasibility test, 36–38, 42–43
 - with flow rate uncertainties, 47–48
 - mixed-integer linear program, 36, 39
 - with piecewise constant heat capacities, 34–40
- resilience test, *see* Resilience test
- slack variables, 35
- with stream splits, 40–47
 - constraints, 40–42
- temperature breakpoint, 34–35
- pinch temperature, 30
- synthesis
 - based on flexibility index target, 65–72
 - class 1 FI target, 85–86
 - future research, 85–89
 - multiperiod, mixed-integer synthesis
 - algorithm, 86–87
 - multiperiod synthesis-analysis-resynthesis algorithm, 88
 - pinch design method, 88
 - using downstream (disturbance) paths, 82–85, 87–88
- systematic methods, 8–11
 - feasibility test, 10
 - resilience index, 10
 - resilience test, 10
 - synthesis, 11
 - vocabulary, 9

S

- Safety, minimum requirements, 283–284
- Safety matrix, 262–265
 - allocating resources, 272
 - application to chemical engineering
 - education, 270–271
 - engineering role, 276–279
 - equipment design factors, 278–279
 - general design factors, 272–278
 - process design factors, 278
 - establishing policy, 271–272
 - failure modes, 265–266
 - intellectual approach to problem solving, 266–268
 - marketing role, 281
 - process review, 294–295
 - programs and procedures, 281–282
 - audits, 310–312
 - critical instruments, 303–396
 - fire and explosion index, *see* Fire and explosion index

- loss prevention principles, 296
- minimum requirements, 282–284
- operating discipline, 297–299
- reactive chemicals, 292–296
- safety training, 306–310
- technology centers, 299–303
- reactive chemicals committees, 294
- research role, 274–275
- role of line management, 272–273
- society's role
 - chemical engineer, 315–316
 - judgement of products, 314–315
 - legislation, 312–314
 - voluntary standards, 268, 270
- Safety meetings, 309–310
- Safety training
 - Dowville Workshop, 306–308
 - industrial hygiene, 309
 - safety meetings, 309–310
 - supervisor training, 308
 - worker training, 308–309
- Shell Bunker-flow conversion, Venezuelan residua, 152
- Slurry-bed reactors, RDS-HDM
 - hydroprocessing technology, 148–151
- Solvent deasphalting, 143–145
- Standards, safety, 268–270
- State legislation, safety role, 313
- Stream split constraints, 40–42
- Sulfur, distribution in petroleum, 114
- Supervisor, safety training, 308

T

- Technology Centers, 299–303
 - design and other guidelines, 300
 - operations interface, 301–302
 - organization, 300–301
 - reviews and audits, 302–303
 - safety role, 302
- Tetradentate-mixed ligands, Ni and V complexes, 107
- Thiele modulus, 180, 210
 - conservation equation, 242
 - deactivation curve effect, 229–230

U

- Urea formaldehyde foam industry, 314–315

V

Vanadium

- associated in partially converted asphaltenes, 190
- catalyst activity after deposition, 214–215
- deposition
 - catalyst particle size effect, 226–227
 - hydrogen partial pressure effect, 222
 - pore structure effect, 225–226
 - reaction temperature effect, 223
- elution profiles, SEC-HCLP, 130–131
- versus nickel reactivity, 192–193
- nonporphyrin metal compounds, 105–107
- petroporphyrins, 101, 103
- ratio of isotropic to anisotropic in asphaltenes, 133

Vanadium sulfide, surface site, reaction mechanism and model, 214

Vanadyl arylporphyrin, 106

Vanadyl compounds, molecular weight, 132–133

Vanadyl hydroporphyrin, 106

Vanadyl nonporphyrin fractions, EPR-derived coordination spheres, 107–108

Vanadyl phthalocyanine, 172

Vanadyl salen, 172

VEBA combi-cracking process, 153

VO-etiochlorophyll, demetallation

- averaged catalyst vanadium loading, 181
- nickel profiles, 176–177
- reaction coefficient matrix, 180
- vanadium profiles, 175–176

VO-porphyrins, diffuse reflectant spectroscopy, 206

VO-tetraphenylporphyrins, demetallation, 162–163

W

Worker, safety training, 308–309